ISSN 0973-8916

Current Trends in Biotechnology and Pharmacy

Volume- 18 issue 3 JULY 2024

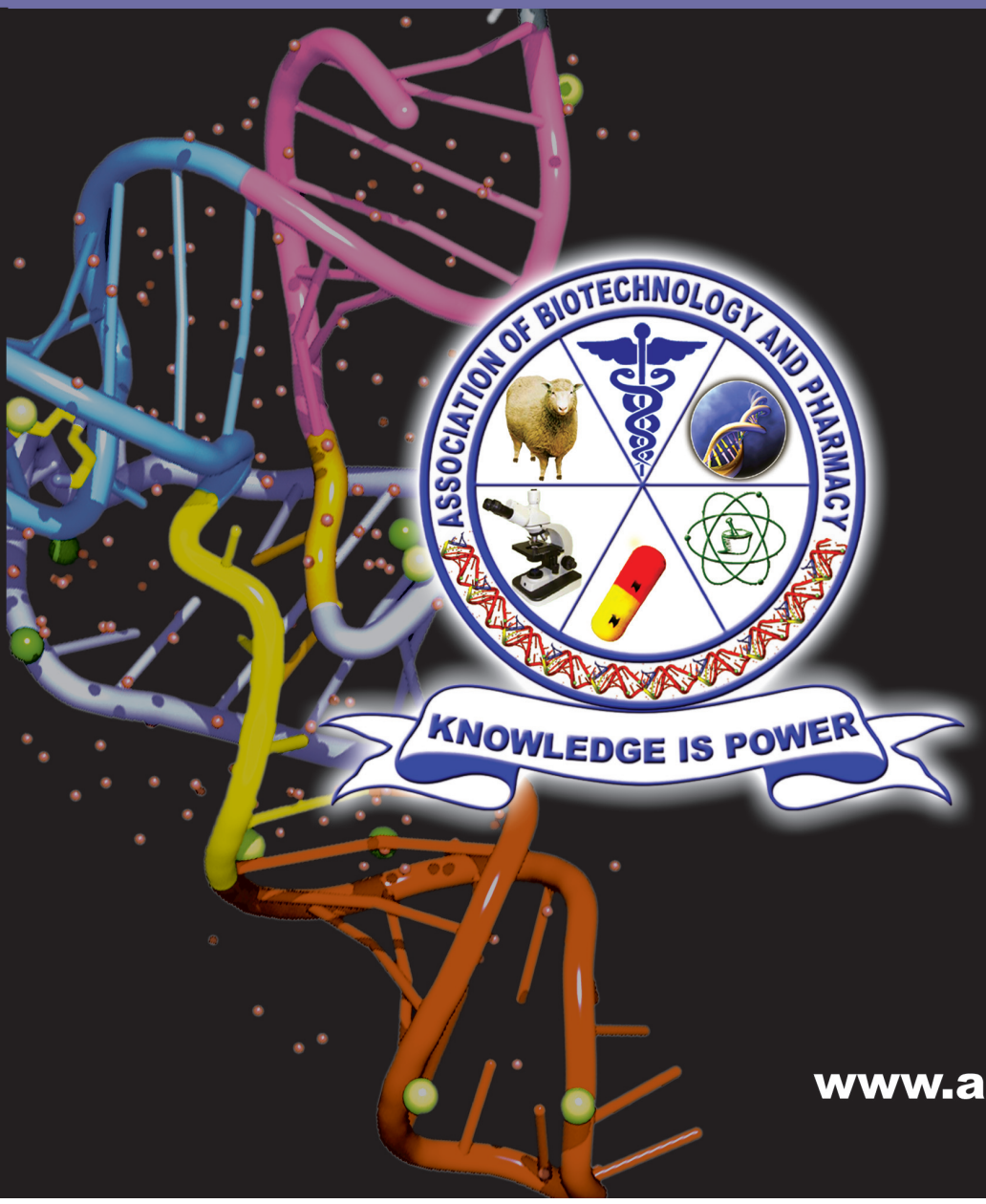

www.abap.co.in

Current Trends in Biotechnology and Pharmacy
ISSN 0973-8916 (Print), 2230-7303 (Online)

www.abap.co.in

ISSN 0973-8916

Current Trends in Biotechnology and Pharmacy

(An International Scientific Journal)

Volume- 18 issue3 JULY 2024

www.abap.co.in

Indexed in Chemical Abstracts, EMBASE, ProQuest, Academic SearchTM, DOAJ, CAB Abstracts, Index Copernicus, Ulrich's Periodicals Directory, Open J-Gate Pharmoinfonet.in Indianjournals.com and Indian Science Abstracts.

Association of Biotechnology and Pharmacy
(Regn. No. 28 OF 2007)

The Association of Biotechnology and Pharmacy (ABAP) was established for promoting the science of Biotechnology and Pharmacy. The objective of the Association is to advance and disseminate the knowledge and information in the areas of Biotechnology and Pharmacy by organising annual scientific meetings, seminars and symposia.

Members

The persons involved in research, teaching and work can become members of Association by paying membership fees to Association.

The members of the Association are allowed to write the title MABAP (Member of the Association of Biotechnology and Pharmacy) with their names.

Fellows

Every year, the Association will award Fellowships to the limited number of members of the Association with a distinguished academic and scientific career to be as Fellows of the Association during annual convention. The fellows can write the title FABAP (Fellow of the Association of Biotechnology and Pharmacy) with their names.

Membership details

(Membership and Journal)	India	SAARC	Others
Individuals – 1 year `	Rs. 600	Rs. 1000	$100
LifeMember	Rs. 4000	Rs. 6000	$500
Institutions – 1 year	Rs. 1500	Rs. 2000	$200
(Journal only) Life member	Rs.10000	Rs.12000	$1200

Individuals can pay in two instalments, however the membership certificate will be issued on payment of full amount. All the members and Fellows will receive a copy of the journal free.

Association of Biotechnology and Pharmacy
(Regn. No. 28 OF 2007)
#5-69-64; 6/19, Brodipet
Guntur – 522 002, Andhra Pradesh, India

Current Trends in Biotechnology and Pharmacy
ISSN 0973-8916

Volume 18 (3) **JULY 2024**

CONTENTS

Information to Authors

The Current Trends in Biotechnology and Pharmacy is an official international journal of Association of Biotechnology and Pharmacy. It is a peer reviewed quarterly journal dedicated to publish high quality original research articles in biotechnology and pharmacy. The journal will accept contributions from all areas of biotechnology and pharmacy including plant, animal, industrial, microbial, medical, pharmaceutical and analytical biotechnologies, immunology, proteomics, genomics, metabolomics, bioinformatics and different areas in pharmacy such as, pharmaceutics, pharmacology, pharmaceutical chemistry, pharma analysis and pharmacognosy. In addition to the original research papers, review articles in the above mentioned fields will also be considered.

Call for papers

The Association is inviting original research or review papers and short comunications in any of the above mentioned research areas for publication in Current Trends in Biotechnology and Pharmacy. The manuscripts should be concise, typed in double space in a general format containing a title page with a short running title and the names and addresses of the authors for correspondence followed by Abstract (350 words), 3 – 5 key words, Introduction, Materials and Methods, Results and Discussion, Conclusion, References, followed by the tables, figures and graphs on separate sheets. For quoting references in the text one has to follow the numbering of references in parentheses and full references with appropriate numbers at the end of the text in the same order. References have to be cited in the format below.

Mahavadi, S., Rao, R.S.S.K. and Murthy, K.S. (2007). Cross-regulation of VAPC2 receptor internalization by m2 receptors via c-Src-mediated phosphorylation of GRK2. Regulatory Peptides, 139: 109-114.

Lehninger, A.L., Nelson, D.L. and Cox, M.M. (2004). Lehninger Principles of Biochemistry, (4th edition), W.H. Freeman & Co., New York, USA, pp. 73-111.

Authors have to submit the figures, graphs and tables of the related research paper/article in Adobe Photoshop of the latest version for good illumination and allignment.

Authors can submit their papers and articles either to the editor or any of the editorial board members for onward transmission to the editorial office. Members of the editorial board are authorized to accept papers and can recommend for publication after the peer reviewing process. The email address of editorial board members are available in website www.abap.in. For submission of the articles directly, the authors are advised to submit by email to krssrao@abap.co.in or krssrao@yahoo.com.

Authors are solely responsible for the data, presentation and conclusions made in their articles/research papers. It is the responsibility of the advertisers for the statements made in the advertisements.

Current Trends in Biotechnology and Pharmacy
Vol. 18(3) 1813-1821, July 2024, ISSN 0973-8916 (Print), 2230-7303 (Online)
10.5530/ctbp.2024.3.29

Unveiling the Effects of Cisplatin and Diallyl Disulfide on MDA-MB-231 Breast Cancer Cells

Kaavya Gunasekaran[1], Priyadharshini Thangavelu[1], Naveen Kumar Kalagatur[2], Rama Jeyaraj[3,4], Suja Samiappan[*1]

[1] Department of Biochemistry, Bharathiar University, Coimbatore – 641 046, India.
[2] DRDO-BU-Center for Life Sciences, Coimbatore – 641 046, India.
[3] Jindal Institute of Behavioral Sciences (JIBS), Jindal Global Institution of Eminence Deemed to Be University, Sonipat – 131 001, India
[4] Director of Clinical Sciences, Northern Territory Institute of Research and Training, Darwin, NT 0909, Australia.
*Corresponding Author: suja.s@buc.edu.in

Abstract

Cancer is one of the most aggressive diseases and is the primary cause of mortality around the world. This can be prevented by combining anti-cancer drugs to reduce the resistance to monotherapy and thereby reduce the toxic effects. Cytotoxic anticancer drugs can potentially elicit cancer cell death by apoptosis or necrosis. Our present study aimed to investigate the combined cytotoxic potential of cisplatin (CDDP) and diallyl disulfide (DADS) on MDA-MB-231 breast cancer cell lines. The clonogenic assay was also performed to assess the effects of the drug on the proliferation of breast cancer cells. The results showed that CDDP/DADS (CDDP and DADS) markedly inhibited cell proliferation and significantly reduced the colony formation potential, migration, and invasion abilities of MDA-MB-231 cells. The apoptosis assay confirmed that cell death was through an apoptotic pathway. Cell cycle analysis results indicated that the combination effect of the drugs resulted in arresting cells in the G2/M phase of the cell cycle. Further, the haemolytic assay revealed that the CDDP/DADS is nontoxic to RBCs. In conclusion, combining these two drugs inhibits the oncogenic properties of TNBC cells, including their growth, survival, migration, and invasiveness.

Keywords: Cancer, wound healing, colony formation, apoptosis, cell cycle, Haemolysis.

Introduction

Cancer is a very complex disease, which is highly heterogeneous, with a multi-step process involving various molecular events underlying the initiation and progression of tumours. According to the GLOBOCAN Statistics 2022, breast cancer (11.5%) is the second most common disease after lung cancer (12.4%). Breast cancer is the second most frequent type of cancer in the world and the fifth most common cause of death from cancer (1). Although it is still the most frequent cause of cancer death in women in underdeveloped regions, in more developed countries, it is the second most frequent cause of cancer death in women (2).

Breast cancer mainly affects women than men; however, this is a rare condition, accounting for less than 1% of cases. Approximately 2.29 million new breast cancer cases were diagnosed in women in 2022, which represents 23.8% of all cancers and over 15.4% of global breast cancer deaths (https://gco.iarc.who.int) (3). It follows, therefore, that numerous people across the world have breast cancer, something which has made it to be regarded as a significant public health

problem due to its extensive research focus. Of all breast cancer-related issues, triple-negative breast cancer (TNBC) is the most aggressive form. Triple-negative breast cancers (TNBCs) are distinguished by the lack of receptors for progesterone and estrogen and the absence of HER2 overexpression (4). These tumours are a distinct subtype of breast cancer, having a poor prognosis. To overcome this problem, it is crucial to understand how complicated the disease is and how it behaves to achieve effective treatment and management measures for patients suffering from the disease.

The cells in the tumour, stromal tumour microenvironment (TME), and extracellular matrix (ECM) significantly impact how the tumour behaves inside the body. The ECM provides structure to cells outside of them, while TME is known for low pH outside of cells with high hypoxia (5). These factors influence the dormant phenotypes of tumour cells, bringing about drug resistance and poor prognosis among cancer patients. Tumours are biologically similar to chronically unhealing wounds, which show continuous inflammation that leads to tumorigenesis, growth and metastasis. Other cells, such as those attracted to the tumour stromal microenvironment, contribute significantly towards cancer growth, metastasis and therapy failure (6). Thus, cancer therapy combines two or more treatments targeting different pathways that stimulate carcinogenesis or facilitate cellular support. Treatment of various types of cancer often entails mono-therapy; however, this traditional approach is frequently less efficacious than combination approaches. Traditional mono-therapeutic techniques are not selective for actively dividing cells but instead, result in killing all non-cancerous ones as well as unhealthy tissues. Chemotherapy may be harmful to a patient, causing numerous side effects and dangers, too (7).

Cisplatin (CDDP) demonstrates significant antitumor activity across various cancers by forming cross-linked adducts with DNA, distorting its structure, and hindering cell division (8). Diallyl disulfide (DADS), found in garlic, exhibits promising anticancer properties by inhibiting the growth of various types of cancer cells and decreasing carcinogen-induced cancers in experimental animals (9). These two compounds differ significantly in terms of their mechanisms of action. Cisplatin damages DNA, while diallyl disulfide has multiple mechanisms of action, including activation of detoxifying enzymes, suppression of DNA adduct formation, antioxidant effects, regulation of cell cycle arrest, induction of apoptosis and differentiation histone modification, and inhibition of angiogenesis and invasion. Both compounds have been studied for their potential role in cancer therapy. Our present study aimed to investigate the combined cytotoxic effects of CDDP and DADS (CDDP/DADS) on MDA-MB-231 breast cancer cell lines.

Our findings, which delve into the effects on migration, apoptosis, cell cycle, and toxicity, hold significant potential to contribute to developing more effective and less toxic breast cancer treatments. This underscores the relevance and impact of our research, inspiring further exploration and advancement in the field.

Materials and Methods

Materials

Cisplatin (CDDP), diallyl disulfide (DADS), and triton X-100 were obtained from Sigma-Aldrich (St. Louis, MO, USA). In addition, Dulbecco's modified eagle's medium (DMEM), fetal bovine serum (FBS), L-glutamine, antibiotics, Crystal violet, and phosphate-buffered saline (PBS) were procured from HI Media Laboratories (Kelton, PA, USA). The apoptosis and cell cycle kits were purchased from Merck (Darmstadt, Germany). All chemicals and solvents used were of analytical grade.

Cell Culture

The MDA-MB-231cell line, a widely used and well-characterized breast cancer cell line known for its triple-negative breast cancer

(TNBC) phenotype, was obtained from the National Centre for Cell Science (NCCS), Pune.

Determination of IC_{50} concentration by MTT assay

All CDDP/DADS treatments for the below experiments were made with the IC_{50} of the drugs, which was determined using the MTT assay (10).

Clonogenic Assay

The clonogenic assay was performed to assess the effects of the drug on the proliferation of breast cancer cells. MDA-MB-231 cells (200 cells/well) were cultured in six-well tissue culture plates for 16 h. Then, drugs were added to the respective wells according to the IC_{50} concentrations (15.78 µM) described in our previous report (11), and the plates were re-incubated for 5–10 days. The media was changed every alternate day, and the plates were observed for colony (clusters of 20 or more cells) formation under an inverted microscope (Nikon, ECLIPSE Ti2, Tokyo, Japan). The colonies were then stained with 0.5% crystal violet solution and scored (12). The data has been represented as % survival derived from the following equation.

% survival = (Number of colonies after treatment/ Number of tumour cells seeded) X100.

Apoptosis assay

The MDA-MB-231 breast cancer cells (1×10^6 cells/well) were seeded and incubated till the cells were attached to the surface. After incubation, cells were treated with IC_{50} concentration of CDDP/DADS (15.78 µM) and allowed to incubate for 24 h. They were then harvested and washed twice with ice-cold PBS. Subsequently, the cells were labelled with Annexin V and the Dead Cell assay kit according to the manufacturer's instructions and incubated for 20 mins in the dark (13,14). This assay is based on the detection of phosphatidylserine (PS) on the apoptotic cell surface using fluorescently labelled Annexin V. The samples were determined by the Muse Cell Analyzer (Millipore, USA) and analysed by software provided by Merck Millipore (15).

Cell cycle analysis

MDA-MB-231 breast cancer cells (1×10^6 cells/well) were seeded in 6-well plates and incubated till the cells were attached to the surface. After incubation, cells were treated with IC_{50} concentration of CDDP/DADS (15.78 µM) and allowed to incubate for 24 h. The cells were detached, pipetted, centrifuged at 500 × g at 4°C for 5 min, and washed once with 1 × Phosphate-buffered saline (PBS). The cells were fixed with 1 ml (70%) of ice-cold ethanol and incubated at 4°C overnight. The ethanol-fixed cells were washed with PBS, and 100 µL of Muse cell cycle reagent was added. The tubes were incubated for 30 min at dark and analysed on a Muse flow cytometer (Millipore, USA). DNA content and cell cycle distribution were analysed using the software provided by Merck Millipore (16).

Haemolysis activity

The haemolytic efficiency of the CDDP/DADS was assessed by following the protocol by Hu *et al*. (2013), with slight modifications (17). A fresh blood sample (5 ml) was collected in heparinised tubes and centrifuged at 2000 rpm for 5 mins. After discarding plasma, the red blood cells were washed three times with phosphate buffer saline. The 2% solution of red blood cells was prepared in phosphate buffer saline for the analysis. 500 µL of the red blood cell solution was added to a micro-centrifuge tube containing CDDP/DADS (IC_{50} concentration) to study the haemolytic activity (18). Phosphate buffer saline was taken as a negative control, and Triton X-100 (10% v/v) as a positive control. The samples were incubated at 37ºC for 3-4 h on the shaker, following the centrifugation at 2000 rpm for 5 mins, and the release haemoglobin content was scanned at 540 nm. The following equation is used to calculate the haemolysis (%):

% of haemolysis = (absorbance of test

compound (CDDP/DADS)-absorbance of PBS)/ (absorbance of Triton X-100)*100

Statistical analysis

Data was expressed as the mean ± standard deviation, and a t-test was performed to identify the significance between groups. The * $p \leq 0.05$ is significant, ** $p \leq 0.01$ is most significant, and 'ns' represents not significant ($p > 0.05$).

Results and Discussions

Clonogenic Assay

The colony formation or clonogenic assay is a widely used method to evaluate cell survival and proliferation under *in vitro* conditions (19). This assay helps estimate cell death before or after treatment with adjuvant therapy or cytotoxic drugs. Studies have shown that CDDP and DADS, as a single therapy modality or combined with other chemotherapeutic drugs, have demonstrated anticancer effects on various human cancer cells (20).

After treating MDA-MB-231 cells with CDDP/DADS for 12 h and 24 h, the control group formed distinct colonies compared to the treatment group. The CDDP/DADS group inhibited colony formation with a 70% reduction in clonogenic ability, and the colonies were much smaller than those formed by the control (Fig. 1).

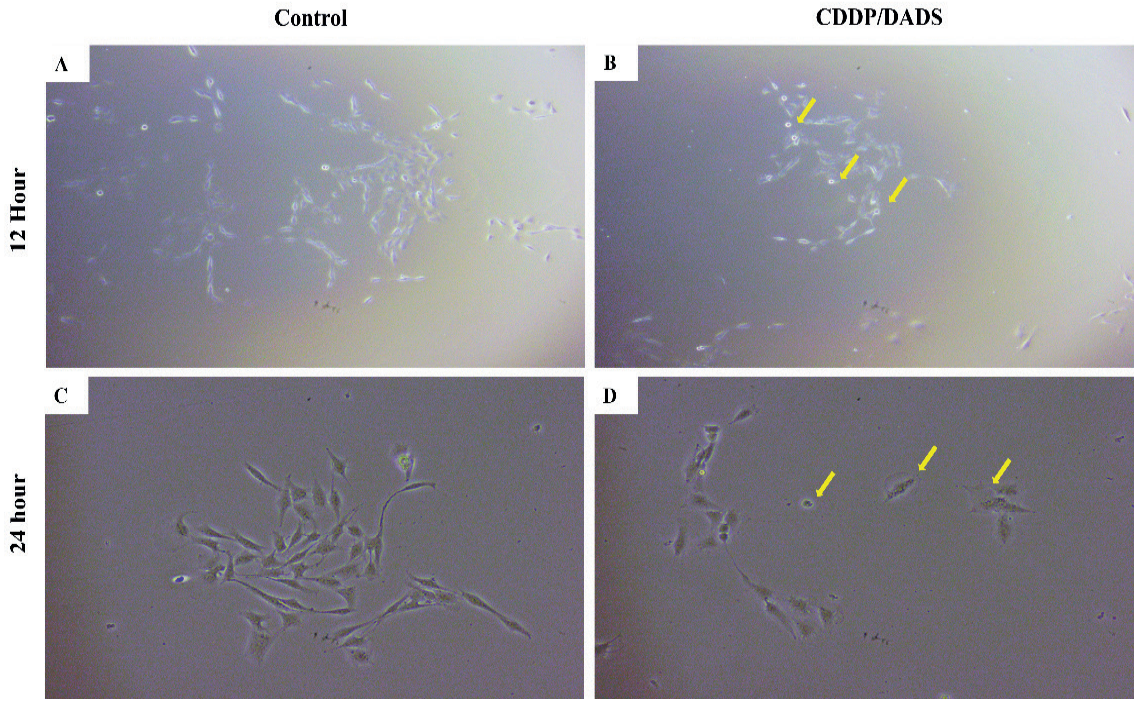

Figure 1: Comparative observation of colony formation in MDA-MB-231 cells subjected to CDDP/DADS treatment with control cells at 12 h and 24 h. The yellow arrow marks denote the apoptosis-undergoing cells in the CDDP/DADS-treated group.

The long-term effects of combination treatment with CDDP/DADS were assessed by clonogenic assay. We found that colony formation in MDA-MB 231 breast cancer cells treated with the combination of these drugs for 24 h was suppressed to 30% (Fig. 2) (21,22).

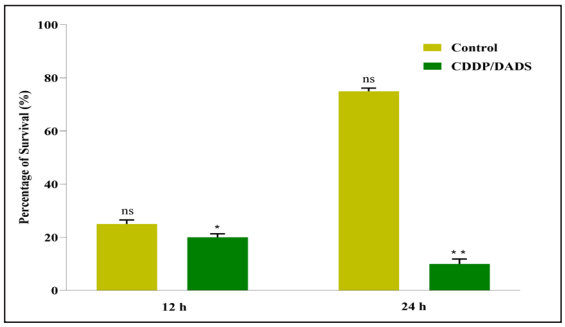

Figure 2: The percentage of MDA-MB-231 cells that survived after treatment with CDDP/DADS compared to the control at 12 and 24 h.

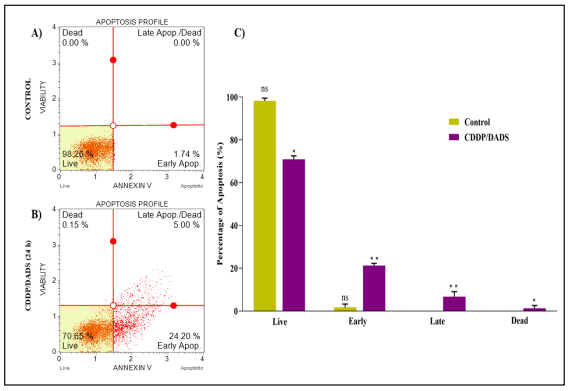

Figure 3: Apoptotic activity of CDDP/DADS on MDA-MB-231 cells. (A) Control cells. (B) CDDP/DADS treated cells. (C) Graph delineating the percentage of apoptosis for each quadrant (live, early, late, and dead).

Cell death (apoptosis)

Cancer cells are potentially killed by necrosis or apoptosis with cytotoxic antitumor drugs. Cell death was identified by analysing the cell trajectories on the dot-plot diagrams of Annexin-V-FITC/PI-stained treated cells. The plots are divided into four quadrants: live cells in the lower left quadrant, early apoptotic cells in the lower right, late-apoptosis cells in the upper right, and dead cells in the upper left (23).

To determine whether the cytotoxic effect of CDDP/DADS was associated with apoptosis, annexin V-FITC/PI double staining was used to determine the number of apoptotic cells by flow cytometry analysis. Phosphatidylserine (PS) is a crucial biomarker of early apoptosis and is translocated to the extracellular domain from the cytosolic portion of the membrane, identified by annexin V-FITC staining. As apoptosis proceeds further, the cell membrane is destroyed, and the PI that goes into the nucleus eventually stains the DNA (24). After treatment, the highest early apoptotic population was 24.20%, with the populations of viable cells at 70.97% in the CDDP/DADS group compared to the control, which had 98.26% live cells (Fig. 3).

Cell cycle analysis

The importance of chemotherapies functioning as cell-cycle modulators has increased due to the recent confirmation of the concomitant involvement of apoptosis and cell-cycle inhibition. Flow cytometry analysis was performed to analyse the various cell cycle checkpoints. We have evaluated the effect of CDDP/DADS on the DNA content of MDA-MB-231 cells by cell cycle phase distribution (G0, G1, S, G2, and M). The analysed data suggested that cells exposed to CDDP/DADS significantly increased the accumulation of DNA contents up to 40% in the G2/M phase. The treatment decreased G0/G1 and S phase cells (Fig. 4). It has been observed that cisplatin arrests cells at sub-G1, S, and G2 phases (25), and diallyl disulfide arrests cells at the G2/M phase. This statement also indicates the accumulation of the DNA contents up to 31% in the G0/G1 phase. The cell cycle analysis results indicate that the combination effect of CDDP/DADS resulted in arresting cells in the G2/M phase of the cell cycle.

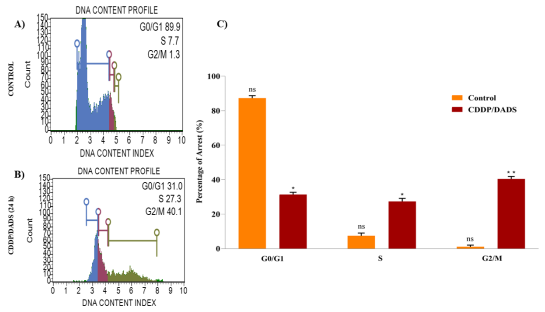

Figure 4: Analysis of cell cycle arrest of CDDP/DADS in MDA-MB-231 cells. (A) Control cells. (B) CDDP/DADS treated cells. (C) Graph presenting the percentage of cell cycle arrest for each phase (G0/G1, S, and G2/M).

Haemolytic Analysis

Haemolysis assay is a commonly used test to evaluate the potential toxicity of compounds on red blood cells. The assay examined the released haemoglobin from the lysis of red blood cells. The haemolytic activity of CDDP/DADS is shown in Figure 5. The results revealed that control and phosphate buffer saline (negative control) showed 0.0% haemolysis. Meanwhile, triton X-100 (positive control) showed 70.60% haemolysis. Moreover, the haemolysis caused by CDDP/DADS at 3% for 12 h and 8% for 24 h was negligible compared to Triton X-100. According to the regulatory guidelines provided by ISO-10993-4: 2107, if the compound causes less haemolysis (below 10% for humans), it is considered a non-haemolytic compound and safe for *in vivo* application. (26,27).

The results (Fig. 5) show that CDDP/DADS in IC_{50} concentration do not show haemolysis activity. According to the percentage of haemolysis activity, a lower concentration of CDDP/DADS was found to be harmless and biocompatible. Thus, the CDDP/DADS combination could be considered non-haemolytic and safe for further applications. The CDDP/DADS combination can be an excellent anticancer agent in preventing breast cancer growth and proliferation.

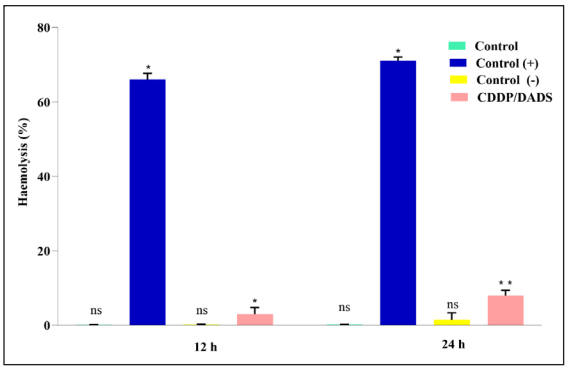

Figure 5: Haemolytic activity of CDDP/DADS at 12h and 24 h. Control is free RBCs, Positive control (control +) is Triton X-100, and Negative control (control -) is PBS.

Conclusions

The combination of CDDP/DADS inhibits various oncogenic properties of TNBC cells, including their growth, survival, migration, and invasiveness. CDDP/DADS can be an excellent anticancer agent in preventing breast cancer growth and proliferation. Additionally, CDDP/DADS induces apoptosis in cancer cells and arrests them in the G2/M phase of the cell cycle. The haemolysis assay showed that CDDP/DADS is non-haemolytic, making them a good choice for various cancer therapies.

Conflict of interest

The authors declare no conflict of interest.

Funding

This research was funded by Rashtriya Uchchattar Shiksha Abhiyan (RUSA) 2.0, India-Bharathiar Cancer Theranostics Research Center (BCTRC) Grant No. BU/RUSA2.0/BCTRC/2020/BCTRC-CT01.

Acknowledgement

The authors were thankful to Bharathiar University for providing the support and facility.

References:

1. Arnold, M., Morgan, E., Rumgay, H., Mafra, A., Singh, D., Laversanne, M., Vignat, J., Gralow, J. R., Cardoso, F., Siesling, S., & Soerjomataram, I. (2022). Current and future burden of breast cancer: Global statistics for 2020 and 2040. The Breast : Official Journal of the European Society of Mastology, 66, 15–23.
2. Sung, H., Ferlay, J., Siegel, R. L., Laversanne, M., Soerjomataram, I., Jemal, A., & Bray, F. (2021). Global Cancer Statistics 2020: GLOBOCAN Estimates of Incidence and Mortality Worldwide for 36 Cancers in 185 Countries. CA: A Cancer Journal for Clinicians, 71(3), 209–249.
3. Cancer Today. (n.d.). Retrieved 14 April 2024, from https://gco.iarc.who.int/today/
4. Kanagaraj, S., & Vadivelu, S. S. (2023). ER Stress Proteins Can be an Effective Target for Epicatechin in Triple Negative Breast Cancer – An in-silico Approach. Current Trends in Biotechnology and Pharmacy, 17(3), 937-945.
5. Zhao, Y., Shen, M., Wu, L., Yang, H., Yao, Y., Yang, Q., Du, J., Liu, L., Li, Y., & Bai, Y. (2023). Stromal cells in the tumour microenvironment: Accomplices of tumour progression? Cell Death & Disease, 14(9), 1–24.
6. Hua, Y., & Bergers, G. (2019). Tumors vs. Chronic Wounds: An Immune Cell's Perspective. Frontiers in Immunology, 10, 2178.
7. Mokhtari, R. B., Homayouni, T. S., Baluch, N., Morgatskaya, E., Kumar, S., Das, B., & Yeger, H. (2017). Combination therapy in combating cancer. Oncotarget, 8(23), 38022–38043.
8. Malinge, J.-M., Giraud-Panis, M.-J., & Leng, M. (1999). Interstrand cross-links of cisplatin induce striking distortions in DNA. Journal of Inorganic Biochemistry, 77(1), 23–29.
9. Mitra, S., Das, R., Emran, T. B., Labib, R. K., Noor-E-Tabassum, Islam, F., Sharma, R., Ahmad, I., Nainu, F., Chidambaram, K., Alhumaydhi, F. A., Chandran, D., Capasso, R., & Wilairatana, P. (2022). Diallyl Disulfide: A Bioactive Garlic Compound with Anticancer Potential. Frontiers in Pharmacology, 13, 943967.
10. Saradhi, G. P., Kalagatur, N. K., Sasidharan, S. S., Thiruppathi, R., Krishna, K., Kunjikulangara, S., & Poda, S. (2022). Preferential Cytotoxic Effect of Vaccinium sect. Cyanococcus Fruit Extract in Human Lung Cancer Cells Related to Normal Cells. Current Trends in Biotechnology and Pharmacy, 16(3), 396-406.
11. Gunasekaran, K., Vasamsetti, B. M. K., Thangavelu, P., Natesan, K., Mujyambere, B., Sundaram, V., Jayaraj, R., Kim, Y.-J., Samiappan, S., & Choi, J.-W. (2023). Cytotoxic Effects of Nanoliposomal Cisplatin and Diallyl Disulfide on Breast Cancer and Lung Cancer Cell Lines. Biomedicines, 11(4), 1021.
12. Aggarwal, S., Bhadana, K., Singh, B., Rawat, M., Mohammad, T., Al-Keridis, L. A., Alshammari, N., Hassan, M. I., & Das, S. N. (2022). Cinnamomum zeylanicum Extract and its Bioactive Component Cinnamaldehyde Show Anti-Tumor Effects via Inhibition of Multiple Cellular Pathways.

Frontiers in Pharmacology, 13.

13. Devi, E. G., & Nisha, M. K. (2024). *In vitro* Antioxidant, Anticancer Effect and GC-MS Analysis of Barleria cuspidata F. Heyne ex. Nees. Current Trends in Biotechnology and Pharmacy, 18(1), 1629-1644.

14. Velemurugan, S., Sethuraman, S. P., & Kamaraj, R. (2024). In-vitro Antioxidant and Cytotoxic Effects of Physalis minima Linn. In HeLa Cell Lines Against Cervical Cancer. Current Trends in Biotechnology and Pharmacy, 18(1), 1581-1585.

15. Lee, C. M., Lee, J., Kang, M.-A., Kim, H. T., Lee, J., Park, K., Yang, Y.-H., Jang, K. Y., & Park, S.-H. (2022). Linifanib induces apoptosis in human ovarian cancer cells via activation of FOXO3 and reactive oxygen species. Arabian Journal of Chemistry, 15(12), 104321.

16. Bhoora, S., Pather, Y., Marais, S., & Punchoo, R. (2020). Cholecalciferol Inhibits Cell Growth and Induces Apoptosis in the CaSki Cell Line. Medical Sciences, 8(1), Article 1.

17. Hu, X., Hao, X., Wu, Y., Zhang, J., Zhang, X., Wang, P. C., Zou, G., & Liang, X.-J. (2013). Multifunctional hybrid silica nanoparticles for controlled doxorubicin loading and release with thermal and pH dual response. Journal of Materials Chemistry B, 1(8), 1109–1118.

18. Sæbø, I. P., Bjørås, M., Franzyk, H., Helgesen, E., & Booth, J. A. (2023). Optimization of the Hemolysis Assay for the Assessment of Cytotoxicity. International Journal of Molecular Sciences, 24(3), 2914.

19. Menyhárt, O., Harami-Papp, H., Sukumar, S., Schäfer, R., Magnani, L., de Barrios, O., & Győrffy, B. (2016). Guidelines for the selection of functional assays to evaluate the hallmarks of cancer. Biochimica et Biophysica Acta (BBA) - Reviews on Cancer, 1866(2), 300–319.

20. Rafehi, H., Orlowski, C., Georgiadis, G. T., Ververis, K., El-Osta, A., & Karagiannis, T. C. (2011). Clonogenic Assay: Adherent Cells. JoVE (Journal of Visualized Experiments), 49, e2573.

21. Pawlak, A., Ziolo, E., Fiedorowicz, A., Fidyt, K., Strzadala, L., & Kalas, W. (2016). Long-lasting reduction in clonogenic potential of colorectal cancer cells by sequential treatments with 5-azanucleosides and topoisomerase inhibitors. BMC Cancer, 16(1), 893.

22. Pandit, B., & Gartel, A. L. (2011). Thiazole Antibiotic Thiostrepton Synergize with Bortezomib to Induce Apoptosis in Cancer Cells. PLOS ONE, 6(2), e17110.

23. Kim, H.-A., Kim, M.-C., Kim, N.-Y., & Kim, Y. (2015). Inhibition of hedgehog signaling reduces the side population in human malignant mesothelioma cell lines. Cancer Gene Therapy, 22(8), 387–395.

24. Noh, J.-I., Mun, S.-K., Lim, E. H., Kim, H., Chang, D.-J., Hur, J.-S., & Yee, S.-T. (2021). Induction of Apoptosis in MDA-MB-231 Cells Treated with the Methanol Extract of Lichen Physconia hokkaidensis. Journal of Fungi, 7(3), 188.

25. Velma, V., Dasari, S. R., & Tchounwou, P. B. (2016). Low Doses of Cisplatin Induce Gene Alterations, Cell Cycle Arrest,

and Apoptosis in Human Promyelocytic Leukemia Cells. Biomarker Insights, 11, 113–121.

26. Khan, H. N., Imran, M., Sanaullah, I., Ullah Khan, I., Sabri, A. N., Naseem, S., & Riaz, S. (2023). *In vivo* biodistribution, antioxidant and hemolysis tendency of superparamagnetic iron oxide nanoparticles – Potential anticancer agents. Arabian Journal of Chemistry, 16(4), 104602.

27. 14:00-17:00. (n.d.). ISO 10993-4:2017. ISO. Retrieved 14 April 2024, from https://www.iso.org/standard/63448.html

Current Trends in Biotechnology and Pharmacy
Vol. 18(3) 1822-1840, July 2024, ISSN 0973-8916 (Print), 2230-7303 (Online)
10.5530/ctbp.2024.3.30

Formulation of Curcumin-based Polyherbal Nanoemulsion Mouthwash and Assessment of its Antioxidant and *in-vitro* Cytotoxic Properties

Norafiqah Yusof[1], Nurhafizah Hamid[1], Nuramalina H Mumin[1], Sheba R David[2], Liyana Ahmad[1], Rajan Rajabalaya[1]*

[1]PAPRSB Institute of Health Sciences, Universiti Brunei Darussalam, Jalan Tungku Link, BE 1410 Gadong, Bandar Seri Begawan, Brunei Darussalam.
[2]School of Pharmacy, University of Wyoming, Laramie, Wyoming, 82071, USA.
*Corresponding author: rajan.rajabalaya@ubd.edu.bn

Abstract

Curcumin is a hydrophobic compound with excellent antibacterial and antioxidative properties but it exhibits poor bioavailability which limits its therapeutic value. Nano emulsion (NE) is a modern drug delivery system that can accommodate the poor bioavailability and solubility of hydrophobic curcumin. The objective of this study was to formulate curcumin-based polyherbal NE mouthwash (Cur-polyherbal NE) and evaluate the antioxidant and cytotoxic properties. The NE formulations were prepared using glyceryl monooleate (GMO), Pluronic® F-127, virgin coconut oil (VCO) and distilled water. Physiochemical characterisation of Cur-polyherbal NE was performed based on FTIR and dynamic light scattering analyses, and their stability at different temperatures was also determined. The antioxidant activity of formulations was evaluated using DPPH scavenging assay, and their in-vitro cytotoxicity was investigated on HEK293 cells. This study demonstrates that the antioxidant activity of Cur-polyherbal NE formulation was superior compared to corresponding non-NE formulation ($p < 0.05$). In-vitro cytotoxicity performed on HEK293 cells revealed better % cell viability in dose-dependent manner. The promising antioxidant activity and non-toxicity on HEK293 cells of Cur-polyherbal NE may suggest its potential use as safer mouthwash alternative.

Keywords: Nano emulsion, curcumin, polyherbal, antioxidant, cytotoxicity

Introduction

Gingival and periodontal disease are commonly affiliated with the chronic accumulation of bacterial plaque due to poor oral hygiene (1). The management of plaque-induced gingivitis focused on regular and appropriate dental hygiene practices including the use of chemical mouthwashes such as chlorhexidine as useful adjuncts for mechanical plaque control measures (2). However, prolonged use of chemical antibacterial mouthwashes are associated with several adverse events (3). As an alternative, plant-derived mouthwash had received substantial importance due to the numerous therapeutic benefits of herbal extracts (4).

Curcumin is a natural polyphenolic compound derived from the rhizomatous herbaceous perennial plant, Curcuma longa Linnaeus (C. longa L.). Curcumin is widely recognised for its wide range of therapeutic properties including antioxidant, antimicrobial and anti-inflammatory properties (5). The therapeutic properties of curcumin are associated with its potent free radical scavenging activity that are linked to various signalling pathways (6). Traditionally, curcumin has been used as an herbal remedy to treat various ailments such as inflammatory diseas-

es, wounds, and ulcers (7). In modern practice, several narratives had reported the utilisation of curcumin for various diseases (8–10). Previous studies demonstrated the topical application of curcumin oral gel had significantly reduced inflammation in severe gingivitis and periodontal infections (8,11). However, several reports had addressed the limitations of native curcumin as a therapeutic agent due to its low bioavailability and poor solubility which greatly hindered its therapeutic efficacy (12). Recently, the emergence of nanotechnology received recognition for its ability to solubilise lipophilic drug and ever since, had drastically improved the efficacious delivery and bioavailability of hydrophobic compounds, such as curcumin (13).

Various nanoparticle-based drug delivery systems (DDS) had been pursued including nanoliposomes, solid-lipid nanoparticle, and nano emulsion to enhance the bioavailability of curcumin (14). Amongst these, nano emulsion had been extensively formulated for the enhancement of solubility and absorption of curcumin (15). Nano emulsion (NE) is a lipid-based colloidal system composed of dispersed oil and aqueous phases stabilised by means of surfactants (16). The organisation of NE system allows the solubilisation of hydrophobic compound and thus, providing better uptake of the compound for therapeutic application (17). Several studies had discussed the promising alternative of NE system in restoring therapeutic properties of curcumin by reducing rapid clearance and promoting controlled-release to minimise toxicity (13,15).

Improved understanding of the pleiotropic effects of herbal plants resulted in the appreciation of polyherbal formulation in achieving greater therapeutic effects that may be unattainable from individual plant (18). Herbal plants generally have high antioxidant content attributed from their secondary metabolites, polyphenols (19). The antimicrobial effect of antioxidants has become considerably recognised as plants' antimicrobial defence mechanism (20). White tea (Camellia sinensis L.) is a renowned therapeutic agent associated with its antioxidative, antimicrobial, and anti-inflammatory properties. The antioxidative properties of white tea are attributed to the high content of catechins and polyphenolic compounds (21). It was previously reported that white tea contains the highest concentration of antioxidants compared to the other tea variants (22). Previous studies had demonstrated the bactericidal properties of white tea against several oral pathogens associated with its polyphenolic compounds (23).

Ginger (Zingiber officinale) is another notable rhizomatous plant possessing a wide range of therapeutic properties including antioxidant, anti-inflammatory, and antimicrobial attributed to several phenolic compounds such as 6-gingerol and shogaols (24). Several narratives had reported the antibacterial activity of ginger against several periodontal and plaque-inducing bacteria strains related to phenolic compounds in ginger that caused destruction of bacterial membrane integrity (25,26). Therefore, the objective of this study was to develop and characterise oil-in-water (o/w) polyherbal nano emulsion mouthwash composed of curcumin, white tea, and ginger extracts, and assessed the antioxidant and in-vitro cytotoxic properties.

Materials and methods

Chemicals

Curcumin and ginger powder extract were Pi Chemicals Ltd. (Shanghai, China). Virgin coconut oil (VCO) was procured from local supermarket, Brunei. White tea (*Camellia Sinensis L.*) extract with product code FSS10580 was purchased from Formulator Sample Shop (FSS®, Bareggio, Italy). Glyceryl monooleate (GMO) was purchased from Croda™ International (East Yorkshire, UK). Pluronic® F-127 (P-F127) was purchased from Sigma-Aldrich (St. Louis, MO, USA).

The human embryonic kidney cells (HEK293) cell line was purchased from American Type Culture Collection (ATCC, USA). Dulbecco's Modified Eagle's Medium (DMEM)

was purchased from Gibco™ (Thermo Fisher Scientific Inc., Waltham, US). 1% penicillin with streptomycin, 10% (v/v) fetal bovine serum (FBS), 3-((4,5-Dimethylthiazol-2-yl))-2,5-diphenyltetrazolium bromide (MTT), and 0.25% trypsin-EDTA, were purchased from Sigma-Aldrich (St. Louis, MO, USA). 6-hydroxy-2, 5, 7, 8-tetramethychroman-2 carboxylic acid (Trolox) and 2,2-diphenyl-1-picrylhydrazyl (DPPH) were purchased from Sigma–Aldrich (St. Louis, MO, USA).

Preparation of curcumin-based polyherbal nano emulsion

Oil-in-water (o/w) curcumin-based polyherbal nano emulsion (Cur-polyherbal NEs) were prepared by performing a two-step low-energy Emulsion Inversion Point (EIP) method (27). Different concentrations of GMO (1%, 2% and 4%) and P-F127 (1%, 2%, 4% and 8%) were used as surfactants, respectively. As seen from the composition of Cur-polyherbal NE formulations on Table 1, the white tea liquid extract (WTE) and filtered ginger liquid extract (GE) contents of Cur-polyherbal NEs were kept at 5% and 20% and curcumin content was either 25 and 50 mg. The aqueous phase solution composed of WTE (5%, w/w), filtered GE (20%, w/w), and surfactant P-F127 was added dropwise to the oil phase mixture composed of VCO, surfactant GMO, and curcumin powder extract (Figure 2). Finally, distilled water was gradually added to mark up the total volume of mixture to 100 mL. The mixture was mixed under continuous magnetic stirring at 400 rpm, 45 – 50°C for 30 minutes to create spontaneous o/w emulsion. The formulation of o/w nano emulsion was achieved by further stirring the emulsion at a higher shear speed of 3000 rpm for another 30 minutes using a L5M-A Laboratory Mixer homogeniser (Silverson® Ltd., Chesham, UK). Obtained nano emulsion formulations were contained in sealed bottles and stored inside a cabinet at room temperature (25 ± 2°C) throughout analysis period.

Physiochemical characterisation of curcumin-based polyherbal nano emulsion

Organoleptic properties

Formulations were evaluated for colour, odour and density. A 100 mL pycnometer was used to determine the density in g/mL of the formulations. Whereas, the colour and odour of the formulations were evaluated based on its intensity(28)50cPs.

pH determination

AE150 pH meter (Fisher Scientific) was used to determine the pH of Cur-Polyherbal NEs. 5 mL of each formulation was diluted with 10 mL of tap water before measuring the pH at room temperature (29).

Dynamic light scattering (DLS) measurements

A Zetasizer Nano ZS (ZEN3600) analyser (Malvern Instruments Ltd., Malvern, UK) was used to measure the particle size, polydispersity index (PdI) and ζ-potential measurements of the o/w nano emulsions. Prior to the experiment, 100 µL of each formulation was diluted with 4 mL of distilled water and sonicated in 37°C water bath for 30 seconds to ensure homogenous scattering of particles. Analysis of formulations was measured at scattering angle of 173° and temperature of 25°C. All measurements were performed in triplicate and results are expressed as mean ± SD (29,30).

Stability study

The stability of formulations was assessed by evaluating the change in organoleptic properties, phase separation, pH, and density at three different temperatures of 4 ± 2°C, 25 ± 2°C, and 40°C ± 2°C with 5% humidity. Measurements were carried out on the day of storage (day 0) and at predetermined time intervals of 14 and 30 days. All formulations were kept in sealed vials (31).

FTIR analysis

Optimised Cur-polyherbal NE formulations were scanned using a Fourier transform infrared spectrometer (FTIR LabSolutions IR, Shimadzu, Columbia, Maryland, USA) at wavelength of 400 – 4000cm^{-1} and resolution of 4 cm^{-1} (32,33)"ISSN":"18469558","abstract":"© 2017 Rajan Rajabalaya et al., published by De Gruyter Open 2017. The purpose of the study was to develop a transdermal tolterodine tartrate (TT.

Antioxidant activity of Cur-polyherbal NE

DPPH assay

In order to analyse the antioxidant activity of Cur-polyherbal NE, DPPH scavenging activity assay was performed based on the capability of the herbal extracts of the formulations in scavenging the DPPH• free radical. A 0.1 mM stock solution of 1,1-Diphenyl-2-picrylhydrazyl (DPPH) in methanol was prepared. All tested sample including free curcumin and Cur-Polyherbal NE formulations (C1-NE and C3-NE) were dissolved in methanol. The non-nanosized formulations (C1-E and C3-E) were also prepared to investigate the effect NE system on the antioxidant capacity of the formulations. The DPPH assay was performed in a 96-well microplate.

The tested compounds containing DPPH free radicals were incubated in the dark for 30 minutes at room temperature to allow free-radical scavenging activity to occur. The antioxidant compounds present in the test formulations reduced DPPH free radicals (purple) to produce 1-Diphenyl-2-picryl hydrazine (yellow). After 30 minutes, the amount of DPPH free radicals remaining was measured using a spectrophotometer microplate reader (EPOCH 2, BioTek Instruments) at 517 nm. The DPPH assay was performed triplicate for each tested compounds and formulations at three independent experiments.

The percentage of radical scavenging activity was calculated according to Equation (1):

$$\% \text{ DPPH scavenging activity } (\%) = \frac{(As - Ai)}{Ac} \times 100\% \quad (1$$

Where, A_s represented the absorbance of sample and DPPH-MetOH solution, A_i represented the absorbance of sample in methanol, and A_c represented the absorbance of DPPH-MetOH solution.

The calculated percentage of DPPH scavenging activity was plotted against sample concentration and IC_{50} values were determined by nonlinear regression analysis.

A powerful antioxidant, Trolox, was used as a reference positive control. A Trolox calibration curve was acquired by measuring the absorbance of 0.1mM DPPH methanolic solution at 517 nm after addition with increasing concentration of Trolox (0 – 30 mM). The absorbance readings were obtained after the DPPH reduction reaction of Trolox at 30 minutes after Trolox addition. Finally, the DPPH radical scavenging capacity were expressed as Trolox equivalent antioxidant capacity (TEAC) in µg/mL of tested compounds (34).

Trolox Equivalent Antioxidant Capacity (TEAC) values were calculated as:

$$\text{TEAC} = \frac{(\text{IC50 of Trolox } (\mu g/mL))}{(\text{IC50 of sample } (\mu g/mL))} \quad (2$$

In-vitro cytotoxicity study

HEK293 cell line

Human embryonic kidney (HEK293) cells were grown in 25 cm^2 culture flasks with complete culture medium containing Dulbecco's Modified Eagle's Medium (DMEM, Gibco, Life Technologies, USA) supplemented with 4mM L-glutamine (Gibco, CA, USA), 10% (v/v) heat inactivated fetal bovine serum (FBS), 100 IU/mL of penicillin and 100 µm/mL streptomycin. The cells were maintained under a controlled humidified atmosphere of 5% CO_2 and 95% humidity at 37°C. Cells were regularly sub-cultured using 0.25% Trypsin-EDTA when 80 – 90% cell confluent was reached. Trypan-blue solution (ThermoFisher) and haemocytometer were used for

cell counting (35)anti-oxidative, and anti-cancer properties but has poor bioavailability. Liquid crystals (LC.

HEK293 cell density optimisation for MTT Assay

Cell density optimisation for MTT assay was performed prior to MTT cytotoxic experiments. Different ranges of cell seeding density (1 x 10^4, 2 x 10^4, 3 x 10^4, and 4 x 10^4 cells/well) were seeded in triplicates on 96-well plate. Each cell density was suspended in complete culture medium.

In-vitro cytotoxicity study of Cur-polyherbal NE using MTT Assay

To evaluate the cytotoxicity of Cur-polyherbal NE formulations, *in-vitro* cytotoxicity using MTT assay was performed on HEK293 cells. HEK293 cells were resuspended in 100 µL complete culture medium, seeded in 96-well culture plate at a density of 2 x 10^4 cells/well and incubated overnight at 37°C, 5% CO_2 and 95% humidity to allow cell attachment. Following overnight incubation, culture medium was removed and cells were treated with 100 µL of culture medium containing different dilutions (1:1000, 1:100, and 1:10) of C1-NE, C3-NE, non-nano-sized formulations (C1-E and C3-E) and empty NE system without herbal extracts (Empty-C1 and -C3) for 24 hours. The HEK293 cells were also treated with 1% of free herbal extracts (curcumin, GE, and WTE) used in the formulation of C1-NE and C3-NE. As negative control, cells were treated with 1% distilled water. The viability of cells was determined after 24-hour of incubation. After 24-hour exposure, 30 µL of MTT (1 mg/mL in PBS) was added to respective wells and incubated at 37°C for 2 hours until purple formazan crystals were formed. The formazan crystals were dissolved in 100 µL of isopropanol and left overnight in the dark before reading the absorbance at 570 nm using spectrophotometer plate reader (EPOCH 2, BioTek Instruments). The measured absorbance is identified as the number of viable cells in respective well. The cell viability was expressed as the percentage of formazan absorbance at 570 nm (36).

Statistical analysis

All tests were performed in triplicates and data are presented as mean ± standard deviation (SD). All statistical analyses were analysed by one-way analysis of variance (one-ANOVA) and multiple comparison by Tukey's test using GraphPad Prism (version 8.4.3). A value of $p < 0.05$ was considered statistically significant.

Results and Discussion

Formulation & preparation of curcumin-based polyherbal nano emulsion (Cur-Polyherbal NE)

Six formulations were prepared in this study by investigating the effect of different concentrations of surfactants (GMO and P-F127)

Table 1. The different formulations prepared with varying concentration of VCO, GMO and P-F127

Formulation code	Oil-phase			Aqueous phase			Phase separation
	VCO (g)	GMO (%)	Cur (mg)	GE (%)	WTE (%)	P-F127 (%)	
F1	5	1	25	20	5	1	No
F2	5	.2	50	20	5	2	No
F3	10	1	25	20	5	1	Yes
F4	10	2	50	20	5	.2	No
F5	5	2	25	20	5	4	Yes
F6	10	4	50	20	5	8	No

and VCO on the stability of the nano emulsion formulations. Amongst these, four formulations (F1, F2, F4, and F6) were successfully produced stabilised nano emulsion with no visible phase separation after 24-hour post-production (Table 1). Therefore, these optimised formulations (C1-NE - C4-NE) were chosen to be further tested for subsequent physiochemical characterisation and stability studies. The optimised formulations with no phase separation are shown at Table 2, and the visualisation for the optimised formulations is shown on Figure 1.

Table 3. The organoleptic properties, pH values and density of the optimised Cur-polyherbal NE

Formulation code	Oil-phase				Aqueous phase		
	VCO (g)	GMO (%)	Cur (mg)	GE (%)	WTE (%)	P-F127 (%)	Distilled water (mL)
C1-NE	5	1	25	20	5	1	70
C2-NE	5	2	50	20	5	2	70
C3-NE	10	2	50	20	5	2	65
C4-NE	10	4	50	20	5	8	65
F5	5	2	25	20	5	4	Yes
F6	10	4	50	20	5	8	No

Abbreviations: VCO, virgin coconut oil; Cur, curcumin; GE, ginger extract; WTE; white tea extract; GMO, glyceryl monooleate.

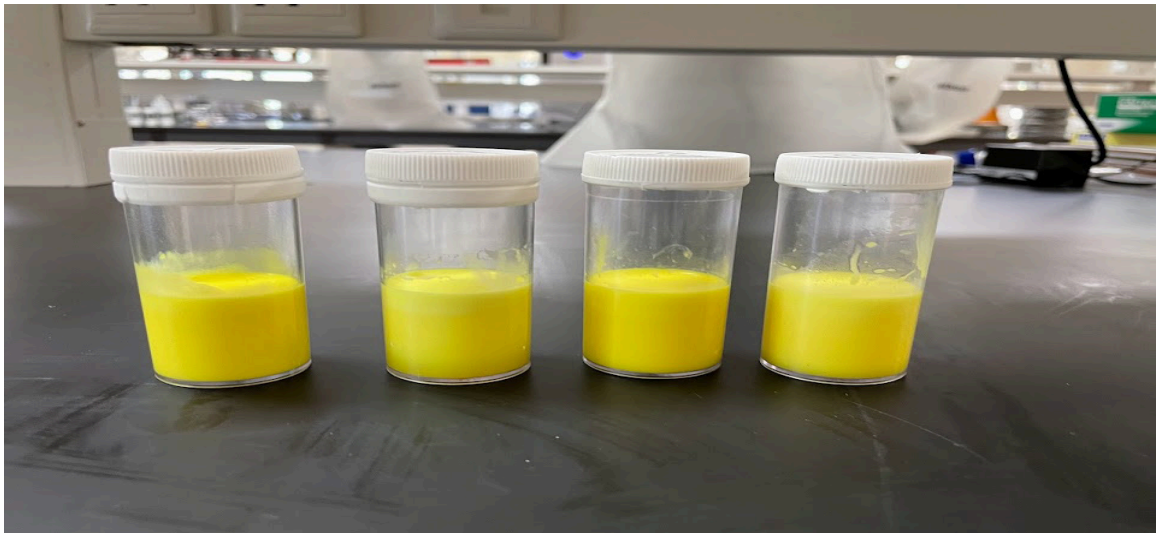

Figure 1. Physical appearance of the optimised oil-in-water curcumin-based polyherbal nano emulsion. From left to right: C1-NE, C2-NE, C3-NE, and C4-NE.

Physiochemical evaluation of optimised Cur-Polyherbal NE

The organoleptic properties, pH, and density of Cur-Polyherbal NE formulations were evaluated. All of the Cur-Polyherbal NE formulations were opaque with pale yellow colour. The measured pH values, density, and odour of the formulations are presented in Table 3.

Table 3. The organoleptic properties, pH values and density of the optimised Cur-polyherbal NE formulations.

Characteristics	Formulation code			
	C1-NE	C2-NE	C3-NE	C4-NE
Colour	Yellow	Yellow	Yellow	Yellow
Odour	Oil-like	Oil-like	Oil-like	Oil-like
(intensity)	(+)	(+)	(+++)	(++++)
pH	5.43	5.40	5.62	6.05
Density (g/mL)	0.977	0.975	0.957	0.994

Note: '+' mild; '+++' moderate; '++++' strong odour.

Stability study

The stability of Cur-Polyherbal NE formulations was assessed based on the measured pH values, density and physical appearance after 30 days storage. At day 30, the Cur-Polyherbal NE formulations presented with acidic pH values ranging from 4.44 – 6.15 (Table 4). All formulations stored at 4 ± 2°C and 40 ± 2°C remained visually stable with no phase separation, although, an increase in density by 0.002 – 0.012 g/mL was observed on most of the formulations (Table 4). Furthermore, reduction in the density of formulation C1-NE and C2-NE was observed by 0.011 g/mL and 0.002 g/mL from its initial density, respectively, when stored at 40 ± 2°C after 30 days. Overall, based on the findings, all formulations presented with relatively acceptable pH values ranging from 5.43 – 6.02 when stored at room temperature (25 ± 2°C) after 30 days. On the other hand, it was shown that formulation C3-NE had the lowest pH values of 4.44 and 4.88 when stored at 4 ± 2°C and 40 ± 2°C, respectively (Table 4).

Table 4. The measured pH values of the Cur-Polyherbal NE formulations at three different storage temperature.

Formulation code	Day	pH			Density (g/mL)		
		4 ± 2°C	25 ± 2°C	40°C ± 2°C	4 ± 2°C	25 ± 2°C	40°C ± 2°C
C1	0	5.43	5.43	5.43	0.977	0.977	0.977
	14	5.35	5.97	4.98	0.977	0.965	0.970
	30	5.61	5.43	4.96	0.978	0.965	0.959
C2	0	5.40	5.40	5.40	0.975	0.975	0.975
	14	5.38	5.52	5.11	0.971	0.963	0.970
	30	5.50	5.50	5.10	0.980	0.963	0.968
C3	0	5.62	5.62	5.62	0.957	0.957	0.957
	.14	4.78	5.60	4.59	0.966	0.956	0.971
	30	4.88	5.79	4.44	0.968	0.962	0.973
C4	0	6.05	6.05	6.05	0.994	0.994	0.994
	14	5.77	5.77	5.78	0.923	0.930	0.931
	30	6.15	6.02	5.58	0.935	0.930	0.931

Particle size, polydispersity index, and zeta potential

The mean particle size, polydispersity index (PdI), and ζ-potential of all four formulations were determined based on Dynamic Light Scattering (DLS) measurements are presented in Table 6. All Cur-polyherbal NEs presented with narrow size distribution (PdI <0.3) and negative ζ-potential values ranging from -0.418 ± 0.373 to -1.12 ± 0.695 (Table 5). It was shown that formulation C3-NE presented the best NE characteristic with relatively smaller mean particle size of 179.8 ± 2.15 nm, PDI of 0.157 ± 0.012, and ζ-potential of -1.12 ± 0.695 mV. In the contrary, formulation C1 presented with relatively larger particle size of 268.3 ± 2.88 nm, PDI of 0.275 ± 0.013, and low ζ-potential of -0.418 ± 0.373 mV. Therefore, due to the distinctive characteristics of C1-NE and C3-NE, these formulations were selected for further antioxidant and cytotoxic studies.

Table 5. Mean particle size, polydispersity index (PdI), and ζ-potential of Cur-polyherbal NEs.

Formulation code	Mean particle size (nm)	Polydispersity Index (PdI)	Zeta (ζ)-potential (mV)
C1-NE	268.3 ± 2.88	0.275 ± 0.013	-0.418 ± 0.373
C2-NE	135.7 ± 2.15	0.169 ± 0.016	-1.027 ± 0.120
C3-NE	179.8 ± 2.15	0.157 ± 0.012	-1.12 ± 0.695
C4-NE	208.1 ± 1.71	0.292 ± 0.004	-0.183 ± 0.352

Data are presented as mean ± SD (n = 3).

FTIR Analysis

The successful incorporation of curcumin, WTE and GE in the Cur-polyherbal NE formulations were analysed using FTIR analysis. The FTIR spectra of formulation C1-NE, C3-NE and individual components of the Cur-polyherbal NE formulations were compared for changes in spectra shifts in the formulations and are depicted in Figure 2. The intense peak at 2926.00 cm^{-1} was revealed to be attributed from the asymmetrical methylene $–CH_2$ (aliphatic) group stretching, whereas, the alkyne –C≡C group stretching resulted in the characteristic dual peaks at 2359.91and 2342.79 cm^{-1} (37). Meanwhile, the disulfide –C-S group stretching resulted in the peak at 668.76 cm^{-1}. Furthermore, these characteristic peaks in FTIR spectra of formulation C1-NE (2926.00, 2359.91, 2342.79 and 668.76 cm^{-1}) were also observed at VCO, GE, GMO, WTE, and curcumin with slight minor shift. Conversely, the characteristic dual peaks observed in formulation C3-NE at 2924.57 and 2854.70 cm^{-1} corresponded to the asymmetrical and symmetrical methylene $–CH_2$ (aliphatic) group stretching, respectively (38)which are sensitive to minute structural changes. The lack of specificity of this technique, on the one hand, permits us to probe directly the vibrational properties of almost all the cofactors, amino acid side chains, and of water molecules. On the other hand, we can use reaction-induced FTIR difference spectroscopy to select vibrations corresponding to single chemical groups involved in a specific reaction. Various strategies are used to identify the IR signatures of each residue of interest in the resulting reaction-induced FTIR difference spectra. (Specific. Meanwhile, the corresponding alkyl carbonate –C=O and nitrate –C=N stretching resulted in strong peak at 1743.91 and 1636.96 cm^{-1}, respectively. Furthermore, the characteristic peaks in formulation C3-NE (2924.57, 2854.70, 1743.91 and 1636.96 cm^{-1}) were also observed at VCO, GMO, P-F127.

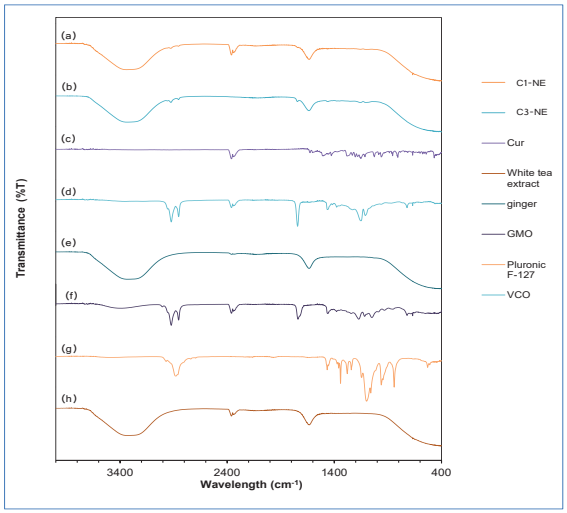

Figure 2. FTIR spectra of (a) C1-NE, (b) C3-NE, (c) curcumin powder extract, (d) VCO, (e) Ginger extract (GE), (f) Glyceryl monooleate (GMO), (g) Pluronic® F-127, and (h) WTE.

Antioxidant activity of Cur-Polyherbal NE

DPPH assay

All tested samples presented with DPPH scavenging activity in a dose-dependent manner (Figure 3). At an equivalent curcumin concentration of 250 µg/mL, C1-NE and C3-NE showed higher DPPH scavenging activity of 96.3 ± 0.577% and 97.7 ± 2.155%, respectively, compared to free curcumin (89.7 ± 1.229%) at the same concentration (Figure 5(a)), although the differences was not significant. When compared between NE and non-NE formulations, the DPPH scavenging activities were significantly reduced ($p < 0.05$) in C1-E (78.6 ± 5.154%) compared to C1-NE (96.3 ± 0.577%) at the same curcumin concentration of 250 µg/mL. Conversely, the reduction in DPPH scavenging activities of C3-NE compared to C3-E was not statistically significant ($p > 0.05$). The DPPH scavenging activities of the three herbal extracts are presented on Table 7. It was revealed that free curcumin and GE presented with excellent antioxidant activities of more than 80%. The IC_{50} values of free curcumin, C1-NE, C3-NE, C1-E and C3-E, from the DPPH scavenging assay, were 3.70, 8.55, 7.74, 16.8, and 11.1µg/mL, respectively (Table 8). The corresponding TEAC values of free curcumin, C1-NE, C3-NE, C1-E and C3-E, are presented in Table 8.

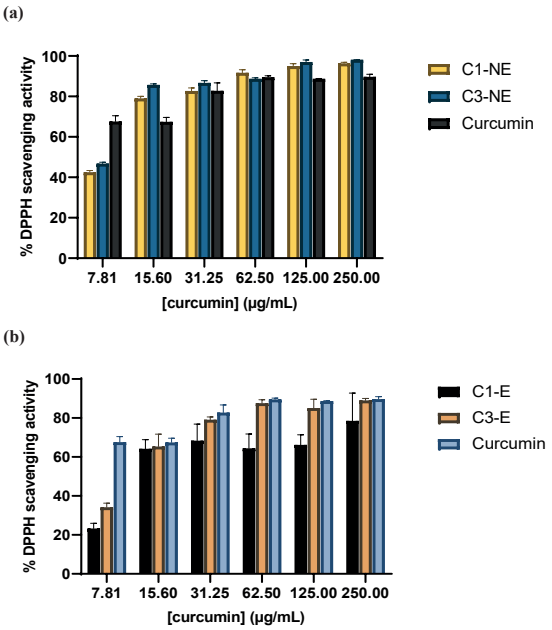

Figure 3. The % DPPH scavenging activity of **(a)** C1-NE, C3-NE, **(b)** C1-E, C3-E at different equivalent curcumin concentrations (7.81 – 250 µg/mL).

Table 6. DPPH radical scavenging antioxidant activity of against the highest concentration of individual herbal extracts used in the development of Cur-polyherbal NE formulations

Herbal extracts	Concentration (µg/mL)	% DPPH scavenging activity
WTE	50	27.0 ± 0.223
GE	200	85.4 ± 0.031
Curcumin	500	90.7 ± 1.15

Table 7. DPPH radical scavenging antioxidant activity (IC_{50}) performed by DPPH assay.

Sample	**IC_{50} (µg/mL) from DPPH assay**	**TEAC (IC_{50}/ IC_{50})**
C1-NE	8.55	0.375

C3-NE	7.74	0.415
C1-E	16.8	0.191
C3-E	11.1	0.289
Curcumin	3.70	0.868
Trolox	3.21	1.000

In-vitro cytotoxicity study

Cell optimisation

Prior to cytotoxic study by MTT assay, determination of the optimal cell density was performed on four different cell seeding density of HEK293 cells. The optimal cell density was selected according to the ability of the cells to reach 80 – 90% confluency after 48 hours on the 96-well plate. This was taken into consideration that HEK293 cells was treated with test samples after overnight incubation and thus, 100% cell confluence should be avoided prior to MTT assay. It was stated that the absorbance for optimum number of cells for MTT assay should be within the range of 0.75 – 1.25 (39). Out of the four cell seeding densities, 2 x 10^4 and 3 x 10^4 cells/well had an appropriate absorbance of 1.07 and 1.16 (Figure 4 (a)). Whereas, 4 x 10^4 cells/well displayed absorbance of 1.80, indicating 100% cell confluence (Figure 4 (b)). Taking into account of the 80 – 90 % cell confluency, 2 x 10^4 cells/well were selected for the MTT assay.

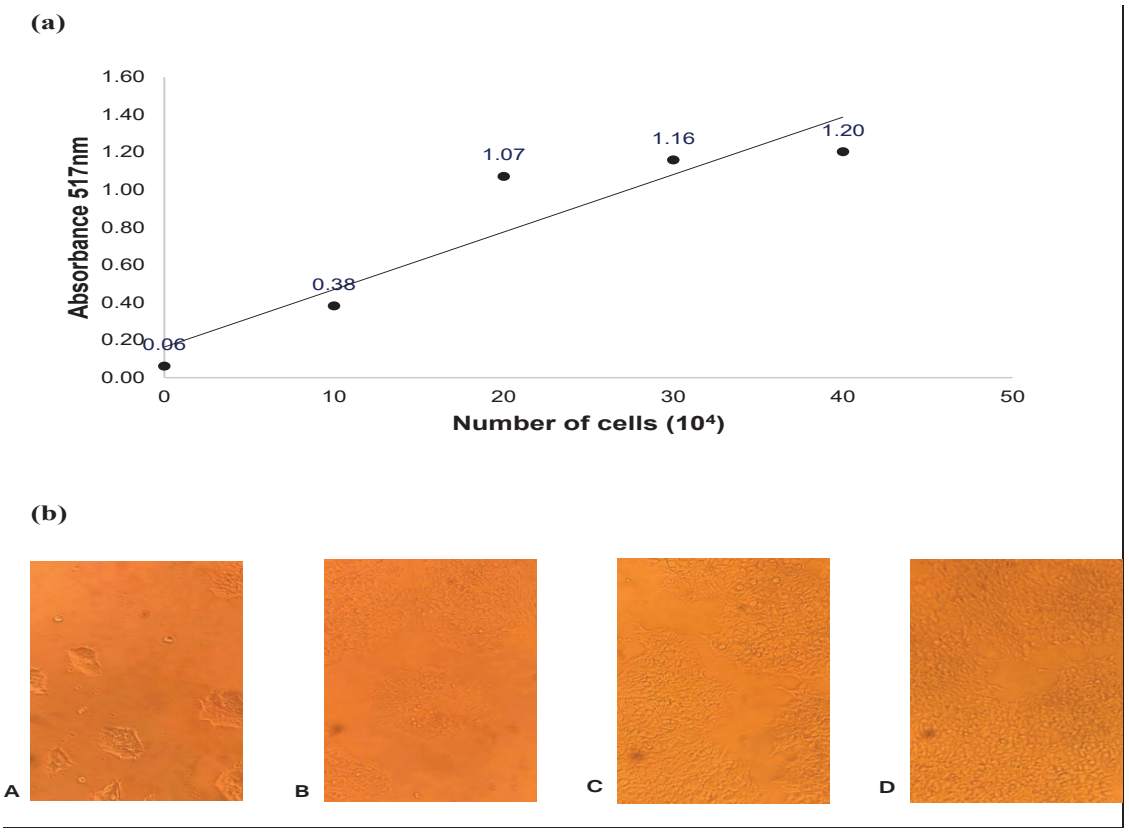

Figure 4 (a) The absorbance (517 nm) of different number of HEK293 cells after 48-hour incubation for cell density optimisation. Figure 4 (b) HEK293 cells viewed under inverted microscope (10x) after 48-hour incubation for cell density optimisation. Note: (A) 1 x 10^4 cells, (B) 2 x 10^4 cells, (C) 3 x 10^4 cells, (D) 4 x 10^4 cells.

In-vitro cytotoxicity of Cur-Polyherbal NE using MTT Assay

In order to determine whether the selected NE formulations (C1-NE and C3-NE) were safe and not toxic to normal cells, different dilutions of the formulations were tested on HEK293 cells and the effect on cell viability was determined by MTT assay. MTT assay was performed on the three herbal extracts used to prepare the NE formulation (curcumin, WTE and GE). It was revealed that free curcumin presented lowest cell viability of 21.3 ± 3.06% followed by WTE with 46.7 ± 2.08%, respectively, after 24-hour incubation (Figure 5). In comparison, GE expressed negligible cytotoxicity with 107.3 ± 4.73% cell viability. Since these NE formulations were prepared in distilled water, the effect of 1% distilled water on cell viability was also tested, and a decrease in cell viability (84.7 ± 4.16%) was observed (Figure 5).

When performed on the NE formulations, the MTT assay revealed a dose-dependent cytotoxicity of C1-NE and C3-NE (Figure 6). Evident cytotoxicity of C1-NE and C3-NE were observed when cells were treated with the formulations diluted at 1:10 which induced a reduction of cell viability of 49.0 ± 2.83 and 44.0 ± 6.66%, respectively. On the other hand, no evident cytotoxicity was observed for C1-NE and C3-NE when diluted at 1:1000 with cell viability above 80%. It was also demonstrated that empty-C1, -C3 and non-nanosized formulations presented a dose-dependent cytotoxicity on HEK293 cells. When compared to NE formulations (C1-NE and C3-NE), the corresponding non-nanosized formulations (C1-E and C3-E) demonstrated a relatively lower cell viability of 36.3 ± 5.34 and 43.6 ± 4.04 % when diluted at 1:10, respectively (Figure 6 (a) and (b)). Conversely, empty-C1 and -C3 did not present with substantial cytotoxicity when diluted at 1:1000 with cell viability above 80%.

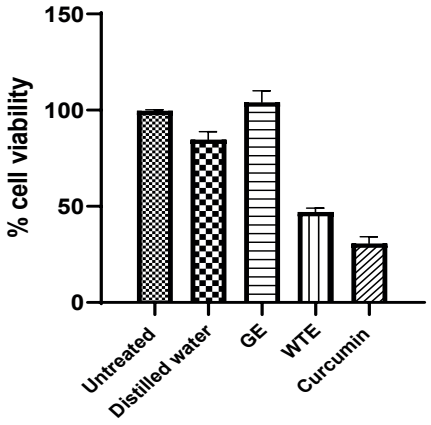

Figure 5. The cytotoxic effects of individual herbal components (GE, WTE and curcumin) on HEK293 cells after 24-hour treatment by MTT assay. Error bars represent standard deviation of triplicate, where n=1.

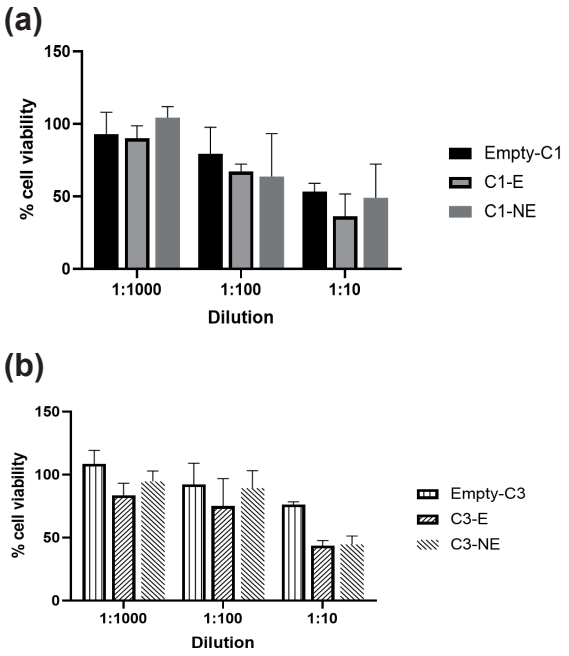

Figure 6. The cytotoxic effect at different dilutions of **(a)** C1-NE, and **(b)** C3-NE on HEK293 cells after 24-hour treatment by MTT assay. Error bars indicate the standard deviation of triplicates, where n=1.

Discussion

Formulation and preparation of Cur-polyherbal NE

Curcumin was able to completely dissolve within oil phase composed of VCO and surfactant GMO. VCO was selected due to its excellent ability to dissolve curcumin attributed to the saturated medium-chain fatty acids (MCFA) contents of VCO that promotes maximum curcumin loading into the NE system (40,41). This is in agreement with previous study whereby VCO demonstrated as a superior plant-based carrier oil for development of NE system for hydrophobic polyphenols such as curcumin (42). Another important consideration during the formulation of NE was to select components that are pharmaceutically acceptable. In this study, non-ionic surfactants (GMO and P-F127) were chosen as they are less toxic compared to the conventional ionic surfactants (43). Previous studies had also described the use of GMO and P-F127 in the development of NE (44), (45). Surfactant is required to create a stabilised interfacial tension present between oil and aqueous phase of NE by ensuring two immiscible phases are sufficiently adsorbed and thereby, providing homogenous NE system (46). Furthermore, it has been reported that the oil-aqueous interfacial tension can be further reduced with increasing surfactant-to-cosurfactant content (47). In this study, the NE system was prepared at varying GMO to P-FF127 ratio contents. Results showed that higher GMO to P-FF127 ratio in combination with higher VCO content exhibited mechanically stable NE system. This is consistent with previous study that reported the incorporation of cosurfactant promoted better interpenetration between surfactants, thereby producing compact interfacial tension that are resistant to particle flocculation (48).

Physiochemical characterisation of Cur-polyherbal NE

Organoleptic properties, pH and density

In this study, the pH values of the optimised formulations were found to be on a slightly acidic pH between 5.40 – 6.04, on average. It has been recommended that the acceptable pH value for mouthwashes should be more than 5.5 to prevent enamel erosion in acidic environment (pH < 5.5) (49). Several factors including chemical reactions and acidic ester contents of VCO might cause the formulations to be slightly acidic (50).

Particle size, PdI and zeta potential

The particle size of the Cur-polyherbal NE formulation served a critical role in providing enhanced curcumin bioavailability (16). The small particle size of NE systems provide greater surface area that enables better drug permeability (51). It was described that the conventional particle size for nano emulsion ranges between 10 – 200 nm in diameter (52). In this study, C1-NE and C4-NE presented with mean particle sizes of more than 200 nm. It was expected that increasing the VCO content with limited concentration of surfactants to compensate for the excessive oil droplet may contribute to the increment of particle size (53). On the other hand, all optimised formulations presented with PdI values less than 0.30 indicating a monodisperse distribution of the particles in the NE system and better stability (54)or lipidic carriers, are being extensively employed to enhance the bioavailability of poorly-soluble drugs. They have the ability to incorporate both lipophilic and hydrophilic molecules and protecting them against degradation in vitro and in vivo. There is a number of physical attributes of lipid-based nanocarriers that determine their safety, stability, efficacy, as well as their in vitro and in vivo behaviour. These include average particle size/ diameter and the polydispersity index (PDI.

The value of zeta potential provides an indication of the physical stability of an NE system and its resistance to particle flocculation based on electrostatic repulsion between the particles (55). It has been reported that an electrostatically stabilised NE system should present with zeta potential values around ± 30mV (56). In

this study, only formulation C2-NE and C3-NE presented with a more negative zeta potential values of -1.027 ± 0.120 mV and -1.12 ± 0.695 mV, relatively, which inherently suggest higher tendency to agglomerate, eventually. The negative zeta potential of the formulations may be due to the dispersion of the anionic fatty acids and glycerol present on GMO and VCO (57). It has been described that the physical stability of NE system is not exclusive to zeta potential values but also on the concentration of surfactant used during the formulation (45). The addition of sufficient surfactant contents may have provided a rigid oil-aqueous interfacial tension which may be sufficient to prevent destabilisation of the NE system.

Stability study

It has been reported that pH alterations due to chemical interactions greatly impact the stability and quality of NE systems due to the electrostatic repulsive interaction that disturb the interfacial tension (58)a major obstacle that remains to be overcome is the capacity of the active molecules in C. asiatica to cross the blood-brain barrier (BBB. Several authors had discussed the influence of pH alteration due to internal chemical reactions which eventually compromise the quality of emulsions. (59). It was also reported that NEs produced using vegetable oil, in this case was VCO, may observe a reduction in pH attributed to the hydrolysis of fatty acid esters (60).

FTIR analysis

The FTIR spectra of Cur-polyherbal NE formulations in comparison to their individual components showed no absence in any functional peaks in any of the spectra. Furthermore, no significant peak shifts or new functional group stretching were observed in the Cur-polyherbal NE formulations (C1-NE and C3-NE). However, some minor shifts in wavelength peaks were observed which may suggest that some interactions occurred between the components of the Cur-polyherbal NE formulations resulting in the broadening of the peaks.

Antioxidant activity

In this study, the selected NE formulations (C1-NE and C3-NE) were investigated for their antioxidant activity using DPPH assay based on the capability of curcumin to scavenge DPPH free radicals when loaded inside the NE system. The increased in DPPH scavenging activity of the NE formulations may be attributed from the well-known antioxidant properties of the polyherbal extracts (WTE, GE and curcumin) present in the NE system which might work synergistically to produce excellent antioxidant activity (61). This observation was expected as both curcumin and GE are renowned for their potent antioxidative properties (62). The increase in antioxidant activity of renowned antioxidant compounds after nanoencapsulation has been reported by some authors (63,64). It has been reported from a previous study that curcumin and resveratrol extracts displayed significant improvement in their antioxidant profile when associated into lipid-nanoencapsulation (65,66). The authors suggested that this was influenced by the kinetic release of antioxidants from the oil core. In-vitro cytotoxicity of Cur-Polyherbal NE using MTT Assay

Cytotoxicity of Cur-Polyherbal NE

In this study, it should be noted that the absolute concentration of the NEs were unable to be deduced as additional assay needs to be performed (67). Thus, in order to assess the cytotoxicity of the formulations, several dilutions of stock NE formulations were made in order to prepare different concentrations of C1-NE and C3-NE, accordingly. However, it was known that C1-NE and C3-NE stock solutions carried curcumin concentration of 250 µg/mL and 500 µg/mL, respectively. Thus, the cytotoxicity of C1-NE and C3-NE towards HEK293 cells were described by taking into account the concentration of curcumin (µg/mL) present at different dilution factors.

In this study, cytotoxicity of C1-NE and C3-NE were in a dose-dependent manner whereby reduction in percentage of cell viability

was observed with increasing concentration of the NE formulations. It can be deduced that C1-NE and C3-NE were evidently cytotoxic towards HEK293 cells when treated with both formulations at a lower dilution of 1:10, whereby, C1-NE and C3-NE had equivalent curcumin concentrations of 25 µg/mL and 50 µg/mL, respectively. This observation is in agreement with previous study that reported higher toxicity of curcumin-loaded NE (< 40% cell viability) at 40 µM on HaCaT cell line (68). Furthermore, the differences in particle sizes between C1-NE (268.3 ± 2.88 nm) and C3-NE (179.8 ± 2.15 nm) may influence the different cytotoxicity observed in this case. It has been reported that NE system with smaller particle size had an increased ability to efficiently deliver loaded drug, in this case was curcumin, across cellular compartments leading more exposure of the drug leading to cytotoxicity especially at a higher dose (69). On the other hand, both empty-C1 and -C3, which comprised of VCO, GMO and P-F127, did not exhibit any inherent cytotoxicity at 1:100 dilution which are in agreement with previous studies that regarded GMO and P-F127 as cytocompatible (70,71).

This study also demonstrated that both C1-NE and C3-NE generally showed higher cell viability when compared with free curcumin. Zheng et al. (72)which was then investigated against human embryonic kidney cells (HEK 293 reported that free curcumin exhibited 50% cytotoxicity at 10 µg/mL compared to curcumin nanoparticle (CNP) with less than 40% cytotoxicity at same concentration after 24 h incubation on HEK293 cells. Several narratives suggested that the reduction in cytotoxicity was accounted from the controlled and sustained release of curcumin when loaded inside NE system (68,73). This suggests that the incorporation of nanotechnology potentially promotes greater bioavailability of curcumin with less toxicity.

One of the limitations of this cytotoxicity study by MTT assay was the lack of independent experimental repeats and statistical analysis was unable to be performed due to the nature of the replicates. Thus, this study cannot conclude whether the cytotoxicity observed in dose-dependent manner between C1-NE and C3-NE was altogether significant. Furthermore, the unknown concentration of NE present on the formulations limits the understanding of the toxicity of formulations associated with NE system. Thus, additional assay should be performed in future studies to determine the concentration of NE present on the formulations. However, as this was only a preliminary study, results obtained from this cytotoxicity study can provide as guidelines for future studies to be performed using a lower concentration of curcumin loaded on NE system and assess its safety profile.

Conclusion

The selected Cur-polyherbal NE formulation (C1-NE and C3-NE) presented with mean particle sizes within 100 to 300 nm, low polydispersity index (PdI) (< 0.3), and acceptable stability when stored at room temperature. This study had shown that the NE formulation (C1-NE and C3-NE) had retained the renowned antioxidant properties of curcumin, WTE and GE, with DPPH scavenging activities over 90%. Moreover, when investigated with the corresponding non-nanosized formulation (C1-E and C3-E), a significant reduction in DPPH scavenging activities were observed ($p < 0.05$) which suggests the importance of nanotechnology in providing better therapeutic effects of the formulation. Whereas, cytotoxicity study of the formulations on HEK293 cells using MTT assay exhibited dose-dependent toxicity. This preliminary study serves as a baseline for further exploration of polyherbal NE formulations as mouthwash alternative. Studies such as antimicrobial study on plaque-inducing pathogens should be evaluated in the future to investigate the efficacy of the Cur-polyherbal NE mouthwash to control gingival and periodontal diseases.

Acknowledgements

The authors would like to acknowledge Universiti Brunei Darussalam, Brunei Darussalam for the funding (UBD/RSCH/1.6/FICB-F(b)/2021/013).

Competing interests

The authors declare that they have no competing interests.

References

1. Murakami S, Mealey BL, Mariotti A, Chapple ILC. Dental plaque-induced gingival conditions. Journal of periodontology. 2018 Jun;89 Suppl 1:S17–27.
2. James P, Worthington H V., Parnell C, Harding M, Lamont T, Cheung A, et al. Chlorhexidine mouthrinse as an adjunctive treatment for gingival health. The Cochrane database of systematic reviews. 2017 Mar;3(3).
3. McCoy LC, Wehler CJ, Rich SE, Garcia RI, Miller DR, Jones JA. Adverse events associated with chlorhexidine use: results from the Department of Veterans Affairs Dental Diabetes Study. Journal of the American Dental Association (1939). 2008;139(2):178–83.
4. Al-Maweri SA, Alhajj MN, Deshisha EA, Alshafei AK, Ahmed AI, Almudayfi NO, et al. Curcumin mouthwashes versus chlorhexidine in controlling plaque and gingivitis: A systematic review and meta-analysis. International journal of dental hygiene. 2022 Feb;20(1):53–61.
5. Menon VP, Sudheer AR. Antioxidant and anti-inflammatory properties of curcumin. Advances in Experimental Medicine and Biology. 2007;595(September 2001):105–25.
6. Tyagi AK, Prasad S, Yuan W, Li S, Aggarwal BB. Identification of a novel compound (β-sesquiphellandrene) from turmeric (Curcuma longa) with anticancer potential: comparison with curcumin. Investigational New Drugs 2015 33:6. 2015 Nov;33(6):1175–86.
7. Hatcher H, Planalp R, Cho J, Torti FM, Torti S V. Curcumin: From ancient medicine to current clinical trials. Cellular and molecular life sciences : CMLS. 2008 Jun;65(11):1631.
8. Farjana HN, Chandrasekaran SC, Gita B. Effect of oral curcuma gel in gingivitis management - a pilot study. Journal of clinical and diagnostic research : JCDR. 2014 Dec;8(12):ZC08-ZC10.
9. Chaturvedi TP. Uses of turmeric in dentistry: an update. Indian journal of dental research : official publication of Indian Society for Dental Research. 2009 Jan;20(1):107–9.
10. Hosadurga RR, Rao S, Jose J, Rompicharla NC, Shakil M, Shashidhara R. Evaluation of the efficacy of 2% curcumin gel in the treatment of experimental periodontitis. Pharmacognosy Research. 2014;6(4):326.
11. Muglikar S, Patil KC, Shivswami S, Hegde R. Efficacy of curcumin in the treatment of chronic gingivitis: a pilot study. Oral health & preventive dentistry. 2013;11(1):81–6.
12. Hassanzadeh K, Buccarello L, Dragotto J, Mohammadi A, Corbo M, Feligioni M. Obstacles against the Marketing of Curcumin as a Drug. International Journal of Molecular Sciences. 2020 Sep;21(18):1–35.
13. Gera M, Sharma N, Ghosh M, Huynh DL, Lee SJ, Min T, et al. Nanoformulations of curcumin: An emerging paradigm for improved remedial application. Oncotarget. 2017;8(39):66680–98.
14. Hettiarachchi SS, Dunuweera SP, Dunuweera AN, Rajapakse RMG. Synthesis of Curcumin Nanoparticles from Raw Turmeric Rhizome. ACS Omega. 2021 Mar;6(12):8246–52.
15. Azami SJ, Teimouri A, Keshavarz H, Amani A, Esmaeili F, Hasanpour H, et al. Curcumin nano emulsion as a novel chemical for the treatment of acute and chronic toxoplasmosis in mice. International journal of

nanomedicine. 2018;13:7363–74.

16. Jaiswal M, Dudhe R, Sharma PK. Nano emulsion: an advanced mode of drug delivery system. 3 Biotech. 2015 Apr 8;5(2):123–7.

17. Wang S, Su R, Nie S, Sun M, Zhang J, Wu D, et al. Application of nanotechnology in improving bioavailability and bioactivity of diet-derived phytochemicals. The Journal of nutritional biochemistry. 2014;25(4):363.

18. Karole S, Shrivastava S, Thomas S, Soni B, Khan S, Dubey J, et al. Polyherbal Formulation Concept for Synergic Action: A Review. Journal of Drug Delivery and Therapeutics. 2019 Feb;9(1-s):453–66.

19. Hano C, Tungmunnithum D. Plant Polyphenols, More than Just Simple Natural Antioxidants: Oxidative Stress, Aging and Age-Related Diseases. Medicines. 2020 May;7(5):26.

20. Ali S, Naqvi R, Nadeem S, Komal S, Naqvi A, Samee Mubarik M, et al. Antioxidants: Natural Antibiotics. Antioxidants. 2019;(1):23–34.

21. Espinosa C, López-Jiménez JÁ, Cabrera L, Larqué E, Almajano MP, Arnao MB, et al. Protective effect of white tea extract against acute oxidative injury caused by adriamycin in different tissues. Food Chemistry. 2012 Oct;134(4):1780–5.

22. Pan J, Jiang Y, Lv Y, Li M, Zhang S, Liu J, et al. Comparison of the main compounds in Fuding white tea infusions from various tea types. Food Science and Biotechnology. 2018 Oct;27(5):1311.

23. Tafazoli A, PhD, Moghadam ET, DDS. Camellia Sinensis Mouthwashes in Oral Care: a Systematic Review. Journal of Dentistry. 2020;21(4):249.

24. Alsahli MA, Almatroodi SA, Almatroudi A, Khan AA, Anwar S, Almutary AG, et al. 6-Gingerol, a Major Ingredient of Ginger Attenuates Diethylnitrosamine-Induced Liver Injury in Rats through the Modulation of Oxidative Stress and Anti-Inflammatory Activity. Mediators of Inflammation. 2021;2021.

25. Park M, Bae J, Lee DS. Antibacterial activity of (10)-gingerol and (12)-gingerol isolated from ginger rhizome against periodontal bacteria. Phytotherapy research : PTR. 2008 Nov;22(11):1446–9.

26. S H, M D, AU K. Inhibitory effect of zingiber officinale towards Streptococcus mutans virulence and caries development: in vitro and in vivo studies. BMC microbiology. 2015 Dec;15(1).

27. Liu Q, Huang H, Chen H, Lin J, Wang Q. Food-Grade Nano emulsions: Preparation, Stability and Application in Encapsulation of Bioactive Compounds. Molecules. 2019 Nov;24(23).

28. Ghosal K, Rajabalaya R, Chakraborty S, Nanda A. Formulation and characterization of both hydrophilic and hydrophobic HPMC based hydrogels containing diclofenac potassium. Latin American Journal of Pharmacy. 2010;29(7).

29. David SR, Refai SA, Yian KR, Mai CW, Das SK, Rajabalaya R. Development and evaluation of liquid crystal systems of combination of 5-fluorouracil and curcumin for cervical cancer cell line. Journal of Pharmacy and Pharmacognosy Research. 2019;7(6):441–53.

30. David SR, Matzidi FNNH, Shanmugam R, Thangavelu L, Balaraman AK, Rajabalaya R. Evaluation of the Chemo-Preventive Effects of Camellia sinensis Silver Nanoparticles and Synergistic Effects with 5-fluorouracil in Colorectal Cancer Induced Rats. Current Trends in Biotechnology and Pharmacy. 2022;16(2):114–29.

31. Muhammad Nuh Musa, Sheba Rani David, Ihsan Nazurah Zulkipli, Abdul Hanif Ma-

hadi, Srikumar Chakravarthi RR. Development and evaluation of exemestane-loaded lyotropic liquid crystalline gel formulations. BioImpacts. 2017;7(4):227–39.

32. Rajan Rajabalaya, Chung Yee Mun, Jestin Chellian, Srikumar Chakravarthi SRD. Transdermal delivery of tolterodine tartrate for overactive bladder treatment: In vitro and in vivo evaluation. Acta Pharmaceutica. 2017;67(3):325–39.

33. Sheba R David, Nurafiqah Malek, Abdul Hanif Mahadi, Srikumar Chakravarthi RR. Development of controlled release silicone adhesive-based mupirocin patch demonstrates antibacterial activity on live rat skin against staphylococcus aureus. Drug Design, Development and Therapy. 2018;12:481–94.

34. Xiao F, Xu T, Lu B, Liu R. Guidelines for antioxidant assays for food components. Food Frontiers. 2020 Mar;1(1):60–9.

35. R David S, Akmar Binti Anwar N, Yian KR, Mai C-W, Das SK, Rajabalaya R. Development and Evaluation of Curcumin Liquid Crystal Systems for Cervical Cancer. Scientia Pharmaceutica. 2020 Mar 23;88(1):15.

36. Idris A, Zulkipli IN, Zulhilmi NR, Lee HF, Rajabalaya R, Lim YC, et al. Melastoma malabathricum Ethyl Acetate Fraction Induces Secondary Necrosis in Human Breast and Lung Cancer Cell Lines. Pharmacognosy Magazine. 2017;13:S688-92.

37. Coates J. Interpretation of Infrared Spectra, A Practical Approach. Encyclopedia of Analytical Chemistry. 2006;1.

38. Berthomieu C, Hienerwadel R. Fourier transform infrared (FTIR) spectroscopy. Photosynthesis Research. 2009 Sep;101(2–3):157–70.

39. Sheba R David, Khairunnasibah Abdullah, Rajeshkumar Shanmugam, Lakshmi Thangavelu, Sanjoy Kumar Das RR. Green Synthesis, Characterization and In Vivo Evaluation of White Tea Silver Nanoparticles with 5-Fluorouracil on Colorectal Cancer. BioNanoScience. 2021;11(4):1095–107.

40. Tabanelli R, Brogi S, Calderone V. Improving Curcumin Bioavailability: Current Strategies and Future Perspectives. Pharmaceutics. 2021 Oct;13(10):1715.

41. Kharat M, McClements DJ. Recent advances in colloidal delivery systems for nutraceuticals: A case study - Delivery by Design of curcumin. Journal of colloid and interface science. 2019 Dec;557:506–18.

42. Zhou H, Zheng B, McClements DJ. Encapsulation of lipophilic polyphenols in plant-based nano emulsions: impact of carrier oil on lipid digestion and curcumin, resveratrol and quercetin bioaccessibility. Food & function. 2021 Apr;12(8):3420–32.

43. Azeem A, Rizwan M, Ahmad FJ, Iqbal Z, Khar RK, Aqil M, et al. Nano emulsion Components Screening and Selection: a Technical Note. AAPS PharmSciTech. 2009;10(1):69.

44. Bharmoria P, Bisht M, Gomes MC, Martins M, Neves MC, Mano JF, et al. Protein-olive oil-in-water nano emulsions as encapsulation materials for curcumin acting as anticancer agent towards MDA-MB-231 cells. Scientific Reports 2021 11:1. 2021 Apr;11(1):1–12.

45. Rachmawati H, Budiputra DK, Mauludin R. Curcumin nano emulsion for transdermal application: Formulation and evaluation. Drug Development and Industrial Pharmacy. 2015;41(4):560–6.

46. Sobhani H, Tarighi P, Ostad SN, Shafaati A, Nafissi-Varcheh N, Aboofazeli R. Formulation Development and Toxicity Assessment of Triacetin Mediated Nano emulsions as Novel Delivery Systems for Rapamycin. Iranian Journal of Pharmaceutical Re-

search : IJPR. 2015;14(Suppl):3.

47. Shafiq-un-Nabi S, Shakeel F, Talegaonkar S, Ali J, Baboota S, Ahuja A, et al. Formulation development and optimization using nano emulsion technique: a technical note. AAPS PharmSciTech. 2007 Apr;8(2).

48. Borrin TR, Georges EL, Moraes ICF, Pinho SC. Curcumin-loaded nano emulsions produced by the emulsion inversion point (EIP) method: An evaluation of process parameters and physico-chemical stability. Journal of Food Engineering. 2016 Jan;169:1–9.

49. Cavalcanti AL, Ramos IA, Leite RB, Oliveira M da C, Menezes K de M, Fernandes LV, et al. Endogenous pH, Titratable Acidity and Total Soluble Solid Content of Mouthwashes Available in the Brazilian Market. European Journal of Dentistry. 2010 Apr;4(2):156.

50. Rajabalaya R, Musa MN, Kifli N, David SR. Oral and transdermal drug delivery systems: role of lipid-based lyotropic liquid crystals. Drug design, development and therapy. 2017;11:393–406.

51. Su R, Fan W, Yu Q, Dong X, Qi J, Zhu Q, et al. Size-dependent penetration of nano emulsions into epidermis and hair follicles: implications for transdermal delivery and immunization. Oncotarget. 2017;8(24):38214.

52. Demisli S, Mitsou E, Pletsa V, Xenakis A, Papadimitriou V. Development and Study of Nano emulsions and Nano emulsion-Based Hydrogels for the Encapsulation of Lipophilic Compounds. Nanomaterials. 2020 Dec;10(12):1–19.

53. Pengon S, Chinatangkul N, Limmatvapirat C, Limmatvapirat S. The effect of surfactant on the physical properties of coconut oil nano emulsions. Asian Journal of Pharmaceutical Sciences. 2018 Sep;13(5):409.

54. Danaei M, Dehghankhold M, Ataei S, Hasanzadeh Davarani F, Javanmard R, Dokhani A, et al. Impact of Particle Size and Polydispersity Index on the Clinical Applications of Lipidic Nanocarrier Systems. Pharmaceutics. 2018 May;10(2).

55. Tamilvanan S. Formulation of multifunctional oil-in-water nanosized emulsions for active and passive targeting of drugs to otherwise inaccessible internal organs of the human body. International journal of pharmaceutics. 2009 Oct;381(1):62–76.

56. Laxmi M, Bhardwaj A, Mehta S, Mehta A. Development and characterization of nano emulsion as carrier for the enhancement of bioavailability of artemether. Artificial Cells, Nanomedicine and Biotechnology. 2015;43(5):334–44.

57. Noor NM, Khan AA, Hasham R, Talib A, Sarmidi MR, Aziz R, et al. Empty nano and micro-structured lipid carriers of virgin coconut oil for skin moisturisation. IET Nanobiotechnology. 2016 Aug;10(4):195.

58. Jusril NA, Bakar SIA, Khalil KA, Saad WMM, Wen NK, Adenan MI. Development and Optimization of Nano emulsion from Ethanolic Extract of Centella asiatica (NanoSECA) Using D-Optimal Mixture Design to Improve Blood-Brain Barrier Permeability. Lim V, editor. Evidence-based Complementary and Alternative Medicine : eCAM. 2022 Mar;2022:1–18.

59. Östbring K, Matos M, Marefati A, Ahlström C, Gutiérrez G. The effect of ph and storage temperature on the stability of emulsions stabilized by rapeseed proteins. Foods. 2021 Jul;10(7).

60. David SR, Abdullah K, Shanmugam R, Thangavelu L, Das SK, Rajabalaya R. Green Synthesis, Characterization and In Vivo Evaluation of White Tea Silver Nanoparticles with 5-Fluorouracil on Colorectal Cancer. BioNanoScience.

2021;11(4):1095–107.

61. Mashhadi NS, Ghiasvand R, Askari G, Hariri M, Darvishi L, Mofid MR. Anti-Oxidative and Anti-Inflammatory Effects of Ginger in Health and Physical Activity: Review of Current Evidence. International Journal of Preventive Medicine. 2013;4(Suppl 1):S36.

62. Sökmen M, Akram Khan M. The antioxidant activity of some curcuminoids and chalcones. Inflammopharmacology. 2016 Jun;24(2–3):81.

63. Ha TVA, Kim S, Choi Y, Kwak HS, Lee SJ, Wen J, et al. Antioxidant activity and bioaccessibility of size-different nano emulsions for lycopene-enriched tomato extract. Food chemistry. 2015 Jul;178:115–21.

64. Zorzi GK, Caregnato F, Moreira JCF, Teixeira HF, Carvalho ELS. Antioxidant Effect of Nano emulsions Containing Extract of Achyrocline satureioides (Lam) D.C.-Asteraceae. AAPS PharmSciTech. 2016 Aug;17(4):844–50.

65. Coradini K, Lima FO, Oliveira CM, Chaves PS, Athayde ML, Carvalho LM, et al. Co-encapsulation of resveratrol and curcumin in lipid-core nanocapsules improves their in vitro antioxidant effects. European Journal of Pharmaceutics and Biopharmaceutics. 2014 Sep;88(1):178–85.

66. Spigno G, Donsì F, Amendola D, Sessa M, Ferrari G, De Faveri DM. Nanoencapsulation systems to improve solubility and antioxidant efficiency of a grape marc extract into hazelnut paste. Journal of Food Engineering. 2013 Jan;114(2):207–14.

67. Ivanov A, Min'kov K, Samoilenko A, Levin G. The Measurement of Nanoparticle Concentrations by the Method of Microcavity Mode Broadening Rate. Sensors (Basel, Switzerland). 2020 Oct;20(20):1–15.

68. De Matos RPA, Calmon MF, Amantino CF, Villa LL, Primo FL, Tedesco AC, et al. Effect of Curcumin-Nano emulsion Associated with Photodynamic Therapy in Cervical Carcinoma Cell Lines. BioMed research international. 2018;2018.

69. Oliveira WN, Alencar EN, Rocha HAO, Amaral-Machado L, Egito EST. Nanostructured systems increase the in vitro cytotoxic effect of bullfrog oil in human melanoma cells (A2058). Biomedicine & Pharmacotherapy. 2022 Jan;145:112438.

70. Menon JU, Kona S, Wadajkar AS, Desai F, Vadla A, Nguyen KT. Effects of surfactants on the properties of PLGA nanoparticles. Journal of biomedical materials research Part A. 2012;100(8):1998–2005.

71. Valente F, Bysell H, Simoni E, Boge L, Eriksson M, Martini A, et al. Evaluation of toxicity of glycerol monooleate nanoparticles on PC12 cell line. International journal of pharmaceutics. 2018 Mar;539(1–2):23–30.

72. Zheng Y, Chen Y, Jin LW, Ye HY, Liu G. Cytotoxicity and Genotoxicity in Human Embryonic Kidney Cells Exposed to Surface Modify Chitosan Nanoparticles Loaded with Curcumin. AAPS PharmSciTech. 2016 Dec;17(6):1347–52.

73. Abruzzo A, Zuccheri G, Belluti F, Provenzano S, Verardi L, Bigucci F, et al. Chitosan nanoparticles for lipophilic anticancer drug delivery: Development, characterization and in vitro studies on HT29 cancer cells. Colloids and surfaces B, Biointerfaces. 2016 Sep;145:362–72.

Current Trends in Biotechnology and Pharmacy
Vol. 18(3) 1841-1849, July 2024, ISSN 0973-8916 (Print), 2230-7303 (Online)
10.5530/ctbp.2024.3.31

Host specific Arbuscular Mycorrhizal Fungi (AMF): A Boost to Growth and Phosphorus Regulation in Cotton (*Gossypium herbaceum*)

Tasleem Sultana and Pavan Kumar Pindi*

Department of Microbiology, Palamuru University, Mahabubnagar-509001, Telangana, India.
* Corresponding Author: pavankumarpindi@gmail.com

Abstract

Cotton holds paramount importance as a natural resource with considerable economic, social, and environmental implications. This study focused on isolating host-specific mycorrhizal spores for the Mahyco cultivar of *Gossypium herbaceum*. A homogenous mixture of soils (HMS) was utilized, incorporating eight widely used cultivars in Mahabubnagar District, and maintained for 60 days. After the designated period, the well-grown Mahyco plant was carefully extracted and transferred to a pot containing sterilized soil, ensuring sterile conditions for 8 weeks. Mycorrhizal colonization was observed in roots, and the soil was sieved to isolate host-specific spores. Abundant spores of *Glomus mosseae* were identified based on the manual by Schenk and Perez (1987). These spores were propagated through a funnel experiment and then transferred to pots for mass cultivation. The efficiency of *Glomus mosseae* was tested with four different soils in Mahabubnagar District. Deep black soil exhibited optimal growth in terms of plant development and phosphorus uptake, followed by shallow black soil. This method demonstrates high host specificity for geographically grown cotton and can be adapted for the sustainable cultivation of cotton.

Keywords: AMF, *Glomus mosseae, Gossypium herbaceum,* HMS.

Introduction

Cotton, a crucial natural fibre and economically significant crop, bestows considerable advantages to humans and stands as a pivotal raw material globally. Despite numerous recent studies affirming the capacity of arbuscular mycorrhizal fungi (AMF) to enhance plant growth (27), yield, quality, and phosphorus acquisition, (5, 11 19) their impact on the economic and agronomic traits of cotton (24) remains largely unexplored. Prior research findings indicate that mycorrhiza-mediated inoculants can potentially reduce the necessity for phosphorus fertilization by at least 25%, and in some cases, up to 50%, without compromising crop yield (7).

Mycorrhizal associations exhibit diverse structures and functions, with the arbuscular mycorrhizal (AM) association being the most prevalent. This association forms between the roots of higher plants and Zygomycete fungi of the order *Glomales* (30). Numerous recent studies affirm that arbuscular mycorrhizal fungi (AMF) enhance plant growth (19), yield, quality, and phosphorus acquisition (24). Fungi play pivotal roles in microbiological and ecological processes, influencing soil fertility (17), decomposition, mineral and organic matter cycling (14), as well as plant health and nutrition (29). A significant effect on host plants is the mobilization of nutrients like N and P from structural and other polymers otherwise inaccessible to plant roots.

Mycorrhizal fungi develop on plants through three main methods: forming spores (4), colonized root fragments, or vegetative hyphae. The latter two are known as propagules, structures containing mycorrhizal fungi capable of initiating new associations. Propagules in mycorrhizae encompass spores, hyphal fragments, or other structures produced by the fungi. Two types of fungus colonize plants: endomycorrhiza or ectomycorrhiza. Endomycorrhiza form 90% of relationships with all plant species (35), while ectomycorrhizal fungi colonize from outside the root cells, forming relationships with approximately 10% of all plant species.

Arbuscular mycorrhizal fungi (AMF) establish symbiotic relationships with plant roots and can enhance the adaptability of host plants (3), particularly by providing additional phosphorus (P), (1), nitrogen (N), and zinc (31). The symbiosis with AMF leads to the extension of root systems, increasing the root surface area utilized for nutrient uptake by more than 100-fold. A diverse range of essential agricultural crops, including wheat, rice, corn, potato, tomato, onion, pulses, cotton, and soybean, can engage in symbiotic associations with AMF, highlighting their significance in global agriculture.

Numerous studies have reported isolating mycorrhizal fungi from plant roots, demonstrating their specificity to particular plants due to their presence in the rhizosphere vicinity. However, confirming that plant growth is solely due to the presence of specific fungi remains challenging. The present study primarily focuses on isolating host-specific mycorrhizae using the HMS (Homogenized Mixture of Soil) method, where the plant (*Gossypium herbaceum*) actively takes up spores beneficial for its growth. This approach empowers the plant with the ability to select the most suitable fungi for optimal development.

Materials and Methods

A uniform blend of soils: Rhizosphere soils associated with cotton plants were gathered from six forest locations, namely Amrabad-Nagarkurnool (Ngkl), Bhadrachalam-Khammam (Khm), Eturunagaram-Warangal (Wrngl), Jannaram-Adilabad (Adb), Kataram-Karimnagar (Krmn), and Narsapur-Medak (Mdk). The soil samples were carefully enclosed in sterile zip-lock bags and transported to the laboratory.

Preparation of soil samples for homogenous mixture of soils (hms)

Elimination of undesired materials such as roots, gravel, stones, and pebbles was conducted upon receiving the soil samples collected from different locations in the laboratory. Subsequently, the bulk soil was reduced to the required quantity using the quartering technique (28), serving as a source for the isolation of efficient mycorrhizae specifically for the Mahyco cultivar of *Gossypium herbaceum*. Before sowing, the seeds underwent washing 2 to 3 times to eliminate adhering impurities and miscellaneous bacteria from the seed surface.

Preparation of Sterile Soil

A sterile soil mixture was created by combining sand and red soil in a 1:1 ratio, followed by autoclaving at 121°C under 15 lbs pressure.

Determination of percentage of mycorrhizal root infection

Roots were cautiously removed and rinsed thoroughly with water to eliminate any adhering soil particles. Subsequently, they were fixed in FAA (Formalin acetic acid alcohol solution). The roots were submerged in a KOH solution and autoclaved for 15-20 minutes, followed by cleaning with distilled water. Acidification was carried out in 5N HCl, and the staining process was performed using lactophenol trypan blue. The clarified roots underwent staining according to the technique outlined in (23). The percentage of infection was determined using the formula provided by (13).

Funnel experiment

Sowing of Mahyco cotton cultivar was conducted using *Glomus mosseae* spores in funnels filled with sterilized soil supplemented with Hoagland's Solution (16).

Spore isolation and identification

A total of 100 grams of soil underwent the process of submersion in 1 litre of water within a beaker. Thorough mixing was accomplished using a glass rod, and the mixture was allowed to settle for a duration of 4 to 5 hours. The suspension was meticulously poured through a series of sieves with mesh sizes of 400, 100, 70, and 50 µm. The residues retained on these sieves were then rinsed onto Whatman filter paper. Subsequently, spores were carefully selected using a needle under a stereo binocular research microscope and arranged on a glass slide, with or without the application of Melzer's reagent for enhanced identification. The identification process relied on a thorough analysis of morphological and subcellular characteristics, with spores being cross-referenced against the original description provided by (26).

Sampling diversity

Soil samples were gathered from various cotton fields in Mahabubnagar District, including shallow black soil from Malleboinpally, red soil from Makthal, deep black soil from Kalwakurthy, and sandy soil from Narayanpet.

Physico-chemical profile of soils in cotton farming environments

Soil's available nitrogen content was assessed using the alkaline potassium permanganate method, as described by (32). The determination of available phosphorous was conducted following the method outlined by Bray and Kurtz in 1945, while potassium levels were determined through flame photometry, following the protocol established by (18).

Results and Discussion

The growth of cotton plants is significantly influenced by Arbuscular Mycorrhizal Fungi (AMF), as observed in the study by (33). Plants that undergo AMF inoculation demonstrate increased adaptability to adverse conditions, as reported by (34). In this study, particular emphasis is placed on the host-specific mycorrhizal spores for the Mahyco cotton cultivar. Eight Cotton cultivars were planted in an HMS mixture (Table-1), and optimal conditions were maintained to facilitate seed germination, allowing the plants to grow for a period of 60 days.

Table-1: Growth parameters of Eight cotton cultivars grown in HMS (aged 50 days)

Cultivar	Mycorrhizal Colonization (%)	Height of the plant (cm)		Plant fresh weight (g)		Plant dry weight (g)	
		Shoot	Root	Shoot	Root	Shoot	Root
Mahyco	82	35.03 ± 0.76	14.5 ± 0.4	10.43 ± 0.35	6.33 ± 0.32	1.91 ± 0.02	1.16 ± 0.02
Rashi	75	29.4 ± 0.29	12.56 ± 0.28	9.76 ± 0.3	4.9 ± 0.26	1.44 ± 0.03	0.86 ± 0.2
kaveri	71	25.63 ± 0.2	11.93 ± 0.25	9.66 ± 0.15	4.53 ± 0.25	1.31 ± 0.02	1 ± 0.04
Marvel	70	24.7 ± 0.19	12.06 ± 0.11	9.13 ± 0.25	4.3 ± 0.2	1.29 ± 0.01	0.93 ± 0
Obama	70	24.23 ± 0.15	11.16 ± 0.25	9.23 ± 0.15	3.9 ± 0.2	1.26 ± 0.01	0.89 ± 0.01
Nusun	68	21.73 ± 0.11	10.6 ± 0.2	8.73 ± 0.2	3.6 ± 0.2	1.21 ± 0.02	0.82 ± 0.02
Raj seeds	62	20.7 ± 0.3	10.23 ± 0.15	8.63 ± 0.11	3.36 ± 0.15	1.12 ± 0	0.79 ± 0.01
Sunny	57	20.56 ± 0.15	9.7 ± 0.2	8.36 ± 0.15	3.33 ± 0.11	1.06 ± 0.01	0.78 ± 0.02

After 50 days of cultivation, the Mahyco cultivar exhibited a peak mycorrhizal colonization rate of 82%, showcasing significant growth in both plant height and weight. Remarkably, it demonstrated maximal shoot and root lengths. Subsequent to the 50-day growth period, the Mahyco plant underwent transplantation into

sterile soil. During this transfer, the root zone underwent three thorough washes with sterile water and received a mercuric chloride treatment to eliminate any adhered particles. The seedling was carefully situated in a pot filled with sterile soil, and stringent laboratory conditions were maintained to foster its robust growth over the ensuing five (5) weeks.

Following a 5-week growth period (Table-2), the roots were carefully extracted to assess mycorrhizal colonization, revealing a recorded rate of 62% based on the methodology outlined by (13). Additionally, 8-10 spores were isolated using the Wet Sieving and Decanting method and subsequently mounted on coverslips for identification, referencing the Schenk and Perez manual from 1987, leading to their classification as *Glomus mosseae*. These spores were then propagated through a funnel experiment, a technique described by (33), spanning a period of 7-14 days.

Throughout this germination phase, the seeds had direct contact with the mycorrhizal spores, minimizing the likelihood of spore unavailability under controlled conditions. Following germination, the setup was transferred to a sterile pot environment for the extensive cultivation of spores.

Table-2: Growth parameters of Mahyco cultivar in sterile soil aged 5 weeks.

Cultivar	Mycorrhizal Colonization (%)	Height of the plant (cm)		Plant fresh weight (g)		Plant dry weight (g)		Isolated Spore
		Shoot	Root	Shoot	Root	Shoot	Root	
Mahyco	85%	44.9±0.19	15.4±0.2	12.46±0.25	7.53±0.23	2.05±0.04	1.26±0.02	Glomus mosseae

Efficacy of Glomus mosseae in four diverse soil samples

Based on the findings outlined in Table-4, it is apparent that the presence of *Glomus mosseae* arbuscular mycorrhizal fungi (AMF) spores significantly contribute to promoting plant growth. In an effort to address poor plant growth conditions, as elaborated in the 'Materials and Methods' section, four distinct soil samples were subjected to NPK and trace element analyses (refer to Table-3). These soils underwent treatment with *Glomus mosseae* AMF spores, with an uninoculated sample serving as a control. The Mahyco cultivar was cultivated in these diverse soils over a 50-day period to assess the efficacy of AMF under natural conditions.

Table-3: Physico chemical characteristics of four diverse cotton soils.

Location	Soil type	pH	N	P	K	S	Fe	Mn	Zn	Cu
Malleboinpally	Shallow black soil	8.0	220.14	91.72	121.84	8.6	2.32	23.24	0.31	0.23
Chitteboinpally	Red soil	7.0	189.68	85.15	102.69	9.8	4.57	25.31	1.02	0.22
Kalwakurthy	Deep black	8.0	235.23	102.58	138.12	8.0	2.12	31.21	0.32	0.52
Divtipally	Sandy soil	8.0	175.87	76.92	91.75	9.8	0.12	12.25	0.18	0.04

Across all soil types, Mahyco exhibited favourable growth parameters and phosphorus content. The most substantial growth and phosphorous content were observed in deep black soil, followed by shallow black soil. Conversely, sandy soil displayed comparatively less growth, and red soil exhibited the least growth and phosphorous content, as detailed in Table-4.

Table-4: Growth parameters of Mahyco inoculated with *Glomus mosseae* (G.m) in four different soils of Mahbubnagar district. (aged 50 days).

Soil Type	Location	Combination	Height of the plant (cm)		Plant fresh weight (g)		Plant dry weight (g)		P content (%)	Mycorrhizal Colonization (%)
			Shoot	Root	Shoot	Root	Shoot	Root		
Sandy Soil	Narayanpet	Control	18.53±0.15	10.76±0.15	2.06±0.15	1.2±0.19	0.55±0.01	0.36±0.02	0.13±0.01	-
		M+G.m	41.7±0.19	20.53±0.15	7.73±0.11	3.5±0.2	1.96±0.02	1.16±0.01	0.17±0.02	57
Deep black Soil	Kalwakurthy	Control	20.63±0.2	12.23±0.15	3.56±0.15	1.7±0.1	1.46±0.02	0.76±0.02	0.2±0.01	-
		M+G.m	50.26±0.11	24.33±0.2	9.23±0.15	4.66±0.15	3.49±0.02	2.13±0.01	0.33±0.02	68
Shallow black Soil	Jadcherla	Control	19.9±0.2	11.13±0.11	2.93±0.15	1.03±0.15	0.96±0.01	0.55±0.01	0.17±0.02	-
		M+G.m	48.53±0.15	23.53±0.15	8.5±0.19	4.16±0.15	3.16±0.01	1.8±0.01	0.27±0.01	65
Red Soil	Makthal	Control	19.33±0.11	11.13±0.15	2.63±0.11	1.33±0.15	0.65±0.01	0.43±0.02	0.16±0.01	-
		M+G.m	44.5±0.2	22.6±0.2	8.03±0.15	3.86±0.15	2.86±0.01	1.55±0.01	0.23±0.02	61

Cotton, being a mycotrophic plant, typically experiences enhanced growth and nutrient uptake through arbuscular mycorrhizal (AM) colonization. The symbiotic relationship between terrestrial plants and AM fungi (AMF) is well-established, and this association commonly results in improved nutritional status and overall fitness for the host plant (8, 27). Nonetheless, the role of slow AM colonization in cotton growth disorders remains uncertain, and it is unclear whether it is a symptom or the underlying cause of reduced plant growth (23).

To address nutrient deficiencies in the soil, mycorrhizal fungi play a crucial role in facilitating the uptake of mineral nutrients, thereby promoting plant growth (22). The symbiotic association of arbuscular mycorrhizal (AM) fungi is particularly impactful in supplying less mobile nutrients like phosphorus to the host plant through the roots, thereby mitigating the adverse effects of salt stress (35).

As highlighted by (23), arbuscular mycorrhizal (AM) fungi are recognized as bio ameliorators of salinity stress due to their adaptability to contaminated soils and their involvement in modulating biochemical processes. The pivotal role of AM fungi in supplying phosphorus to the plant is of significant importance, with the ability to solubilize phosphorus from the surrounding areas and make it available to the roots (28). In the case of the Mahyco variety, inoculation with AMF demonstrated the most substantial impact on both plant growth and nutrient uptake, accompanied by a noticeable increase in mycorrhizal root colonization.

Some authors assert that the most significant growth stimulation in plants by beneficial bacteria and fungi occurs when the plants face stressful conditions. In contrast, non-treated plants under similar conditions tend to exhibit poor performance (12, 23)

Research findings indicate that the initial colonization of arbuscular mycorrhizal (AM) fungi in cotton roots can commence within 2-4 weeks after planting, as noted by (2). During

seed germination in HMS, a symbiotic relationship forms with specific fungi in the rhizosphere, significantly promoting the growth of the cultivar and exhibiting high specificity for that particular cultivar. The fungi, as part of their reproductive cycle, produce spores. These spores may be released into the soil when conditions are suitable for dispersal and germination, as reported by (38) and (37). However, the precise timing of spore release from root-associated fungi may not follow a strict schedule or predictable timeline. This variability is influenced by diverse environmental and biological factors, including plant age, growth stage, soil temperature, moisture levels, and nutrient availability, all of which impact both the growth of mycorrhizal fungi and the propensity of cotton roots to establish symbiotic relationships. The fifty-day mark post-sowing is a critical juncture for assessing arbuscular mycorrhizal fungi (AMF) colonization; hence, agricultural traits were examined during this period. Within 36 days, over 80% of cotton roots situated 25 cm below the soil surface had developed mycorrhizal associations at the inoculation point, with subsequent secondary spread occurring in a span of 10–13 days (13, 36).

The HMS Host-Specific Selection method emerges as a promising solution to address challenges posed by climate change and the obstacles associated with developing efficient bioinoculants, including cost, time, and the complex study of genetic factors influencing specificity. This innovative approach ensures the long-term sustainability of agricultural productivity. The method, as demonstrated, successfully identifies and isolates geographically specific arbuscular mycorrhizal fungi (AMF) spores tailored to the host plant, such as the Mahyco cultivar and *Gossypium herbaceum,* emphasizing high plant specificity within forest soil HMS. Given its reliance on the availability of various spores under specific climatic conditions and its adaptability to interactions between the plant and soil, this method holds global applicability for developing efficient bio-inoculants tailored to specific plants. The overarching aim is to contribute to environmentally friendly and sustainable agricultural practices worldwide.

Unlike traditional random selection for mycorrhizal spore, this method distinguishes itself by referring to and exploring natural combinations. This technique could be the most effective for isolating novel, efficient mycorrhizal spore. This method demonstrates that the isolated spores are specific to the Cotton cultivar Mahyco.

The efficiency of *Glomus mosseae* was assessed across four distinct cotton soil samples, revealing varying degrees of colonization, plant growth, and phosphorous content. Among these, deep black soil exhibited the highest levels, followed by shallow black soil, showcasing maximum colonization, plant growth, and phosphorous content. In contrast, sandy soil demonstrated the least colonization, plant growth, and phosphorous content, with red soil exhibiting values intermediate between sandy and black soils.

Conclusion

Successfully identifying and isolating geographically specific organisms for *Gossypium herbaceum*, particularly the highly plant-specific mycorrhizal spores from forest soil HMS, demonstrates the efficacy of our method. The approach relies on the availability of various mycorrhizal spores to the cotton plant under specific climatic conditions. The selection process is intricately determined by the interaction between the plant and mycorrhizae. As a result, this method holds universal applicability for developing efficient mycorrhizal spores tailored to the specific needs of cotton plants worldwide. The versatility of this method proves advantageous for fostering environmentally friendly and sustainable agricultural practices.

References

1. Abbott, L. K. and Robson, A. D. (1991). Factors influencing the occurrence of vesicular-arbuscular mycorrhizas. Agric Eco-

syst Environ, 35: 121–150.

2. Abdul Qayyum (2013). Impact of Mycorrhizal Fungi on Cotton Yield and Nutrient Uptake in Calcareous Soil. Pakistan Journal of Botany.

3. Allen, M. F. (1996). The ecology of arbuscular mycorrhizas: a lookback into the 20th century and a peek into the 21st. Mycol Res, 100: 769–782.

4. Babu, K. S. and Manoharachary, C. (2003). Occurrence of Arbuscular Mycorrhizal fungi in Rhizosphere soils of some medicinal plants. Indian Phytopathology, 56: 223-227.

5. Bona, E. et al. (2017). Arbuscular mycorrhizal fungi and plant growth-promoting pseudomonads improve yield, quality and nutritional value of tomato: a field study. Mycorrhiza, 27: 1–11.

6. Bray, R. H. and Kurtz, L. T. (1945). Determination of total, organic, and available forms of phosphorus in soils. Soil Science, 59: 39-45.

7. Ceballos, I. et al. (2013). The in vitro mass-produced model mycorrhizal fungus, rhizophagus irregularis, significantly increases yields of the globally important food security crop cassava. PLoS One 8, e70633.

8. Daniella Hoffmann., Vierheilig H., Riegler P., and Schausberger, P. (2009). Arbuscular mycorrhizal symbiosis increases host plant acceptance and population growth rates of the two-spotted spider mite Tetranychus urticae, Oecologia, 158: 663–671.

9. David, B. Nehl., Allen, S. J. and Brown, J. F. (1998). Slow arbuscular mycorrhizal colonisation of field-grown cotton caused by environmental conditions in the soil, Mycorrhiza 8:159–167.

10. David, J. Read. (1998). Mycorrhiza - the state of the art. In: Varma A., Hock B. (eds) Mycorrhiza, Springer, Berlin, 3–34.

11. Delavaux, C. S. et al. (2017). Nutrient enrichment effects on mycorrhizal fungi in an Andean tropical montane Forest. Mycorrhiza, 27: 311–319.

12. Dilfuza Egamberdieva. (2013). Response of Maize to Bacterial Inoculants under Different Soil Conditions, Turkey International Plant Nutrition Colloquium, XVII: 583-585.

13. Feng, G., Zhang, FS., Li, X. L., Tian, C. Y., Tang, C. X., Rengel, Z. (2002). Uptake of nitrogen from indigenous soil pool by cotton plant inoculated with arbuscular mycorrhizal fungi. Communications In Soil Science and Plant Analysis, 33: 3825-3836.

14. Giovannetti, M. and Mosse, B. C. (1980). An evaluation of techniques for the measuring VAM infection in roots. New Phytologist, 84: 489-500.

15. Gosling, P. et.al., (2006). Arbuscular mycorrhizal fungi and organic farming. Agriculture, Ecosystem and Environment, 133: 17-35.

16. Gu Feng., Zhang, F.S., Li, X. l., Tian, C.Y., Tang C., and Rengel, Z. (2002). Improved tolerance of maize plants to salt stress by Arbuscular mycorrhiza is related to higher accumulation of soluble sugars in roots, Mycorrhiza, 12: 185–190.

17. Hoagland and Arnon. (1938). *The water-culture method for growing plants without soil* (Circular (California Agricultural Experiment Station), 347. ed.), Berkeley, Calif.: University of California, College of Agriculture, Agricultural Experiment Station. OCLC 12406778.

18. Irene, M., Cardoso., Thomas., and Kuyper, W. (2006). Mycorrhizas and tropical soil fertility. Agriculture, Ecosystem and Environment. 116: 72-84.

19. Jackson, M. L. (1973). Soil chemical analysis, prentice hall of India Pvt. Ltd., New Delhi, India, 498: 151-154.

20. Majewska, M. L., Rola, K. & Zubek, S. (2016). The growth and phosphorus acquisition of invasive plants Rudbeckia laciniata and Solidago gigantea are enhanced by arbuscular mycorrhizal fungi. Mycorrhiza, 27: 83–94.

21. McGee, P. A., Torrisi, V. & Pattinson, G. S. (1999). The relationship between density of *Glomus mosseae* propagules and the initiation and spread of arbuscular mycorrhizas in cotton roots. Mycorrhiza, 9: 221–225.

22. Mozafar Sharifi., Ghorbanli, M., and Ebrahimzadeh, H. (2007). Improved growth of salinity-stressed soybean after inoculation with salt pre-treated mycorrhizal fungi. Plant Physiol, 164:1144–1151.

23. Neera Garg, Baher, N. (2013). Role of arbuscular mycorrhizal symbiosis in proline biosynthesis and metabolism of Cicer arietinum L. (Chickpea) Genotypes Under Salt Stress. Plant Growth Regul, 32: 767–778.

24. Nehl, D. B., Allen, S.J. and Brown, J.F. (1998). Slow arbuscular mycorrhizal colonisation of field grown cotton caused by environmental conditions in the soil. Mycorrhiza, 8(3):159-167.

25. Phillips, J.M., (1970). Hayman's improved procedure for clearing and staining parasitic and vesicular-Arbuscular mycorrhizal fungi for assessment of infection. Transactions of the British Mycological Society, 55: 158.

26. Rahimzadeh, S. & Pirzad. (2017). Arbuscular mycorrhizal fungi and Pseudomonas in reduce drought stress damage in flax (Linum usitatissimum L.)-a field study. Mycorrhiza, 27:s 537–552.

27. Read, D. J., Ducket, T. J. G., Francis, R., Ligrone, R. and Russell, A. (2000). Symbiotic fungal associations in lower land plants. Royal Society, Phil Trans R Soc, 815-831.

28. Rishi, K., Behl., Sharma, H., Kumar, V., and Narula, N. (2003). Interactions amongst mycorrhiza, Azotobacter chroococcum, and root characteristics of wheat varieties. Agronomy and Crop Science, 189:151–155.

29. Schenck, N. C., and Perez, Y. (1987). Manual for the identification of Vesicular Arbuscular Mycorrhizal INVAM. Florida University, Gainseville, USA. Pp. 245.

30. Schübler, A., Krüger, C. & Urgiles, N. (2016). Phylogenetically diverse AM fungi from Ecuador strongly improve seedling growth of native potential crop trees. Mycorrhiza, 26: 199–207.

31. Schumacher, B. A., Shines, K. C., Burton, J. V., and Papp, M. L. (1990). Comparison of three methods for soil homogenization. Soil Science Society of America Journal, 54(4): 1187-1190.

32. Smith Sally, E., and Andrew Smith, F. (2011). Roles of Arbuscular Mycorrhizas in Plant Nutrition and Growth: New Paradigms from Cellular to Ecosystem Scales. Annual Review of Plant Biology, 62: 227-250.

33. Smith, S. E. and Read, D. J. (2008). Mycorrhizal symbiosis. Q Rev Biol, 3: 273–281.

34. Smith, S.E., and Read, D.J. (2008). Mycorrhizal symbiosis. 3rd edn. Academic press. Spring Harbor Laboratory Press, New York.

35. Subbiah, B.V., Asija, G.L. (1956) A rapid procedure for the estimation of available nitrogen in soils. Curr Sci, 25: 259-260.

36. Tasleem Sultana., and Pavan Kumar Pin-

di. (2012). Role of Arbuscular Mycorrhizae (AM) Fungi and Multi Bioinoculants in Cotton Plant Growth. British Microbiology Research Journal, 2(3): 123-130.

37. Tian, C.Y., G. Feng., Li, X.L. and Zhang, F.F. (2004). Different effects of arbuscular mycorrhizal fungal isolates from saline or non-saline soil on salinity tolerance of plants. Appl Soil Ecol, 26: 143-148.

38. Vazquez, M., Cesar, S., Azcon, R., Barea, J.M. (2000). Interactions between arbuscular mycorrhizal fungi and other microbial inoculants (Azospirillum, Pseudomonas, Trichoderma) and their effects on microbial populations and enzyme activities in the rhizosphere of Maize plants. Appl Soil Ecol, 15(3): 261-272.

39. Xinpeng, Gao., Huihui Guo., Qiang Zhang., Haixia Guo., Li Zhang., Changyu Zhang., Zhongyuan, Gou., Yan Liu., Junmei Wei., Aiyun chen., Zhaohui chu. and Fanchang Zeng. (2020). Arbuscular mycorrhizal fungi (AMF) enhanced the growth, yield, fiber quality and phosphorus regulation in upland cotton (*Gossypium hirsutum L*.). Scientific Reports, 10: 2084. https://doi.org/10.1038/s41598-020-59180-3.

40. Xiu-Hua Chen., Feng-Ling Wang., Rui Zhang., Ling-Ling Ji., Zheng-un-Yang., Hui Lin. and Bin Zhao. (2016). Evidences of inhibited arbuscular mycorrhizal fungal development and colonization in multiple lines of *Bt* cotton. Agriculture Ecosystems & Environment, 230: 169-176.

41. Zak, J.C., McMichael, B., Dhillion, S., Friese, C. (1998). Arbuscular-mycorrhizal colonization dynamics of cotton (*Gossypium hirsutum L*) growing under several production system on the southern high plains, Texas. Agriculture Ecosystem and Environment, 68(3): 245-254.

Current Trends in Biotechnology and Pharmacy
Vol. 18(3) 1850-1865, July 2024, ISSN 0973-8916 (Print), 2230-7303 (Online)
10.5530/ctbp.2024.3.32

Development and Evaluation of Sulfate-Free Charcoal Toothpaste from Coconut Shell and Rice husk

Sheba R David[1], Norhadyrah Izazie Ahad[2], Ashok Kumar Balaraman[3], Rajan Rajabalaya[2]*

[1]School of Pharmacy, University of Wyoming, Laramie, Wyoming, 82071, USA
[2]PAPRSB Institute of Health Sciences, Universiti Brunei Darussalam, Jalan Tungku Link BE1410, Bandar Seri Begawan, Brunei Darussalam
[3]Centre for Research and Innovations, University of Cyberjaya, Persiaran Bestari 63000 Cyberjaya, Malaysia
*Corresponding author: rajan.rajabalaya@ubd.edu.bn

Abstract

Toothpaste containing sulfate is one major concern as it is known as irritating and causes adverse effects in the oral cavity. Hence, a sulfate-free toothpaste is much more preferred nowadays. This research paper discusses on three sulfate-free toothpaste formulations that were prepared and optimized containing two types of charcoal namely activated coconut shell charcoal and rice husk charcoal. The formulations differ in the binding agents and surfactants used and they are evaluated based on 13 physiochemical characterizations including organoleptic properties, pH, foamability, spread ability, tube extrudability, moisture content, FTIR spectroscopy, cleaning test, toxicity assay, stability, abrasiveness, grittiness and morphological evaluation. One commercial toothpaste was also included in the test to be used as comparison. The objectives of this research are to prepare and optimize sulfate-free toothpaste formulations with natural charcoal from coconut shell and rice husk, evaluate the toothpaste formulations for physiochemical characterization, stability, toxicity and their effectiveness (cleaning test). Menthol crystals were dissolved in Propanediol and rice husk charcoal were grinded with mortar and pestle. All solid ingredients (including activated coconut shell charcoal, carrageenan, sodium dodecyl sulfate (SDS) and Sangelose) were then mixed together with a small amount of distilled water. After transferring to a white tile, liquid ingredients were added to the solid mixtures and mixed thoroughly using spatulas. The liquid ingredients included were dissolved menthol, liquid surfactants (including decyl glucoside (DG) and Tween-80 (T-80), glycerin, triethanolamine and coconut oil. Finally, distilled water was added gradually until a paste consistency was formed. Three toothpaste formulations have been developed namely F1, F2 and F3 of which varied in the binding agent and surfactant used. All toothpaste formulations showed results similar to commercial toothpaste in terms of appearance, odour, smoothness, tube extrudability, cleaning test and grittiness. F1 have the highest basic pH (9.78) and highest foamability (14 mL) among the toothpaste formulations. However, F1 have the lowest germination index (48.1%) indicating that it is most toxic than the others including the commercial toothpaste. In conclusion, all three toothpaste formulations were able to achieve the desired and acceptable characteristics with the physiochemical characterization. This study might provide good scope and be useful for further research as being a sulfate-free toothpaste that uses renewable waste activated coconut shell charcoal and rice husk charcoal as the abrasive ingredients and is capable of improving and maintaining oral hygiene.

Keywords: Charcoal toothpaste, Sulfate-free toothpaste, Coconut shell, Rice husk

Introduction

Around 300 to 500 BC, toothpaste formulation designs can be found to begin in China and India where squashed bones and clamshells were used as abrasives to clean teeth (1,2). In the Middle Ages, the primary ingredients used to clean teeth in the Arab were fine sand and pumice (3). In 2020, about 307 million people in the United States have used toothpaste and this might rise to 316 million in 2024 (4). Toothpaste can be defined as a semi-solid dentifrice that cleans and maintains good oral health of teeth by removing food particles, reduce plaque formation, reduce stain, polish the tooth surface and refreshes the breath (2, 5, 6). They present in the form of paste, gel, liquid or powder dentifrices and is to be used with a toothbrush simultaneously (3, 5). Toothpaste promotes and maintains oral hygiene with the help of the ingredients in the toothpaste and brushing mechanism from the toothbrush. Brushing twice a day for 2 minutes each is the most well-known recommendation as a daily oral care routine.

Recently, a number of commercial dentifrices have been using coconut shell activated charcoal in their ingredient, either in the form of powder or paste and are used to whiten teeth. A coconut shell is the hard outer part of a coconut fruit located between the coconut husk and coconut flesh. Charcoal is produced by the process of removing water and other volatile elements from carbon-based materials such as coconut shell, coconut husk and wood. Moreover, charcoal can be activated with high temperature and gases to increase its porosity which results in activated charcoal (7).

Historically, in India, burnt rice husk in powder form have been used to clean the teeth over centuries and nowadays, activated charcoal made from rice husk was seen to be available, but not widely, as powder for teeth-cleaning. Rice husk, also referred as rice hull, is the outermost layer of the rice grain. They provide protective cover to the grain and have an elongated convex shape (8). Rice husks are the by-product of rice production milling process and are considered as agricultural wastes obtained from the milling process in large quantity. They have been recycled to be used for various purposes including as fuel to be burnt as energy, used in manufacturing, strengthening construction materials and used as raw materials such as for metal polishing agent (8,9).

Numerous common ingredients can be found in toothpaste including abrasives, binders, surfactants, humectants, preservatives, sweeteners and flavours (6). Glycerine functions as a humectant that prevents loss of moisture from the toothpaste (10). It ensures that the toothpaste remains in a moist condition preventing the toothpaste formulation from drying out (3, 11). Like thickening agents, humectants also affect the consistency and stability of the toothpaste in a long term. Having good water retention will result in glossy or shiny toothpaste formulation with an appealing texture within the mouth (12). In cosmetic industry, triethanolamine functions as preservatives, pH adjusters as well as surfactants (13). Sorbitol acts as a primary sweetening agent and humectant (10). Sweeteners work together with the flavorings by adding sweetness to the toothpaste formulation (12). One common flavouring agent is menthol that are used to refresh oral cavity and gives off cooling sensation (14). While, propanediol function as a solvent that helps in dissolving low-soluble ingredients, boosts preservative and enhance viscosity (13).

Common toothpaste usually uses Sodium Lauryl Sulfate (SLS) as the surfactant or foaming agent. However, SLS is known to be an irritating ingredient and might cause adverse effects such as oral mucosa inflammation which might develop into aphthous mouth ulcers or canker sores. It can also cause skin and eye irritation (3, 5, 15). Being a sulfate-free toothpaste has the advantage of being less irritating than those toothpaste containing Sodium Lauryl Sulfate. This is a common ingredient found

in commercial toothpastes and they are known to might cause adverse effects affecting the oral mucosa and skin (3). Hence, a more natural-based and sulfate-free toothpaste is usually much preferred.

Therefore, this is the first study to combine coconut shell charcoal and rice husk charcoal to develop a natural-based, safe and effective sulfate-free toothpaste formulation. In order to determine whether the formulated toothpaste is ideal, physiochemical characterization was done. Common tests that were done in previous literature include foamability, stability test, abrasiveness and cleaning test to check toothpaste effectiveness as well as toxicity assay to ensure the safety of the toothpaste formulation. An ideal toothpaste must be non-toxic, have a good abrasive effect for cleaning, non-irritant, have a prolonged effect keeping the mouth clean and fresh, impart no stain on the teeth, stable in a long-term and is easily available at an affordable price (2). The objectives of this research are to prepare and optimize sulfate-free toothpaste formulations with natural charcoal from coconut shell and rice husk, evaluate the toothpaste formulations for physiochemical characterization, stability, toxicity and their effectiveness (cleaning test).

Materials and methods

Chemicals

Activated coconut shell charcoal (Micronized activated charcoal powder, Take it Global, Penang, Malaysia) and rice husk charcoal (prepared in UBD) were used as abrasives. Carrageenan (Sigma-Aldrich, Missouri, United States of America) and Hydroxypropyl Methylcellulose Stearoxy Ether (Sangelose 60L, Daido Chemical Corporation, Osaka, Japan) were used as binding agents. Three surfactants were included which were Sodium dodecyl sulphate (Surechem Products Ltd, Suffolk, England), Decyl glucoside (C18-C16 Glucoside, Ecosense 3000, Dow Chemicals, United States of America) and Tween-80 (Polysorbate 80, Merck KGaA, Darmstadt, Germany). Glycerin (Propane-1,2,3, triol, Surechem Products Ltd, Suffolk, England) as humectant, triethanolamine (Glentham Life Sciences, Corsham, United Kingdom) as preservative, sorbitol (D-Sorbitol, Glentham Life Sciences, Corsham, United Kingdom) as sweetening agent, Menthol (L-Menthol, Glentham Life Sciences, Corsham, United Kingdom) as flavouring agent. Propanediol (Propane-1,3-diol, Zemea, Formulator Sample Shop, Milan, Italy) was used as dissolvent to dissolve the menthol crystals. Finally, Cocos Nucifera (Coconut) oil, bought from local market, as a defoaming agent and distilled water as the carrier. Three toothpaste formulations were developed and their compositions are shown in Table 1.

Table 1 Ingredients and compositions of the toothpaste formulations

No.		Formula (%w/w)		
	Formulation code	F1	F2	F3
	Ingredients			
1	Activated coconut shell charcoal	32.3	32.3	32.3
2	Rice husk charcoal	1.0	1.0	1.0
3	Carrageenan	1.7	-	-
4	Sangelose	-	1.7	1.7
5	Sodium Dodecyl Sulphate (SDS)	6.7	-	-
6	Decyl Glucoside (DG)	-	6.7	-
7	Tween-80 (T80)	-	-	6.7
8	Glycerin	1.7	1.7	1.7
9	Triethanolamine	1.7	1.7	1.7
10	Sorbitol	2.0	2.0	2.0
11	Menthol	1.0	1.0	1.0
12	Propanediol	13.3	13.3	13.3
13	Coconut oil	3.3	-	-
14	Distilled water	q.s.	q.s.	q.s.

w/w: weight by weight; F1: Formulation 1; F2: Formulation 2; F3: Formulation 3; q.s.: quantum sufficient

Menthol crystals were dissolved in Propanediol and rice husk charcoal were grinded

with mortar and pestle. All solid ingredients (sequence blue) were then mixed together with a small amount of distilled water. After transferring to a white tile, liquid ingredients were added to the solid mixtures and mixed thoroughly using spatulas. The liquid ingredients included were dissolved menthol, liquid surfactants (DG and T80), glycerin, triethanolamine and coconut oil. Finally, distilled water was added gradually until a paste consistency was formed (16).

Physiochemical characterization

The three toothpaste formulations as well as one commercial toothpaste were evaluated according to the 13 physiochemical characterizations listed below.

Organoleptic properties

The organoleptic properties evaluated were colour, appearance, odour and smoothness (texture) of the toothpaste formulations. The colour and appearance were checked visually and the odour was checked by smelling the formulation. While the smoothness was assessed by rubbing the formulation in between the fingers (1,16)

pH

The pH was measured by using a digital pH meter FiveEasy (Mettler Toledo, Greifensee, Switzerland). A suspension of the toothpaste was made by taking 1g of the formulation in a 25mL beaker with 10mL of distilled water. Then after stirring well, the pH was determined within 5 minutes (2)

Foamability

About 1g of formulated toothpaste was taken and stirred with 5 mL of distilled water in a 25 mL beaker. Taken into a 25mL measuring cylinder and V2 was recorded (volume of water only). With a gloved hand covering the top, the measuring cylinder was shaken vertically for 10 times. Foams were formed and V1 was recorded (volume of foam with water) (1,16,17)

The foamability can be determined by using the formula below:

where,

V1 – Volume of foam with water (mL)

V2 – Volume of water only (mL)

Spreadability

About 1g of the toothpaste formulation was placed on a white tile. A glass petri dish below a conical flask containing water (total weight was about 400g) was placed carefully at the centre of the formulation. Then, the diameter of the toothpaste was measured after 15 minutes have passed (18)

Tube extrudability

The formulated toothpaste was filled in a small plastic tube. Tube extrudability was determined by pressing the tube with normal force at room temperature and checking whether the toothpaste extrude homogeneously (19)

Moisture content

Moisture content was determined by using moisture analyzer MOC63U (Shimadzu Corporation, Kyoto, Japan) and the temperature was set at 105°C. About 1g of the formulated toothpaste was placed and the final moisture content was recorded (20).

Fourier transform infrared spectroscopy

Fourier transform infrared (FTIR) spectrophotometer IRSpirit (Shimadzu Corporation, Kyoto, Japan) was used to confirm the functional groups in the formulated toothpaste. They were characterized in attenuated total reflection mode over a wavenumber range from 4000 to 500 cm-1. A number of 30 scans was set and the measurement mode was in percentage transmittance (21)

Cleaning test

Eggshells were used due to their high amount of calcium, resembling tooth enamel

and hence were suitable for the cleaning test. About 200ml of water were boiled in a beaker and 15 ml of vinegar as well as 20 drops of red food colour were added. A hard-boiled egg was immersed in the beaker and let sit for 5 minutes to be stained. After that, a line was drawn dividing the egg into half (one side of the egg was the control). A pea-sized (about 0.25g) formulated toothpaste was taken on to a moist toothbrush and brushed on one side of the egg with circular and back-and-forth motion for a total of 10 strokes. Then, the egg was rinsed and the red stain removal was inspected for presence or absence (19)

Toxicity assay

In order to check for the toxicity of the formulated toothpaste, a toxicity assay was done based on seed germination index. Mung beans were soaked overnight for about 12 hours. Once sterilized with distilled water, 20 seeds were placed in each container containing cotton wool pads (each container for each formulation). For a period of 5 days, about 5-10 mL of formulated toothpaste suspensions and distilled water (as control) were added to their respective containers for twice daily at room temperature to grow the seeds. Then, relative seed germination (RSG), relative root length (RRL) and germination index (GI) were determined according to the formulas below (11).

$$RSG\ \% = \frac{number\ of\ seeds\ germinated\ in\ test}{number\ of\ seeds\ germinated\ in\ control} \times 100$$

$$RRL\ \% = \frac{average\ root\ length\ in\ test}{average\ root\ length\ in\ control} \times 100$$

$$GI = \frac{RSG\ \% \times RRL\ \%}{100}$$

Stability

The formulated toothpaste was filled in Scott bottles and were stored at two different conditions which were 25°C ± 2°C with 60% ±5% relative humidity (RH), and at 40°C ± 2°C with 75% ±5% RH for a period of 30 days (Day 0 as control). The organoleptic properties, pH, foamability, spreadability, tube extrudability, moisture content and cleaning test were then evaluated for stability (16,17)

Abrasiveness

On a plastic microscopic slide, a pea-sized amount (about 0.25g to 0.5g) of formulated toothpaste was placed and 2 drops of distilled water was added. In a back-and-forth motion, the formulated toothpaste was rubbed using a cotton swab with short strokes (about 2 cm) for 30 times. The slide was rinsed carefully and dried with soft tissue. Then, the intensity of scratches on the surface of the slide was rated visually with a scale of 0 (no scratch) to 5 with 5 having a high degree of scratches (19)

Grittiness

A pea-sized amount (0.25g to 0.5g) of formulated toothpaste was placed on a piece of butter paper and was rubbed using a finger with 30 strokes in a back-and-forth motion. The grittiness was determined as present or absent (19).

Morphological evaluation

About 1-2 drops of formulated toothpaste suspension was placed on a microscope slide. After a cover slip was set, the slide was taken to the digital microscope imager (Celestron, California, United States of America) which was used to observe and capture high resolution images. Then, morphological evaluation was done.

Statistical analysis

Each test was performed in triplicates. Mean, standard deviation (SD) and one-way ANOVA (analysis of variance) statistical analysis were done using GraphPad Prism (version 8.4.3). Data were presented as mean ± SD and p-value less than 0.05 were reported as statistically significant.

Results and Discussion

The results obtained from this research are presented in the tables below. Table 2

shows 9 physiochemical characterization results. A comparison can then be made between each toothpaste formulations and the commercial toothpaste. With reference to Table 2, excluding the colour, the toothpaste formulations and commercial toothpaste have similar organoleptic properties which have a smooth texture, a paste-like appearance and gave off a pleasant smell with minty odour. They also showed good tube extrudability, good cleaning ability and absence of gritty matters. All toothpaste formulations resulted with a scale of 4 in abrasiveness test while commercial toothpaste have a scale of 2.

Table 2: Physiochemical characterization results

Formulations	F1	F2	F3	Commercial
Colour	Matte black	Glossy black	Glossy black	Glossy white-grey stripes
Appearance	Paste-like	Paste-like	Paste-like	Paste-like
Odour	Pleasant	Pleasant	Pleasant	Pleasant
Smoothness	Smooth	Smooth	Smooth	Smooth
pH	9.78 ± 0.01***	9.33 ± 0.02***	9.39 ± 0.01***	7.03 ± 0.01
Foamability (mL)	14.00 ± 1.00	3.00 ± 1.00***	3.00 ± 1.00***	16.00 ± 1.00
Spreadability (cm)	2.60 ± 0.10***	4.03 ± 0.35***	3.47 ± 0.15***	5.20 ± 0.17
Tube extrudability	Good	Good	Good	Good
Moisture content (%)	50.39 ± 0.40***	55.16 ± 1.64***	55.63 ± 0.32***	29.06 ± 0.26
Cleaning test	+	+	+	+
Abrasiveness	4.0	4.0	4.0	2.0
Grittiness	Absent	Absent	Absent	Absent

+: Presence. n=4. F1: Formulation 1; F2: Formulation 2; F3: Formulation 3. Asterisks (*) represents significant differences as compared to the commercial toothpaste (*** for p-value < 0.001). ANOVA with Tukey post-hoc test was done.

The pH of all toothpaste formulations was significantly higher than the commercial toothpaste ($p<0.001$). The pH ranges around pH 9 with F1 having the highest pH of 9.78 and F2 having the lowest pH of 9.33. While the commercial toothpaste has a lower pH with pH 7.03. Both F2 and F3 have similar foamability of 3mL which were significantly lower ($p<0.001$) than F1 and commercial toothpaste with 14mL and 16mL respectively. Furthermore, all toothpaste formulations showed significantly lower spreadability compared to commercial toothpaste ($p<0.001$). F1 gave the lowest spreadability of 2.60cm and F2 gave the highest with 4.03cm. However, commercial toothpaste gave a higher spreadability with 5.20cm. With significant results ($p<0.001$) compared to commercial toothpaste, F3 gave the highest moisture content of 55.63% and F1 have the lowest with 50.39%. On the other hand, commercial toothpaste has a much lower moisture content with 29.06%. According to Table 3, all tested samples obtained a relative seed germination of 100%. After measuring and obtaining the relative root length, germination index (GI) was calculated. Both F2 and F3 gave a high GI (100.8% and 103.2% respectively), while F1 have a significantly lower GI than the control with 48.1% ($p<0.001$) and the commercial toothpaste shows a GI of 70.6%.

Table 3: Toxicity assay results

Seed germination	F1	F2	F3	Commercial	Control
Number of seeds germinated	20	20	20	20	20
Relative seed germination (%)	100	100	100	100	-
Averageroot length (cm)	4.12 ± 2.00***	8.63 ± 3.59	8.84 ± 4.12	6.04 ± 2.17	8.56 ± 3.90
Relativeroot length (%)	48.1	100.8	103.3	70.6	-
Germination index (%)	48.1	100.8	103.2	70.6	-

n=5; F1: Formulation 1; F2: Formulation 2; F3: Formulation 3; Relative comparison with control; (distilled water); Root length assessment conducted on Day 6 (n=20); Relative Root Length was compared to the control (distilled water); Asterisks (*) represents significant differences as compared to the control (distilled water) (*** for p-value < 0.001). ANOVA with Bonferroni post-hoc test was done.

After completing the 30 days period for stability test, all formulations have shown to remain stable when tested (Table 4). ANOVA with Bonferroni post-hoc test was used for statistical analysis. The pH of all toothpaste formulation has decreased significantly ($p<0.05$) after 30 days in both storage conditions. The moisture content was shown too increased significantly as well in all formulations ($p<0.01$). On the other hand, there were no significant changes in foamability and spreadability.

Table 4 Stability results

Formulations	F1			F2			F3		
Day	0	30		0	30		0	30	
Temperature(°C)	25	25	40	25	25	40	25	25	40
Relative humidity (%)	60	60	75	60	60	75	60	60	75
Colour	Matte black	Matte black	Matte black	Glossy black	Glossy black	Glossy black	Glossy black	Glossy black	Glossy black
Appearance	Paste-like	Paste-like	Paste-like	Paste-like	Paste-like	Paste-like	Paste-like	Paste-like	Paste-like
Odour	Pleasant	Pleasant	Pleasant	Pleasant	Pleasant	Pleasant	Pleasant	Pleasant	Pleasant
Smoothness	Smooth	Smooth	Smooth	Smooth	Smooth	Smooth	Smooth	Smooth	Smooth
pH	9.78 ± 0.01	8.60 ± 0.01*	8.45 ± 0.02*	9.33 ± 0.02	8.53 ± 0.01*	8.32 ± 0.01*	9.39 ± 0.01	8.66 ± 0.01*	8.36 ± 0.01*
Foamability (mL)	14.00 ± 1.00	7.67 ± 0.58	11.33 ± 0.58	3.00 ± 1.00	2.67 ± 0.58	2.33 ± 0.58	3.00 ± 1.00	2.33 ± 0.58	2.00 ± 0.00
Spreadability (cm)	2.60 ± 0.10	2.90 ± 0.26	2.80 ± 0.10	4.03 ± 0.35	3.93 ± 0.06	4.37 ± 0.25	3.47 ± 0.15	4.30 ± 0.10	3.87 ± 0.12
Tube extrudability	Good	Good	Good	Good	Good	Good	Good	Good	Good
Moisture content (%)	50.39 ± 0.40	56.30 ± 1.64**	55.88 ± 3.01**	55.16 ± 1.64	59.96 ± 0.62**	61.69 ± 1.18**	55.63 ± 0.32	61.36 ± 0.38**	61.54 ± 0.28**
Cleaning test	+	+	+	+	+	+	+	+	+

+: Presence. n=6: F1: Formulation 1; F2: Formulation 2; F3: Formulation 3; Asterisks (*) represents significant differences as compared to the control, Day 0 at 25°C (* for p-value < 0.05 and ** for p-value <0.01). ANOVA with Bonferroni post-hoc test was done

FTIR analysis were done to observe the functional groups in the formulations. In Figure 1-4, FTIR spectra of toothpaste formulations have been compared with the coconut shell charcoal, rice husk charcoal as well as their respective distinctive ingredients (binding agent and surfactants). The microscopical images of simple mixture of activated coconut shell charcoal (microparticle) and rice husk charcoal shown in the Figure 5A. It is clear that, microparticle based coconut shell charcoal uniformly distributed and appeared, whereas rice husk charcoal (non-microparticle) appeared clump mass in the images. Formulated toothpaste and commercial toothpaste microscopical photographs are Figure 5, such as B - F1, C- F2, D - F3 and E- commercial toothpaste (F1- SDS; F2- DG; F3- T80 & commercial - SLS) respectively. The images were observed from different toothpaste formulation prepared by using different surfactants showing different morphological properties.

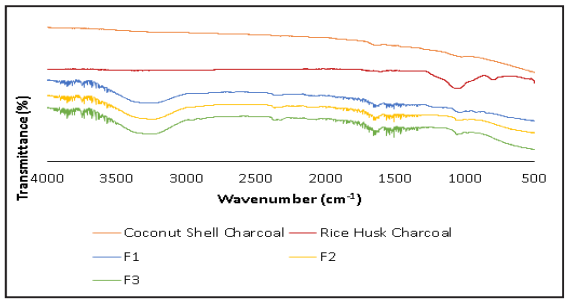

Figure 1 FTIR spectra of Coconut shell charcoal, Rice husk charcoal with the three toothpaste formulations. Abbreviations: F1 Formulation 1, F2 Formulation 2, F3 Formulation 3

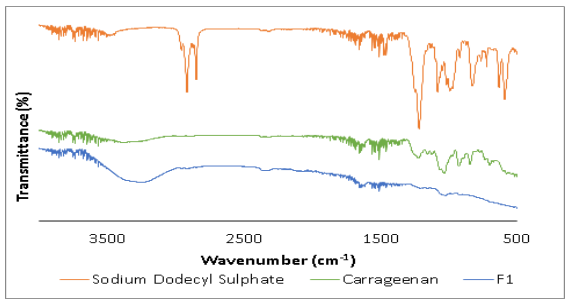

Figure 2 FTIR spectra of F1, Carrageenan and Sodium Dodecyl Sulphate (SDS). Abbreviations: F1 Formulation 1

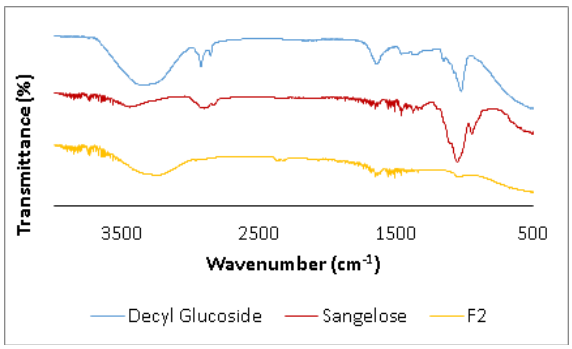

Figure 3 FTIR spectra of toothpaste F2 with Sangelose and Decyl Glucoside (DG). Abbreviations: F2 Formulation 2

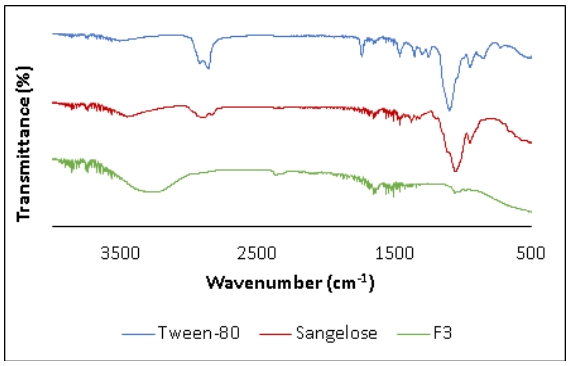

Figure 4 FTIR spectra of F3 with Sangelose and Tween-80 (T80). Abbreviations: F3 Formulation 3

Discussion

Coconut shells and rice husk are known as agricultural wastes generated in large quantities and are potential sources of carbon. They are often used as alternative energy sources by burning them, however, due to their abundant wastes, they can cause disposal problems. Hence, agricultural waste recycling should be done to solve this environmental pollution. One way is to use them as natural ingredients in producing safe and effective toothpaste.

Three different surfactants were used to formulate sulfate-free toothpaste which were Sodium Dodecyl Sulphate (SDS), Decyl Glucoside (DG) and Tween-80 (T80). Furthermore, carrageenan and Sangelose were used as the binding agents. In F1, the reason behind the

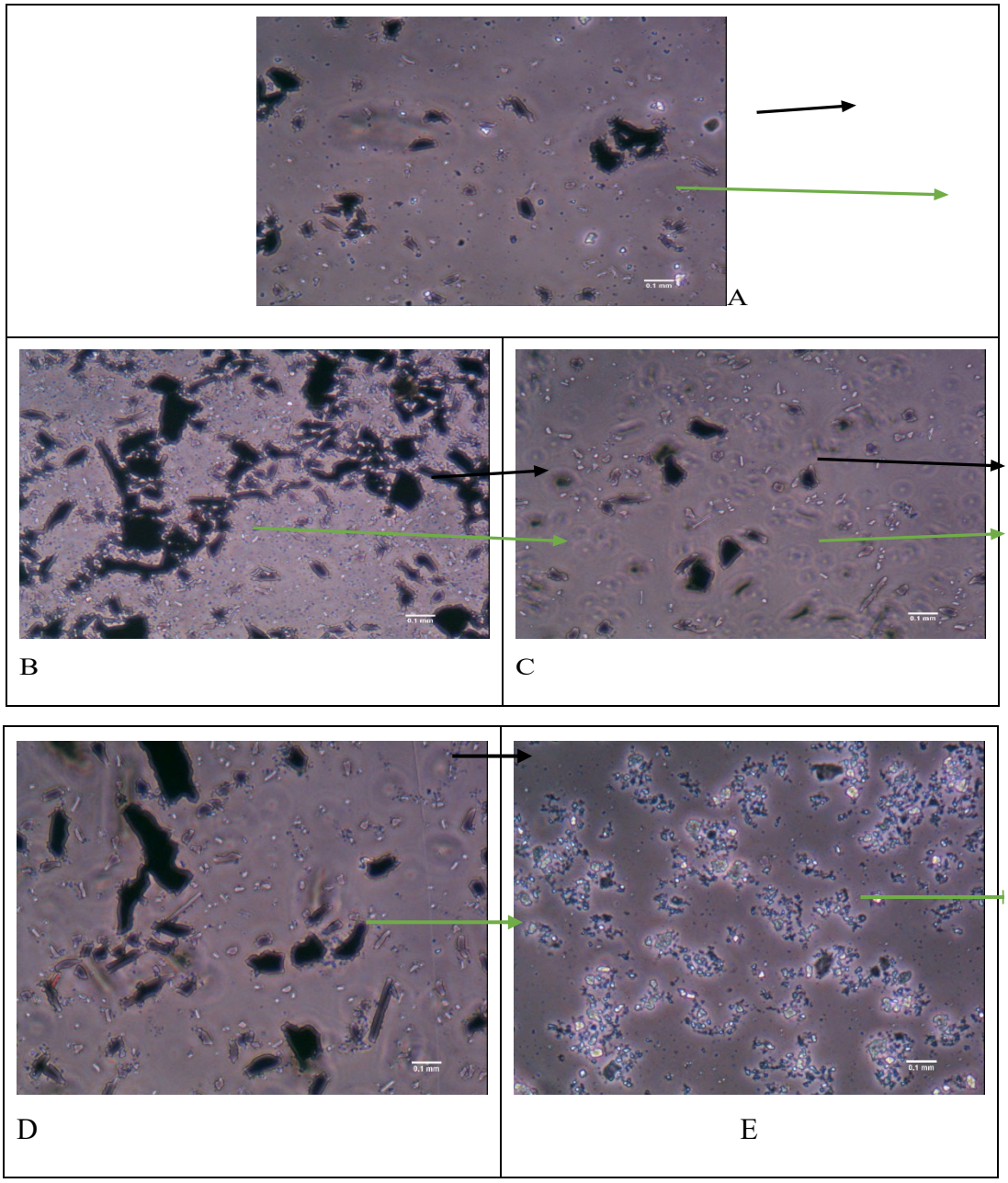

Figure 5: Microscopical photographs (20X) Figure 5A - Mixture of coconut shell charcoal and rice husk charcoal. With mixture of activated coconut shell charcoal and rice husk charcoal, toothpaste formulations were prepared by using different surfactants (Figure 5B- Sodium Dodecyl Sulphate; Figure 5C- Decyl Glucoside; Figure 5D- Tween-80). Figure 5E - Commercial toothpaste with SLS surfactant. BLACK LINE - Activated coconut shell charcoal (micro-particle); GREEN LINE - Activated rice husk charcoal (non-microparticle).

preparation stage. Thus, coconut oil acts as a defoaming agent to control foaming.

All three formulations appeared black colour which is due to the abundant main ingredient, activated coconut shell charcoal (32.3%) which is black in nature. Although glycerin plays a role in providing glossy or shiny appearance with appealing texture (12), the matte and glossy appearance of the formulation may also be due to the surfactants used. Both DG and Tween-80 produced a glossy finish while SDS gave off a matte appearance. All formulations have similar organoleptic properties with the commercial toothpaste that have a smooth texture, paste-like appearance and pleasant smell with minty odour. The minty odour in the formulations comes from the menthol crystals added (1%). These organoleptic properties of the formulation may enhance marketability (19).

All toothpaste formulation has obtained a pH lower than 10.5 which is the maximum pH for an ideal toothpaste (22). The pH in all three toothpaste formulations were in the alkaline region that ranges between 9.33 to 9.78. Alkaline pH was shown to cause less adverse changes to the surface of the teeth (19). While, a lower pH toothpaste promotes greater alteration to the enamel surface (23). The pH of a toothpaste is important in order to maintain the basic pH of the mouth. Basic medium prevents bacteria growth in the mouth that may cause teeth damage such as cavities, gum disease and tooth decay (24). The pH values were slightly varied between each formulation and this may be due to the acidic or alkali nature of their distinctive ingredients. Among the formulation, F1 have the highest pH of 9.78 indicating that carrageenan and SDS might be more basic in nature. Both F2 and F3 resulted in having similar pH values with 9.33 and 9.39 respectively and this may be due to having the same binding agent, Sangelose.

Both F2 and F3 have a lower foamability with 3mL. On the other hand, F1 and commercial toothpaste have a foamability of 14mL and 16mL respectively. These differences suggests that the quantity of the surfactants in F2 and F3 is insufficient (6.7%). Thus, in further study, the quantity of the surfactants will need to be increased which will lead to higher foamability. Surfactant or also called as a foaming agent. It generates foam during brushing that facilitates wetting the tooth surfaces, dispersing the toothpaste in the mouth and food debris removal from the oral cavity (10,12). The surfactant used in the commercial toothpaste is the commonly used detergent, Sodium Lauryl Sulfate (SLS). High foamability suggest that there is a high concentration of SLS. High concentration of SLS causes a concern as it raises oral irritation among those who are prone to mouth ulcers or canker sores (19). Decyl glucoside, on the other hand, is gentle and less irritating. Tween-80 is also a good surfactant alternative to SLS. When using sulfate-free toothpaste, mouth ulcers may feel less painful and recovery time is faster. Sulfate-free toothpaste may also help reduce teeth sensitivity pain when compared to using SLS containing toothpaste (15).

Producing and using consumer products usually involve filling, pumping and discharge from their packaging. These processes are related with the complex rheological properties of the materials. Rheological properties that are controlled in toothpaste are ingredients such as polymer thickeners and particulate abrasives. Typical polymers include carboxymethyl cellulose, xanthan gum and carrageenan (25). Newton's law of viscosity can be defined as the relationship between shear stress and shear rate of a fluid when mechanical stress was applied. Fluids can be categorized into Newtonian fluids and non-Newtonian fluids. Toothpaste is considered as non-Newtonian fluids which does not obey Newtonian's law of viscosity where the ratio of shear stress to shear rate is not constant and depends on the shear rate (26). In other words, non-Newtonian fluids are affected by factors other than temperature, opposite with Newtonian fluids which temperature is the only factor affecting their viscosity. An example

of Newtonian fluid is water. The viscosity of water will remain constant no matter how they are forced to flow through a pipe. However, when temperature is applied, the water will become less viscous and will flow easily. On the other hand, the viscosity of non-Newtonian fluids will change only when pressure, agitation or shear stress is applied. When shear stress is applied, the viscosity decreases making the fluid to flow easily and these fluids are known as shear-thinning fluids (27). Thus, toothpaste is a non-Newtonian fluid with shear-thinning behavior. In this study, there are two tests that evaluates the rheological properties of the toothpaste which are tube extrudability and spreadability.

One essential factor to consumer is the toothpaste ability to be squeezed easily from the tubes and apply on the toothbrush. In this research, all toothpaste formulations have good tube extrudability indicating that there are no difficulty obtaining the toothpaste formulation during tube extrusion (19). Spreadability can be defined as the extent of the area to which the paste readily spreads on the application area. Possessing good spreadability is an essential criterion to be an ideal toothpaste (2). F2 have the highest spreadability with 4.03cm, while F1 have the lowest spreadability of 2.60cm. The variation might be caused by the different binding agents and surfactants used. From the results, carrageenan and SDS seem to significantly decrease the spreadability of the toothpaste formulation. On the other hand, the commercial toothpaste has a higher spreadability with 5.20cm despite having carrageenan in its composition as well. This may be due to the toothpaste having a higher amount of glycerin content affecting the ability to spread. High spreadability leads to high chances of wide performance range (19).

Dry mouth can be prevented with the presence of moisture in the toothpaste. Moisture content affects the physical properties and quality of the toothpaste. As mentioned, humectants help retain moisture preventing toothpaste from drying out. Common humectants include glycerine, sorbitol as well as water (24). Among the formulations, F3 have the highest moisture content (55.63%) and F1 have the lowest with 50.39%. While, the commercial toothpaste has a much lower moisture content with 29.06%.

Toothpaste is usually stored for months before they are being used hence it is important for toothpaste to have good stability. Stability test gives a close approximate of the shelves lives of products. For example, a sample stored at 45°C for 8 weeks is equivalent to storing at room temperature for one year (19). Although there was a significant decreased in pH value ($p<0.05$) and significant increase in moisture content ($p<0.01$), all toothpaste formulations have shown to have good stability after 30 days of storing in two different conditions (25°C and 40°C).

FTIR spectroscopy helps to confirm the presence of functional groups in the toothpaste formulations. Coconut shell charcoal and rice husk charcoal peaks can be seen in all three toothpaste formulation spectra. Absorption bands found in the FTIR spectrum of coconut shell charcoal at 1644.09 cm-1 and 1030.94 cm-1 represents C=C stretching and C-O stretching respectively (28,29). While, the peak at 1050.91 cm-1 in rice husk charcoal spectrum represents secondary alcohol C-C bond or Si-O-Si stretch (30). With similar peaks in F1 spectrum, the peak at 3385.15 cm-1 and 1035.22 cm-1 shown in the carrageenan spectrum might corresponds to O-H stretching and C-OH with S=O bonds respectively (31). The peak at 1079.43 cm-1 in SDS spectrum suggests C-C band stretching (32). Three peaks in F2 spectrum can also be seen in FTIR spectrum of Sangelose and DG. Absorption band at 1050.91 cm-1 indicates the presence of glucose ring in Sangelose (33). On the other hand, in the DG spectrum shows the presence of OH groups, C-C from ring stretching and C-O-C bonds respectively (34). FTIR spectrum of F3 have two similar peaks with those in Sangelose and T80 as well. The peak seen in T80 spectrum at 1093.68 cm-1 is attributed to C-O-C

stretching (35).

Presence of gritty matters in the toothpaste can cause wear to the teeth enamel and injury to skin. Therefore, test for grittiness is done by checking the presence of solid in the formulation (19). The results showed that there was absence of gritty matters in all three toothpaste formulations. All toothpaste formulations have shown to have good cleaning ability, thus the ability in cleaning tooth enamel (19). Cleaning effectiveness is another important property of an ideal toothpaste. It depends on its ability to remove stains on the teeth surface. The cleaning can be done by the abrasive ingredients contained in the toothpaste aided by the brushing mechanism of the toothbrush (36). In this study, the coconut shell charcoal (32.3%) and rice husk charcoal (1.0%) are the abrasive ingredients in the toothpaste formulations. The high compositions of these abrasives in the formulations may have caused the high abrasive potential. All toothpaste formulations have better abrasive potential than the commercial toothpaste. This can be supported by the cleaning test conducted. Based on observations, the cleaning ability of the commercial toothpaste has shown to be present but have lower cleaning ability compared to the toothpaste formulations. Upon inspecting the red stain removal after 10 brushing strokes, the toothpaste formulations were able to remove stain more than the commercial toothpaste suggesting that high abrasive potential has better stain removal (19).

Besides abrasive particles, surfactants also aid in cleaning the oral cavity. They act as foaming agents that produces foam while brushing. The foam would give an enjoyable sensation to the consumer, helps in wetting the surface of the teeth, allowing dispersion and free movement of the toothpaste as well as helping in loosening and removing debris and plaque in the oral cavity (12,14). Surfactants are amphiphilic molecules that contains hydrophilic heads and hydrophobic tails (37). When surfactants are dissolved in water, they would form spherical shapes aggregates called micelles where the hydrophilic heads are on the outside in contact with the surrounding water and hydrophobic tails are in the core of the micelles protected inside away from the water. When brushing with toothpaste, the hydrophobic tails in the surfactant molecules will attract and trap food debris into the core of the micelles. As micelles are suspended in water, they can be easily washed away from the oral cavity along with the food debris inside, cleaning the oral cavity (38).

To evaluate the abrasive effects of the formulated toothpaste, two activated charcoal mixture such as coconut shell charcoal (micro-particle) and rice husk charcoal (macro-particles) were mixed in the ratio of 32.3 is to 1. The image of toothpaste F1 in Figure 5B shows mixtures of micro and macroparticles of activated charcoal clearly appeared. This may be due to the adsorption as well as blocking the pores onto macro size particle of activated rice husk charcoal by SDS. The process of adsorption of SDS-coated RHC (rice husk charcoal) might be governed by chemisorption (39). Whereas, micrometer size activated coconut shell charcoal (CSC) has been recognized as a good candidate in adsorption process due to having a high specific surface (40). This may be due to having high number of pores that is typically acts as a better adsorbent in the application of activated charcoal in whitening toothpastes, however, Sodium dodecyl sulfate (SDS), an anionic surfactant, is used as cleaning and hygiene products (41,42). Also, adsorption layer between SDS and RHC appeared enlarged due to addition of water before observation in the microscopic evaluation. This may be due to disturbances of surfactant micelles on the coating of the microparticles. The image of toothpaste F2 in Figure 5C showed strong adsorption on the CSC where head group micelles re-enlarged with water addition before microscopical observation. Less adsorption on RHC may be the reason that clump mass was not observed in the F2 formulation. Decyl glucoside is a mild non-ionic surfactant that were used in variety of cosmetic formularies due to the safety of green surfac-

tant. It is a biodegradable surfactant that results in products with low toxicity and friendly properties to the environment (43). The image of toothpaste F3 in Figure 5D, shows similar pattern of micelles appear like DG containing toothpaste F2, and it has been reported that activated charcoal and Tween 80 for a high wetting power. The image of commercial toothpaste in Figure 5E, which contains Sodium Lauryl Sulfate (SLS) surfactant, have shown to utilizing uniform particle size and hence, it appeared with uniform particle size without any clumpy masses compared to formulated toothpaste.

Cosmetic products usually have some level of toxicity and this could cause a major concern. Therefore, toxicity assay is vital in order to prove better performance of the toothpaste formulation. Toxicity assay was performed based toward seed germination index (11). Phytotoxicity is defined as plant growth inhibition and a delay of seed germination (44). A germination index value of more than 80% usually indicates no phytotoxicity (45). Among the formulations, only F2 and F3 have a GI of 100.8% and 103.2% respectively, surpassing the target GI%. Therefore, F2 and F3 are less toxic in nature which may be due to the toothpaste formulations being sulfate-free. F1 and commercial toothpaste, on the other hand, have a lower GI value of less than 80% with 48.1% and 70.6%. F1 are more toxic suggesting the toxicity of SDS, while SLS presence is causing the toxicity in the commercial toothpaste. This evidence has further proven the toxicity of sulfate-containing toothpaste.

In this study, all objectives have been achieved. Sulfate-free toothpaste formulations have been prepared and optimized that contains coconut shell charcoal and rice husk charcoal. Evaluation have been done that shows all toothpaste formulation of their cleaning effectiveness, toxicity, stability and other properties. A number of limitations should be acknowledged in this research study. Additional tests could have been conducted on the toothpaste formulations such as SEM-EDX analyses where particle shapes could have been observed through micrographs. Another test would be a cleaning test that uses turmeric powder to stain artificial teeth. Due to shortage of time, stability test could only be done after 30 days when in fact, stability test was usually conducted after two to three months of storage. The undesirable foamability results of F2 and F3 formulations suggest improvement should be made by increasing the composition of the surfactants in future study.

Conclusion

As expected, the toothpaste formulations were able to achieve the desired and acceptable characteristics with the physiochemical characterization. This study might provide good scope and be useful for further research as being a sulfate-free toothpaste that uses renewable waste activated coconut shell charcoal and rice husk charcoal as the abrasive ingredients and is capable of improving and maintaining oral hygiene. Upon successful formulation, the toothpaste formulations have the chance of being patented and to be produced commercially.

Acknowledgements

We sincerely thank PAPRSB Institute of Health Science, Universiti Brunei Darussalam for providing laboratory and animal facilities.

Competing interests

The authors declare that they have no competing interests.

References

1. Gupta A, Mishra A. Development and Characterization of Herbal Toothpaste containing Neem Bark Powder as Abrasive. International Journal of Recent Advances in Medical & Pharma Research 2019; 2:2–4.

2. Jagtap AM, Kaulage SR, Kanse SS, Shelke VD, Gavade AS, Vambhurkar GB, et al. Preparation and Evaluation of Toothpaste. Asian Journal of Pharmaceutical Analysis 2018; 8:191. https://doi.org/10.5958/2231-5675.2018.00035.2.

3. Iqbal K, Asmat M, Jawed S, Mushtaque A, Mohsin F, Hanif S. Role of different ingredients of tooth pastes and mouthwashes in oral health. Journal of the Pakistan Dental Association 2011; 20:163–70.

4. U.S.: Usage of toothpaste 2011-2024. Statista Research Department 2020. https://www.statista.com/statistics/287376/usage-of-toothpaste-in-the-us-trend/ (accessed January 29, 2021).

5. Vrani E, La A, Mehmedagi A, Uzunovi A, Dağ C, Özalp N. Formulation Ingredients for Toothpastes and Mouthwashes. Bosn J Basic Med Sci 2004; 4:51–8.

6. Phalke PL, Rukari TG, Jadhav AS. Formulation and evaluation of toothpaste containing combination of aloe and sodium chloride. Int J Pharm Sci Res 2019; 10:1462–7. https://doi.org/10.13040/IJPSR.0975-8232.10(3).1462-67.

7. Machla F, Mulic A, Bruzell E, Valen H, Stenhagen ISR. In vitro abrasivity and chemical properties of charcoal-containing dentifrices. Biomater Investig Dent 2020; 7:167–74. https://doi.org/10.1080/26415275.2020.1838284.

8. Carlile WR, Raviv M, Prasad M. Organic soilless media components. Soilless Culture: Theory and Practice Theory and Practice, Elsevier; 2019, p. 303–78. https://doi.org/10.1016/B978-0-444-63696-6.00008-6.

9. Kumar A, Mohanta K, Kumar D, Parkash O, Scholar R. Properties and Industrial Applications of Rice husk: A review. International Journal of Emerging Technology and Advanced Engineering 2012; 2:86–90.

10. Formulating Toothpaste using Carbopol Polymers. Lubrizol Pharmaceutical Bulletin 24 2010:1–18.

11. Kumar R. Development of Biosurfactant Based Cosmetic Formulation of Toothpaste and Exploring its Efficacy. Advances in Industrial Biotechnology 2018; 1:1–5. https://doi.org/10.24966/aib-5665/100005.

12. Stovell AG, Newton BM, Lynch RJM. Important considerations in the development of toothpaste formulations for children. Int Dent J 2013;63 Suppl 2:57–63. https://doi.org/10.1111/idj.12083.

13. Fiume MM, Heldreth B, Bergfeld WF, Belsito D V., Hill RA, Klaassen CD, et al. Safety Assessment of Triethanolamine and Triethanolamine-Containing Ingredients as Used in Cosmetics. Int J Toxicol 2013; 32:59S-83S. https://doi.org/10.1177/1091581813488804.

14. Pader M. Dentifrices. Kirk-Othmer Encyclopedia of Chemical Technology 2012:1–9.

15. Abdel Hamid M. SLS free toothpaste v Regular Toothpaste. Mouthpower Org 2021. https://www.mouthpower.org/toothpaste/sls-free-toothpaste-v-regular-toothpaste/#alternatives-to-sodium-lauryl-sulfate (accessed January 29, 2021).

16. Nishad U, Ali M, Maurya A. Formulation and Evaluation of a Polyherbal Toothpaste using Medicinal Plants. Journal of Pharmaceutical Sciences and Research 2020; 12:105–11.

17. Kamalapurkar KA, Gote PM, Pathan MA, Surwase PR, Shiddanagoudar KJ. Development and Characterization of Herbal Toothpaste containing Neem Extract; Compared with marketed product. World J Pharm Pharm Sci 2019; 8:936–42. https://doi.org/10.20959/wjpps20194-13409.

18. Anju T, Aiswarya K. Formulation and antimicrobial evaluation of toothpastes containing arginine and proline. International Journal of Advances in Pharmacy, Biology and Chemistry 2016;5(2):143–7.

19. Ogboji J, Y. Chindo I, Jauro A, Boryo D, N. M. L. Formulation, physicochemical evaluation and antimicrobial activity of green toothpaste on streptococcus mutans. International Journal of Advanced Chemistry 2018; 6:108. https://doi.org/10.14419/ijac.v6i1.10808.

20. Gautam D, Palkar P, Maule K, Singh S, Sawant G, Kuvalekar C, et al. Preparation, evaluation and comparison of herbal toothpaste with marketed herbal toothpaste. Asian Journal of Pharmacy and Technology 2020; 10:165. https://doi.org/10.5958/2231-5713.2020.00028.8.

21. Maçon ALB, Valliant EM, Earl JS, Jones JR. Bioactivity of toothpaste containing bioactive glass in remineralizing media: Effect of fluoride release from the enzymatic cleavage of monofluorophosphate. Biomedical Glasses 2015; 1:41–50. https://doi.org/10.1515/bglass-2015-0005.

22. Dentistry-Toothpastes-Requirements, test methods and marking. 1995.

23. Hilgenberg SP, Pinto SCS, Farago PV, Santos FA, Wambier DS. Physical-chemical characteristics of whitening toothpaste and evaluation of its effects on enamel roughness. Braz Oral Res 2011; 25:288–94. https://doi.org/10.1590/S1806-83242011005000012.

24. Omar KA, Ismail AK, Amin CM, Jalal MS, Qadr SN, Rafiq ZF. Physicochemical characteristics of toothpastes and natural powder and their antibacterial activity against Viridans Streptococci bacteria. Oriental Journal of Chemistry 2017; 33:2566–72. https://doi.org/10.13005/ojc/330553.

25. Ahuja A, Luisi G, Potanin A. Rheological measurements for prediction of pumping and squeezing pressures of toothpaste. J Nonnewton Fluid Mech 2018; 258:1–9. https://doi.org/10.1016/j.jnnfm.2018.04.003.

26. George HF, Qureshi F. Newton's Law of Viscosity, Newtonian and Non-Newtonian Fluids. Encyclopedia of Tribology, Springer US; 2013, p. 2416–20. https://doi.org/10.1007/978-0-387-92897-5_143.

27. Rohrig BB. Newtonian versus non-Newtonian fluids. ChemMatters - Amercian Chemical Society 2017.

28. Kumarasinghe KDMSPK, Kumara GRA, Rajapakse RMG, Liyanage DN, Tennakone K. Activated coconut shell charcoal based counter electrode for dye-sensitized solar cells. Org Electron 2019; 71:93–7. https://doi.org/10.1016/j.orgel.2019.05.009.

29. Pranoto, Martini T, Astuti F, Maharditya W. Test the Effectiveness and Characterization of Quartz Sand/Coconut Shell Charcoal Composite as Adsorbent of Manganese Heavy Metal. IOP Conf Ser Mater Sci Eng 2020;858. https://doi.org/10.1088/1757-899X/858/1/012041.

30. Mishra A, Taing K, Hall MW, Shinogi Y. Effects of Rice Husk and Rice Husk Charcoal on Soil Physicochemical Properties, Rice Growth and Yield. Agricultural Sciences 2017; 08:1014–32. https://doi.org/10.4236/as.2017.89074.

31. Prado-Fernández J, Rodríguez-Vázquez JA, Tojo E, Andrade JM. Quantitation of κ-, ι- and λ-carrageenans by mid-infrared spectroscopy and PLS regression. Anal Chim Acta 2003; 480:23–37. https://doi.org/10.1016/S0003-2670(02)01592-1.

32. Singh MK, Agarwal A, Gopal R, Swarnkar RK, Kotnala RK. Dumbbell shaped nickel nanocrystals synthesized by a laser induced fragmentation method. J Mater Chem 2011; 21:11074–9. https://doi.org/10.1039/c1jm12320c.

33. Akinosho H, Hawkins S, Wicker L. Hydroxypropyl methylcellulose substituent analysis and rheological properties. Car-

bohydr Polym 2013; 98:276–81. https://doi.org/10.1016/j.carbpol.2013.05.081.

34. Deyab MA. Decyl glucoside as a corrosion inhibitor for magnesium-air battery. J Power Sources 2016; 325:98–103. https://doi.org/10.1016/j.jpowsour.2016.06.006.

35. (35) Kura AU, Hussein-Al-Ali SH, Hussein MZ, Fakurazi S. Preparation of Tween 80-Zn/Al-levodopa-layered double hydroxides nanocomposite for drug delivery system. The Scientific World Journal 2014;2014. https://doi.org/10.1155/2014/104246.

36. Varnadoe C. Toothpaste. 2018.

37. de Oliveira Rangel Yagui C, Lineu Prestes A, Rangel-Yagui CO, Pessoa-Jr A, Costa Tavares L. Micellar solubilization of drugs. J Pharm Pharmaceut Sci 2005; 8:147–63.

38. Davies R. Surfactants: explainer. Science & Technology Facilities Council 2019. https://www.isis.stfc.ac.uk/Pages/SH19_Surfactants.aspx (accessed May 8, 2021).

39. Que W, Jiang L, Wang C, Liu Y, Zeng Z, Wang X, et al. Influence of sodium dodecyl sulfate coating on adsorption of methylene blue by biochar from aqueous solution. Journal of Environmental Sciences 2018; 70:166–74. https://doi.org/10.1016/j.jes.2017.11.027.

40. Bhatnagar A, Hogland W, Marques M, Sillanpää M. An overview of the modification methods of activated carbon for its water treatment applications. Chemical Engineering Journal 2013; 219:499–511. https://doi.org/10.1016/j.cej.2012.12.038.

41. Vaz VTP, Jubilato DP, Oliveira MRM de, Bortolatto JF, Floros MC, Dantas AAR, et al. Whitening toothpaste containing activated charcoal, blue covarine, hydrogen peroxide or microbeads: Which one is the most effective. Journal of Applied Oral Science 2019; 27:1–8. https://doi.org/10.1590/1678-7757-2018-0051.

42. Fu W, Qu F, Yu G, You J. High selectivity for sodium dodecyl sulphate by polymer nanoparticles and detection of proteins based on the polymer nanoparticles-sodium dodecyl sulphate system. Sens Actuators B Chem 2017; 245:774–9. https://doi.org/10.1016/j.snb.2017.01.175.

43. Fiume MM, Heldreth B, Bergfeld WF, Belsito D V., Hill RA, Klaassen CD, et al. Safety Assessment of Decyl Glucoside and Other Alkyl Glucosides as Used in Cosmetics. Int J Toxicol 2013; 32:22S-48S. https://doi.org/10.1177/1091581813497764.

44. Blok C, Baumgarten A, Baas R, Wever G, Lohr D. Analytical methods used with soilless substrates. Soilless Culture: Theory and Practice Theory and Practice, Elsevier; 2019, p. 509–64. https://doi.org/10.1016/B978-0-444-63696-6.00011-6.

45. Luo Y, Liang J, Zeng G, Chen M, Mo D, Li G, et al. Seed germination test for toxicity evaluation of compost: Its roles, problems and prospects. Waste Management 2018; 71:109–14. https://doi.org/10.1016/j.wasman.2017.09.023.

Current Trends in Biotechnology and Pharmacy
Vol. 18(3) 1866-1880, July 2024, ISSN 0973-8916 (Print), 2230-7303 (Online)
10.5530/ctbp.2024.3.33

Design and Development of Machine Learning Model for Antibody Design: Rituximab a Case Study

Harit Kasana[1,2], Harish Chander[1], and Ashwani Mathur[2*]

[1]National Institute of Biologicals (Ministry of Health and Family Welfare, Government of India) A-32, Sector-62, NOIDA-201 309, India
[2]Department of Biotechnology, Jaypee Institute of Information Technology Noida, A-10, Sector-62, Noida, 201309, Uttar Pradesh, India
*Corresponding Author: ashwani.mathur@mail.jiit.ac.in

Abstract

The design of antibodies using machine learning has emerged as a cutting-edge approach in the field of medical sciences and therapeutics. This study delves into the principles, methods, and deployment of machine learning approach for antibody design. The present study showed use of extensive antibody databases to train computational models, facilitating the prediction of antibody-antigen interactions. Seven different encoders were used for the vectorization of the antibody and antigen sequences. Conjoint triad showed unsurpassed performance in the machine-learning algorithm with 0.78 correlation and outperformed other encoding methods. The case study of Rituximab was used to demonstrate the practical application of the machine-learning model that was developed. The affinity score predicted by the model was utilised to select the most promising rituximab sequence. Structural investigation employed molecular dynamics (MD) simulation to authenticate the novel sequence (variant) of rituximab. Rituximab variant showed -45.44 kcal/mole compared to the wild type that had -37.66 kcal/mole as a binding free energy for the antigen-antibody complex. Free energy landscape (FEL) was calculated on the first two principal components (PC1 and PC2). The wild type has three minimum energy basins, whereas this variant exhibited only one. This showed that complex produced by antibody variant has a greater capacity to attain global minima. This study sheds light on the innovative application of machine learning in antibody design and also provides compelling evidence of its efficacy through the case study of rituximab. Present study opened new avenues for the development of antibodies with enhanced binding capabilities.

Keywords: Rituximab, Machine Learning, Immunogenicity, Molecular Dynamic Simulation.

Introduction

Monoclonal antibodies (MAbs) also known as therapeutic antibodies (TAbs)(1). Therapeutic antibodies are classified as protein-based therapeutic agents that have undergone engineering to recognise and bind to specific molecules (e.g., proteins, cells, and disease-associated molecules) within the organism. The creation of these antibodies is facilitated using specialized techniques that enable the generation of substantial quantities of identical antibodies capable of recognizing and engaging with a specific target (1). A range of therapeutic antibodies were introduced in the mid-1990s and have since been implemented in clinical settings (2). Currently, the quantity of licenced therapeutic antibodies (TAbs) stands

at approximately one hundred, with a greater number in the process of development this includes various designed and modified antibody formats. TAbs are commonly employed in the management of diverse severe diseases, including cancer, rheumatoid arthritis, multiple sclerosis, Crohn's disease and leukaemia(3). The therapeutic efficacy of these TAbs can be attributed to one or more mechanisms, including target binding and neutralization, direct cytotoxicity, antibody-dependent complement-dependent cytotoxicity, antibody-dependent cellular cytotoxicity, or other unidentified mechanisms (4). The range of disease areas that can be targeted by therapeutic antibodies has expanded significantly. Antibodies are now being used as medicines in various fields, including cancer, inflammatory illness, organ transplantation, cardiovascular disease, infection, respiratory disease, ophthalmologic disease, and others (2).

The essential role of immune-mediated effector functions in therapeutic antibodies targeting tumour cells is their specific binding to targets via the antibody-binding fragment (Fab) region(5), followed by the induction of immune responses via the fragment crystallizable (Fc) region. Cross-linking of cell-bound antibodies with Fc gamma receptors (FcRs) is responsible for activating immune effector cells. This interaction results in natural killer (NK) cells mediating antibody-dependent cellular cytotoxicity (ADCC). Similarly, antibody-dependent cellular phagocytosis (ADCP) is initiated by the interaction between FcRs and macrophages. This process involve the internalisation of antibody-opsonized target cells into phagosomes, where they are degraded via phagosome maturation and acidification(6).

The therapeutic antibody interacts with the antigen at a specific epitope region. The epitope refers to a spatial arrangement acknowledged by the complementary paratype of an antibody (7). The binding affinity between antibody and antigen can be determined by various traditional methods, including surface plasmon resonance (SPR) and enzyme-linked immunosorbent assay (ELISA). Although these are effective methods, there are still some limitations, such as time, cost, and potential variation in results (8).

$$Kd = \frac{koff}{kon}$$

The equilibrium dissociation constant, denoted as 'kd', represents the ratio of the dissociation rate constant ('koff') to the association rate constant ('kon') for the binding interaction between an antibody and its corresponding antigen (9). An inverse relationship exists between 'kd' and affinity. The 'kd' value is a measure of the antibody concentration required for a specific experiment. A lower kd value indicates a stronger affinity of the antibody, as it corresponds to a lower concentration needed (10). Various traditional techniques were used to determine kd during antibody –antigen interactions, including flow cytometry and ligand tracer (11). Traditional methods for determining the dissociation constant (kd) in antibody-antigen interactions face difficulties such as the assumption of 1:1 binding, affinity heterogeneity, omission of kinetic information, inability to account for conformational changes, reliance on equilibrium conditions, and potential interference from immobilization and sample matrix effects. Moreover, the other factors that affect the antigen-antibody interaction are temperature, pH, ionic strength, concentration antigen-antibody(12). With all of these factors, it may be difficult to determine an accurate kd value.

In the light of the challenges for determining the binding affinity between Antibody and Antigen, Therefore, in this study, a machine learning (ML) model to determine kd was proposed. The ML model was trained on antigen and antibody protein sequences with known kd values. It presents a novel machine learning (ML) approach for the efficient determination of kd, utilising existing kd values of antigen and antibody protein sequences. Determining the binding affinity using the sequence made the calculation faster. This could allow modifying the antibody sequence to improve the sensitivity and speci-

ficity against the given antigen. Later, this study demonstrated a case study of application of this method on the Rituximab. Engineered Rituximab was designed and validated using molecular dynamics simulation.

Materials and Methods

Data collection

Collection

The study focuses on the structural characteristics and binding affinity of antigen-antibody complexes, using data obtained from the SAbDab database(13, 14). (SAbDab is an in-depth database of antibody-antigen pairs. Every structure is accompanied with several information, including experimental details, antibody nomenclature (e.g., pairings of heavy and light chains), curated affinity data, and sequence annotations. As of July 25, 2023, 15,065 antigen-antibody complexes were accessible. After eliminating blanks in affinity and removing incorrect entries, 916 antigen-antibody pair remained that had affinity values (kd). These antibody sequences have heavy chain and light chain both. In the creating the data for machine learning model the heavy and light chain sequences were concatenated. Antigen sequences were also fed separately to the model with the sequence of the antibody and the kd value.

Machine learning model

DeepPurpose framework(15) was used for building the machine learning model. This framework is essentially constructed for drug-target interaction (DTI) used in drug repurposing and virtual screening. However, it also has model for protein-protein interaction. The source codes were sourced from github repository (kexinhuang12345/DeepPurpose: A Deep Learning Toolkit for DTI, Drug Property, PPI, DDI, Protein Function Prediction (Bioinformatics) (github.com)). DeepPurpose was preferred due to its user-friendly design which facilitated the use of multiple encoders for encoding the sequence of proteins and multiple evaluation metrics such as MSE, R-squared and Concordance Index. It also enabled the support for custom model architecture with utilities for training and evaluating the models. Here, 8 different encoders were used for encoding the protein sequence and result was evaluated: 'CNN', 'AAC', 'PseudoAAC', 'Conjoint_triad', 'Quasi-seq', 'ESPF', 'Transformer', 'CNN_RNN'. ‘CNN’ and 'Conjoint_triad' encoder outperformed the others and thus used as preferred encoding technique. Though DeepPurpose library enabled the utilisation of some pretrained models, a custom deep learning model was developed combining two different neural network architectures. The combined neural network architectures were, Convolutional Neural Network (CNN) and Message Passing Neural Network (MPNN). The configuration of the model used was, 100 epochs, 0.001 learning rate and 128 batch sizes, these parameters along with other essential parameters are represented in Table 1. The interaction prediction for antibodies was complex due to their large sequence length. Thus, such custom model was utilised with testing on multiple encoders to ensure highly accurate predictions. The model was trained on 70% of the known dataset of antibody-antigen pairs with their corresponding Kd values in log. The example data is shown below:

Antibody

EVQLVESGGGLVQPGGSLRLS-
CAASGYTFTNYGMNWVRQAPGKGLEWVG-
WINTYTGEPTYAADFKRRFTFSLDTSK-
STAYLQMNSLRAEDTAVYYCAKY-
PHYYGSSHWYFDVWGQGTLVTVSSAST-
KGPSVFPLAPSSKSTSGGTAALGCLVKDYF-
PEPVTVSWNSGALTSGVHTFPAVLQSSGLYS-
LSSVVTVPSSSLGTQTYICNVNHKPSNTK-
VDKKVEPKSCDKTHTXXXDIQMTQSPSSL-
SASVGDRVTITCSASQDISNYLNWYQQKP-
GKAPKVLIYFTSSLHSGVPSRFSGSGSGTD-
FTLTISSLQPEDFATYYCQQYSTVPWTFGQ-
GTKVEIKRTVAAPSVFIFPPSDEQLKSGT-
ASVVCLLNNFYPREAKVQWKVDNALQSGN-
SQESVTEQDSKDSTYSLSSTLTLSKADYEKH-
KVYACEVTHQGLSSPVTKSFNRGEC

Antigen

GQNHHEVVKFMDVYQRSYCHPIETL-VDIFQEYPDEIEYIFKPSCVPLMRCGGCCN-DEGLECVPTEESNITMQIMRIKPHQGQHI-GEMSFLQHNKCECRPKKD

kd:1.22

The model used 10% of the data for validation while rest 20% for testing (coefficient of determination), making the split ratio of the dataset to be 70:10:20, where each ratio part corresponds to train, validation and test respectively. The regression score (r^2) was used as evaluation metric to calculate the performance.

Table 1. Parameters associated with the machine learning model.

Experimental Parameter	Value
Learning rate	0.001
Batch size	128
Epoch	100
Hidden layer dimension	1024, 1024, 512
Size of hidden layers in MPNN	128
Number of layers in the MPNN	3
Number of filters in convolutional layer	32, 64, 96
Size of the filters in each convolutional layer	4, 8, 12

CDR Identification

The recognition of Complementarity Determining Regions (CDR) sequences plays a crucial role in augmenting the properties of antibodies, such as their binding affinity, specificity, and overall therapeutic effectiveness. AbRSA tool(16) was used to predict the CDR regions, which is a tool specifically stands for Antibody Numbering and CDR Delimiting. This tool was employed to predict the Complementarity Determining Regions (CDR) for both the VH (Heavy chain) and VL (Light chain) of each antibody.

Rituximab structure

The structure of rituximab was sourced from protein data bank (PDB)(17), numerous structures of rituximab were submitted in the PDB. Here, the structure with PDB ID: 2OSL(18, 19) was downloaded for determining the known interaction of CDR region and epitope of antigen.

Sequence engineering

In this study, the Complementarity Determining Region (CDR) of rituximab was focused on, being a pivotal component guiding the binding specificity and affinity. A comprehensive computational analysis was undertaken to explore all possible amino acid combinations within the CDR.

Structure model building

Novel sequence of the rituximab that predicted the maximum affinity with the antigen was modelled using a machine learning (ML)-based technology provided by the SAbPred server(20). The ABodyBuilder-ML module, which is a component of the SAbPred server, was utilised for the purpose of novel rituximab structure modelling using sequence data. The ABodyBuilder-ML programme was applied to predict the structure of the variable domains of the antibody, namely VH (heavy chain) and VL (light chain), that are commonly referred to as the Fv (fragment variable).

MD Molecular Dynamics Simulation was performed for the top-selected antigen-antibody complexes. GROMACS2022 package was the software that was used to carry out the molecular dynamic simulations of the top-selected antigen-antibody complexes for a time period of 100 ns(21–23). The CHARMM force field parameters (24)were used to define the topological parameters, which were then allocated to both the antibodies and the antigen. The Ewald Particle Mesh approach was used with the purpose to perform the calculations necessary to determine the distance electrostatic force (25). In order to establish a neutral system, Na+ and Cl- ions were introduced, and the TIP3P water cube model was employed with the purpose to

solvate the system. The steepest descent (SD) method, which consists of 50,000 minimization steps, was used on the system with the aim of removing any steric conflicts. In addition, the temperature of the entire system was raised to 310 K, and the timestep was set to 2 fs for 100 ps of simulation time (NVT). After that, the system underwent additional equilibration at a pressure of 1 bar for a duration of 1 ns during the simulation time (NPT). GROMACS was able to simulate at a constant temperature by employing the velocity-rescaling strategy in conjunction with a temperature coupling scheme (26). Temperature control was linked with pressure coupling, and the result was the NPT ensemble. The pressure coupling employed was the Parrinello-Rahman pressure coupling(27). Using the SHAKE approach(28), all hydrogen bonds were constrained, and after that, the coordinates of the structure were recorded after every 10 ps during the entire 100 ns (100,000 ps) production run. The conformational stability and variation of the antigen-antibody complexes were determined by post MD analysis. The results of the 100 ns MD simulation were analysed with the RMSD (root mean square deviation) tool in GROMACS. Following the MD simulation, clustering was performed on the complexes by applying the gromos cluster method using the g_cluster packages of GROMACS(29, 30) with a threshold RMS of 0.3 nm. Later, these clusters were used for further analysis and interpreting the stability and flexibility of the antigen-antibody complexes. Furthermore, the binding free energy of the antigen-antibody was calculated using the MM/GBSA approach as mentioned in the section 1.6. Here, the middle cluster of the most popular cluster was used for determination of binding free energies. All the clusters generated were used for SASA determination, which were compared with the epitopes of the spike protein.Results and Discussion

Data collection

Data was collected from the SAbDab database, eventually 916 entries with their PDB ids and Kd values that had units in nanomolar. These Kd values were further converted to log values under the normalization process. The logarithmic values of the Kd are shown in Figure1, most data points were ranged in between 10^{-6} to 10^{-11}. There were few outliers in the datasheet for Kd values. Corresponding sequence of the antibodies and antigens were extracted from the protein data bank using the PDB Ids sourced from the SAbDab database. These sequences were for the Fab region of the antibody with their heavy and light chains sections. Both heavy and light chains were merged together as a single component of antibody. Similarly, antigen sequences were also extracted as a separate input for the machine learning model.

Building machine learning model

Encoders, ‘CNN’, ‘AAC’, ‘PseudoAAC’, ‘Conjoint_triad’, ‘Quasi seq’, ‘ESPF’, ‘Transformer’, ‘CNN_RNN’ were used for encoding the protein sequences of antibodies and antigens. All these encoders were used serially to encode the sequence of the target protein sequence and used in the DeepPurpose machine-learning model. Table 2 shows the performance of each encoder for predicting the Kd values. The original values of Kd were in nM and the magnitude was converted into log scale after multiplying with 10^9. Figure 1(a) shows the original Kd values and converted logarithmic values. As observed in the plot that original Kd values are skewed towards 0 as most of the datapoints had low Kd values in nano molar. This skewedness can affect the performance of the prediction and thus they were converted into log scale after multiplying with 10^9. Figure 1(b) showed the normalized values of CNN and ConjointTriad performed similarly in the pearson correlation with the coefficient value of 0.78. However, mean square error for CNN was 4.08 while for ConjointTriad it was 4.14. Other encoders, AAC, ESPF and Transformer also showed correlation coefficient greater than 0.7.

Table 2. Performance of the different encoder on the data set to predict the Kd values.

Encoder	MSE	Pearson Correlation Coefficient	p-value	Concordance Index
CNN	4.08	0.78	7.32E-37	0.82
AAC	5.28	0.71	1.04E-27	0.78
PseudoAAC	8.82	0.39	1.18E-07	0.66
ConjointTriad	4.14	0.78	1.43E-36	0.83
Quasi-Seq	8.79	0.42	1.12E-08	0.63
ESPF	4.96	0.73	6.68E-30	0.80
Transformer	5.60	0.71	4.88E-28	0.81
CNN_RNN	7.90	0.50	3.51E-12	0.67

ConjointTriad model showed the best performance for correlation coefficient and mean square error and thus selected for the further processing. ConjointTriad is widely used for dealing with the sequential data including protein sequence. The architecture comprises multiple convolutional layers and encodes the sequence within a 1D encoder, thereby capturing the features and patterns inherent in the sequence. As the sequence of the protein was of different length thus the padding was also used during the ConjointTriad encoder. Moreover, p-values in the Table 1 shows the relevance score of the prediction for their correlation co-efficient. As shown in the table that all the p-values are lower than 0.05 and thus the confidence was greater than 90% for the calculated correlation coefficients. The concordance index evaluates how well the model's predicted probabilities of survival align with the actual outcomes. The ConjointTriad model has the highest concordance index value of 0.83, while CNN also has a close value of 0.82. Considering all the evaluation metrics, Conjoint Triad encoder moder was selected as the best performing model. Moreover, various studies used machine learning models based deep convolutional neural networks, that used in both bio-medical and sensor-based study(31–34)deep convolutional neural networks have demonstrated dominant performance in human activity recognition (HAR.

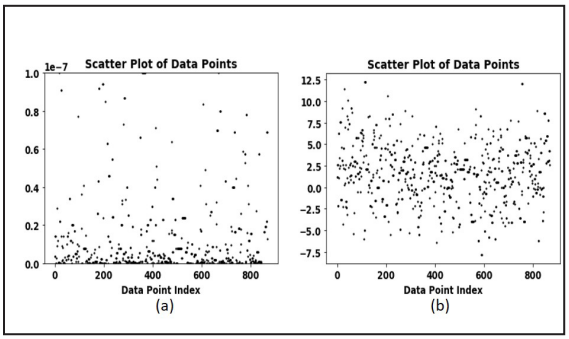

Figure 1. Plot of Kd values with respect to each 916 entries of the antibodies (a) original Kd (b) logarithmic values of the kd.

CDR and structure of rituximab

Once the ML model was selected with the best performing encoder technique (ConjointTriad), the Fab sequence of the Rituximab was collected. PDB ID: 6VJA was sourced from protein databank for extracting the sequence of heavy and light chains of the Fab segment of the Antibody. Sequence of heavy and light chains were submitted to the AbRSA tool for detecting the CDRs. Complementarity-determining regions (CDRs) are immunoglobulin (Ig) hypervariable domains that regulate particular antibody (Ab) binding(35)fungi, protozoa and viruses. The possibility that isolated CDRs, represented by short synthetic peptides, may display antimicrobial, antiviral and antitumor activities irrespective of Ab specificity for a given antigen

is addressed here.\nMETHODOLOGY/PRINCIPAL FINDINGS: CDR-based synthetic peptides of murine and human monoclonal Abs directed to: a.

The chains are shown below with the coloured CDR region detected by AbRSA tool:

> RITUXIMAB FAB HEAVY CHAIN

1 QVQLQQPGAELVKPGASVKMSCKASGYTFTSYNMHWVKQTPGRGLEWIGAIYPGNGDTSY 60
61 NQKFKGKATLTADKSSSTAYMQLSSLTSEDSAVYYCARSTYYGGDWYFNVWGAGTTVTVS 120
121 AASTKGPSVFPLAPSSKSTSGGTAALGCLVKDYFPEPVTVSWNSGALTSGVHTFPAVLQS 180
181 SGLYSLSSVVTVPSSSLGTQTYICNVNHKPSNTKVDKKVEPKSC

> RITUXIMAB FAB LIGHT CHAIN

1 QIVLSQSPAILSASPGEKVTMTCRASSSVSYIHWFQQKPGSSPKPWIYATSNLASGVPVR 60
61 FSGSGSGTSYSLTISRVEAEDAATYYCQQWTSNPPTFGGGTKLEIKRTVAAPSVFIFPPS 120
121 DEQLKSGTASVVCLLNNFYPREAKVQWKVDNALQSGNSQESVTEQDSKDSTYSLSSTLTL 180
181 SKADYEKHKVYACEVTHQGLSSPVTKSFNRGEC

Heavy chain showed 3 CDR segments, CDR1 coloured as red, CDR2 coloured as orange while CDR3 coloured as green. In heavy chain, CDR3 is the longest with 12 residues while CDR2 showed 8 residues and CDR1 with 7 residues, respectively. In contrast, CDR1 has the maximum length of 10 in light chain, while CDR2 has the minimum of 7 amino acids. Structure of Rituximab is submitted in the PDB with PDB ID: 6VJA, this entry has CD20 B-lymphocyte antigen bound with the antibody structure. Figure 2, shows the Antigen and Antibody structures. Only the Fab segment that interacts with Antigen is submitted in the protein databank, heavy chain has 224 amino acids while light chain has 213 amino acids. CD20 antigen has 278 amino acids in the PDB entry.

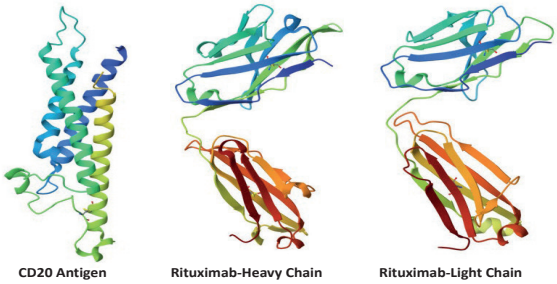

Figure 2. Structure of CD antigen that complexed with Rituximab using heavy and light chain of Fab segment, deposited in protein data bank with PDB ID: 6VJA.

Antigen in the structure is deposited as dimer in this structure with chain C and D while H and L are the heavy and light chains of the antibody. SER95, TRP100, HIS35, ASN33, SER58, TYR52, and ASP56 from the heavy chain was interacting with the chain C of the antigen while SER28, SER29, SER31, TRP91, and ASN94 from the light chain was involved in the antigen antibody interaction. It is noteworthy that SER28, SER29, and SER31 interacting residues from the light chain were from CDR1, while TRP91, and ASN94 were from CDR3. Similarly, SER58, TYR52, and ASP56 were from CDR2 of the heavy chain, while SER95, and TRP100, also seen as interactive residues, were from CDR3. In overall, the outcome provides a comprehensive analysis of the molecular composition and binding properties of the Rituximab antibody, with specific emphasis on its interaction with the CD20 antigen, which is crucial for its therapeutic efficacy.

Modification of antibody sequence

Later, the CDR segments of antibody were targeted for the substitution of single amino acids serially. This resulted in generation of 969 sequences that constitute of all possible combination of amino acid for a given substitution.

Essentially, this created a vast library of Rituximab variants. These new sequences of heavy/light chains were constitutively fed to the trained machine-learning model along with the original sequence of CD20 antigen. The model predicted log (Kd) values which further converted into antilog to deduce the original Kd value in nano Molar. The Kd value is a standard measure of the binding affinity between an antibody and an antigen; lower Kd values indicate higher affinity(36). Figure 3, shows the top three sequences of the Rituximab that predicted the minimum Kd values in the ML model. The Top sequence showed 0.000024 nM Kd and it was considered and best modified Antibody sequence at the CDR that can bind with CD20 antigen with the highest affinity. In this sequence, SER31 was converted to LEU31. This specific mutation significantly increased the binding affinity of the antibody to the CD20 antigen.

Figure 3. Top three sequences of the Rituximab with minimum Kd values from the ML model.

Structure modelling

Protein structure of Rituximab and CD20 antigen peptide was collected from the protein data bank (PDB). The required modification in the rituximab was imposed in the complex structure using SWISS Pdb viewer tool. Swiss-PdbViewer is an application that provides a user friendly interface allowing to evaluate many proteins at the same time(37). The structure was further simulated under physiological condition for 100 ns to achieve the most stable conformation. Both wild and new variant of rituximab was simulated for 100 ns. Various evaluation metrics were further computed on the simulation trajectory.Root mean square deviation (RMSD)

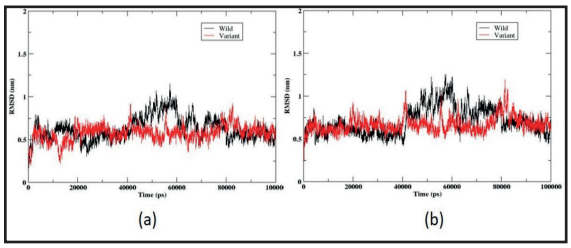

Figure 4. Root mean square deviation (RMSD) for the (a) antibody (rituximab) and (b) antigen (CD20) for wild type and variant type in the complex.

The deviation of antigen-antibody complex from the equilibrated structure achieved after the NVT and NPT ensemble equilibration. This deviation showed the change in the conformational space of the antigen-antibody complex. Root-mean-square deviation (RMSD) was calculated over the 100 ns for the rituximab (antibody) and CD20 (antigen). The RMSD is a metric that quantifies the average distance between the atoms, typically the backbone atoms, of molecules that have been superimposed(38). Both antigen and antibody showed high RMSD during the 100 ns simulation. Here, the wild and variant both started with the similar pattern in the RMSD for antibody as shown in Figure 4 (a) at 0.75 nm from the initial conformation. Until the 40 ns of the simulation trajectory, they behaved similarly. However, post 40 ns, wild type showed a high peak of RMSD compared to variant. Moreover, after 80 ns, they re-showed the similar pattern of RMSD. Similarly, in antigen the RMSD of wild type showed the higher peak between 40 ns to 80 ns. Following an 80-nanosecond interval, they subsequently realign and attain a stable configuration, converging at a distance of 0.75 nanometers, as visually represented in Figure 4 (b). Plots shown in Figure 4, illustrate the higher deviation in the wild conformation of the protein compared to the variant (both for antibody and antigen). Here, the reference structure used for alignment was the

complete complex while the RMSD was calculated for the antigen and antibody separately. The plots showed that RMSD of the antibody and antigen behaved similarly as per their deviation pattern from the initial docked conformation. Here, the complete complex was taken as reference for the alignment and RMSD was calculated for antibody and antigen individually. This suggest that antibody showed translation motion in the given complex. The interaction site has changed to limited extent during the course of the simulation. This happened to find the stronger interaction with the antigen. However, it is noted that variant that designed in this case study has shown lower deviation than the wild type. This specify that if the variant antibody interact with the antigen in native like conformation, then the chances of formation of stable pose is higher compared to the wild type. Both the plots showed a jump in same period (40-70 ns) that indicate the disturbance of the conformation. However, it settled in the later phase to achieve more stability. Overall, this outcome provides significant understanding into the dynamic characteristics of the Rituximab-CD20 complex, highlighting the variations in stability and structural modifications between the original and modified versions of the antibody. These findings hold great importance in understanding the molecular foundation of interactions between antibodies and antigens, and can provide assistance in developing therapeutic antibodies that are more stable and efficient.

Root mean square fluctuation (RMSF)

The root mean square fluctuation (RMSF) quantifies the variation of each atom along the whole trajectory. Later, the root mean square fluctuation (RMSF) was calculated for wild and variant antibody to compare the fluctuation at residue level. The plot shown in Figure 5, shows that both wild type and variant showed the similar trend of RMSF. In heavy chain of the wild type other than the terminal residues LYS-129, SER-130, and SER-132 showed the high RMSF, crossing 0.3 nm cutoff while LYS-129 and SER-130 also showed the similar RMSF pattern in variant type. However, none of these residues were part of the CDR region. In contrast, light chain showed more stability and only terminal residues showed the high RMSF while rest of the residues were settled in their conformation. The graphical representation of the RMSF is shown in the Figure 5. As observed from the plots that both wild and variant type behaved similarly in the simulation and common residues showed the jump in the RMSF.

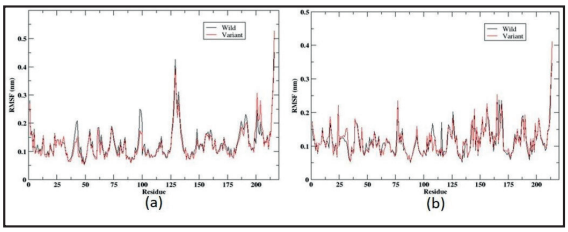

Figure 5. RMSF plots of (a) heavy chain and (b) light chain for both wild and variant types. X axis shows the residue number and Y axis shows the RMSF in nm scale.

Free energy landscape (FEL)

Free energy landscapes are commonly used in computational chemistry and biophysics to represent and simulate the process of protein folding, ligand-receptor interaction, enzyme mechanisms, and other dynamic molecular processes. They offer valuable information regarding the thermodynamics and kinetics of these processes(39). Here, the top two principal components of the conformational motion were calculated to represent the maximum deviation. This presents the movement of the protein along the principal component to achieve an energetically stable state. Moreover, it also presents the variation in the structure of the protein that signifies the overall stability of the molecule. The antibody antigen complexes (wild and variant) was simulated for 100 ns and their principal components were detected, the motion and the energy term were calculated as shown in the 3D energy landscape in Figure 6. The free energy was shown in relative scale where the most stable state or the minimum free energy state was considered as reference. Therefore, the energy

scale started from 0 (minimum) and went to high scale. Moreover, in the funnel shape plot, it is shown that wild type has multiple basins while the variant has single basin. These basins are minimum energy state that was achieved for the given complex. It is noteworthy that going from one basin to another basin there are energy barrier that needs to be crossed. Navigating these energy barriers presents a formidable challenge within the conformational space, and there is a significant likelihood of a given structure becoming trapped in these local energy minima. As shown in the Figure 6, that variant has no energy barrier in their its free energy landscape and this showed that complex has high possibility to reach the global minima without getting trapped in the local minima. On the other hand, wild type has energy barriers and there is more chance that conformation would trap in the local minima and will not be eligible to reach global minima. It is also been seen that basins in the wild type have not the similar energy states conformation as depicted by the colour gradient and the depth of the basin. In conclusion, this investigation shows the significance of studying the energy landscapes of molecular complexes. The outcome is that the mutated version of the antibody-antigen complex is more prone to achieving a stable structure with ease, without the obstruction of energy obstacles, in contrast to the original form. The understanding acquired from this observation is extremely helpful in the realm of drug design and protein engineering, as it pertains to the crucial aspects of molecular interactions' stability and efficiency.

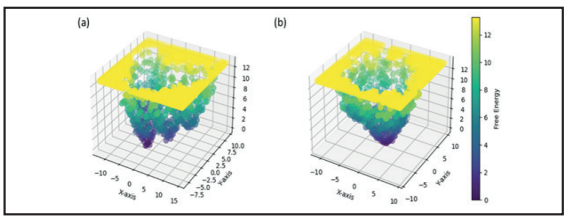

Figure 6. Free energy landscape of the antigen (CD20) and antibody (rituximab) complex for 100 ns simulation calculated over first two principal components for (a) wild type and (b) variant type.

Gibbs binding free energy (∆G)

MM/PBSA and MM/GBSA have been extensively employed in biomolecular studies, particularly in the investigation of protein folding, protein−ligand binding, and protein−protein interactions(40). Here, binding free energy of the antigen-antibody complex was calculated for the last 20 ns of the simulation. MM/GBSA (Molecular mechanics with generalised Born and surface area solvation) method was employed to calculate the binding free energy. This energy has multiple energetic terms that includes gas and solvation term of gibbs energy. Gas energy term has Van der Waal and electrostatic energy components. However, solvation term has both polar and non-polar components. Average values for all the terms were calculated van der Waal showed the most favourable energy (-63.07 kcal/mole) for the wild while for variant electrostatic component dominated (-70.55 kcal/mole). Polar solvation energy was positive in both the cases, wild has 50.08 kcal/mole while for variant it is 129.57 kcal/mole. Overall, the average binding free energy for wild and variant was comparative but variant showed more stability with -45.44 kcal/mole and the wild type had -37.66 kcal/mole. This showed that variation in the antibody provided stronger interaction with the antigen that further resulted in the more stable complex formation. Figure 7, showed the binding free energies for wild and variant types with their various energetic components.

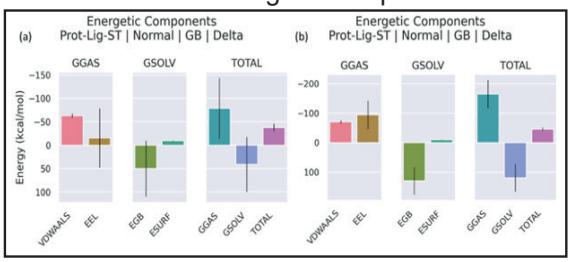

Figure 7. Binding free energy calculated using MM/GBSA techniques for (a) wild type and (b) variant type.

Further, the binding free energy was recorded for each frame, 20 frames were gen-

erated for the last 20 ns. Energy in each of the frame is shown in Figure 8. The energy was stable for the variant the standard deviation was 6.21. In the wild type the energy continuously fallen and reached to minimum at 100 ns.

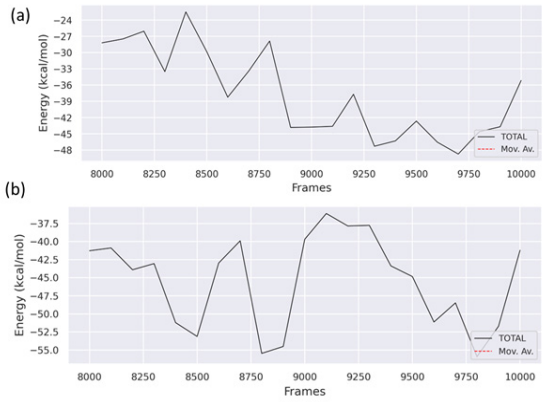

Figure 8. Binding free energy of each frame for (a) wild type and (b) variant type for the rituximab and CD20 complex over last 20 ns simulation trajectory.

RMSD and RMSF shown earlier in the calculation conveyed that the conformation of wild and variant type showed similar trend. However, variant had relatively more stable conformational behaviour during the simulation trajectory. This showed that more stability was attained in the complex after the change imposed in the rituximab sequence. This change was guided by the ML method demonstrated in this study. Later, it was also showed that the variant had similar level of residual fluctuation. The variant had favourable binding free energy calculated from the MM/GBSA. Overall, the variant of rituximab showed stronger binding with the antigen than the wild type.

Discussion

The therapeutic application of monoclonal antibodies (mAbs) is among the most promising areas within the domain of immunotherapy. Immunogenicity is one of the most significant factors that can limit the therapeutic and diagnostic applications of mAbs. The advancement of biological therapeutics has been greatly accelerated by the integration of computational technologies with high-throughput technology(41–43). Numerous cases of in silico vaccine design have been successful, including the vaccine design initiated by Correia et al. through computational protein design(44). They used in-silico methods to design small, thermally and conformationally stable protein scaffolds. Additional testing has shown that these protein scaffolds successfully imitate the structure of the viral epitope and stimulate powerful antibodies that can neutralise the virus.

The present study demonstrated the conceptualization and construction of a resilient machine learning framework for forecasting the antigen-antibody binding affinity. The conjoint triad encoder method demonstrated the highest degree of accuracy, as evidenced by its correlation coefficient of 0.78. An additional application of the method was to illustrate its efficacy on rituximab through the generation of original sequences that targeted the CDR region. Rituximab induces apoptosis, complement activation, and antibody-dependent cell-mediated cytotoxicity by binding to the CD20 marker expressed on B lymphocytes (Miranda-Hernández MP, López-Morales CA, Ramírez-Ibáñez ND, Piña-Lara N, Pérez NO, Molina-Pérez A, et al. Assessment of physicochemical properties of rituximab related to its immunomodulatory activity(45, 46). The study identified the optimal sequence exhibiting the greatest affinity for the CD20 antigen. A molecular dynamics (MD) simulation study was conducted to investigate the binding characteristics and structure of the variant rituximab. The RMSD of this variant was lower than that of the wild type. This indicates that the probability of stable pose formation is greater for variant antibodies that interact with the antigen in a native-like conformation, as opposed to the wild type. The binding free energy of the antigen-antibody complex was -45.44 kcal/mole for the Rituximab variant and -37.66 kcal/mole for the wild type. This showed that variation in the antibody provided stronger interaction with the antigen that further resulted

in the more stable complex formation. A free energy landscape (FEL) was calculated by utilising the initial two principal components (PC1 and PC2). In contrast to the wild type, which possesses three minimum energy basins, this variant displayed only one. Thus, it was demonstrated that the antibody variant-produced complex is more capable of achieving global minima. In the machine learning model, the variant that was generated and justified demonstrated a higher level of stability and affinity with the antigen. Thus, the methodology that was presented in the study has the potential to be utilised in the design of antibodies in order to produce therapeutic antibodies that are more effective.

Conclusion

This study showed the design and development of a robust machine learning model to predict the binding affinity between antigen and antibody. Conjoint triad encoder method showed the highest accuracy with 0.78 correlation coefficient. The method was further used to demonstrate its application on rituximab by generating novel sequences by targeting the CDR region. The study detected the best sequence that showed the highest affinity for the CD20 antigen. The structure of the variant rituximab was modelled and the binding characteristics was explored in MD simulation study. The variant generated and justified in ML model showed the higher stability and affinity with the antigen. The method presented in the study has potential to be used in antibody design to generate more efficacious therapeutic antibody.

Acknowledgements: The authors acknowledge Jaypee Institute of Information Technology, NOIDA, Uttar Pradesh and National Institute of Biologicals, NOIDA for providing infrastructure and support

Conflict of Interest: The authors declare that there are no conflicting interests.

Funding: There is no funding to report

Authors Contribution: H.K. wrote the manuscript. A.M. conceived the idea and methodology. H.C. and A.M. edited the manuscript. All authors read and approve the manuscript

References

1. Berger, M., Shankar, V., & Vafai, A. (2002). Therapeutic Applications of Monoclonal Antibodies. *The American Journal of the Medical Sciences*, *324*(1), 14–30. https://doi.org/10.1097/00000441-200207000-00004
2. Suzuki, M., Kato, C., & Kato, A. (2015). Therapeutic antibodies: their mechanisms of action and the pathological findings they induce in toxicity studies. *Journal of Toxicologic Pathology*, *28*(3), 133–139. https://doi.org/10.1293/tox.2015-0031
3. Quinteros, D. A., Bermúdez, J. M., Ravetti, S., Cid, A., Allemandi, D. A., & Palma, S. D. (2017). Therapeutic use of monoclonal antibodies: general aspects and challenges for drug delivery. In *Nanostructures for Drug Delivery* (pp. 807–833). Elsevier. https://doi.org/10.1016/B978-0-323-46143-6.00025-7
4. Houen, G. (2022). Therapeutic Antibodies: An Overview. In G. Houen (Ed.), *Therapeutic Antibodies* (Vol. 2313, pp. 1–25). New York, NY: Springer US. https://doi.org/10.1007/978-1-0716-1450-1_1
5. Lu, L. L., Suscovich, T. J., Fortune, S. M., & Alter, G. (2018). Beyond binding: antibody effector functions in infectious diseases. *Nature Reviews. Immunology*, *18*(1), 46–61. https://doi.org/10.1038/nri.2017.106
6. Kamen, L., Ordonia, B., Myneni, S., & Chung, S. (2022). Method for Measurement of Antibody-Dependent Cellular Phagocytosis. In G. Houen (Ed.), *Therapeutic Antibodies* (Vol. 2313, pp. 305–312). New York, NY: Springer US. https://doi.org/10.1007/978-1-0716-1450-1_19
7. Akbar, R., Robert, P. A., Pavlović, M., Je-

liazkov, J. R., Snapkov, I., Slabodkin, A., … Greiff, V. (2021). A compact vocabulary of paratope-epitope interactions enables predictability of antibody-antigen binding. *Cell Reports*, *34*(11), 108856. https://doi.org/10.1016/j.celrep.2021.108856

8. Beeg, M., Nobili, A., Orsini, B., Rogai, F., Gilardi, D., Fiorino, G., … Gobbi, M. (2019). A Surface Plasmon Resonance-based assay to measure serum concentrations of therapeutic antibodies and anti-drug antibodies. *Scientific Reports*, *9*(1), 2064. https://doi.org/10.1038/s41598-018-37950-4

9. Huber, W., & Mueller, F. (2006). Biomolecular Interaction Analysis in Drug Discovery Using Surface Plasmon Resonance Technology. *Current Pharmaceutical Design*, *12*(31), 3999–4021. https://doi.org/10.2174/138161206778743600

10. Frenzel, A., Roskos, L., Klakamp, S., Liang, M., Arends, R., & Green, L. (2014). Antibody Affinity. In S. Dübel & J. M. Reichert (Eds.), *Handbook of Therapeutic Antibodies* (pp. 115–140). Weinheim, Germany: Wiley-VCH Verlag GmbH & Co. KGaA. https://doi.org/10.1002/9783527682423.ch6

11. Spiegelberg, D., Stenberg, J., Richalet, P., & Vanhove, M. (2021). KD determination from time-resolved experiments on live cells with LigandTracer and reconciliation with end-point flow cytometry measurements. *European Biophysics Journal*, *50*(7), 979–991. https://doi.org/10.1007/s00249-021-01560-2

12. Reverberi, R., & Reverberi, L. (2007). Factors affecting the antigen-antibody reaction. *Blood Transfusion*. https://doi.org/10.2450/2007.0047-07

13. Schneider, C., Raybould, M. I. J., & Deane, C. M. (2022). SAbDab in the age of biotherapeutics: updates including SAbDab-nano, the nanobody structure tracker. *Nucleic Acids Research*, *50*(D1), D1368–D1372. https://doi.org/10.1093/nar/gkab1050

14. Dunbar, J., Krawczyk, K., Leem, J., Baker, T., Fuchs, A., Georges, G., … Deane, C. M. (2014). SAbDab: the structural antibody database. *Nucleic Acids Research*, *42*(D1), D1140–D1146. https://doi.org/10.1093/nar/gkt1043

15. Huang, K., Fu, T., Glass, L. M., Zitnik, M., Xiao, C., & Sun, J. (2021). DeepPurpose: a deep learning library for drug–target interaction prediction. *Bioinformatics*, *36*(22–23), 5545–5547. https://doi.org/10.1093/bioinformatics/btaa1005

16. Li, L., Chen, S., Miao, Z., Liu, Y., Liu, X., Xiao, Z., & Cao, Y. (2019). AbRSA: A robust tool for antibody numbering. *Protein Science : A Publication of the Protein Society*, *28*(8), 1524–1531. https://doi.org/10.1002/pro.3633

17. Berman, H. M., Westbrook, J., Feng, Z., Gilliland, G., Bhat, T. N., Weissig, H., … Bourne, P. E. (2000). The Protein Data Bank. *Nucleic Acids Research*, *28*(1), 235–242. https://doi.org/10.1093/nar/28.1.235

18. Bank, R. P. D. (n.d.). RCSB PDB - 2OSL: Crystal structure of Rituximab Fab in complex with an epitope peptide. Retrieved October 14, 2023, from https://www.rcsb.org/structure/2OSL

19. Du, J., Wang, H., Zhong, C., Peng, B., Zhang, M., Li, B., … Ding, J. (2007). Structural Basis for Recognition of CD20 by Therapeutic Antibody Rituximab *. *Journal of Biological Chemistry*, *282*(20), 15073–15080. https://doi.org/10.1074/jbc.M701654200

20. Dunbar, J., Krawczyk, K., Leem, J., Marks, C., Nowak, J., Regep, C., … Deane, C. M. (2016). SAbPred: a structure-based antibody prediction server. *Nucleic Acids Research*, *44*(Web Server issue), W474–W478. https://doi.org/10.1093/nar/gkw361

21. Berendsen, H. J. C., van der Spoel, D., & van Drunen, R. (1995). GROMACS: A message-passing parallel molecular dynamics implementation. *Computer Physics Communications*, *91*(1), 43–56. https://doi.org/10.1016/0010-4655(95)00042-E

22. Abraham, M. J., Murtola, T., Schulz, R., Páll, S., Smith, J. C., Hess, B., & Lindahl, E. (2015). GROMACS: High performance molecular simulations through multi-level parallelism from laptops to supercomputers. *SoftwareX*, *1*, 19–25. https://doi.org/10.1016/j.softx.2015.06.001

23. GROMACS 2022 Manual. (n.d.). https://doi.org/10.5281/zenodo.6103568

24. Huang, J., & MacKerell, A. D. (2013). CHARMM36 all-atom additive protein force field: validation based on comparison to NMR data. *Journal of Computational Chemistry*, *34*(25), 2135–2145. https://doi.org/10.1002/jcc.23354

25. Darden, T., York, D., & Pedersen, L. (1993). Particle mesh Ewald: An N·log(N) method for Ewald sums in large systems. *The Journal of Chemical Physics*, *98*(12), 10089–10092. https://doi.org/10.1063/1.464397

26. Bussi, G., Donadio, D., & Parrinello, M. (2007). Canonical sampling through velocity rescaling. *The Journal of Chemical Physics*, *126*(1), 014101. https://doi.org/10.1063/1.2408420

27. Parrinello, M., & Rahman, A. (1981). Polymorphic transitions in single crystals: A new molecular dynamics method. *Journal of Applied Physics*, *52*(12), 7182–7190. https://doi.org/10.1063/1.328693

28. Xu, Y., Gnanasekaran, R., & Leitner, D. M. (2012). Analysis of Water and Hydrogen Bond Dynamics at the Surface of an Antifreeze Protein. *Journal of Atomic and Molecular Physics*, *2012*, e125071. https://doi.org/10.1155/2012/125071

29. Valdés-Tresanco, M. S., Valdés-Tresanco, M. E., Valiente, P. A., & Moreno, E. (2021). gmx_MMPBSA: A New Tool to Perform End-State Free Energy Calculations with GROMACS. *Journal of Chemical Theory and Computation*, *17*(10), 6281–6291. https://doi.org/10.1021/acs.jctc.1c00645

30. Miller, B. R. I., McGee, T. D. Jr., Swails, J. M., Homeyer, N., Gohlke, H., & Roitberg, A. E. (2012). MMPBSA.py: An Efficient Program for End-State Free Energy Calculations. *Journal of Chemical Theory and Computation*, *8*(9), 3314–3321. https://doi.org/10.1021/ct300418h

31. Bu, C., Zhang, L., Cui, H., Yang, G., & Wu, H. (2023). Dynamic Inference via Localizing Semantic Intervals in Sensor Data for Budget-Tunable Activity Recognition. *IEEE Transactions on Industrial Informatics*, *PP*, 1–13. https://doi.org/10.1109/TII.2023.3315773

32. Cheng, D., Zhang, L., Bu, C., Wang, X., Wu, H., & Song, A. (2023). ProtoHAR: Prototype Guided Personalized Federated Learning for Human Activity Recognition. *IEEE Journal of Biomedical and Health Informatics*, *27*(8), 3900–3911. Presented at the IEEE Journal of Biomedical and Health Informatics. https://doi.org/10.1109/JBHI.2023.3275438

33. Mirrashid, M., & Naderpour, H. (2023). Incomprehensible but Intelligible-in-time logics: Theory and optimization algorithm. *Knowledge-Based Systems*, *264*, 110305. https://doi.org/10.1016/j.knosys.2023.110305

34. Xu, S., Zhang, L., Tang, Y., Han, C., Wu, H., & Song, A. (2023). Channel Attention for Sensor-Based Activity Recognition: Embedding Features into all Frequencies in DCT Domain. *IEEE Transactions on Knowledge and Data Engineering*, *35*(12), 12497–12512. Presented at the IEEE Transactions on Knowledge and

Data Engineering. https://doi.org/10.1109/TKDE.2023.3277839

35. Polonelli, L., Pontón, J., Elguezabal, N., Moragues, M. D., Casoli, C., Pilotti, E., … Travassos, L. R. (2008). Antibody complementarity-determining regions (CDRs) can display differential antimicrobial, antiviral and antitumor activities. *PloS One*, *3*(6), e2371. https://doi.org/10.1371/journal.pone.0002371

36. Van Regenmortel, M. H. V., & Azimzadeh, A. (2000). Determination of Antibody Affinity. *Journal of Immunoassay*, *21*(2–3), 211–234. https://doi.org/10.1080/01971520009349534

37. Guex, N., & Peitsch, M. C. (1997). SWISS-MODEL and the Swiss-Pdb Viewer: An environment for comparative protein modeling. *ELECTROPHORESIS*, *18*(15), 2714–2723. https://doi.org/10.1002/elps.1150181505

38. Benson, N. C., & Daggett, V. (2012). A Comparison of Multiscale Methods for the Analysis of Molecular Dynamics Simulations. *The Journal of Physical Chemistry B*, *116*(29), 8722–8731. https://doi.org/10.1021/jp302103t

39. Camacho, C. J., Weng, Z., Vajda, S., & DeLisi, C. (1999). Free Energy Landscapes of Encounter Complexes in Protein-Protein Association. *Biophysical Journal*, *76*(3), 1166–1178. https://doi.org/10.1016/S0006-3495(99)77281-4

40. Wang, E., Sun, H., Wang, J., Wang, Z., Liu, H., Zhang, J. Z. H., & Hou, T. (2019). End-Point Binding Free Energy Calculation with MM/PBSA and MM/GBSA: Strategies and Applications in Drug Design. *Chemical Reviews*, *119*(16), 9478–9508. https://doi.org/10.1021/acs.chemrev.9b00055

41. Carter, P. J. (2006). Potent antibody therapeutics by design. *Nature Reviews Immunology*, *6*(5), 343–357. https://doi.org/10.1038/nri1837

42. Reichert, J. (2008). Monoclonal Antibodies as Innovative Therapeutics. *Current Pharmaceutical Biotechnology*, *9*(6), 423–430. https://doi.org/10.2174/138920108786786358

43. Nelson, A. L., & Reichert, J. M. (2009). Development trends for therapeutic antibody fragments. *Nature Biotechnology*, *27*(4), 331–337. https://doi.org/10.1038/nbt0409-331

44. Correia, B. E., Bates, J. T., Loomis, R. J., Baneyx, G., Carrico, C., Jardine, J. G., … Schief, W. R. (2014). Proof of principle for epitope-focused vaccine design. *Nature*, *507*(7491), 201–206. https://doi.org/10.1038/nature12966

45. Weiner, L. M., Dhodapkar, M. V., & Ferrone, S. (2009). Monoclonal antibodies for cancer immunotherapy. *The Lancet*, *373*(9668), 1033–1040. https://doi.org/10.1016/S0140-6736(09)60251-8

46. Tsurushita, N., Hinton, P. R., & Kumar, S. (2005). Design of humanized antibodies: From anti-Tac to Zenapax. *Methods*, *36*(1), 69–83. https://doi.org/10.1016/j.ymeth.2005.01.007

Current Trends in Biotechnology and Pharmacy
Vol. 18(3) 1881-1896, July 2024, ISSN 0973-8916 (Print), 2230-7303 (Online)
10.5530/ctbp.2024.3.34

Synergistic Effect of Chemical and Physical Treatments on *Azolla pinnata* for Cadmium Ions Removal from Synthetic Wastewater Systems

Kaakarlu Shivakumar Vinanthi Rajalakshmi[1] and Kuppusamy Alagesan Paari[1*]

[1*]Department of Lifesciences, CHRIST (Deemed to be University), Bangalore, India- 560029
*Corresponding Author : paari.ka@christuniversity.in

Abstract

Azolla pinnata, an aquatic fern has been utilized as an effective biofiltering and adsorbent agent to complement many conventional treatment methods for the removal of environmental pollutants. This study is designed to develop an effective regime to treat metal pollutants of industrial and urban waste discharge using a novel strategy involving *Azolla pinnata*. In the present study, cell surface modification by physical treatments that include heating (muffle furnace), and mechanical waves (ultrasonication) and chemical treatments as sulphuric acid and ethanol were employed to enhance the adsorption of metal pollutants. Factors such as biosorbent dose, contact time, initial metal ion concentration, temperature, and solution pH were optimised in batch mode. The point of zero charge of the adsorbent was determined to be at 5.85 pH. The results of surface morphology, elemental analysis, crystallinity, recorded through SEM, FTIR and XRD confirmed the adsorptive properties in both modified and unmodified biomass. The intensity peaks linked to O-H, C-H, C-N, N-H and C=O stretching bands was intense in the treated *A. pinnata* groups indicating the induction of the active groups. Out of the two chemical pre-treatments, the batch adsorption experiment with ethanol found to chelate Cd^{+2} metal ions to a higher extent (94.36%) in contrast to the results obtained from H_2SO_4 treated biomass. Whereas, the physical treatments exhibited the strong adsorption (83.28 and 96.92±0.55%) for ultrasonicated and muffle furnace pre-treated biomass respectively for the dosage of 0.25g. The adsorption efficiency of physically modified sorbent revealed the cent percent removal of Cd^{+2} ions from the aqueous phase with the dosage of 1.0g in 15min of contact time which is due to the incorporation of new binding sites. Moreover, these results proved that the highest rate of cadmium adsorption onto *A. pinnata* is in result of the modifications caused onto surface structure, porosity and the addition of functional groups on the surface of the treated biomass.

Keywords: *Azolla pinnata*, phytoremediation, cadmium chelation, surface properties, chemical and physical modifications.

Introduction

Rapid population explosion coupled with industrialization and urbanization has given way to increased ecosystem degradation (1). The major environmental issue raised throughout the world is the egression of toxic pollutants in water bodies due to the disposal of toxic wastes originated from automobile engines, industrial sectors and domestic operators

(2). Wastewater, especially discarded from the industries, contain a wide range of heavy metals such as Cd, As, Fe, Cr, Zn, Cu, Mn, Pb, Ni, etc, turns out to be a major environmental concern due to their bioaccumulation properties (3). Being a simple and persistent element, cadmium cannot be broken down into less toxic forms in the environment. Accumulation of such toxicants into the water either in the form of organic or inorganic compounds successively enter the food chain leading to various health hazards (4). The conventional treatment methods for metal removal from aqueous streams such as chemical precipitation, lime coagulation, ion exchange, reverse osmosis and solvent extraction etc. are not economical besides posing toxicity (5,6). Among the existing technologies, adsorption method meets the requirements to maximize the removal of heavy metals, supporting the objective of identifying the most effective water treatment system. Adsorption is widely regarded as the most popular technique for removing heavy metals from systems as it is cheap, easy to use, readily available in a wide variety of adsorbents, highly efficient, easy to operate, reversible, and ability to regenerate (7). As release of hazardous pollutants are inevitable with industrial revolution, employment of novel remedial measures such as bioremediation and phytoremediation using adsorbents may mitigate the toxic effects caused by the pollutants.

Utilization of aquatic plants to hyperaccumulate the pollutants from wastewater and their application in biomonitoring of pollution had been well reported (8). Aquatic macrophytes are considered to be strong indicators of heavy metal pollution in aquatic ecosystems, acting as biological filters by absorbing heavy metals (9,10,11). *Azolla pinnata*, an aquatic pteridophyte commonly known as water fern, has emerged as a promising candidate due to its remarkable characteristics such as rapid growth rate, high biomass production, and efficient nutrient uptake (12). *Azolla*'s high biomass productivity, ability to proliferate in diverse aquatic habitats, and relatively short lifecycle further enhance its suitability for remediation studies (13). Despite such promising attributes, the precise mechanisms underlying *Azolla*-mediated heavy metal removal, as well as its efficacy under varying environmental conditions, remain unclear. Moreover, *Azolla* species possess an exceptional capacity to accumulate heavy metals from surrounding water, attributed to mechanisms such as adsorption, chelation, and bioaccumulation. This study aims to provide a comprehensive overview of the current state of knowledge regarding the role of *Azolla pinnata* in heavy metal remediation and to assess the efficiency of the native, chemically and physically modified *Azolla pinnata* to uptake the metal Cd. Experimental findings of this research seek to elucidate the factors that should be considered in the removal of Cd from wastewaters by native, and modified *A. pinnata*.

Materials and methods

Biomass preparation

The healthy biomass of *Azolla pinnata* was collected from the experimental site (pollution-free site) and thoroughly rinsed with distilled water to eliminate soil and dust contaminants, followed by desiccation in a shaded environment for a duration of 3 days. Subsequently, it was subjected to oven drying at a controlled temperature of 40°C for a period of 24 hours. The dried material was pulverized using blender and sieved to obtain constant size particles (0.85–1.70 mm) and was used for characterization without any prior chemical treatment and stored in aliquots for further study (14).

Health properties by pigmentation analysis

Transmission, absorption, and reflection, along with many other plant stress and pigment indicators was measured using CI-710s Spectra Vue Leaf Spectrometer (CID Bio-Science, USA). The operating environment of the instrument was maintained at -10°C to 50°C with non-condensing humidity (0% - 90%). The

detector with the wavelength range of 360-1100 nm and the spectrometer with the minimum leaf size of 20mm x 20mm was used to allow full operation in a handheld form factor with a 7inch 1024 x 600 IPS touchscreen display (Integration time of 30µs – 60s). The quantification of chemical concentrations, pigment analysis, and the quantification of physical or optical properties such as film thickness, index of refraction, and extinction coefficient were analysed with a full suite of the built-in indices' software (15).

Chemical modification of azolla pinnata biomass

Sulphuric acid treatment

10g of biomass of *A. pinnata* was added to 100 ml of 0.1N H_2SO_4 and the solution was then placed on a rotary shaker at 40 °C, at 105 rpm, for 24 h. The adsorbent was then cooled to room temperature and was separated by filtration using Whatman No.1 Ashless filter paper. Following filtration, the biomass was thoroughly washed with distilled water until pH 6-7 was obtained and was dried in an oven at 70 °C overnight until the constant weight was acquired. The material was sieved and stored in a desiccator prior to further analysis (16).

Ethanol treatment

Azolla biomass of about 10g was exposed to 25% ethanol solvent for 4hrs at 40 °C and was placed in a shaking incubator overnight at 105 rpm. The solution mixture was then subjected to filtration and washed with distilled water until the solution reaches neutral pH. Then the activated biomass was dried overnight at 60°C and stored in air tight container for the further study (17).

Physical modifications of azolla pinnata biomass

Ultrasonication treatment

In this type of physical modification, the powders was ultrasonicated at an amplitude of 20 for the time interval of 1hr, followed by washing with distilled water and was oven dried for one day at 70°C. The resultant biosorbents, modified via physical means, were then evaluated for their effectiveness in the biosorption of cadmium metal ions (18).

Muffle furnace treatment

Thermal treatment was carried out at 300°C with no external air or gas supply for 1 h in a muffle furnace. The yield of char obtained was 52%. The prepared biosorbents were tested directly for the biosorption of cadmium metal ions from the aqueous solutions (18).

Preparation of metal stock solution

The analytical grade of $Cd(NO_3)_2.\ 4H_2O$ of 99% assay was used in this study. The standard metal stock solution was prepared using standard procedures, with varying initial concentrations by dissolving $Cd(NO_3)_2.\ H_2O$ in distilled water. All glassware utilized in the biosorption studies was frequently rinsed with HNO_3 followed by extensive washing with distilled water to mitigate interference from contaminants. The pH of each solution was determined using a digital pH meter and subsequently adjusted using 0.1 M HCl or 0.1 M NaOH solutions.

Biosorption studies and research design

Biosorption potential of raw chemically, and physically modified *Azolla pinnata* was tested. The effect of experimental factors such as biosorbent dose, metal ion concentration, contact time, temperature and pH was investigated independently for Cd^{+2} ion biosorption onto *Azolla pinnata* biomass. Each parameter was analysed stepwise in batch mode while keeping one constant against other suitable variables. To test the biosorption efficiency, known biomass of Azolla was exposed to varying concentrations of Cd^{+2} (15.75ppm and 500 ppm). The batch of test tubes were placed on a rotary shaker with a constant shaking of 100 rpm with pre-defined temperature and exposure time.

The solution was filtered and the biomass was separated from the filtrate using filter paper. The concentration of Cd^{+2} metal ion in the filtrates were analysed by atomic adsorption spectroscopy (AAS). Two controls, including metal-free and biosorbent-free blanks were employed.

Batch adsorption experiments were conducted with different pH (5-9), adsorbent doses (0.25-1.0g), Cd^{+2} ion concentrations (15.75-500ppm), temperatures (15-45 ^{o}C) at different time intervals (15 ,30,60 and 180mins).

Metal adsorption capacity (qe) is defined as the quantity of metal adsorbed per gram of biosorbent and can be calculated using the following equation Eq. (1) and expressed in mg/g:

$$qe = (C_i - C_e) \times V/m \ldots\ldots\ldots (1)$$

where m is the mass of biosorbent (g), V is the volume of solution (L), C_i is the initial metal-ion concentration (mg/L), and Ce is the equilibrium concentration of metal ions (mg/L). The percentage of metal removed was computed using equation Eq. (2) as follows:

$$\text{Removal efficiency } (\%) = (C_i - C_e)/C_i \times 100 \ldots\ldots\ldots (2)$$

Instrumental characterization of unmodified and modified azolla pinnata biomass

The adsorbent developed by chemical and physical modification were characterized to understand the surface morphology, surface chemistry, and to analyse the functional sites of the adsorbent. The interaction of cadmium ions with the biosorbent material was detected using analytical tools. The surface morphology, chemical characterization and elemental composition of the adsorbent was analysed using Apreo S LoVac Scanning Electron Microscopy (SEM, ThermoFisher Scientific Corporation). The active sites and functional groups on the adsorbent were assessed by Fourier transform infrared (FTIR) spectrophotometer with QATR-S single reflection ATR accessory having extended range diamond crystal (Shimadzu Model IR Spirit). The nature and chemical composition of metal on the surface of *Azolla* sorbent was detected through Rigaku Mini Flex Powder X-ray Diffractometer (XRD, Rigaku Corporation) with Cu Kα radiation. The generator voltage and current were set at 35 KV and 25 mA respectively. The *A. pinnata* samples were scanned in the 2θ ranges 20-80°C in continuous scan mode with a 10°/ min scan speed (19).

Statistical analysis

The statistical analysis was carried out by using SPSS statistics software version 27. The results were interpreted by One-way Analysis of Variance (ANOVA) to verify the significance using Duncan's Test by the probability less than $p<0.05$.

Results and discussion

` *Azolla* species was identified and authenticated as *Azolla pinnata* R. Br. (Voucher no.1094) by Central Ayurveda Research Institute, Bangalore, India. The fresh *Azolla* collected from the study site and was subjected to CI-710s Spectra Vue Leaf Spectrometer to detect the health properties of *A. pinnata* before its utilization in various environmental applications. The present investigations showed the existence of chlorophyll *a* and chlorophyll *b* that was approximately in the standard range of ¼ and ¾ with total chlorophyll content of 6.9821±0.3943ugcm^{-3} (Table 1). The presence of anthocyanin (0.3695±0.0780), flavanols (0.0643±0.0376) and carotenoid (0.0186±0.0046) indices signified the ability of the plant to protect against biotic and abiotic stresses. The decrease in the chlorophyl content index due to water stress in plant was recorded in previous studies and a strong correlation with the amount of chlorophyll in the plant was observed (20,21). Further research on the pigmentation and its correlation to plant stress properties in aquatic plants is required as the information is scarce.

Table 1. Pigmentation index, health and stress of *A. pinnata*

Sl. no.	Index	Abbrev	Index value
1	Anthocyanin Reflectance Index	ARI	0.3695±0.0780
2	Carotenoid Reflectance Index	CRI	0.0186±0.0046
3	Chlorophyll A ($ugcm^{-3}$)	CPHLA	1.7563±0.1648
4	Chlorophyll B ($ugcm^{-3}$)	CPHLB	5.4326±0.2720
5	Chlorophyll Total ($ugcm^{-3}$)	CPHLT	6.9821±0.3943
6	Chlorophyll Content Index	CCI	1.3390±0.1717
7	Chlorophyll Normalized Difference Vegetation Index	CNDVI	0.2077±0.0205
8	Flavanols Reflectance Index	FRI	0.0643±0.0376
9	Greenness Index	G	2.1098±0.1715
12	Photochemical Reflection Index	PRI	0.2998±0.0224
13	Plant Senescence Reflectance Index	PSRI	0.1049±0.0186
16	Water Band Index	WBI	1.8289±0.0335

Optimization factors affecting the cadmium biosorption potential of Azolla pinnata

Main parameters such as pH, temperature, contact time, biosorbent dosage and heavy metal initial concentration that influence the biosorption of cadmium was investigated. The present biosorption experiments were carried out using varying adsorbent dosages to determine the effect of each factor at different mass of *A. pinnata* biomass. The results depicted in Table 2. show that the percentage of Cd^{+2} removal increased from 52.46 to 89.62% with the increase in adsorbent concentration from 0.25 to 1g/25mL in the metal solution (500mg/L). Increased adsorption is due to the more availability of unsaturated active sites on the biomass surface for the attachment of the metal ions (22). The rate of adsorption above the optimal dose of 1g/25ml of 500mg/L was found to be remain unchanged or decreased due to insufficient Cd^{+2} ion concentration to fit all the active sites on surface of the adsorbent, which is in consistent with the results of earlier reports (23). However, at a lower adsorbent dosage, the interaction of Cd^{+2} ions with adsorbent decreases because of the limited biding sites available for adsorption (24).

Effect of metal ion concentration at varying adsorbent dosages

The mechanism of metal uptake is dependent on the initial metal ion concentration in the solution. The present study evaluated the highest amount of Cd^{+2} ions that could be up taken by the adsorbent at a 0.25g dose at a pH of 6.6 is up to 408.65mg/L when the time of exposure increased from 15min to 24hr. The rate of Cd^{+2} adsorption onto *A. pinnata* at different concentrations (15.75 to 500mg/L) of Cd^{+2} ions is displayed in Table 2. The removal efficiency increased proportionally with the increase in initial metal concentration from 15.47 to 365.95mg/L of Cd^{+2} respectively in 15min of contact time. Similarly, the decrease in the percent removal from 99.24 to 81.58% when concentration of Cd^{+2} increased from 20 to 200 mg/L was reported (25). Nonetheless, increasing the Cd^{+2} ion concentration from 15.75 to 250 mg/L did not show further increase in the rate of uptake and attained equilibrium (95.82 ± 3 % of adsorption) after 1hr of exposure. Further increase in the initial Cd^{+2} concentration (500mg/L) decreased the rate to 89.62%, which is in strong agreement with the recent studies (26,27). This could be due to weak and inconsistent force of contact

between metal ions and the surface of adsorbent indicating the saturation point, which may lead to diffusion of ions into the aqueous phase or due to limited availability of active sites on the adsorbent (22,28).

Table 2. Factors influencing on the cadmium biosorption onto untreated *Azolla pinnata*.

Metal Concentration (mg/L)	15min	30min	1hr	3hr	6hr	12hr	24hr
BD: 0.25g							
500	262.3	278.9	368.3	375.15	381.05	379.85	385.65
250	163.2	181.02	201.57	210.2	213.1	217.32	222.57
125	89.07	96.46	112.14	115.26	115.4	115.95	117.36
62.5	50.26	51.33	58.9	60.74	60.82	61.63	60.93
31.25	26.95	27.85	30.05	30.27	30.71	31.51	31.19
15.75	14.85	14.92	15.13	15.28	15.12	15.32	15.54
BD: 0.50g							
500	339.1	358.15	416.2	423.95	432.7	434.45	441.65
250	188.37	197.95	221.77	235.8	237.96	238.72	239.55
125	97.89	106.82	116.54	120.9	121.09	121.28	122.15
62.5	52.26	54.64	60.32	60.93	61.35	61.72	62.14
31.25	28.83	29.73	30.74	30.92	31.12	31.04	31.18
15.75	15.12	15.37	15.71	15.57	15.68	15.7	15.73
BD: 0.75g							
500	350.05	374.8	430.5	432.8	436.85	439.7	445.83
250	202.82	210.35	228.2	237.83	239.67	241.03	242.9
125	105.26	111.46	119.7	123.79	123.97	124.25	124.79
62.5	55.11	58.29	61.44	61.56	61.67	62.31	62.48
31.25	29.7	30.85	30.9	30.98	31.13	30.82	31.22
15.75	15.15	15.23	15.42	15.53	15.61	15.67	15.73
BD: 1.0g							
500	365.95	376.3	448.1	451.04	456.6	460.55	461.6
250	215.53	223.58	233.42	239.8	241.21	242.33	244.1
125	113.49	117.13	121.39	123.6	124.07	124.28	124.91
62.5	58.14	60.44	61.26	61.94	61.71	61.58	61.42
31.25	30.6	30.92	30.53	31.03	31.11	31.2	31.15
15.75	15.47	15.52	15.61	15.65	15.58	15.71	15.74

BD- Biosorbent dosage, mg/L- milligram per litre

Effect of contact time at varying adsorbent dosages

Contact time is one of the significant factors that possess a major impact on the adsorption rate of the *Azolla* biomass. The rate of adsorption of Cd^{+2} ions onto the surface of *A. pinnata* at various contact times (15 min, 30 min, 1hr, 3hr, 6hr, 12hr, and 24hr) with respect to varying metal ion concentration and adsor-

bent dosages is listed in Table 2. The uptake of Cd^{+2} ions was found to be increase rapidly during the first 15min-1hr which is due to the abundancy of unsaturated active sites on the biomass surface (demonstrating an adsorption process occurs through surface binding with no energy-mediated reactions). Similar to the present findings, the rate of adsorption of Cd^{+2} ions increased from 83.7% to 87.2%, when the contact time raised from 15min to 3hrs at the dosage of 0.25g/100ml (25). After 1hr of biosorption, the removal of metal ions gradually decreased and eventually reached equilibrium due to the attainment of saturation point (29). The time required for the metal ions in a solution to become constant is an equilibrium time of adsorption. The maximum biosorption rate for Cd^{+2} uptake was 461.6 mg/g and the removal percentage was 92.32% within 1hr of adsorbent - adsorbate contact time. According to the present investigation, a rapid absorption rate (365.95 - 448.1mg/g) was noted till 1hr, followed by a slower adsorption during the 3 - 6hr (453.82 ± 2.78 mg/g) and, eventually reached an equilibrium. Due to the rapid increase in metal bio-adsorption rate, the more efficient contact time required for the further batch experiments was considered to be 30mins-1hr.

Effect of temperature at varying adsorbent dosages

The temperature is the main factor that influences the adsorption process. The adsorption capacities of *A. pinnata* for the Cd^{+2} ions at different temperatures with varying adsorbent dosages are shown in Figure 1. A temperature ranges between 5 °C to 45 °C with the differences of 10 °C were studied. It was observed that adsorption increased slightly with increasing temperature from 5 °C to 25 °C. But it was analysed that the percentage of Cd^{+2} ion adsorption onto *A. pinnata* was higher between 25 °C and 35 °C up to 99.7%.

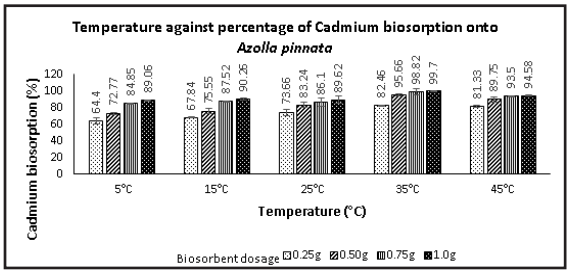

Figure 1. Effect of solution temperature on the removal of Cd^{+2} ions (initial conc.= 500mg/L, exposure time = 60min, pH = 7, agitation speed = 100rpm)

Based on the present findings, the adsorption of the Cd^{+2} metal ions onto the *A. pinnata* biomass increased with the rise in temperature which indicates the endothermic nature of the adsorption process due to higher diffusion rate and increased transportation of metal ions (30,31). The adsorption decreased approximately 5-10 % when the temperature was further raised to 45 °C. for the same dosages of unmodified *A. pinnata* biomass and Cd^{+2} metal ion concentration. Several studies have reported the reduced metal ion uptake by increasing temperature (32). This decrease is due to the tendency of the Cd^{+2} ion molecules to migrate from the adsorbent (solid phase) to the metal medium (liquid phase) or due to weak adsorptive forces between the Cd^{+2} ions adsorbed and the active sites on the biomass and also between adjacent Cd^{+2} molecules adsorbed on the adsorbent surface (33). This indicated that the adsorption process using unmodified biomass is physisorption.

Effect of pH at varying adsorbent dosages

The point of zero charge (pH_{PZC}) refers to the pH at which the surface charge density of the adsorbent is electrically neutral exhibiting minimal interaction with metal solution (34). In the present study, pH_{PZC} of the adsorbent was determined to be 5.85 (Figure 2). Consequently, at pH of metal solution below 5.85, the adsorbent surface acquires positive charge enhancing its attraction to anions. Conversely, when

the pH exceeds the pH_{PZC}, the adsorbent surface becomes negatively charged, creating conditions conducive to the adsorption of cationic species (35).

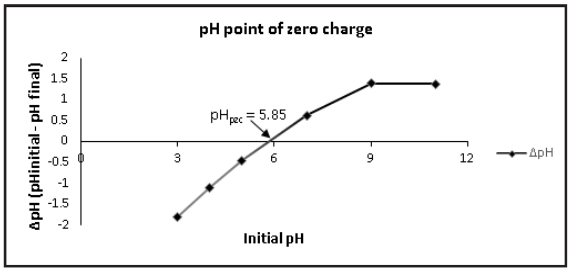

Figure 2. Point of zero charge of untreated *Azolla pinnata* biomass

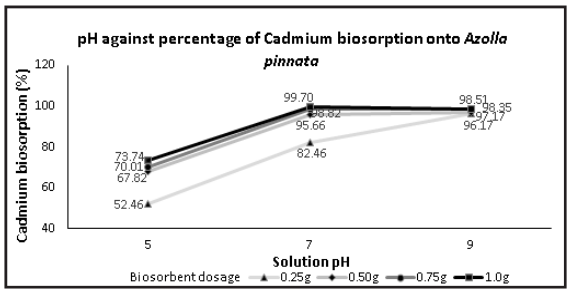

Figure 3. Effect of solution pH on the removal of Cd^{+2} ions (initial conc.= 500mg/L, exposure time = 60min, temperature = 35°C, agitation speed = 100rpm)

The effects of pH on the biosorption of Cd^{+2} ions onto *Azolla pinnata* biomass were investigated at a pH ranging from 5 to 9 are shown in Figure 3. The biosorption capacities of adsorbent (qe; mg/L) for Cd^{+2} cations increased with the increasing pH from pH 5 to pH 7. Under alkaline conditions, the anions on the biosorbent surface increases, so, the biosorption efficiencies increases rapidly from 52.46 to 99.7%. This occurs due to the decrease in competitive adsorption between metal cations (Cd^{+}) and protons (H^{+}) to bind onto the same functional groups/ active sites (ion exchange mechanism) (36). Beyond the optimum pH, metal cations react with hydroxide ions and precipitate as metal hydroxide (precipitation mechanism) which could have cause the diffusion of Cd^{+2} ion from the adsorbent surface into the medium above pH 7 and decreases the efficiencies of adsorption gradually to 96.17% (37). But due to the formation of insoluble metallic hydroxide and to ignore the effect of precipitation of Cd^{+2} ions, further adsorption studies were performed at pH 7.

Characterization of Azolla for adsorptive properties

FTIR analysis

FTIR spectroscopy was used as a major tool to detect the characteristic functional groups present on the surface of biomass which may facilitate the binding sites for the attachment of Cd^{+2} ions. The adsorbent spectra of the showed multiple types of vibrational frequencies in peaks due to the presence of distinct functional groups. The FTIR graphs of the physically and chemically modified *A. pinnata* biomass before and after cadmium adsorption (in the range of 400–4000 cm^{-1}) are shown in Figure 4.

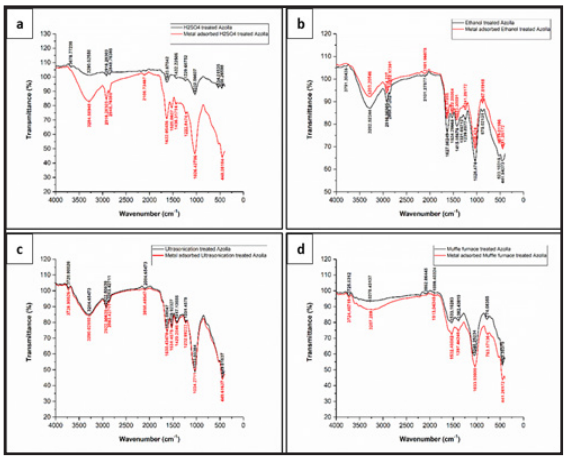

Figure 4. FTIR spectra of H_2SO_4 (a), EtOH (b), ultrasonication (c), and muffle furnace (d) treated *Azolla* biomass before (black line) and after (red line) adsorption of cadmium ions.

The FTIR spectroscopic graph of H_2SO_4 treated *Azolla* biomass before Cd^{+2} adsorption revealed strong adsorption bands at 3290 cm^{-1}, confirming the presence of N-H and O-H broad stretching. Peaks at 1623 cm^{-1} and 1032 cm^{-1} were linked to N-H and C-N representing amine

bending and stretching respectively. However, the Cd^{+2}-loaded H_2SO_4 treated adsorbent displayed supplementary peaks around 2916 (C-H stretching), 2848 (C–H stretching), 1525 (–COO- anti-symmetric stretching), and 448 (C–H bending) cm^{-1} in Figure 4a. Whereas, the ethanol modified biomass displayed the significant peaks at 3282, 2916, 1627, 1415 and 1028 cm^{-1} for O-H stretching, C-H alkane stretching, N-H amine bending, O-H carboxylic acid bending, and C-O ether stretching respectively. Only shift in few peaks with no significant changes after Cd load onto EtOH treated biomass surface was noticed (Figure 4b).

Similarly, the FTIR graphs for physically modified biomass showed overlapping peaks with no changes even before and after Cd^{+2}-load onto the ultrasonicated biomass surface (Figure 4c). The muffle furnace treated *Azolla* biomass displayed strong bands at 3278 (O-H stretching) and 1048 cm^{-1} revealing major changes after Cd^{+2} accumulation (Figure 4d). Overall, the FTIR spectroscopic graphs for Cd-loaded physically and chemically modified sorbent showed significant shifting and disappearance of some peaks revealing the strong bonds between the Cd ions and the biomass surface (38). Noticeably, the appearance of some new peaks in the graph evidencing the fact that, the functional groups on the surface of the *A. pinnata* biomass are more affective in the adsorption of Cd^{+2} ions. In comparison to the unmodified *A. pinnata*, the strength of the O-H, N-H, C=O and C-H stretching bands on treated *A. pinnata* biomass surface increased as a result of modifications, indicating the increase in the active groups (19)

XRD analysis

The degree of crystallinity of adsorbent material was determined by X-ray diffraction analysis of *Azolla* biomass before and after treatments and Cd adsorption onto their surface. Figure 5 depicts the high intensity peak at angle of 2θ: 26.8° which disappeared after Cd- load onto acid treated adsorbent. However, few broad peaks obtained for EtOH treated adsorbent at angles 29.6°, 36.2°, 39.7°, 43.5°, 47.7° and 48.8° indicating the semi-crystalline structure after Cd^{+2}-load (Figure 5a,b).

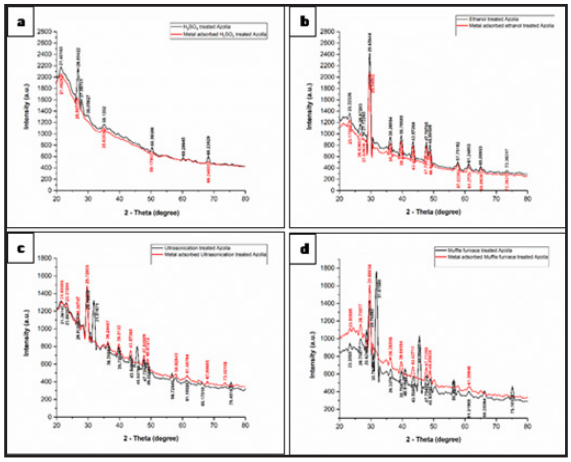

Figure 5. XRD pattern of H_2SO_4 **(a)**, EtOH **(b)**, ultrasonication **(c)**, and muffle furnace **(d)** treated *Azolla* biomass before (black line) and after (red line) adsorption of cadmium ions.

The physically modified adsorbents showed the diffraction peaks between 2θ: 30° to 50° for ultrasonicated biomass confirming the crystalline structure. More significant shift in the broad diffraction peak from 2θ: 31.8° to 2θ: 29.7° and disappearance of peaks at angles 2θ: 45.5°, 56.7° and 75.45° was observed that may due to the interaction of Cd^{+2} ions with sorbent surface. Similarly, the high intensity peaks at angles 2θ: 28.6°, 31.8°, 45.6°, 56.4° and 75.1° found to be reduced after Cd^{+2}-load representing the transition of crystalline to the amorphous structure for furnace modified adsorbent (Figure 5c,d). Although XRD analysis does not directly elucidate the mechanism of the adsorption process between the adsorbent material and Cd^{+2} ions, its significance remains paramount due to the high crystallinity that was exhibited by all treated adsorbent structures. The strong bonds between heavy metals and sorbent were evidenced by a reduction in crystallinity, and was indicated by shifts or broadening of diffraction peaks, along with the emergence of new peaks (39). Moreover, variations in crystallinity, wheth-

er increased or decreased, further confirm the interaction of the adsorbent with heavy metal ions after the adsorption of Cd^{+2} ions.

Scanning Electron Microscope analysis

The surface morphological features of blank and Cd^{+2}-loaded *Azolla* biomass was demonstrated in Figure 6a, b. The dominance of a complex pore matrices and coarse holes on its preceding structures, which were significant for the adsorption process, can be noticed in the raw (unmodified) biomass surface (Figure 6a) with average pore size up to 253.5nm. In fact, these properties such as rough morphology, porous surface, greater pore size are found to be highly favourable and supportive for metal ion attachment in the adsorption process (31). The adsorption of Cd^{+2} ions caused the untreated biomass to form a smoother surface and tight structures throughout the visualization (Figure 6b).

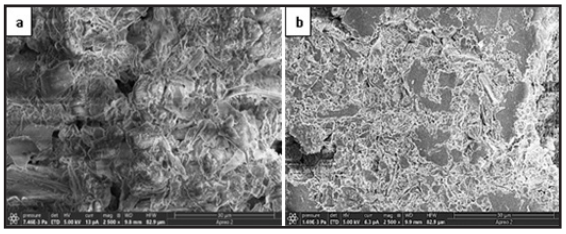

Figure 6. SEM analysis of raw (unmodified) *Azolla* biomass before **(a)** and after **(b)** adsorption of cadmium ions.

SEM analysis of treated adsorbents revealed the visualization of minor structural alterations on its surface (Figure 7a, b, c, d). From the SEM images of chemical and physical modified adsorbent, all treated biomass can be described as having porosity with many fragments scattered on its surface and inside the pores before metal adsorption (40). The porous size of treated biomass was slightly increased up to 290.03 nm for H_2SO_4 treated biomass and 4-fold increase of pore size up to 1.043 µm was seen in EtOH treated *Azolla* biomass. The porosity on the physical modified biomass surface ranged between 158.7 nm and 217.3 nm due to the reduction of particle size after treatments. Unlike these possibilities, the number of pores on the surface of ultrasonicated and muffle furnace treated biomass may increase by facilitating the chelation of Cd^{+2} ions to a greater extent. The formation and distribution of the new pores over the entire surface of the material is expected to improve the performance of the biomass as an adsorbent, which may due to the modifications on its surface either physically or chemically (18).

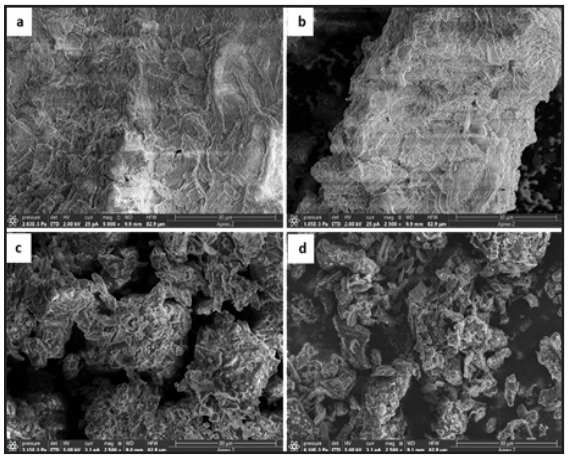

Figure 7. SEM analysis of H_2SO_4 (a), EtOH (b), ultrasonication (c), and muffle furnace (d) treated *Azolla* biomass before adsorption of cadmium ions.

Cadmium-loaded *Azolla* biomass was also analysed to observe the morphological changes (Figure 8). The disappearance of previously detected pores, transition of rough to smoother surface, and modulation of small scattered fragments into larger fragments, (41,42) which affirmed the attachment of Cd^{+2} ions to the active binding sites on the surface and pores of *A. pinnata* biomass (Figure 8a,b). The surface characterization of physical modified adsorbent was completely varied after Cd^{+2} adsorption exhibiting shininess (Figure 8c,d) as described by the earlier report (43).

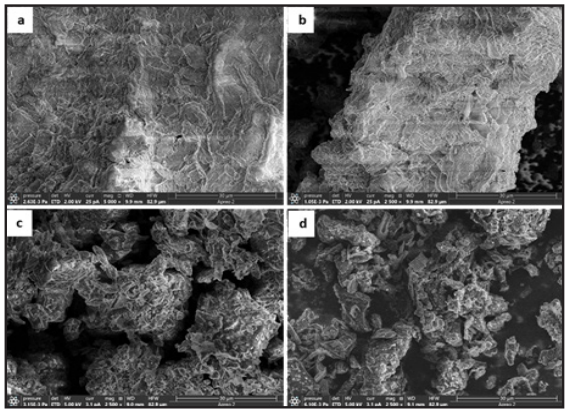

Figure 8. SEM analysis of H_2SO_4 (a), EtOH (b), ultrasonication (c), and muffle furnace (d) treated *Azolla* biomass after adsorption with cadmium ions.

Biosorption efficiency of chemically and physically modified A. pinnata biomass

The adsorption experiments were conducted using different chemical and physical modified *A. pinnata* sorbents. The results obtained from the optimization studies for some factors such as initial Cd^{+2} ion concentration= 500mg/L, temperature = 35°C, pH=7.0 were maintained during the experimentation. The contact time is found to be saturated at 60min. But the exposure time of 15min with agitation speed of 100rpm were considered for further studies with treated adsorbents to understand the short time of exposure required for its applicability at pilot scale.

Table 3. The percentage of metal recovered from treated and untreated *A. pinnata* adsorbents

	Untreated	Chemical treatments		Physical treatments	
Biosorbent dosage	**Raw**	**H_2SO_4**	**EtOH**	**Ultrasonication**	**Muffle furnace**
0.25g	71.43±1.36^{c}	64.72±0.92^{d}	94.36±1.58^{b}	83.28±2.62^{c}	96.92±0.50^{c}
0.50g	86.49±0.52^{b}	77.95±1.88^{c}	99.21±0.60^{a}	91.12±1.22^{b}	98.82±1.17^{b}
0.75g	90.76±4.65^{ab}	87.22±3.55^{b}	100.22±0.87^{a}	96.47±2.81^{a}	100.78±0.91^{a}
1.0g	91.80±1.64^{a}	91.12±2.84^{a}	100.36±0.68^{a}	99.44±2.88^{a}	100.74±0.61^{a}
***p* value**	**< 0.001**	**< 0.001**	**< 0.001**	**< 0.001**	**0.001**

Values are expressed as mean ± SD (%) for triplicates, SD: Standard deviation, H_2SO_4: Sulphuric acid treated adsorbent, EtOH: Ethanol treated adsorbent. *p value significant ($p \leq 0.05$) accordance to Duncan's multiple range test in different treatments are expressed in increasing order as a-d.

Based on the earlier reports, the analytical investigations have revealed that the modifications of biomass surface result in notable changes in their adsorptive properties such as hydrophobic properties, water absorption characteristics, ion exchange capacity, resilience against microbial degradation, and thermal stability. Therefore, in the present study some methods such as physical treatments which include heating (muffle furnace), and mechanical waves (ultrasonication) and chemical treatments as acid solutions (sulphuric acid) and organic compounds (ethanol) were employed for the modification of cell surface.

The cadmium removal efficiency of different chemical and physical treated and untreated *A. pinnata* adsorbents is displayed in Table 3. The results obtained from these adsorption studies showed the metal recovery of up to 71.43% and later increased to 91.80% when the dose of untreated biomass increased from 0.25 – 1.0g. The chemical treatment with ethanol has showed faster adsorption kinetics as well as higher biosorption for Cd^{+2} ions than the virgin *A. pinnata* biomass. In contrast, H_2SO_4 pre-treatment showed the significant decrease in the Cd^{+2} biosorption onto *Azolla* biomass of about 64.72% which is lesser than its untreated

counterpart. This may occur due to the formation of large amount of oxygen functionalities in narrow pore openings and closure of some micropores and mesopores which in turn result in decrease of surface volume and surface area on biosorbent (44). Whereas, the physical treatments exhibited the strong adsorption that are reported to be 83.28 and 96.92±0.55% for ultrasonicated and muffle furnace pre-treated biomass (BD: 0.25g) respectively. Further reached 99.44 to 100% (maximum up to 500ppm) revealing the cent percent removal of Cd^{+2} ions from the aqueous phase with the dosage of 1.0g in 15min of contact time which is due to the incorporation of binding sites. The introduction of various cell surface modifications such as phosphorylation and carboxylation of hydroxyl group, amination of hydroxyl and carboxyl group, carboxylation of amine groups, saponification of carboxylate ester groups, oxidation, etc. has led to an increased biosorptive efficiency (45). Thus, it can be concluded that that the functional groups on the biomass facilitated the occurrence of a polar and hydrophilic surface, which enabled the binding or absorption of cationic metal ions.

Conclusion

In conclusion, the modifications undertaken to enhance the adsorptive properties on biomass surface has witnessed *Azolla pinnata* as an effective adsorbent for cadmium remediation from synthetic wastewater, which entails a balance between heightened adsorption potential, prolonged stability, production costs and environmental implications. The present research findings demonstrate the utilization of organic solvents and heat in chemical and physical treatments as a novel exploration in phytoremediation, respectively. As the current investigation focuses solely on cadmium as the target metal, modifications involving chemical agents (such as sulphuric acid and ethanol) and physical techniques (such as ultrasonication and muffle furnace treatment) may not uniformly enhance adsorption for all contaminants. Consequently, ongoing research aims to explore more efficient chemical and physical methodologies for surface modifications and metal desorption techniques to mitigate environmental and human health risks. Hence, a meticulous assessment of the optimistic treatment approaches is essential in making well-informed decisions regarding the adoption of these technologies.

Acknowledgement

The laboratory facilities and support for this study was provided by CHRIST (Deemed to be University) which the authors gratefully acknowledge and would like to extend their sincere gratitude to Centre for research for providing necessary facilities (MRP DSC - 1936).

Conflict of Interest

The authors declare no conflict of interest

References

1. Kobilov, E., Batirov, K., & Ozdamirova, E. (2023). Urban Ecosystems of Uzbekistan and Ways of Their Ecologization. BIO Web of Conferences. https://doi.org/10.1051/bioconf/20236303002.
2. Lin, L., Yang, H., & Xu, X. (2022). Effects of water pollution on human health and disease heterogeneity: a review. Frontiers in environmental science, 10:880246. https://doi.org/10.3389/fenvs.2022.880246.
3. Kumar, P., Gacem, A., Ahmad, M. T., Yadav, V. K., Singh, S., Yadav, K. K., ... & Cabral-Pinto, M. (2022). Environmental and human health implications of metal (loid) s: Source identification, contamination, toxicity, and sustainable clean-up technologies. Frontiers in Environmental Science, 10:949581. https://doi.org/10.3389/fenvs.2022.949581.
4. Vinanthi Rajalakshmi, K. S., Liu, W. C., Balamuralikrishnan, B., Meyyazhagan, A., Sattanathan, G., Pappuswamy, M., ... & Lee, J. W. (2023). Cadmium as an Endocrine Disruptor That Hinders the Repro-

ductive and Developmental Pathways in Freshwater Fish: A Review. Fishes, 8:589. https://doi.org/10.3390/fishes8120589.

5. Razzak, S. A., Faruque, M. O., Alsheikh, Z., Alsheikhmohamad, L., Alkuroud, D., Alfayez, A., ... & Hossain, M. M. (2022). A comprehensive review on conventional and biological-driven heavy metals removal from industrial wastewater. Environmental Advances, 7:100168. https://doi.org/10.1016/j.envadv.2022.100168.

6. Karim, A., Raji, Z., Karam, A., & Khalloufi, S. (2023). Valorization of Fibrous Plant-Based Food Waste as Biosorbents for Remediation of Heavy Metals from Wastewater—A Review. Molecules, 28:4205. https://doi.org/10.3390/molecules28104205.

7. Türkmen, D., Bakhshpour, M., Akgönüllü, S., Aşır, S., & Denizli, A. (2022). Heavy metal ions removal from wastewater using cryogels: A review. Frontiers in Sustainability, 3:765592. https://doi.org/10.3389/frsus.2022.765592.

8. Ali, S., Abbas, Z., Rizwan, M., Zaheer, I. E., Yavaş, İ., Ünay, A., ... & Kalderis, D. (2020). Application of floating aquatic plants in phytoremediation of heavy metals polluted water: A review. Sustainability, 12(5):1927. https://doi.org/10.3390/su12051927.

9. Kristanti, R. A., & Hadibarata, T. (2023). Phytoremediation of contaminated water using aquatic plants, its mechanism and enhancement. Current Opinion in Environmental Science & Health, 100451. https://doi.org/10.1016/j.coesh.2023.100451.

10. Sarojini, G., Kannan, P., Rajamohan, N., & Rajasimman, M. (2023). Bio-fabrication of porous magnetic Chitosan/Fe3O4 nanocomposite using Azolla pinnata for removal of chromium–Parametric effects, surface characterization and kinetics. Environmental Research, 218:114822. http://dx.doi.org/10.1016/j.envres.2022.114822.

11. Sharma, K., Saxena, P., & Kumari, A. (2023). Phytoremediation of Heavy Metals by Azolla filiculoides Lam. From Fly Ash Polluted Water Bodies. Water, Air, & Soil Pollution, 234(7):419. http://dx.doi.org/10.1007/s11270-023-06423-4.

12. Kumar, S., Thakur, N., Singh, A. K., Gudade, B. A., Ghimire, D., & Das, S. (2022). Aquatic macrophytes for environmental pollution control. In Phytoremediation Technology for the Removal of Heavy Metals and Other Contaminants from Soil and Water (pp. 291-308). Elsevier. https://doi.org/10.1016/B978-0-323-85763-5.00023-4.

13. Sachdeva, S., & Sharma, A. (2012). Azolla: role in phytoremediation of heavy metals. Int J Eng Sci, 1: 9698. http://dx.doi.org/10.13140/RG.2.1.1276.0407.

14. Bhatt, N., Chandra, R., Kumar, S., Singh, K., & Pratap, N. (2020). Nutritive analysis of Azolla pinnata and its cultivation during winter season. Int. J. Curr. Microbiol. App. Sci, 9:2012-2018. https://doi.org/10.20546/ijcmas.2020.903.233.

15. Kupčinskienė, A., Brazaitytė, A., Rasiukevičiūtė, N., Valiuškaitė, A., Morkeliūnė, A., & Vaštakaitė-Kairienė, V. (2023). Vegetation Indices for Early Grey Mould Detection in Lettuce Grown under Different Lighting Conditions. Plants, 12:4042. https://doi.org/10.3390/plants12234042.

16. Li, Z., Teng, T. T., Alkarkhi, A. F., Rafatullah, M., & Low, L. W. (2013). Chemical modification of imperata cylindrica leaf powder for heavy metal ion adsorption. Water, Air, & Soil Pollution, 224:1-14. https://doi.org/10.1007/s11270-013-1505-5.

17. Argun, M. E., & Dursun, S. (2006). Removal of heavy metal ions using chemically modified adsorbents. J. Int. Environ. Appl. Sci, 1:27-40. https://www.researchgate.net/publication/266888800.

18. Aswani, M. T., & Kumar, M. P. (2019). A novel water hyacinth based biosorbent for 2, 4-dichlorophenoxyacetic acid (2, 4-D) removal from aqueous solution. Desalin. Water Treat., 165:163-176. https://doi.org/10.5004/dwt.2019.24581.

19. Rajalakshmi, K. S. V., & Paari, K. A. (2023). A comprehensive study on the assessment of chemically modified Azolla pinnata as a potential cadmium sequestering agent. Int. J. Exp. Res. Rev, 36:01-19. https://doi.org/10.52756/ijerr.2023.v36.001.

20. Ghasemi M, Arzani K, Yadollahi A, Ghasemi S, Khorrami SS (2011). Estimate of leaf chlorophyll and nitrogen content in Asian pear (Pyrus serotina Rehd.) by CCM-200. Not. Sci. Biol., 3:91-94. https://doi.org/10.15835/nsb315623.

21. Khaleghi, E., Arzani, K., Moallemi, N., & Barzegar, M. (2012). Evaluation of chlorophyll content and chlorophyll fluorescence parameters and relationships between chlorophyll a, b and chlorophyll content index under water stress in Olea europaea cv. Dezful. International Journal of Agricultural and Biosystems Engineering, 6:636-639. https://doi.org/10.5281/zenodo.1082211.

22. Yousaf, A., Athar, M., Salman, M., Farooq, U., & Chawla, F. S. (2017). Biosorption characteristics of Pennisetum glaucum for the removal of Pb (II), Ni (II) and Cd (II) ions from aqueous medium. Green Chemistry Letters and Reviews, 10:462-470. https://doi.org/10.1080/17518253.2017.1402093.

23. Manzoor, Q., Nadeem, R., Iqbal, M., Saeed, R., Ansari, T.M. (2013). Organic acids pretreatment effect on Rosa bourbonia phyto-biomass for removal of Pb (II) and Cu (II) from aqueous media. Bioresour. Technol. 132:446-452. https://doi.org/10.1016/j.biortech.2013.01.156.

24. Fawzy, M., Nasr, M., Abdel-Gaber, A., & Fadly, S. (2016). Biosorption of Cr (VI) from aqueous solution using agricultural wastes, with artificial intelligence approach. Separation Science and Technology, 51:416-426. https://doi.org/10.1080/01496395.2015.1115068.

25. Kumar, P., & Kumar, P. (2019). Removal of cadmium (Cd-II) from aqueous solution using gas industry-based adsorbent. SN Applied Sciences, 1:1-8. https://doi.org/10.1007/s42452-019-0377-8.

26. Ding, Z., Hu, X., Wan, Y., Wang, S., & Gao, B. (2016). Removal of lead, copper, cadmium, zinc, and nickel from aqueous solutions by alkali-modified biochar: Batch and column tests. Journal of Industrial and Engineering chemistry, 33:239-245. https://doi.org/10.1016/j.jiec.2015.10.007.

27. Sazali, N., Harun, Z., & Sazali, N. (2020). A review on batch and column adsorption of various adsorbent towards the removal of heavy metal. Journal of Advanced Research in Fluid Mechanics and Thermal Sciences, 67:66-88. https://akademiabaru.com/submit/index.php/arfmts/article/view/2854.

28. Nassar, N.N. (2010). Rapid removal and recovery of Pb (II) from wastewater by magnetic nanoadsorbents. J. Hazard. Mater, 184:538–546. https://doi.org/10.1016/j.jhazmat.2010.08.069.

29. Taha, A. A., Shreadah, M. A., Heiba, H. F., & Ahmed, A. M. (2017). Validity of Egyptian Na-montmorillonite for adsorption of Pb2+, Cd2+ and Ni2+ under acidic conditions: characterization, isotherm, kinetics, thermodynamics and application study. Asia-Pacific Journal of Chemical Engineering, 12:292-306. https://doi.org/10.1002/apj.2072.

30. Deosarkar, S. D., & Hangirgekar, S. P. (2012). Cu (II) adsorption from aqueous

solution by Punica granatum L. husk. Journal of Chemical and Pharmaceutical Research, 4:4651-4656. http://jocpr.com/vol4-iss10-2012/JCPR-2012-4-10-4651-4656.pdf.

31. Alharbi, R. M., Sholkamy, E. N., Alsamhary, K. I., Abdel-Raouf, N., & Ibraheem, I. B. M. (2023). Optimization Study of the Capacity of Chlorella vulgaris as a Potential Bio-Remediator for the Bio-Adsorption of Arsenic (III) from Aquatic Environments. Toxics, 11:439. https://doi.org/10.3390/toxics11050439.

32. Gupta, V. K., Rastogi, A., & Nayak, A. (2010). Biosorption of nickel onto treated alga (Oedogonium hatei): application of isotherm and kinetic models. Journal of colloid and interface science, 342:533-539. https://doi.org/10.1016/j.jcis.2009.10.074.

33. Funtua, M. A., & Ugbe, F. A. (2015). Adsorption of heavy metals from aqueous waste water using unmodified and ethylenediaminetetraacetic acid (EDTA) modified maize cobs. Int. J. Curr. Res. Biosci. Plant Biol. Int. J. Curr. Res. Biosci. Plant Biol. Int. J. Curr. Res. Biosci. Plant Biol, 2: 98-103.

34. Borba, L. L., Cuba, R. M. F., Terán, F. J. C., Castro, M. N., & Mendes, T. A. (2019). Use of adsorbent biochar from Pequi (Caryocar Brasiliense) husks for the removal of commercial formulation of glyphosate from aqueous media. Brazilian Archives of Biology and Technology, 62. https://doi.org/10.1590/1678-4324-2019180450.

35. Tsegaye, F., Taddesse, A. M., Teju, E., & Aschalew, M. (2020). Preparation and sorption property study of Fe3O4/Al2O3/ZrO2 composite for the removal of cadmium, lead and chromium ions from aqueous solutions. Bulletin of the Chemical Society of Ethiopia, 34:105-121. https://doi.org/10.4314/bcse.v34i1.10.

36. Božić, D., Stanković, V., Gorgievski, M., Bogdanović, G., & Kovačević, R. (2009). Adsorption of heavy metal ions by sawdust of deciduous trees. Journal of hazardous materials, 171:684-692. https://doi.org/10.1016/j.jhazmat.2009.06.055.

37. Yao, Z. Y., Qi, J. H., & Wang, L. H. (2010). Equilibrium, kinetic and thermodynamic studies on the biosorption of Cu (II) onto chestnut shell. Journal of Hazardous Materials, 174:137-143. https://doi.org/10.1016/j.jhazmat.2009.09.027.

38. Balarak, D., Al-Musawi, T. J., Mohammed, I. A., & Abasizadeh, H. (2020). The eradication of reactive black 5 dye liquid wastes using Azolla filiculoides aquatic fern as a good and an economical biosorption agent. SN Applied Sciences, 2:1-11. https://link.springer.com/article/10.1007/s42452-020-2841-x.

39. Maponya, T. C., Makgopa, K., Somo, T. R., & Modibane, K. D. (2022). Highlighting the Importance of Characterization Techniques Employed in Adsorption Using Metal–Organic Frameworks for Water Treatment. Polymers, 14:3613. https://doi.org/10.3390/polym14173613.

40. Oladipo, B., Govender-Opitz, E., & Ojumu, T. V. (2021). Kinetics, thermodynamics, and mechanism of Cu (II) ion sorption by biogenic iron precipitate: using the lens of wastewater treatment to diagnose a typical biohydrometallurgical problem. ACS omega, 6:27984-27993. https://doi.org/10.1021/acsomega.1c03855.

41. Kavand, M., Asasian, N., Soleimani, M., Kaghazchi, T., & Bardestani, R. (2017). Film-pore-[concentration-dependent] surface diffusion model for heavy metal ions adsorption: single and multi-component systems. Process Safety and Environmental Protection, 107:486-497. https://doi.org/10.1016/j.psep.2017.03.017.

42. Charazińska, S., Burszta-Adamiak, E., & Lochyński, P. (2022). The efficiency of removing heavy metal ions from industrial electropolishing wastewater using natural materials. Scientific Reports, 12:17766. https://doi.org/10.1038/s41598-022-22466-9.

43. Huang, F., Guo, C. L., Lu, G. N., Yi, X. Y., Zhu, L. D., & Dang, Z. (2014). Bioaccumulation characterization of cadmium by growing Bacillus cereus RC-1 and its mechanism. Chemosphere, 109:134-142. https://doi.org/10.1016/j.chemosphere.2014.01.066.

44. El-Hendawy, A. N. A. (2003). Influence of HNO3 oxidation on the structure and adsorptive properties of corncob-based activated carbon. Carbon, 41: 713-722. https://doi.org/10.1016/S0008-6223(03)00029-0.

45. Gupta, V. K., Nayak, A., & Agarwal, S. (2015). Bioadsorbents for remediation of heavy metals: current status and their future prospects. Environmental engineering research, 20:1-18. https://doi.org/10.4491/eer.2015.018.

Current Trends in Biotechnology and Pharmacy
Vol. 18(3) 1897-1903, July 2024, ISSN 0973-8916 (Print), 2230-7303 (Online)
10.5530/ctbp.2024.3.35

Molecular Studies to Understand Brain Networking in Linguistic, Cognition and Emotions: Current and Future Challenges.

Pavani A[1@#], Emani L S [2#], Vasuja Devi M. [3] and Satyanarayana Rao TS [4]

[1.] Department of English, KLEF deemed to be University, Vaddeswaram-522302, India
[2.] Department of Biotechnology, KLEF Deemed to be University, Vaddeswaram-522302, India
[3.] Department of CSE, Mangalayatan University, Jabalpur, Madhya Pradesh, India
[4.] Department of Psychiatry, JSS Institute for Higher Education and Research, Mysore, India
Both are equal first authors
*Corresponding author: pavanilinguist@kluniversity.in

Abstract

Bilingual language process is a key factor in left side of the brain. The cognition of the learning modalities is very crucial for assimilation, organization, and interpretation of knowledge. The neurochemical events like estrogen, testosterone, dopamine 5HT, Oxytocin, nerve growth factor (NGF) play as neuro-endocrine brain axis for learning to cognition. The human cognition recognises the language in five stages that is input, status of language, getting access over the literature of that language, interaction with family, and finally social network communication. The factors influence the bilingual aspects include language exposure, genes, perception and receiving, neurochemical pathways, social communication, and environmental conditions. Apart from these elements the other external influencing factors like health humanities and technological advances and make a lot of impact on cognition processes and mental health.

Key words: Human Brain, Language, Alertness, Orientation, Cognition, Clinical Factors, Neurochemicals, Networking

Introduction

Brain is a unique organ in the body controlling all body functions and providing holistic functional efficiency coordinating human brain to body. The brain weighs 1.5 Kgs. and contains trillions of neurons with high interconnectivity leading to the efficient biological function. Healthy ageing of brain is a crucial biological phenomenon and understanding of healthy ageing still an open challenge. Any alterations in neurological integrity leads to brain disorders like cognitive deterioration, memory loss, movement disorders, loss of emotions and body coordination (1). Currently, 55million people are affected by brain disorders and by 2050 this number touches 155 million. The lack of early bio markers, cognitive and movement disorders disturbances are the critical challenges in the neurology clinics. The present paper highlights molecular understanding of brain and cognition and language interlinking leading to mental health.

The complexity of brain language

Language is a cognitive process in which brain involves and evolves while using. Language is a process involves brain include frontal, temporal and parietal lobes, and some posterior regions (1). Brain involvement and influence in using language as the brain centres express and increase extensively during the process of communication. This mechanism of language differs with second language as brain centres function differently while using a native language and executing a target language.

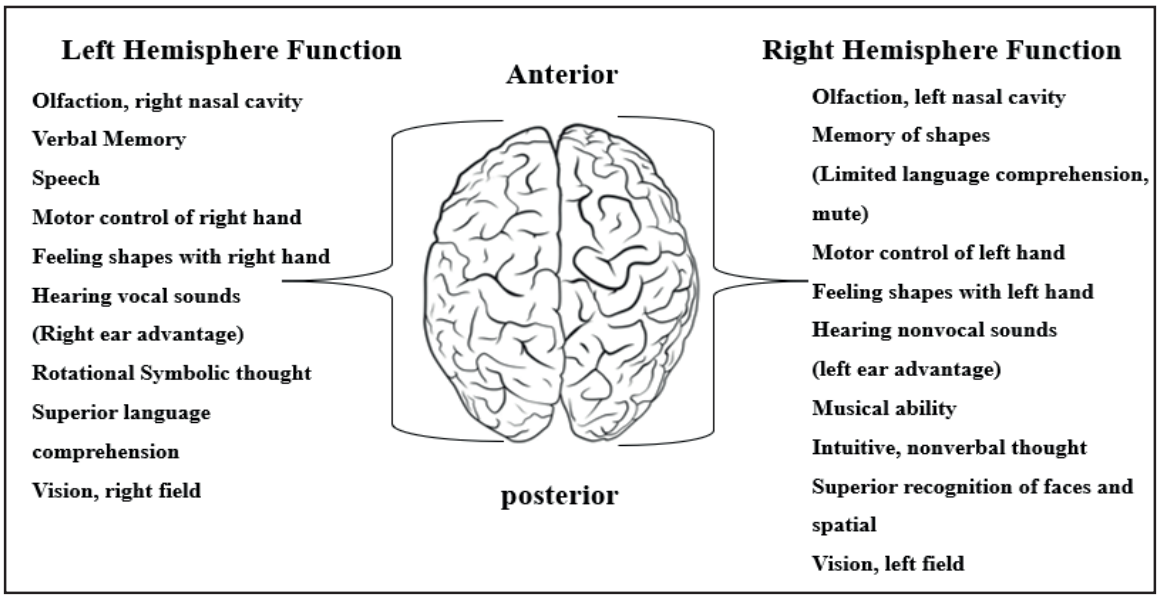

Figure 1: Function of Left and Right Hemisphere Brain

The above picture (Fig 1) replicates the brain and how the cognitive analysis take part. On the right side of the brain, the study, logic, and aptitude make brain receive the signals through study or observation thinks logically based on the aptitude calculations which memorizes on the left part of the brain it is shown in the picture which together forms the cognitive analytical process of brain function.

However, cognitive process of usage of language is synchronized with nonverbal patterns which strengthens and give emphasis to the communication. The language includes nonverbal which strengthens the communication (2). The process of neuro imaging enhances and supports the nonverbal patterns during the process of speaking and communicating. The context-based communication in expressions, the process of neuro imaging plays pivotal role to decode the message effectively. Hence, the cognitive outcomes of the bilingual concept are based on brain and its functions, exclusively the three active parts alertness, orientation, and detection of that language. This paper throws light on how these three patterns function in brain while using second language in expressing the thoughts to others effectively (3).

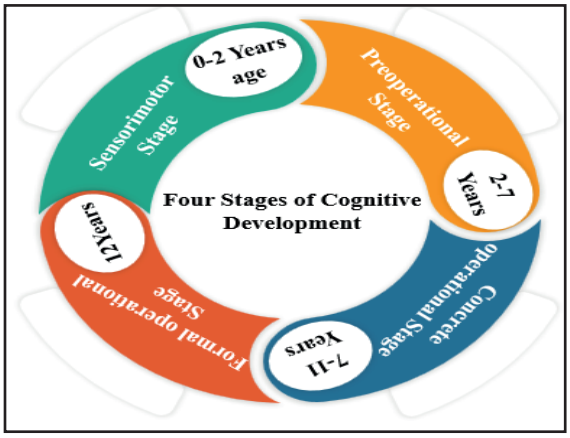

Figure 2: Developmental Stages of Cognitive Development

The above picture (Fig 2) connects with the cognitive process development once after its evolvement which is divided into four parts which finally leads to sensory motor where the destination of cognitive development of language understanding takes place based on the environment created amidst to them.

The early studies indicate that the anxiety and apprehension levels are high while using second language exclusively when compared it

with the native language (4). The process of using second language includes three main stages. The first stage is the influence of language, and the second stage is the execution of that and the third is contextual understanding and reproducing it in the second language accordingly. These three patterns influence, execution of language and contextual replica in expressions are the major mechanisms to emphasize on to avoid apprehensions using second language (5).

The major controlling power of fear while expressing thoughts during communication process is nothing but brain. As the process of cognitive analysis during the reciprocation takes place in brain, the understanding of brain patterns, controlling of brain and counselling of modules in brain are needed to avoid such challenges in using second language. While executing the bilingual language, the phobia, fear, and inhibitions in communication during the process of cognitive analysis there are mainly controlling processes involve in implications (6). As per the research studies till date, there are no authentic or concrete reasons found for the cause of fear, phobia and inhibitions in using of second language in public (7-10). The inhibitory controlling models to avoid anxiety while speaking in second language through the interferences phase in brain patterns. The second language usage in communication lead to many distractions in the adaptation of language. The configuration process in brain patterns while using when second language is used by the speaker as the two languages to be composed and executed at a time. The amalgamation process during the conversion of the context from understanding in native language to second language includes a major cognitive analytical process in brain patterns. The major challenge takes place in this due process. There is still a lot of research going on where the researchers are finding out the concrete and abstract reasons behind it.

As per the research done in the process of second language speaking, execution and challenges, the research says that the cognitive challenges are not similar in all age groups, as it differs based on gender, age, intelligence, socio-economic status as well. The notion that bilingualism could have generalized consequences for nonverbal cognitive ability originated in research in human beings. There is a belief that bilingualism was detrimental for intelligence reported better performance by bilingual children than monolinguals on both verbal and nonverbal tasks.

As per the research done by the Hakuta *et al,* (11) the major challenges in using of second language without phobia, inhibitions and fear has become the need of the hour. Though the cognitive neuroscience has augmented the neurological challenges and problems of the usage of second language, still many more to be known which are prevailing in usage of second language by the native language speakers. The reason behind this is the process of mono lingual pattern in brain is different from bilingual usage as there are three factors influence the brain, they are alertness, orientation, and detection. These three are to be more activated through Inhibitory Control Model control in brain to face the challenges while using the second language eloquently without fear and inhibitions.

Hormones cognitive networking

Brain is a hall mark centre for neuron endocrine centre controlling many biological functions. The brain endocrine access links holistic cognitive networking. The following figure 3 highlights the role of thyroxin which takes care of mental health all the life. While Dopamine enhances memory circuits, emotions and decision making while love hormone oxytocin controls social cognition. The estragon influences the brain integrity while progesterone, enhances memory and testosterone enhances the function of cognitive through NGF. There is still lot of debate on role of endocrines in cognitive networking as the detailed mechanism is not still clear (12)

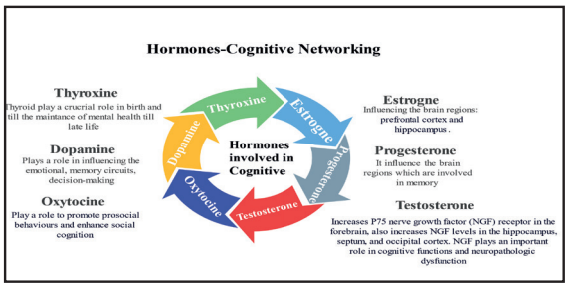

Figure 3: Hormone-cognitive networking in the brain

The brain cognitive process patterns

The constant effort and control over the cognitive process while using the bilingual languages can be made by overcoming through Inhibitory Control Model control in brain. It is observed by the researchers that while using the second language by native speakers, the situations, responses, reactions are similar in both languages while presenting, explaining, and writing as well while speaking. However, the nonverbal signs are additional points to the expressions (13). However, the inhibitions are similar in using the second language in all speakers however, the inhibitory control systems can be overcome with the assistance of pictures, contextual points, and appropriate representation. Inhibitory Control Model (Mechanism for Bilingual Effects) in which it was argued that bilingual language processing was based on an attention system, the Supervisory Attention System that inhibited the unwanted language so that processing could proceed in the target language (14).

The controlling process for Inhibitory Controls in brain play key role in second language (15). To avoid the interference of the other languages while using the second language, there should be a strong cognitive control system is a pre-requisite, which leads to attention, mental configuration while proceeding to bilingual communication. It is also observed that these control systems vary and differ based on socio linguistic, socio economic intelligent quotient levels and so on. The major effect of using multi languages is flexibility, switching over and monitoring (16).

The process of magneto encephalography

The measurement of the magnetic field produced by neuronal electrical activity is known as magneto encephalography, or MEG. The main application of MEG is as a non-invasive tool that uses suitable source localization techniques to identify the epileptic focus by detecting interictal epileptic discharges such as spikes (17). While scalp EEG is sensitive to electrical fields produced by extracellular currents, MEG predominantly detects the magnetic fields induced by intracellular currents. Currently, MEG is approved for usage in two situations: pre-operative brain mapping and epilepsy surgery.

By applying signal processing and source reconstruction algorithms to MEG sensor data, brain imaging with MEG sensor data is made possible (18). This results in highly dynamic maps of brain activation across a wide range of neural oscillatory frequencies with a high degree of spatiotemporal precision that is not possible with other imaging techniques. Across widely dispersed brain areas, this imaging method is perfectly adapted to monitor dynamic neuronal activity and simultaneously characterize their interconnections (19-20).

MEG systems to measure brain signals is the process of isolating miniscule brain-related signals from the massively greater signals from outside the brain. Thus, MEG has required the development of very exquisitely sensitive sensors, filtering, and a method to shield the sensors from recording outside noise (20).

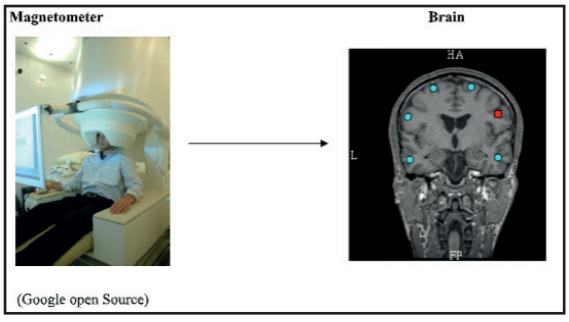

Figure 4: Magneto encephalography and its analysis.

The patient lies inside the scanner (Fig 4), which is equipped with a few insulated sensors. Ionic currents that are passing through the dendrites are the source of the signals (bottom). There is no detectable field produced by action potentials (21). The magnetometer displays the brain cross sectional image with detailed features of the brain (22-25).

Risk Factors Influence Cognitive Functionalities/Function

Cognition is a crucial parameter in brain function**.** There are number factors influences brain-cognition axis. Fig 5 indicates the role of clinical parameters like sugar, hypertension, high lipids etc play a key role in modulating cognition integrity in brain. Cognitive disorders are crucial in diabetes, hypertension etc in age and related disorders. The cognitive integrity and functionality are also influenced by neurochemical, Psychological and these factors cause changes in neural networking leading to changes in memory and cognition and finally influencing mental health as represented in Fig 6. The psychologies and psychiatrists are trained to use counselling using the factors influencing cognition as a source in their therapeutic modalities. As presented in Figure brain and cognition is influenced by multi factorial and the complex biological to environmental to sociological hence, the complex aetiology is still not clear for cognition.

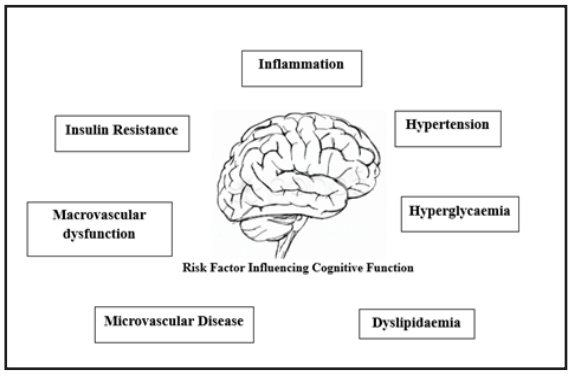

Figure 5: Clinical risk factors for cognitive dysfunctions

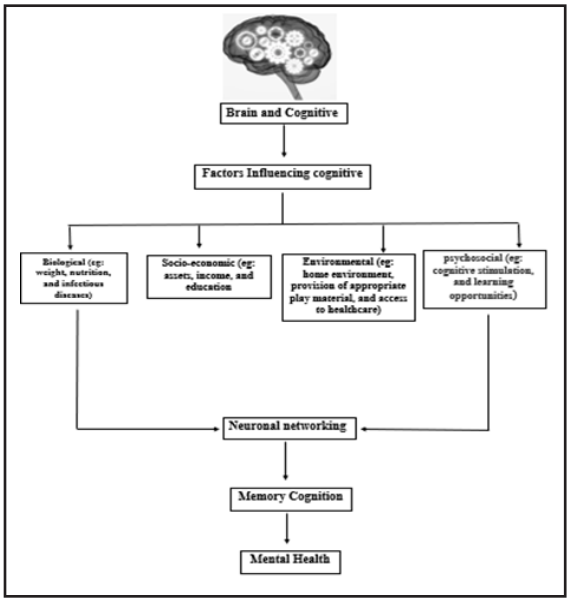

Figure 6: Factors Influence cognitive function.

Conclusion

Human brain is overwhelmed with abundant cognitive thoughts with innumerable wave patterns. Second language acquisition is purely a cognitive approach which needs a lot of attentiveness and alertness while using it. The deviations which happen in brain in using the second language can be controlled through the alertness, orientation and detection which is already proved by Russell and team in their research. Further research how the Inhibitory control model is developed and how the brain patterns recognised, reorganized, and restructured to overcome the inhibitions to be done in detail in further research.

Future Challenges

The studies highlighted very complex challenges in understanding brain and cognition and also focussing on mental health challenges in brain like autism, speech problem, language assimilation, and memory challenges etc., currently, scientists trying to understand from the basics to clinics to face the clinical challenges in cognitive disorders. People also looking at new concepts like artificial intelligence, deep

brain stimulations, re generative medicine computational aided learning etc., (29-31). It is also necessary to understand the total architectural and functional entity of the brain with reference to regions involved in cognitive networking and this may help for cognitive understanding and resolving issues in near future.

Acknowledgements: LSE thankful to KLEF for doctoral fellowship

References:

1. Friederici, A. D. The brain basis of language processing: From structure to function, Physiological Reviews, 91, pp.1357–1392 (2011).
2. Bialystok, E., & Viswanathan, M. Components of executive control with advantages for bilingual children in two cultures, Cognition, 112, pp.494 –500 (2009).
3. Kroll, J. F., & Gollan, T. H. Speech planning in two languages: What bilinguals tell us about language production, The Oxford handbook of language production? pp. 165–181 (2014).
4. Bialystok, E., Craik, F. I. M., Green, D. W., & Gollan, T. H. Bilingual Minds, Psychological Science in the Public Interest, 10, pp.89 – 129 (2009).
5. Miyake, A., & Friedman, N. P. The nature and organization of individual differences in Executive Functions: Four general conclusions, Current Directions in Psychological Science, 21, pp.8 –14 (2012).
6. Green, D. W., & Abutalebi, J. Language control in bilinguals: The adaptive control hypothesis, Journal of Cognitive Psychology, 25, pp.515– 530 (2013).
7. Peal, E., & Lambert, W. The relation of bilingualism to intelligence, Psychological Monographs, 76 (Whole No. 546), pp.1–23 (1962).
8. Carroll, J. B. Research on teaching foreign languages, Handbook of research on teaching. pp. 1060–1100 (1963).
9. Horwitz, E. K., Horwitz., M. B., & Cope, J. Foreign language classroom anxiety, Modern Language Journal, 70, pp.125–132 (1986).
10. Lalonde, R. N., & Gardner, R. C. Investigating a causal model of second language acquisition: Where does personality fit? Canadian Journal of Behavioural Science, 16, pp.224–237 (1984)
11. Hakuta, K., & Cancino, H. Trends in Second-Language- Acquisition Research. Harvard Educational Review, 47, pp.294-316 (1977).
12. Ali SA, Begum T, Reza F. Hormonal Influences on Cognitive Function. Malays J Med Sci. (4) pp:31-41 (2018).
13. Bialystok, E., Craik, F., & Luk, G. “Cognitive control and lexical access in younger and older bilinguals, Journal of Experimental Psychology: Learning, Memory, and Cognition, 34, pp. 859 – 873 (2008).
14. Green, D. W. ‘Mental control of the bilingual lexico-semantic system, Bilingualism: Language and Cognition, pp. 67– 81 (1998).
15. Green, D. W., & Abutalebi, J. Language control in bilinguals: The adaptive control hypothesis, Journal of Cognitive Psychology, pp. 25, 515– 530 (2013).
16. Dukelow T, Vassilev P, Lawrence EG, Jacobson L, Koychev I, Muhammed K, Kennelly SP. Barriers to brain health behaviours: results from the Five Lives Brain Health Ireland Survey. Front Psychol. 24;14:1101514 (2023).
17. Chen, Y.; Guo, R.; Wang, J.; Yu, M.; Zhao, M.; Zhao, L. Theoretical Study on Performing Movement-Related MEG with Kr-Based Atomic Comagnetometer. Photonics, 10, 1302. (2023).

18. Pan R, Yang C, Li Z, Ren J, Duan Y. Magnetoencephalography-based approaches to epilepsy classification. Front Neurosci. 2023 12;17:1183391. (2023).

19. Zhang H, Hao Y, He H, Roberts N. EEG based brain functional connectivity analysis for post-autoimmune encephalitis (AE) patients with epilepsy. Epilepsy Res. 193:107166. (2023).

20. Miller KJ, Fine AL. Decision-making in stereotactic epilepsy surgery. Epilepsia. 63(11), pp.2782-2801 (2022).

21. Shih JJ. Magneto encephalography-Established but not yet Essential. Epilepsy Curr. 12;20(2), pp.75-77 (2020).

22. Katagiri M, Wang ZI, Hirfanoglu T, Aldosari MM, Aung T, Wang S, Kobayashi K, Bulacio J, Bingaman W, Najm IM, Alexopoulos AV, Burgess RC. Clinical significance of ictal magnetoencephalography in patients undergoing epilepsy surgery. Clin Neurophysiol. 145. Pp.108-118. (2023).

23. Cao F, Gao Z, Qi S, Chen K, Xiang M, An N, Ning X. Realistic three-layer head phantom for optically pumped magnetometer-based magneto encephalography. Comput Biol Med. 2023. pp. 107318. (2023).

24. Cherukuri, A. S. S., Modi, V. K., Baraskar, B., Sood, S., Reguram, R., Palvia, D., Gopalakrishnan, K., Damani, D. N., Gaddam, S., Samaddar, P., Katukuri, N., Shivaram, S., Dey, S., Mitra, D., Roy, S., Linden, D. R., Beyder, A., Kulkarni, K., & Arunachalam, S. P. Microwave-Based Dielectric Properties as an Electrophysiological Biomarker: Future Perspectives. *Electronics (Switzerland)*, *12*(15), Article 3276. (2023).

25. Yang Y, Luo S, Wang W, Gao X, Yao X, Wu T. From bench to bedside: Overview of magnetoencephalography in basic principle, signal processing, source localization and clinical applications. Neuroimage Clin. 20; 42:103608. (2024).

26. Hsu, HC., Bai, CH. Individual and environmental factors associated with cognitive function in older people: a longitudinal multilevel analysis. BMC Geriatr 22, 243 (2022).

27. Kim M, Park JM. Factors affecting cognitive function according to gender in community-dwelling elderly individuals. Epidemiol Health. 15;39: e2017054 (2017).

28. Adolphs, R. The social brain: neural basis of social knowledge. Annu. Rev. Psychol. 60, pp. 693–716. (2009).

29. Frantzidis CA, Peristeri E, Andreou M and Cristea AI Editorial: New challenges and future perspectives in cognitive neuroscience. Front. Hum. Neurosci. 18:1390788. (2024)

30. Hertrich I, Dietrich S and Ackermann H. The Margins of the Language Network in the Brain. Front. Commun. 5:519955 (2020).

31. National Academies of Sciences, Engineering, and Medicine; Health and Medicine Division; Board on Health Sciences Policy; Committee on Preventing Dementia and Cognitive Impairment; Downey A, Stroud C, Landis S, et al., editors. Preventing Cognitive Decline and Dementia: A Way Forward. Washington (DC): National Academies Press (US); 22. 4, (2017).

Current Trends in Biotechnology and Pharmacy
Vol. 18(3) 1904-1912, July 2024, ISSN 0973-8916 (Print), 2230-7303 (Online)
10.5530/ctbp.2024.3.36

Supercritical Fluid for Retama Raetam Porous Film Production: A Strategy for Advancing Drug Dosage

Hatem Ksibi[1,2]

[1]LAMEEE Laboratory, University of Gafsa, Campus Universitaire Sidi Ahmed Zarroug – 2112, Gafsa, Tunisia.
[2]University of Sfax, IPEIS, P.B. 1172 Sfax 3018, Tunisia.
*Corresponding author: Hatem.ksibi@ipeis.usf.tn

Abstract

This proposal outlines a novel approach for fabricating porous films designed specifically for therapeutic formulations. These biodegradable films are sourced from Retama Raetam shrub branches through the innovative Supercritical Anti-Solvent (SAS) process. Renowned for their efficacy in managing hypertension and serving as diuretics, these films also excel in enhancing the entrapment of additional active ingredients. Furthermore, they enhance the entrapment of other active ingredients, thereby improving the stability and composition of tablets or capsules. Notably, the resulting film displays an exceptionally narrow and uniform distribution of pore sizes. Employing conditions of 10MPa and 40°C, carbon dioxide is utilized as the antisolvent to fabricate thin films sourced from Retama Raetam. These films boast a median area of approximately 7μm², underscoring their precise and consistent characteristics.

Keywords: Drug delivery, porous film, *Retama Raetam*, SAS process, Supercritical CO_2.

Introduction

Recent studies have shown a significant interest in innovative drug delivery systems. One such innovation is the development of orally disintegrating tablets pills, which turn solid drugs into forms that dissolve fast in the mouth. There is a wide variety of oral dosage forms available, including tablets, chewable tablets, sublingual tablets, capsules, and liquids. Traditional tablets and capsules can be problematic for patients who have difficulty swallowing, whereas liquids can suffer from stability issues and imprecise dosing. An alternative approach to improve drug delivery involves incorporation of active ingredients into a porous film. This biodegradable film has a precisely distributed network of pores, ensuring rapid disintegration upon ingestion and eliminating the need for water consumption. Not all drugs dissolve uniformly within a short time, and patients often need to consume water concurrently, which can be inconvenient.

To address the challenges posed by active ingredients that cannot be combined with biodegradable materials in tablet formulations, the primary goal is to fabricate a porous film that possesses both robust mechanical strength and exceptional flexibility, while maintaining a uniform distribution of fine pores. This porous matrix serves as an ideal medium for the absorption or seamless incorporation of the specific active ingredient in question.

Various methods have been employed to deposit films and multilayers in pharmaceutical applications. These methods include dipping,

centrifugation, coating, and spraying. Dipping involves coating the substrate with a solution containing polycations and polyanions, followed by rinsing Decher et al. (1). The use of coating techniques has been extended to the field of pharmaceuticals, as demonstrated by Lee et al. (2). These adaptations enable precise and uniform deposition of coatings, ensuring accurate drug release profiles and enhancing the overall performance of pharmaceutical formulations. In addition, spray coating has garnered extensive application across various industries. This versatile technique is employed to efficiently apply coatings, both inorganic and organic, to a wide array of substrates.

In addition, the utilization of supercritical fluid technology enables the creation of an exceedingly thin, porous film, further enhancing the efficiency and precision of this manufacturing process. There has been growing interest in crystallization processes that use fluids at supercritical state. In fact, the crystallization using supercritical carbon dioxide (CO_2) has received considerable attention in the pharmaceutical industry, Chakravarty et al. (3). It has converted as the favorite alternative to conventional processes such as evaporative and antisolvent crystallizations. Carbon dioxide presents an array of appealing attributes, primarily owing to its abundant accessibility, cost-effectiveness, eco-friendly nature, widespread recognition as safe, and its relatively low critical temperature, making it an ideal choice for applications requiring gentle operating temperatures, particularly when dealing with heat-sensitive materials. Supercritical crystallization, employed for microparticle production, arises from the substantial supersaturation achieved through rapid depressurization or swift mass transfer between the solution and the supercritical fluid antisolvent. This method finds relevance in the pharmaceutical sector, as indicated by De Marco (4) and also Franco et al. (5). Furthermore, it enables the projection of a thin, porous film with meticulously controlled micropores.

Conventional methods for extracting natural active ingredients from shrub and plant derivatives, such as grinding, spray drying, and solvent evaporation, have limitations when it comes to producing thin deposits that are free from solvents. The presence of solvents in these formulations can potentially lead to inaccuracies in dosing, which is a critical concern in pharmaceutical and related industries.

The RESS (Rapid Expansion of Supercritical Solutions) technique marked the beginning of the search for more efficient extraction techniques. Notably, Ksibi and Subra (6) showed that this method was effective at extracting α- and β- carotene microparticles that were enclosed in lipid films. According to Sharma and Jagannathan (7), this early success encouraged the investigation of additional applications, such as the use of a thin film of ibuprofen produced using also the RESS technique. Morphologies and shapes may be precisely altered with minimal changes to pressure or temperature, which has enormous promise for therapeutic items as highlighted by Ksibi et al. (8).

In sections that follow, we look into the Supercritical Anti-Solvent (SAS) method as a feasible option for generating thin films, particularly in certain thermodynamic conditions. The findings of the SEM analysis of the resulting deposits are also shown. These outcomes demonstrate the pore distribution pattern that is closely narrow. This appears to be a key component with the potential to raise production efficiency for thin, biodegradable films.

Materials and Methods

The Retama Raetam is an abundant shrub used in southern Mediterranean traditional medicine to cure a number of diseases throughout the year as mentioned by Hayet et al. (9). It was used for diabetes, hepatitis, jaundice, skin diseases, rheumatism, fever, and several types of inflammation as noticed by Leon-Gonzalez et al. (10). Moreover, this shrub is employed in Tunisia as a traditional treatment for snake bites, as documented by Saada et al. (11). Moreover, further studies have revealed

that extracts from the seeds of Retama raetam possess diuretic and hypoglycemic properties. Consequently, these seed extracts have the potential to lower plasma triglyceride levels, as demonstrated by Maghrani et al. (12).

Several authors have noted the utilization of *Retama Raetam* as a homeopathic resource. Edziri et al. (13) highlighted the antimicrobial, antioxidant, and antiviral properties found in the flower extracts of *Retama Raetam* Forssk. Furthermore, Eddouks et al. (14) underscored the antihypertensive and diuretic effects observed in the aqueous extract of *Retama Raetam* Forssk. leaves, which were investigated in both normotensive and spontaneously hypertensive rats as mentioned by Eddouks et al. (14).

Numerous research efforts have been dedicated to the comprehensive exploration and characterization of various elements derived from the *Retama Raetam* shrub. These investigations encompass a wide range of aspects related to the plant's composition and properties. One notable study conducted by Hayet et al. (9) investigated deeply into the intricate phenolic composition found within *Retama Raetam* flower oil. This research shed light on the specific phenolic compounds present in the oil, elucidating their potential applications and benefits. In fact, Oil from flower contains a total of 50 components mainly nonanal, linalool, myrcene and many others polyaldehydes and terpenes with a low percentage. In a separate study, El Yadini et al. (15) provided a detailed account of the composition of *Retama raetam* monosperma stems and seeds found in the arid expanse areas and across the Middle Atlas in Morocco. This research not only highlighted the nutritional and chemical makeup of these seeds but also contributed to our understanding of the plant's adaptability to challenging environmental conditions.

Beyond these, several other research endeavors have focused on unraveling the intricate constituents found within different genus of *Retama Raetam*, Leon-Gonzalez et al., (10). These investigations aim to unravel the plant's complex chemical profile, potentially uncovering novel compounds with diverse applications in various fields, from agriculture to medicine.

Furthermore, recent research has unveiled the antimicrobial and antioxidant potential of essential oils derived from Retama raetam, indicating their suitability for applications in the food and pharmaceutical sectors. Notably, a prior investigation conducted by our research team has underscored the antioxidant and antimicrobial attributes of this extract, as reported in Rejab and Ksibi (16).

Figure 1- Retama Raetam shrub flowers and seeds

Our primary emphasis lies in the application of eco-friendly natural solvents and the development of innovative technology systems for utilizing supercritical fluids, separation processes, and material production. As an illustration, eco-conscious chemical methods that involve carbon dioxide, with traits closely resembling those of organic solvents in their supercritical state, provide both ease of handling and eco-friendliness

Supercritical fluid technology is a promising route for the extraction, separation and shaping of divided solids including the SAS process which leads to homogeneous precipitation and recrystallization of materials into microscale size with generally narrow distribution. More-

over, materials regenerated from vegetable matrices using SAS supercritical fluids offer an appealing approach for recrystallizing numerous organic compounds sourced from plants. This method is particularly advantageous for substances that are challenging to fragment or recrystallize, such as extremely long-chain pharmaceuticals that necessitate the production of uniform ultrafine particles with consistent morphology, De Marco (4). The use of the SAS technique allows an accurate control of the crystallization process, resulting in very small and uniform particles, Rejab and Ksibi, (17). Furthermore, the separation of the anti-solvent from the particles after precipitation was readily accomplished. This allows for the avoidance of substantial solvent by-products and the potential establishment of an advantageous solvent and anti-solvent flow.

As the substance *Retama Raetam* is not soluble in supercritical CO_2, it is first solubilized in a supercritical organic solvent (itself soluble in CO_2). Then, the solution is confined in an atomization tank through a coaxial spray nozzle where it is brought into contact with CO_2 which will separate the molecule from the organic solvent, leading to precipitation. Simultaneously, the solvent evaporates in the supercritical phase, elevating the solute's concentration. This dual-directional mass transfer is the key factor behind the swift supersaturation of the solute, resulting in its nucleation.

The application of this process to pharmaceutical compounds involves specific constraints. Particular attention must be paid to the choice of the solvent. The choice of the solvent is based on three requirements. The first is its good miscibility with the anti-solvent (CO_2). The usual solvents such as ethanol, toluene and acetone show complete mutual miscibility with SC-CO_2. The second is the solubility of the solid to be crystallized and the third is its human safety. Indeed, the solvent must generally belong to class 3 (non-toxic) of the pharmaceutical guidelines. SAS precipitation results in the production of solvent-free materials, affording precise control over the morphology, size, and polymorphic phase of the precipitated material.

Figure 2 illustrates a schematic representation of the apparatus employed in the Supercritical Anti-Solvent (SAS) process. From literature, we can underline potentialities of the kind of crystallization as the tiny during the process which occur a very fine droplet and a high specific surface area for mass transfer. The freshly precipitated aggregates are retained within the system, while the supercritical fluid and organic solvent are continuously drained from the system. As the carbon dioxide is used in this process, it can be removed easily from the system by depressurizing. We mention that precipitations were obtained at the inner of the vessel. The experiments conducted in this study are mainly focused on the variation of carbon dioxide pressure, temperature on porous film dimensions and distribution.

The SAS process commences by pressurizing CO_2 to the desired level within the precipitator, followed by precise temperature control. CO_2 is methodically transitioned into a supercritical state, ensuring meticulous attainment of the designated pressure (10 and 12 MPa) within a high-pressure vessel. This prepares the groundwork for executing Supercritical Anti-Solvent (SAS) experiments, as per established protocols. The selection of a 2 kg/h CO_2 flow rate is a judicious decision, informed by prior research, particularly the findings of Rejab and Ksibi (17) which demonstrated its effectiveness in achieving solution atomization.

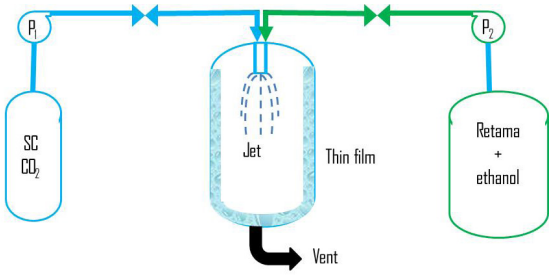

Figure 2- A schematic representation of the SAS process

Within this meticulously controlled environment, a liquid solution is introduced, comprising a carefully crafted mixture of powdered *Retama Raetam* and ethanol. This solution is expertly sprayed into the reactor using a purpose-designed nozzle, where the solvent undergoes rapid diffusion. This diffusion process causes the solution droplets to disperse into the bulk supercritical fluid, initiating the intricate sequence leading to the solute's precipitation. The culmination of these precisely engineered conditions results in the formation of a porous film, as detailed in Table 1.

Subsequently, we undertake a washing step, during which the precipitator is depressurized to atmospheric levels, and the film that has precipitated on the inner wall of the precipitator is meticulously collected for further analysis and examination. Our experimental runs were conducted to assess the process's efficiency in generating thin *Retama Raetam* films with controlled pore structures. Such films hold promise for addressing challenges associated with the incorporation of additives that are difficult to swallow, ensuring precise dosing, and maintaining consistent particle sizes. During each run, we systematically varied the operating conditions to explore the effects of different combinations. The results derived from each operational run are derived from observations made during a stabilized operating period under a specific set of operating conditions.

Table 1- Operating Run conditions

Run	T °C	P MPa	Volume of solution /ml
1	30	10	40
2	40	10	25
3	40	10	40
4	50	12	40

Results and Discussion

The application of film coating or deposition in general, to achieve customized surface properties holds significant relevance in the fields of pharmaceuticals, cosmetics, and food manufacturing. Through the engineering of plant materials, it becomes possible to impart specific physical, chemical, biochemical, and pharmaceutical characteristics by creating a thin, porous film over active principle particles. This versatility allows for the fine-tuning of critical parameters such as operating pressure, temperature, dissolution rate, chemical reactivity, and flow rate, thereby accommodating a wide spectrum of applications, Souiy et al. (18). Several studies show that SAS is not merely an effective process for nucleated material morphology control and scalability. Conducting processing under mild conditions can additionally enhance the stability of biopharmaceuticals without compromising their conformational structure.

Nevertheless, it is crucial to highlight a notable observation from our experiments. Instead of adhering to the intended surfaces, the film coating unexpectedly occurred within the chamber, specifically on the inner wall of the precipitator and its bottom. We subsequently scraped the film coating from these surfaces and subjected it to examination under a scanning electron microscope (SEM).

Biopharmaceuticals processed with SAS process are also submitted to atomization spray formation. However, several studies have shown that RESS, PGSS and other supercritical processes conduct only particle (spheres and sticks) after nucleation and separation. The tunable properties of $scCO_2$ mean that material engineering can speed up the process. Habulin and Knez (19) found that an increase of supercritical carbon dioxide flow rate led to a loss of relative activity and therefore, a narrow distribution of particle size with a quasi-uniform morphology. It is important to call attention to the fact that no excipients were used during drying and the product (thin film or particles) is free of solvent.

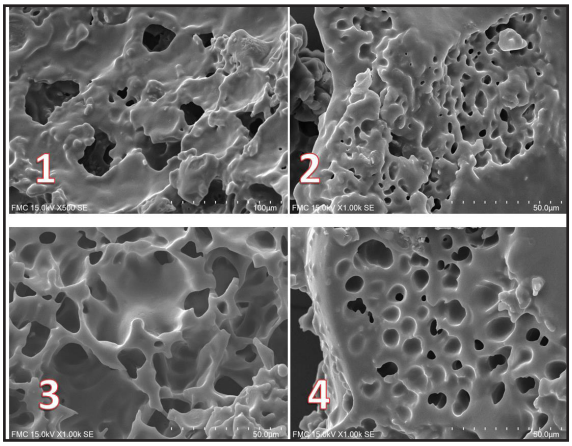

Figure 2- formed films on the inner wall vessel for several run cases

The present study delves into the analysis of various film deposits within a defined study area using ImageJ software. Our primary objective is to determine the average pore area within the blackened regions and establish a corresponding distribution function for each experimental condition. With reported porosity levels ranging from 40-50%, as per Rejab and Ksibi (16), we noted differences in the average pore class distribution across various study locations.

Figure 3 presents the outcomes from multiple experimental runs, revealing the consistent formation of spongy thin films in each case. The figures depicting *Retama Raetam* deposits at a microscopic scale offer insights into the internal structure of the atomization slot and the resulting film. These variances in pore size can be attributed to working temperature, pressure conditions, and the volume to be dissolved, highlighting the intricate relationship between these factors in film deposition. The examination of regenerated Retama Raetam film surfaces was carried out using a *Zeiss Auriga Compact* focused ion beam scanning electron microscope (FIB-SEM) with an accelerating voltage set at 10 kV. The scale was chosen at 50 µm to get a clear idea about pores morphology, area, distribution and depth. Thin films obtained by the SAS process have exhibited the highest organic porous film efficiency offering a best stability to incorporate active principles. With SAS process, it would be interesting to study optimal conditions *Retama Raetam* extract deposition from spray-drying as thin film.

Discussion

Utilizing digital processing techniques on these microphotographs, which involved the use of image analysis software and *Gnuplot* surface tracing, we were able to gain valuable insights into the cumulative intensity within the porous regions, both along and across the deposited material as shown in figure 3.

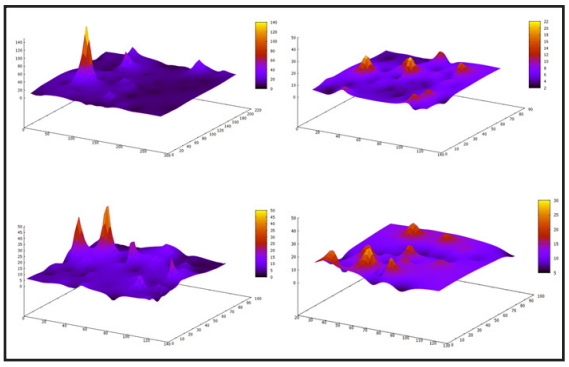

Figure 3- Cumulative Porous Area Intensity (µm²) of the Film from Bidirectional PSD Compilation in Multiple Run Cases

Notably, in the cases of runs 1 and 3, we observed a significant accumulation of porous zones. This accumulation suggests that the *Retama Raetam* -based matrix created in these runs has a substantial capacity for incorporating additional pharmaceutical additives. The various peaks evident in these cases reflect the varying degrees of incorporation within the matrix, shedding light on the potential for controlled release and distribution of these additives.

Conversely, when we examine the diagrams for runs 2 and 4, we notice that the peaks are much lower. This implies a more consistent and evenly distributed porous structure throughout the film. The quasi-regularized distribution in these cases may have its own advantages, de-

pending on the intended use and desired characteristics of the pharmaceutical coating or film.

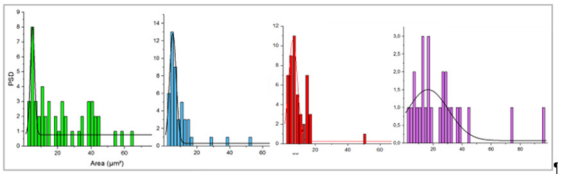

Figure 4- Pore Size Distribution in Various Deposition Films

Figure 4 illustrates the distribution of porous area intensity in the Retama Raetam film deposits, corresponding to the images in Figure 2. Various pore shapes and sizes were achieved by adjusting key parameters. By referencing Table 1 and the pore area distributions depicted in Figure 4, it becomes evident that the operational conditions of the SAS process had a substantial impact on both thin film morphology and pore size distribution.

In the first experiment, Run 1, we conducted operations at a pressure of 10 MPa, maintaining the temperature in close proximity to the critical point of CO2. Our objective was to fabricate a thin film characterized by micron-scale porosity. In this instance, we observed that the medium pore area averaged around 5µm², albeit with the presence of some larger pores.

Moving on to Manipulation Run 3, we maintained the same pressure as the previous run while elevating the temperature beyond the critical point (T=40°C). This adjustment resulted in a subtle increase in pore size, with an average exceeding 10µm but displaying a narrower distribution. A careful examination of the Particle Size Distributions (PSDs) presented in Figure 5 clearly indicated the absence of large pores in this scenario.

In Run 2, we replicated the thermodynamic conditions of Run 3 but introduced a modification by reducing the volume of the solution (comprising *Retama Raetam* and ethanol) from 40ml to 25ml. Under these altered conditions, the film collected within the precipitation chamber exhibited an average pore size of 5µm, distinguished by a considerably narrower distribution. Consequently, the reduction in solution volume not only led to a shortened deposition time but also restricted the growth time of film porosity.

Lastly, in Run 4, we conducted experiments under high-pressure and high-temperature settings, yielding a deposited film characterized by a diverse range of pore sizes. Consequently, the pore area exhibited variations spanning tens of microns, resulting in a distribution that extended widely across the spectrum.

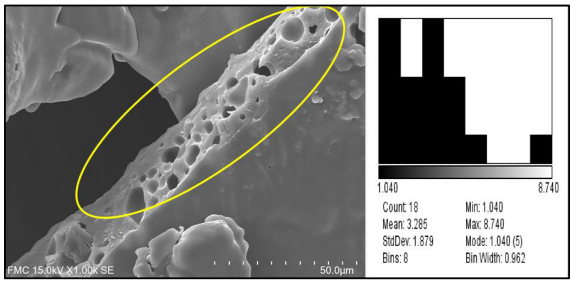

Figure 5- Run 2 Film thickness and Corresponding Pore Area Distribution

During the second experimental run (Run 2), we succeeded in producing a film with an impressive thickness of approximately 18 µm. This film displayed distinct, visually observable pores, as illustrated in Figure (b). What sets this particular material apart is its classification as a truly uniform porous medium. The average pore area within this medium measures approximately 3.5 µm², serving as compelling evidence of the remarkable uniformity and consistent distribution of pores throughout the entire film.

This level of uniformity and controlled porosity is of significant interest in various applications, such as drug delivery systems or materials with specific filtration requirements. The findings from Run 2 highlight the potential for creating materials with precisely engineered porosity, which can be instrumental in achieving desired characteristics and performance in various fields of science and technology.

Conclusion

The SAS coating technique holds significant potential as an environmentally mindful approach for potentially entrapping microparticles through pore creation. This is achieved by generating porous, thin films using vegetable matrices like Retama Raetam. This method finds application in the pharmaceutical industry and other sectors where preventing chemical interactions is of paramount importance.

The figures depicting *Retama Raetam* deposits via SAS process at a microscopic scale offer insights into the internal structure of the atomization slot and the resulting film. These variances in pore size can be attributed to working temperature, pressure conditions, and the volume to be dissolved, highlighting the intricate relationship between these factors in film deposition. In fact increasing pressure led to very close pore distribution and a mean area pore about 7µm² whereas increasing temperature favorites the formation of film with large pores.

List of abbreviations

SAS: Supercritical AntiSolvent process

SC-CO_2: Supercritical carbon dioxide

FIB-SEM: focused ion beam scanning electron microscope.

CPA : Cumulative Pore Area

PSD : Particle Size Distribution

References

1. Decher G., Hong J.D., Schmitt J., (1992) Buildup of ultrathin multilayer films by a self-assembly process: III. Consecutively alternating adsorption of anionic and cationic polyelectrolytes on charged surfaces. Thin Solid Films, 210–211(2), p. 831. https://doi.org/10.1016/0040-6090(92)90417-A.

2. Lee S.H., Bajracharya R., Min J.Y., Han J.-W., Park B.J., Han H.-K., (2020) Strategic approaches for colon targeted drug delivery: An overview of recent advancements. Pharmaceutics. 12, p. 68. https://doi.org/10.3390/pharmaceutics12010068.

3. Chakravarty P., Famili A., Nagapudi K., Al-Sayah M.A., (2019) Using Supercritical Fluid Technology as a Green Alternative During the Preparation of Drug Delivery Systems. Pharmaceutics. 25, 11(12), p. 629. https://doi.org/10.3390/pharmaceutics11120629.

4. De Marco I., (2022) The supercritical antisolvent precipitation from a sustainable perspective: A Life Cycle Assessment, Journal of CO_2 Utilization, 55, 101808. https://doi.org/10.1016/j.jcou.2021.101808.

5. Franco P., De Marco I., (2020) Supercritical Antisolvent Process for Pharmaceutical Applications: A Review. Processes, 8, p. 938. https://doi.org/10.3390/pr8080938

6. Ksibi H., P Subra P., (1996) Powder coprecipitation by the RESS process. Advanced Powder tech. 7 (1), p. 21. https://doi.org/10.1016/S0921-8831(08)60888-2.

7. Sharma S. K. and Jagannathan R., (2019) Synthesis of high throughput ibuprofen nanoparticles via supercritical CO_2 processing, IEEE 19th International Conference on Nanotechnology (IEEE-NANO), Macao, China, p. 203. https://doi.org/10.1109/NANO46743.2019.8993945.

8. Ksibi, H., Moussa, A.B. and Baccar, M. (2006) 'Powder Structure Transition under the Recrystallization Conditions in the RESS Process,' Chemical Engineering & Technology, 29(7), pp. 868–874. https://doi.org/10.1002/ceat.200600094.

9. Hayet, E., Maha, M., Samia, A. et al. (2008) Antimicrobial, antioxidant, and antiviral activities of Retama raetam (Forssk.) Webb flowers growing in Tunisia. World J Microbiol Biotechnol 24, p 2933. https://doi.org/10.1007/s11274-008-9835-y.

10. Leon-Gonzalez A. J.. Navarro I.. Acero N.. Munoz Mingarro D., Martın-Cordero C., (2018) Genus Retama: a review on traditional uses, phytochemistry, and pharmacological activities, Phytochem. Rev. 17, p701. https://doi.org/10.1007/s11101-018-9555-3.

11. Saada M., Falleh H., Jalleli I., Snoussi M., Ksouri R., (2014) Phenolic profile, biological activities and fraction analysis of the medicinal halophyte Retama raetam, South African Journal of Botany, 94, p. 114. https://doi.org/10.1016/j.sajb.2014.06.010.

12. Maghrani M, Zeggwagh NA, Haloui M, Eddouks M., (2005) Acute diuretic effect of aqueous extract of Retama raetam in normal rats. J. Ethnopharmacol. 13, 99(1), p 31. https://doi.org/ 10.1016/j.jep.2005.01.045.

13. Edziri H, Mastouri M, Cheraif I, Aouni M. (2010) Chemical composition and antibacterial, antifungal and antioxidant activities of the flower oil of *Retama Raetam* (Forssk.) Webb from Tunisia, Nat Prod Res. 24(9), p789. https://doi.org/10.1080/14786410802529190.

14. Eddouks M, Maghrani M, Louedec L, Haloui M, Michel JB., (2007) Antihypertensive activity of the aqueous extract of Retama raetam (Forssk.) leaves in spontaneously hypertensive rats. J. Herb Pharmacother. 7(2), p 65. https://doi.org/ 10.1300/j157v07n02_05.

15. El Yadini, A.; Elouafy, Y.; Amiri-Ardekani, E.; Shafiee, M.; Firouzi, A.; Sasani, N.; Khalid, A.; Abdalla, A.N.; Bakrim, S.; Tan, C.S., (2023) A Comprehensive Review of the Pharmacological Properties and Bioactive Components of *Retama monosperma*. Molecules *28*, 1708. https://doi.org/10.3390/molecules28041708.

16. Rejab A., Ksibi H., (2019) Phenolic and flavonoid contents of some plant extracts from Tunisia southern landscape by using different extraction techniques: the case of Retama raetam. Med Aromat. Plants (Los Angeles), 8 (4), p 337. https://doi.org/10.35248/2167-0412.19.8.337.

17. Rejab A., Ksibi H., (2023) Particle crystallization by supercritical antisolvent processing techniques: the case of Retama raetam powder for pharmaceutical purposes. International Journal of Chemical Reactor Engineering, 21(6), p. 717. https://doi.org/10.1515/ijcre-2022-0119.

18. Souiy Z., Ben Moussa A., Ksibi H., (2007) Numerical simulation of heat and mass transfers in a supercritical dissolution column. Chem. Engineering & Technology, 30 (6), p. 715. https://doi.org/10.1002/ceat.200600371.

19. Habulin M., Knez Z., (2001) Activity and stability of lipases from different sources in supercritical carbon dioxide and near-critical propane, J Chem Technol Biotechnol 76, (12) p. 1260. https://doi.org/10.1002/jctb.514.

Current Trends in Biotechnology and Pharmacy
Vol. 18(3) 1913-1921, July 2024, ISSN 0973-8916 (Print), 2230-7303 (Online)
10.5530/ctbp.2024.3.37

Exploring the Therapeutic Synergistic Intervention of *Ceriops decendra* with enriched protein of *Cyamopsis tetragonoloba* against Sreptozotocin Nicotinamide induced type-2 Diabetes

Md Mustahedin Hoque1, Md. Aminul Islam1, Suparna Ghosh1, Barun Dasgupta1, Sanjib Bhattacharya2, Pulok Kumar Mukherjee1, Pallab Kanti Haldar1*

[1]School of Natural Product Studies, Jadavpur University Kolkata 700032, West Bengal, India
[2]West Bengal Medical Services Corporation Ltd., GN 29, Sector V, Salt Lake City, Kolkata 700091, West Bengal, India
*Corresponding author: pallab_haldar@rediffmail.com

Abstract

In this study the synergistic antihyperglycemic effect of the medicinal plant *Ceriops decendra* stem hydro-alcoholic extract (CD) and protein component isolated from *Cyamopsis tetragonoloba* seed (CT) was evaluated *in vitro* in α-glucosidase and α-amylase inhibitory bio-assays and *in vivo* against streptozotocin (STZ)-nicotinamide-induced diabetic rats with metformin as reference in a 28 days standard treatment protocol. The blood serum biochemical parameters and tissue (liver and kidney) antioxidative parameters were analysed. Histopathology of pancreas was also studied. The animal groups treated with the combination of both CD and CT have demonstrated a remarkable inhibition of α-glucosidase and α-amylase activities and restoration of diabetes-induced serum biochemical and tissue antioxidant parameters with improved pancreatic histology as compared to the above groups indicating the synergistic effect. The findings of present study infers that, combination of both CD and CT exerted a synergistic action exhibiting more potent antihyperglycemic effect indicating the beneficial role of protein component in management of diabetic complications.

Keywords: *Ceriops decendra*, gel electrophoresis, protein, diabetes, synergy.

Introduction

A concerned lifestyle disease called diabetes mellitus has grown into a problem on a global scale. According to the 2015 Diabetes Atlas published by the International Diabetes Federation (IDF), there are 415 million individuals worldwide who have been identified as having diabetes, or 8.8% among individuals aged 20 to 79. By 2040, it is expected that there will be more than 640 million adults worldwide who have diabetes. Since over 80% of all persons with diabetes who have not been diagnosed live in low- and middle-income countries, which account for 75% of the global population, the increase in numbers will be greatest there. China and India will have the largest increases in the number of diabetics among developing nations. Urban locations in developing economies have a higher rate of diabetes prevalence (1, 2). Rapid socioeconomic shifts brought on by industrialisation and urbanisation are the primary causes of the global diabetes epidemic, which is also largely driven by population expansion, poor lifestyle choices, and a lack of vigorous physical activity. Diabetes is a silent disease that can cause deadly and severe complications as well as raise expenditures. Nearly every system in the body is impacted by diabetes' long-term problems, but the eyes, kidneys, heart, feet, and nerves are particularly vulnerable. Anatomical,

structural, and functional alterations as a result of the micro- and macrovascular complications result in numerous organ dysfunction (3).

India is undergoing a shift in the prevalence of diabetes from urban to rural areas, the affluent to the less privileged, and older to younger individuals. India ranks second after China in the world in terms of the diabetes epidemic. In both urban and rural parts of India, the prevalence of diabetes has been rapidly rising. The most common form of diabetes is type 2, which is also the main cause of the diabetes epidemic in India. Type 1 diabetes is becoming more common in India as well. Type 2 diabetes prevalence increased gradually in the 1990s and significantly more quickly after 2000. Diabetes now affects more people than it did in 2000, when there were 32.7 million cases. compared to 35.5 million in 2003, in 2007 there were 40.9 million, 50.8 million people in 2010, 2013 saw 65.1 million, 69.2 million people in 2015, The predicted number in 2040 is 1.23 billion. The first study on the prevalence of diabetes in India was carried out in Calcutta (now Kolkata) in 1938. After verifying 96 300 medical records, it was discovered that 1% of the population had diabetes. Between 1973 and 2015, the prevalence of diabetes ranged from 1.1% in urban Lucknow to 25.2% in New Delhi. Few nationwide studies on the level of prevalence of this disorder have been conducted, and the majority of those studies used capillary fasting and a two-hour post glucose load to diagnose diabetes. The countrywide prevalence of diabetes has been reported to be 2.1% in the multi-centre study done between 1972 and 1975 by the Indian Council of Medical Research (ICMR) in six cities (Trivandrum, Calcutta, Cuttack, Delhi, Poona and Ahmadabad) and nearby rural areas (1, 4).

Physical, environmental, metabolic, chemical, and genetic elements all have a direct or indirect impact in the development and progression of diabetes. A diet heavy in antioxidant-rich fruits and vegetables lowers the incidence of diabetes, strongly indicating that these antioxidants may be useful diabetes-inhibiting agents (5). Protein consumption induces the release of glucagon, a hormone that aids in controlling blood sugar levels. In contrast to insulin, glucagon encourages the liver's stored glucose to be released, keeping blood sugar levels from falling too low. This system promotes glucose homeostasis and guards against hypoglycaemia. Consuming protein activates the hormone the insulin's release, which aids in the uptake and utilization of glucose by cells. For those with diabetes, especially type 2 diabetes patients who may have resistant to insulin, a sufficient protein intake maintains sufficient hormone synthesis and secretion (6).

Medicinal plants have long been known to serve as medicinal recourse to the mankind (7). *Ceriops decandra* (Griff.) Ding Hou (Rhizophoraceae) commonly known as Indian mangrove or spurred mangrove in English and *Garan* in Bengali is a shrubby mangrove tree widely distributed throughout the tropical Asia including India and Bangladesh. This plant has traditionally been used against diseases like ulcers, diarrhoea, dysentery, angina, boils, diabetes, hepatitis and wounds (8, 9). The objective of the present study is to explore the synergy effect of *Ceriops decendra* (CD) stem extract with the protein isolated from *Cyamopsis tetragonoloba* (CT) seeds against strepotozotocin nicotinamide-induced type 2 diabetes in rats.

Materials and methods

Extraction of Ceriops decendra stem

The plant *Ceriops decandra* (Griff.) Ding Hou (Rhizophoraceae) was collected on March 2022 from Jharkhali, South 24-Pgs., West Bengal, India and it was authenticated from the Central National Herbarium, Botanical Survey of India, Howrah, West Bengal, India. The air-dried stem (250 g) was extracted with the hydro-alcoholic extraction by ethanol-water (70: 30) in a Soxhlet apparatus at a temperature 60-70°C. Then the solvent extract was then filtered in a member filter (Whatman paper). To exclude the solvent from the filtrate material a

solvent are then transfer into a rotary vacuum evaporator at a reduced pressure at 55°C. then concentrated sample were taken to a dryer for 24 Hour at 40°C then the extract was subjected to transfer in a lyophilise machine for 48 hours. The final yield was 13%.

Chemicals

All the chemicals used were of analytical grade obtained commercially.

Phytochemical screening

Preliminary phytochemical screening was performed on the foregoing extract to detect the presence of various phytochemicals (10).

Isolation of protein from Guar powder

Guar seed powder (procured from M/s Alona Pvt. Ltd.) was defatted by acid-alkali treatment followed by removal of phenolics and flavonoids as per previously reported protein acid salt alkaline methods (11). Then the resultant material was subjected to polyacrylamide gel electrophoresis followed by staining and de-staining. The identification of band are observed in the UV light at 254 and 366 nm and as the running capability depends upon the molecular weight of the sample, Here as a standard bovine serum albumin (BSA) has been used which molecular weight is about 65.5 Kda, its shows that it run up to the bottom of the gel, whereas the sample band run less compare to the standard it means it has higher the molecular weight based on the running capability its expected the molecular weight of the band are lies in between 75-80 Kda (12). Purity of isolated protein was assessed by the micro-Kjeldahl method (83%).

Animals

Adult Wistar albino rats of either sex were used. The animal was feed with the normal diet for 5 Days in a animal house in acclimatize condition relative humidity 55%, temp. 22±5°C. The experimental procedure started after review and the approval by the IAEC reference no. JU/IAEC-22/43.

In vitro antioxidant activity

The radical scavenging or antioxidant activity of DPPH is determined by its capacity to receive an electron. Strong antioxidants will rapidly transfer an electron to DPPH, significantly reducing the amount of purple that DPPH exhibits. The amount of colour change is related to the tested compound's antioxidant strength (13).

Prepare a stock solution with a 0.1 mM suggested concentration by dissolving the DPPH powder in a suitable solvent (such as methanol or ethanol). Weight 1.97 gram of DPPH in 50 ml of methanol. Molecular weight of DPPH 394 gram/mol. Make careful to thoroughly mix the DPPH powder until it dissolves. Cover the container with aluminium foil and store the DPPH solution in an amber bottle to shield it from light.

One well should be designated as a blank control that solely contains the solvent and DPPH solution. This well will assist in making any background absorbance corrections. 100 µL of each sample or antioxidant standard should be added to the appropriate microplate wells. Add 100 µL of the DPPH solution to each well containing the samples or standards. Set the timer for 30 minutes and allow the plate or cuvette to incubate there in the dark and at room temperature. During this period, the samples' antioxidant chemicals will interact with the DPPH radical. Utilising a spectrophotometer, determine each well's absorbance following the incubation time at a certain wavelength, commonly 517 nm. Utilise the blank control effectively to clean the spectrophotometer.

In vitro alpha amylase and alpha glucsidase inhibitory assay

Alpha-amylase is an enzyme involved in the digestion of carbohydrates, and the alpha-amylase inhibitory test measures a sub-

stance's capacity to block its activity.

Preparation of enzyme solution: 1 mg of enzyme solution = 30 unit of enzyme.

For the preparation of 1 unit/ ml of enzyme solution take 1 mg of enzyme and dissolved it in the 30 ml of buffer. And then store it in -20 Degree Celsius for the further use of the enzyme.

Preparation of starch substrate

1% W/V 100 mg of starch dissolved in 10 ml of buffer solution and shake it gently and dissolved it in a hot water contact and shake the system over and over again.

Preparation of 5.3 M Potassium sodium tetrahydrate solution

Dissolved 14.96 gram (PST) in 10 ml 2 M NaOH solution. And before that prepare 2 M NaOH solution by dissolving 1.6 Gram of NaOH are dissolved in 20 ml, of distilled water.

Prepare of 96 mM DNSA solution: 21.9 mg/ml 438 mg of DNSA in 40 ml of buffer solution.

Sample preparation: prepare the stock solution of test sample and in different concentration right from to lower to upper conc. 10,20,40,60,80, 100 µg/ ml .

Procedure: 30 µl of phosphate buffer or plant extracts Acarbose was used as a positive control after 30 µl of -amylase enzyme solution was combined with it and pre-incubated at 37°C for 10 minutes. Following this, 40 µl of starch solution (the substrate) was added, and the reaction was started at 37 °C for 30 minutes. The stop reagent, 20 µl of DNSA solution, was then added and heated in a water bath for 5 minutes. The mixture was diluted with 80 µl of buffer and warmed to room temperature. At 540 nm, the mixture's absorbance was measured using a Spectramax ID3 spectrophotometer (4).

In vivo study for anti-diabetic activity

For the experiment in each group 6 animal was selected which has average body weight more than = 170 gram

Initially 110 mg/kg nicotinamide was injected then wait for 20 min after all 40 mg/kg streptozotocin (STZ) was injected. Then the animal was provided dextrose water for three days after three days blood glucose was measure.

No significant raise of blood glucose Average blood glucose was – 125 mg /dl. Then again animal was feed for five days with the normal diet when the animal become healthy then 35 mg/dl STZ was injected.

After three days blood glucose measure, average blood glucose of each group. Blood glucose was measure in a regular interval (5 days) interval

Fasting Blood Glucose measurement in a regular interval

Group- A Standard control (Metformin) 50 mg/kg

Group-B Diabetics control (Nicotinamide + STZ) Induced

Group -C Normal control (Vehicle control)

Group-D Test control *Ceriops decendra* extract (Nicotinamide + STZ induced) CD extract 250 mg/kg)

Group-E Test control CD+CT (Nicotinamide + STZ induced) CD 250 mg/kg + CT 0.9 gram /kg enriched protein

After 28 days of foregoing treatments the animals were sacrificed and the serum biochemical parameters and tissue (liver and kidney) antioxidative parameters were analysed by the fully automated Auto-Analyser SELECTRA. Histopathological study of pancreas was performed at 40x (2, 6).

Statistical analysis

For the analysis of the mean blood glucose level of various group Two-way ANOVA group analysis use for the measurement of mean difference between and within the group (Mean ± SD). The analysis shows there is significant different between test control supplement with the extract group ***P < 0.0001 compare

to the *Ceriops decendra* dose group and the alpha value = 0.05 compare to the standard treatment group and significant diff. among means. It means the average blood glucose of the combinational drug is much more effective compare to the drug extract along or the standard treatment.

Results and Discussion

Table 1: Preliminary phytochemical test of *Ceriops decendra* and *Cyamopsis tetragonoloba* (+) presence (-) Absent.

Sl. No.	Test Name	Ceriops decendra	Cyamopsis tetragonoloba
1	Flavonoids	++	-
2	Alkaloids	++	+
3	Phenol	++	-
4	Saponin	-	-
5	Tannin	+	-
6	Glycoside	+	+
7	Protein	-	+++
8	Terpenoids	++	--

Table 2: *In vitro* antioxidant assay.

Concentration µg/ml	Control	Sample	%RSA	IC50 Value
50	0.521	0.312	40.11516	1.709
100	0.510	0.192	62.35294	5.855
150	0.521	0.122	76.58349	10.002
200	0.452	0.067	85.17699	14.149
250	0.512	0.045	91.21094	18.295
300	0.511	0.021	95.88235	22.442

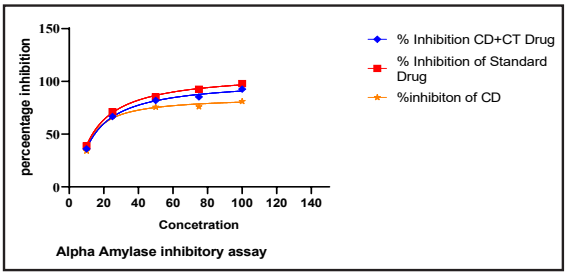

Figure 1: Alpha Amylase inhibitory assay. IC_{50} value of CD+CT= 7.554 & Standard= 8.186 And IC_{50} value of CD is = 9.12.

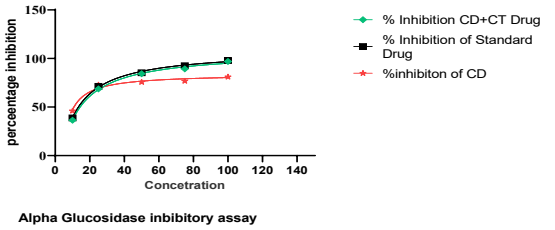

Figure 2: Alpha Glucosidase inhibitory assay. IC50 value of CD+CT= 7.152 Std= 7.819 CD IC50 = 8.219.

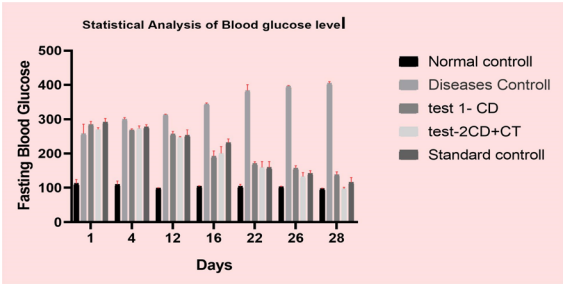

Figure 3: Antidiabetic effect of plant extract and its combination with protein.

Table 3: Oral glucose tolerance test.

Fasting Blood Glucose (Group-A) *Mg/dl*	Fasting Blood Glucose (Group-B) *Mg/dl*	Fasting Blood Glucose (Group-C) *Mg/dl*	Fasting Blood Glucose (Group-D) *Mg/dl*	Fasting Blood Glucose (Group-E) *Mg/dl*
298 ±2	298±7	110±8	299±4	300±8
285±3	314±5	102 ±7	286±3	285 ±2
265 ±2	325±3	105 ±5	*268*±4	*272* ±4
191±4	346±4	106±4	193 ±6	161±3
165±5	372±2	112±3	168±4	163±4
145±3	410±3	108 ±4	152 ±3	152 ±2
133±5	418±4	112±2	142 ±5	131 ±3

Table 4: Serum biochemical parameters.

Test Name	Standard Control	Diabetics control	Normal control	Test control *Ceriops decendra*	Test control CD+CT
Total cholesterol	50± 5mg/dl	68± 3mg/dl	48±2mg/dl	53±8mg/dl	42±6mg/dl
Total Protein	90±2 g/l	115±6 g/l	95±3 g/l	126± g/l	115±g/l
SGPT	38±2 U/l	72±8 U/l	35± u/l	52±6 u/l	41±u/l
SGOT	44±3 IU/l	83±3 IU/l	38±2 IU/l	63±3 IU/l	51±2 IU/l
ALT	162±2IU/l	182±3IU/l	150±5IU/l	175±3IU/l	164±3IU/l
AST	35±3IU/l	65±3IU/l	46±3IU/l	42±3IU/l	55±3IU/l
Bilirubin	4.8±0.5mumol/l	7.8±0.5mu mol/l	3.8±0.2mu mol/l	2.8±0.3mu mol/l	3.8±0.4mu mol/l
HbA_1C	7.2±0.5	9.2±0.3	6.2±0.4	7.2±0.2	6.8±0.3
HDL	35±2 mg/dl	25± mg/dl	38±3 mg/dl	34 ± 2 mg/dl	31±5mg/dl±
LDL-C	78±3 mg /dl	91±2 mg /dl	70±3 mg /dl	88±2 mg /dl	80±4mg /dl
Urea	78.70±8 mg/dl	112.50±3mg/dl	65.70±2 mg/dl	88±8 mg/dl	75.70±8 mg/dl

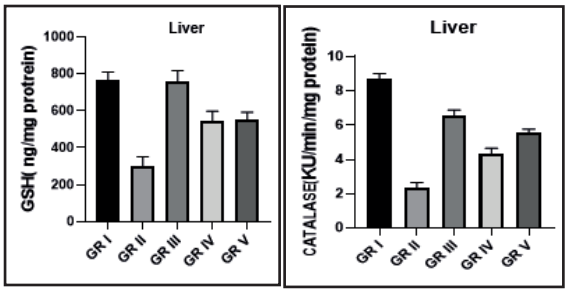

Figure 4: Hepatic antioxidant parameters. P-Value <0.001, with 95.00% CI of diff., Mean Diff. 2.052, SE of diff. 0.1109

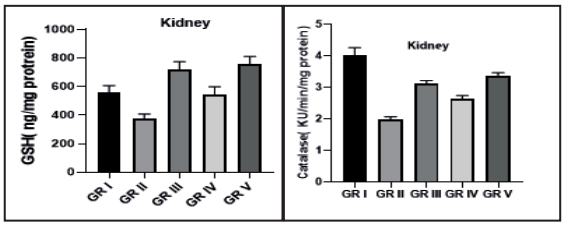

Figure 5: Renal antioxidant parameters. P-Value <0.0001, SE of diff. 41.30, Mean Diff. 466.6 Compare to negative control and p** compare to the standard and followed by the treatment, CI of diff. 95.0%

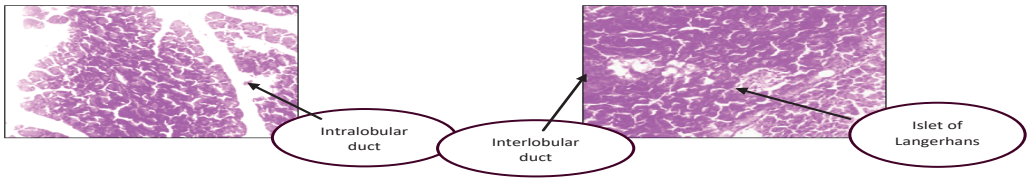

Fig. 6A: CD 250 mg/kg dose pancreatic beta cell the density of the beta-cell is less s compare to standard or the supplementary dose group. (Magnification - 10x40)

Fig. 6B: Test control Treatment CD + CT treatment the cluster beta cell- can be seen the test supplementary group and cell are dense. (Magnification - 10x40)

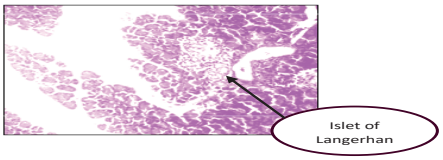

Fig. 6C: Negative control Nicotinamide +STZ induced; Here the number of beta-cell count decrease Gradually
(Magnification - 10x40)

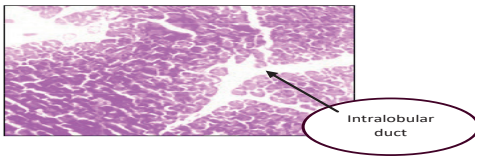

Fig. 6D: Another picture of CD 250 mg/kg treatment pancreas the density of the cell is less compare to the standard and supplementary dose group animal pancreas (Magnification - 10x40)

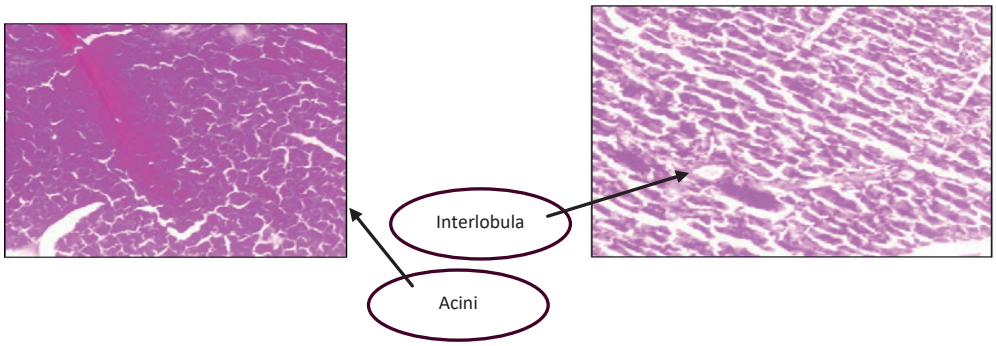

Fig. 6E: Normal control Without diabetes here the density of the cell is normally distributed (Magnification - 10x40)

Fig. 6E: Standard control Metformine dose 50 mg/kg (Magnification - 10x40)

Figure 6: Pancreatic tissue histopathology.

Discussion

Prevalence and co-morbidity in Type-2 diabetes is quite higher, currently. Synthetic molecule uses which targeting the many pathways, has decorates consequence in long term, Medicinal plants contain various phytochemicals which are responsible for the therapeutics benefits (14). In the present experiments the sole objective was to identify the effect of protein component over pre-clinical study with the plant extract of a mangrove plant *Ceriops decendra*. This mangrove plant has their several implications on therapeutics in-terms of traditional use. On the other hand, the protein component are used widely now a days as supplementary component for the treatment of diabetics patient. *Ceriops decendra* used for the treatment of diabetics traditionally and the protein component has their significant role on the metabolism process. Here in this study, we have evaluated the effect of foregoing plant extract with the enriched protein *Cyamopsis tetragonoloba* on pre-clinical study type-2 diabetes.

Right from the collection and identification of the sample here we have evaluated the comparative effectiveness and the enzyme-inhibitory assay. With solvent enrichment method purification of protein was carried out then it was supposed to quantify the enriched protein the purification was about 83%, analysis was carried out by the micro-Kjhadal method. After purification of the protein, we have assessed the anti-oxidant and in-vitro alpha-amylase inhibitory assay with combination of drug extract and the purified protein which show very promising result as compare to the plant extract along. In the *in vitro* level we have analyse the combinational anti-oxidant activity DPPH assay and the comparative enzyme inhibitory assay (15). The enzyme assay was quite surprising on the combination result its work as close to the standard drug acarbose. The IC50 value for the combination of isolated protein and the extract was 7.152 whereas the reference drug IC50 value 7.819 and *Ceriops decendra* is 8.219 which is quite differ from each other for the alpha-glucosidase enzyme. On the other hand, the enzyme inhibitory assay alpha – amylase has their own way of inhibitory potency the IC50 value of different drug and drug combination as follows IC50 value of CD+CT= 7.554 and standard = 8.186 and IC50 value of CD is = 9.12. In *in vivo* study, there were five group in there after the 28 days dose treatment each of the group except the normal control and the negative control group the mean blood glucose level after the 28 days which shows significantly lower as compare to the standard and the only extract treatment group. Significance on the statistical

analysis the p value is < 0.001 with the 95% confidence interval.

Overall, the tissue anti-oxidant parameter is then use to analyse the effect of each and individual group of their effect on the anti-oxidant property. In every anti-oxidant parameter, the combination supplementary dose group shows good effect on GSH and catalase activity and the statistical analysis ANOVA was conducted to determine the significance level of those individual group.

The experiment has fewer limitation that the assessment of the proper protein band is quite important due improper estimation of the band can lead to wrong interpretation of the molecular weight detection. During the experiment it was an little challenge to understand the protein band here after the gel electrophoresis this limitation need to assess again for to make the experiment robustness. As the protein plays a greater role on the metabolic dysfunction a proper amount of protein specially essential and semi-essential has greater impact on the metabolic regulation directly and indirectly. Based on the above experiment here we need to make robustness of the data by the multiple time study and look the importance of the natural occurring plant supplement for the treating the diabetes. Further studies in this way can yield an effective natural regime against diabetes.

Acknowledgements

The authors are thankful to Department of Biotechnology, Govt. of India, New Delhi for financial supports and the authority of Jadavpur University, Kolkata, West Bengal, India for providing the necessary facilities.

Conflict of interest

The authors declare that there is no conflict of interest.

References

1. Dash S, Pattnaik G, Kar B, Sahoo N, Bhattacharya S. An approach towards method development to investigate the anti-diabetic activity on experimental animals. Curr Trends Biotechnol Pharm 2021; 15: 330-348.
2. Dash S, Sahoo N, Pattnaik G, Ghosh G, Rath G, Bhattacharya S, Kar B. Antihyperglycemic effect of *Annona squamosa* leaf and oleanolic acid combination in diabetic albino rats. Curr Trends Biotechnol Pharm 2023; 17: 1004-1012.
3. Martinez-Sanchez A, Sałowka A. Molecular mechanisms of nutrient mediated regulation of microRNAs in pancreatic β-cells. Front Endocrinol 2021; 12: 704824.
4. Patra S, Bhattacharya S, Bala A, Haldar PK. Antidiabetic effect of *Drymaria cordata* leaf against streptozotocin–nicotinamide-induced diabetic albino rats. J Adv Pharm Technol Res 2020; 11: 44-52.
5. Biswas M, Kar B, Bhattacharya S, Kumar RBS, Ghosh AK, Haldar PK. Antihyperglycemic activity and antioxidant role of *Terminalia arjuna* leaf in streptozotocin-induced diabetic rats. Pharm Biol 2011; 49: 335-40.
6. Kumari R, Goldar WA, Mondal S, Patra S, Bhattacharya S, Haldar PK. Protective effect of *Basella alba* leaf against diabetic nephropathy in rats. Adv Tradit Med 2021; 21: 111-119.
7. Bhattacharya S. A review on experimentally proven medicinal plants and their constituents against fluoride toxicity. J Environ Pathol Toxicol Oncol 2023; 42: 51-64.
8. Nabeel MA, Kathiresan K, Manivannan S. Antidiabetic activity of the mangrove species *Ceriops decandra* in alloxan-induced diabetic rats. J Diabetes 2010; 2: 97-103.
9. Mahmud I, Shahria N, Yeasmin S, Iqbal A, Mukul EH, Gain S, Shilpi JA, Islam MK. Ethnomedicinal, phytochemical and pharmacological profile of a mangrove

plant Ceriops Decandra GriffDin Hou. J Complement Integr Med 2018; 16: 2017-0129.

10. Shaikh JR, Patil M. Qualitative tests for preliminary phytochemical screening: An overview. Int J Chem Studies 2020; 8: 603–608.

11. Asati V, Sharma PK. Purification and characterization of an isoflavones conjugate hydrolyzing β-glucosidase (ICHG) from *Cyamopsis tetragonoloba* (Guar). Biochem Biophys Rep 2019; 20: 100669.

12. Ladner-Keay CL, Turner RJ, Edwards RA. Fluorescent protein visualization immediately after gel electrophoresis using an in-gel trichloroethanol photoreaction with tryptophan. Meth Mol Biol 2018; 1853: 179–190.

13. Bhattacharya S, Haldar PK, Zaman MK. Anti-inflammatory and *in vitro* antioxidant property of *Zanthoxylum nitidum* root. Curr Trends Biotechnol Pharm 2010; 4: 774-783.

14. Bhattacharya S. Antineoplastic potential of *Trichosanthes dioica* root: A treatise. Indian J Nat Prod Resour 2023; 14: 202-209.

15. Bhattacharya S, Haldar PK, Zaman MK. Anti-inflammatory activity and antioxidant role of *Zanthoxylum nitidum* bark. Orient Pharm Exp Med 2011; 11: 271-277.

Current Trends in Biotechnology and Pharmacy
Vol. 18(3) 1922-1934, July 2024, ISSN 0973-8916 (Print), 2230-7303 (Online)
10.5530/ctbp.2024.3.38

Virtual Screening of New azo Coumarin Derivatives as Possible Alkaline Phosphatase Inhibitors

Anees Pangal[1], Javed Shaikh[1], Ranjit Kadam[2], Ravindra Kodag[2] and Khursheed Ahmed[1]*

[1]Advanced Scientific Research Laboratory, Abeda Inamdar Senior College of Arts, Science and Commerce (Autonomous), Azam Campus, Pune – 411001, India.
[2]Department of Chemistry and Research Centre, Abeda Inamdar Senior College of Arts, Science and Commerce (Autonomous), Azam Campus, Pune – 411001, India.
*Corresponding author: khursheedahmed@azamcampus.org

Abstract

To develop new alkaline phosphatase inhibitors, a series of new azo coumarin derivatives were designed by using computer aided drug designing and virtually assessed using online platforms. At first, the compounds were screened for ADMET, physicochemical properties, drug-likeness, toxicity studies and target prediction using pKCSM, SwissADME, SwissTargetPrediction and ProTox-II tools. The predictions were supported by *in silico* molecular docking with alkaline phosphatase enzyme using CB-Dock2 molecular docking tool. The compounds possessed good ADMET and physicochemical properties, drug-likeness and devoid of any immunotoxicity and cytotoxicity. The evaluated binding energy values reveal that all compounds fit favorably into the alkaline phosphatase active site displaying hydrogen bonding with different amino acid residues of the target protein and could be good scaffolds for designing new alkaline phosphatase inhibitors. These results collectively framed the way for the development of new azo coumarin derivatives as possible alkaline phosphates inhibitors.

Keywords: Alkaline phosphatase, coumarin, ADMET, Drug-likeness, Molecular docking.

Introduction

In recent years, the strategy of making hybrids of two or more than two biologically active motifs has emerged as a popular approach that involves conglomeration of two or more pharmacophores in one molecular scaffold to develop multifunctional biological agents (1-2). These hybrid structures are expected to exhibit multiple biological activities, modified selectivity profile, different or dual modes of action without reduced or no undesired side effects due to mixing of different pharmacophores in a single molecule (3-4). The cheminformatic tools, have played a major role in the development of therapeutically important small molecules or drugs including the Prediction of Activity Spectra for Substances (PASS), Lipinski's rule of five, predictions of absorption, distribution, metabolism, excretion, and toxicity (ADMET) are useful applications for the optimization and well-targeting of chemical synthesis, biological testing, and drug discovery (5). ADMET Predictor is a designed program of the computer for estimating pharmacokinetic parameters or properties of drug-like compounds from their molecular structures (6). Being highly bioactive and low toxic by a drug/drug-like compound are not good enough criteria to qualify the compound as a good can-

didate. A better profile of pharmacokinetic is exclusively important for a novel compound and it is very significant to evaluate the ADMET profile of new compounds earlier to avoid waste of time and resources (7).

Alkaline phosphatase is a hydrolase enzyme found in many organisms from bacteria to human and has been known to play a crucial role in various biological functions (8). It is used as tumor marker in various types of cancers like seminomas and ovarian cancer. Elevated levels of alkaline phosphatase have been found in several multifactorial disorders viz. bones diseases, thyrotoxicosis, hepatic or liver diseases, intestinal disease, cancerous growth (tumors) and rheumatoid arthritis etc. indicating it to be an interesting target for drug discovery (9).

On the other hand, coumarin or 2-oxo-2H-chromene derivatives are also known as therapeutic agents with broad and diverse biological activities (10) such as antioxidant (11), antimicrobial (12-13), antiviral (14), anti-inflammatory (15), antidepressant (16), anti-asthmatic (17), anti-HIV (18), anti-tubercular (19) and antitumor (20-21) are only few of them. The role of coumarin moiety in medicinal chemistry as a good therapeutic agent is well established and a number of different natural and synthetic coumarin based molecules have been reported as a potent alkaline phosphatase inhibitor (22-23).

Moreover, heterocyclic compounds are the exceptional targets for anticancer research and drug discovery (24). Among them, nitrogen containing compounds have shown excellent effects than non-nitrogen containing compounds (25). Further, it is reported that the combination of distinct pharmacophores produces compounds with improved activity (26). At the same time synthesis of hybrid structures from different class of compounds is one of the popular strategies for the development of drug candidates with increased activity and improved specificity (27-28).

Finding possible medicinal compounds is a major issue for many researchers because there are many drugs fail to arrive in clinical trials owing to their unsuitable drug likeness and poor ADMET (absorption, distribution, metabolism, elimination and toxicity) properties (29). In the design and development of new biological agents, molecular hybridization is a useful strategy and is based on the combination of two or more pharmacophoric units in the same molecule (30). In order to obtain a good pharamcophore with better activities and higher selectivity, we designed the target compounds by virtual screening using the computational tools like ADMET, pharmacokinetic, physicochemical and drug-likeness properties and molecular docking. The new coumarin analogs were designed by joining 4-hydroxycoumarin with different aromatic amines like aniline, 2-aminopyridine, 2-aminopyrimidine, 3-aminopyridazine and 2-aminopyrazine through the diazotization reaction as shown in the following Figure 1.

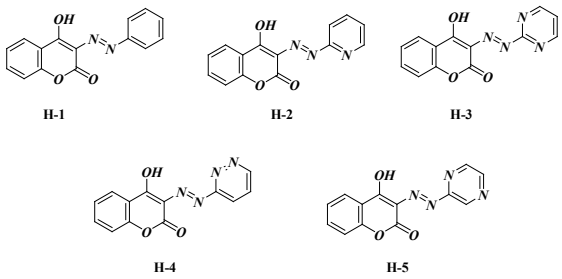

Figure 1. Designed azo coumarin derivatives

Materials and methods

The designed new azo coumarin derivatives (H-1 to H-5) were subjected to an in silico screening for ADMET, pharmacokinetic, physicochemical and drug-likeness properties, target prediction, toxicity prediction and molecular docking using the computational tools the pkCSM, SwissADME, ProTox-II and CB-Dock2 as online tools (31-32). These web servers were selected because they are freely accessible and provide strongly built computational methods to estimate a universal judgment of the pharmacokinetics and toxicity of small molecules.

ADMET prediction

The ADMET studies are significant to estimate the pharmacodynamics of the designed compounds, which could be a candidate agent in drug design and discovery studies. SMILES format of the designed molecules are uploaded on the pKCSM web server (https://biosig.lab.uq.edu.au/pkcsm/prediction). The pkCSM web server provide the information with respect ADMET parameters like gastrointestinal (GI) absorption, blood-brain barrier (BBB) permeability, CYP2D6 and CYP3A4 substrates and inhibitors, human skin permeability coefficients (log Kp), Caco-2 permeability, volume of distribution at steady state (VDss), CNS permeability, total clearance, AMES toxicity, maximum recommended tolerated dose (MRTD) human, oral rat acute toxicity (LD50) and hepatotoxicity, skin sensitization etc.

Pharmacokinetic, physicochemical properties and drug-likeness prediction

The designed molecules were estimated for pharmacokinetic, physicochemical properties and drug-likeness properties using SwissADME (http://www.swissadme.ch/). SwissADME is a web-based platform that lets users upload or draw their target compounds with structure or SMILES code. This tool supplies many parameters like lipophilicity (iLOGP, XLOGP3, WLOGP, MLOGP, SILICOS-IT, Log Po/w), water solubility – Log S (ESOL, Ali, SILICOS-IT), drug-likeness rules (Lipinski, Ghose, Veber, Egan, and Muegge) and Medicinal Chemistry (PAINS, Brenk, Leadlikeness, Synthetic accessibility) methods.

Target prediction

SMILES codes of the designed compounds were uploaded to the SwissTargetPrediction website (https://www.swisstargetprediction.ch) to analyze their putative off-targets in the human organism.

Toxicity prediction

Toxicological predictions for bioorganic compounds are essential to estimate the amount of tolerability of the lead compounds before *in vitro*, *in vivo,* and clinical studies. ProTox-II is virtual lab software used for the prediction of toxicities of the designed molecules. The SMILES codes of the designed molecules were uploaded to the The ProTox-II website (https://tox-new.charite.de/protox_II/) to analyze their acute toxicity, hepatotoxicity, cytotoxicity, carcinogenicity, mutagenicity, immunotoxicity, adverse outcome pathways (Tox21) and toxicity targets.

Molecular docking

CB-Dock2 is an improved version of the protein-ligand blind docking tool that inherits the curvature-based cavity detection procedure and the AutoDock Vina-based molecular docking procedures. In order to understand the probable binding affinities of the designed azo coumarin derivatives, molecular docking studies were carried out at active site of human alkaline phosphatase (PDB ID: 1EW2) using online molecular docking platform CB-Dock2 (https://cadd.labshare.cn/cb-dock2). The docking results were saved as PDB file and the PDB were processed for observing the interactions according to the literature.

Results and Discussion

ADMET prediction

A compound with better bioactivity and lesser toxicities should be investigated in the drug discovery to reduce the wastage of time and resources (33). These compounds could be developed into new medication when the target has been validated with sufficiently high quality ADMET properties. The ADMET properties of the designed analogs (H-1 to H-5) were predicted by using pkCSM web server and their drug potential was elaborated. The predicted results are shown in Table 1.

Table 1: ADMET properties of new azo coumarin derivatives calculated from pkCSM

Property	Model Name	H-1	H-2	H-3	H-4	H-5
Absorption	Water solubility[a]	-3.931	-3.494	-3.306	-3.2	-3.136
	Caco-2 permeability[b]	0.819	0.926	1.299	1.152	1.247
	Intestinal absorption (human)[c]	91.113	93.421	95.887	97.861	100
	Skin Permeability[d]	-2.837	-2.915	-2.851	-2.904	-2.872
Distribution	VDss (human)[e]	-0.13	-0.271	-0.275	-0.39	-0.334
	Fraction unbound (human)	0.118	0.248	0.199	0.228	0.221
	BBB permeability[f]	-0.222	-0.474	-0.68	-0.68	-0.68
	CNS permeability[g]	-1.697	-2.774	-2.897	-2.682	-2.896
Metabolism	CYP2D6 inhibitor[h]	No	No	No	No	No
	CYP3A4 inhibitor[h]	No	No	No	Yes	No
Excretion	Total Clearance[i]	0.199	0.251	0.333	0.063	0.248
Toxicity	Max. tolerated dose (human)	0.328	-0.261	0.067	-0.005	-0.004
	Oral Rat Acute Toxicity (LD50)	2.158	2.535	2.554	2.514	2.532
	Oral Rat Chronic Toxicity (LOAEL)	1.382	1.314	0.989	1.097	0.976
	Minnow toxicity	0.255	0.379	-0.079	-0.388	0.01
	Hepatotoxicity[h]	No	No	Yes	Yes	Yes
	Skin Sensitization[h]	No	No	No	No	No
	AMES toxicity	Yes	Yes	Yes	Yes	Yes

Note: [a](log mol/L), [b](log Papp in 10^{-6} cm/s), [c](% Absorbed), [d](log Kp), [e](log L/kg), [f](Fu), [g](log PS), [h](Yes/No), [i](log ml/min/kg), [j](LD50 in mol/kg), [k](LOAEL in log mg/kg_bw/day)

Log S (S in mol/L) is a parameter used to evaluate aqueous solubility. All of the derivatives were found to show good solubility values ranging from -3.136 to -3.931 mol/L. The analog H-1 is more soluble in water than all other analogs. More than 0.90 value of the Papp coefficient and more than 30% intestinal absorption indicates the compound has high Caco-2 permeability and good gastrointestinal absorption. All the derivatives showed poor gastrointestinal absorption and compound H-1 possessed the highest value of intestinal absorption among. The distribution of the compound or the drug in the body is characterized by Volume of distribution (VDss), blood-brain barrier permeability (logBB), and CNS permeability. Drugs can bind extensively to proteins in the plasma. The free or unbound fraction of a drug is usually the portion that is responsible for a pharmacologic effect. The designed molecules showed the unbound fraction in the range of 0.118 to 0.248 and the analog H-2 may show good pharmacological effect as it showed highest unbounded fraction of the drug. All the hybrids were poorly distributed within the tissues. The penetration of drug through Central Nervous System (CNS) is measured by parameter log PS, for all the analogs is less than -3 which indicates inability of these analogs to penetrate the CNS. Cytochrome P450s is an important enzyme system for drug metabolism in liver and the CYP2D6 and CYP3A4 are the two main subtypes of cytochrome P450. The molecules were unable to inhibit these enzymes and restrain the metabolism of the xenobiotics in the body. The prediction of total clearance helps to determine the feasibility of clinical dosing for the starting dose during clinical trial studies and it depends on

the molecular weight and hydrophilicity of the compound. The prediction showed that the total clearance of H-3 is highest followed by H-2 and other analogs H-5, H-4 and H-1 will not be eliminated from the body which may be associated with certain types of toxicities. The maximum recommended tolerated dose (MTD) provides an estimate of the toxic dose threshold of drugs in humans. From the values for MTD it is clear that the high dose is required for toxicity. All analogs have LD50 values above 0.5 mM and are non-toxic as per the predictions. For a compound, the predicted LOAEL is expressed in log (mg/kg_bw/day) and all the derivatives shows LOAEL in the range of 0.976 to 1.382. The predicted results show that the analogs H-1 and H-2 are non-hepatotoxic while all these analogs may not have skin sensitization. The designed analogs depicted LC50 values greater than 0.5 mM and are non toxic. Furthermore, all these analogs act as non-carcinogenic which is depicted from negative AMES toxicity test. These overall results of ADMET studies disclosed that the compounds have got good pharmacokinetic properties.

Furthermore, the BOILED-Egg profile enables the perceptive consideration of passive gastrointestinal absorption (HIA) and brain penetration (BBB) in the function of the position of the molecules in the WLOGP-vs-TPSA referential was screened for the selected five compounds (34). In this model, the white area corresponds to a high probability of passive absorption in the GIT, while the yellow area is for a high probability of brain penetration. Also, the marks are colored in blue if predicted as actively effluxes by P-gp (PGP+) and in red if estimated as non-substrate of P-gp (PGP−). All designed compounds were estimated to be well-absorbed but not accessing the brain, and all compounds were not subject to active efflux (red dot) (Figure 2).

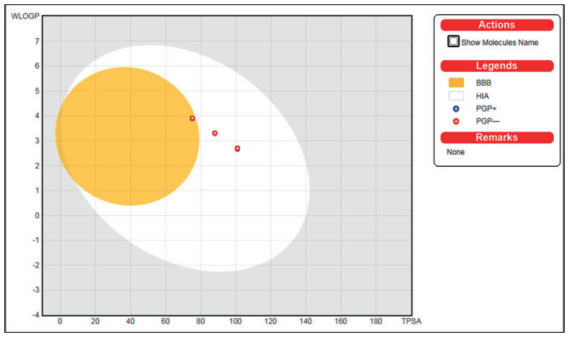

Figure 2. BOILED-Egg presentation of the compounds

Table 2. Physicochemical properties of the new azo coumarin derivatives

Properties		H-1	H-2	H-3	H-4	H-5
Molecular weight (g/mol)		266.25	267.24	268.23	268.23	268.23
No. of Heavy atoms		20	20	20	20	20
No. of Arom. heavy atoms		16	16	16	16	16
No. of Rotatable bonds		2	2	2	2	2
No. of H-Bond acceptors		5	6	7	7	7
No. of H-Bond donors		1	1	1	1	1
Molar Refractivity		75.13	72.92	70.72	70.72	70.72
Total polar surface area Å²		75.16	88.05	100.94	100.94	100.94
Solubility	Log S (ESOL)	-4.00	-3.54	-3.14	-2.91	-2.88
	Log S (Ali)	-4.51	-4.02	-3.61	-3.24	-3.18
	Log S (SILICOS-IT)	-5.65	-5.28	-4.91	-4.91	-4.91
Lipophilicity	MLOGP	2.07	1.81	1.16	1.56	0.75
	WLOGP	3.91	3.31	2.70	2.70	2.70
	XLOGP3	3.26	2.52	1.87	1.51	1.45

Physicochemical properties and drug-likeness prediction

The physicochemical properties give a comprehensive depiction of the structures of derivatives such as molecular weight (MW), molar refractivity (MR), topological polar surface area (TPSA), number of rotatable bonds, heavy atoms and hydrogen bond acceptors and donors. The physicochemical properties of the designed azo coumarin derivatives (H-1 to H-5) were predicted by using the SwissADME and the results are presented in Table 2. The bioavailability properties exhibited by the analogs are within the range except the lipophilicity that indicates they are excellent drug candidates. Hence form these physicochemical properties, we can be concluded that these compounds have excellent pharmacological properties and are orally bioavailable.

The bioavailability predictions of the compounds displayed a rapid evaluation of drug likeness. The drug likeness was evaluated based on the physicochemical properties to find oral drug candidates. There are five different rule-based filters (35) which are used to predict whether the chemical compounds can act as drug. The result of drug likeness evaluation of analogs is shown in Table 3 –

Table 3. Drug Likeness evaluation of the new azo coumarin derivatives

Rule-based filters	H-1	H-2	H-3	H-4	H-5
Lipinski violations	0 violation	0 violation	0 violation	0 violation	0 violation
Ghose violations	0 violation	0 violation	0 violation	0 violation	0 violation
Veber violations	0 violation	0 violation	0 violation	0 violation	0 violation
Egan violations	0 violation	0 violation	0 violation	0 violation	0 violation
Muegge violations	0 violation	0 violation	0 violation	0 violation	0 violation
Bioavailability Score	0.55	0.55	0.55	0.55	0.55
PAINS No. of Alerts	1 alert azo	1 alert azo	1 alert azo	1 alert azo	1alert azo
Brenk No. of Alerts	2 alerts: coumarin, diazo group	2 alerts: coumarin, diazo group	2 alerts: coumarin, diazo group	2 alerts: coumarin, diazo group	2 alerts: coumarin, diazo group
Lead likeness No. of Violations	0 violation	0 violation	0 violation	0 violation	0 violation
Synthetic accessibility	3.35	3.29	3.14	3.33	3.38

All the test compounds showed good drug similarity and can be a good drug candidates. They have zero violation for druglikeness according to the five laws framed by Lipinski, Ghose, Veber, Egan and Muegge. The Brenk and Pan Assay INterference compoundS (PAINS) structural alerts used in medicinal chemistry for the identifying unstable, reactive, toxic fragments present in the structure. Among the compounds examined, all molecules resist Brenk's rule due to coumarin and diazo groups. All analogs contain azo bond responsible for one alert in PAINS. However, all the compounds showed no violations in Lead likeness due to smaller molecular weight. Thus, these preliminary results provide the lead for the design of more potent drug. Furthermore, the bioavailability radar of the compounds is given in Figure 3, and the colored zone depicts suitable physicochemical space for oral bioavailability. The Bioavailability

Radar gives a first glance at the drug-likeness of the compounds. The pink area represents the optimal range for each property (lipophilicity: XLOGP3 between −0.7 and +5.0, size: MW between 150 and 500 g/mol, polarity: TPSA between 20 and 130 Å2, solubility: log S not higher than 6, saturation: fraction of carbons in the sp3 hybridization not less than 0.25, and flexibility: no more than 9 rotatable bonds.

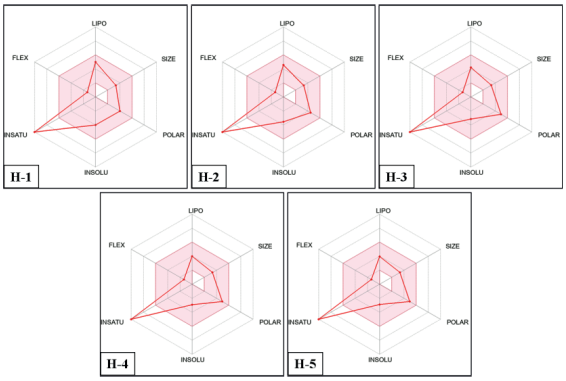

Figure 3. The Bioavailability Radar for drug-likeness of the new azo coumarin derivatives.

Target Prediction

The target prediction of all compounds was performed using the SwissTargetPrediction platform (36) and the results are depicted as a pie-chart (Figure 4). The H-1, containing phenyl ring linked to coumarin through diazo bond was predicted as 33.3% oxidoreductase. All other derivatives H-2 to H-5, containing 1 to 2 nitrogen atoms in the phenyl ring were predicted as enzymes inhibitors with varying percentages, as given in Figure 4.

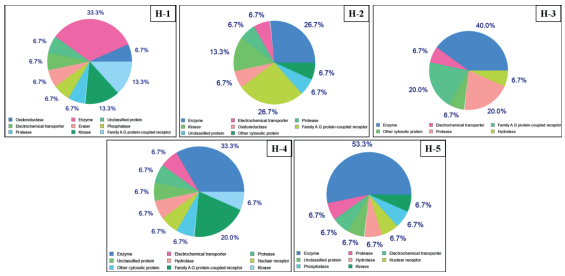

Figure 4. SwissTargetPrediction of the designed compounds.

Toxicity Prediction

The new azo coumarin derivatives were evaluated for toxicity, LD50 and classification by ProTox-II. The compound H-1 was found in class V toxicity while H-2 to H-5 were in class IV, which indicates if swallowed they may be harmful and toxic to human being at a concentration of (2000 < LD50 ≤ 5000) mg/kg body weight. The lethal dose varies from 2000 to 3200 mg/kg weight for all the compounds. The average similarity of the designed compounds ranged between 39.79 to 53.28% with the prediction accuracy of 23 to 67.38%. The ProTox-II platform is divided into five different classification steps: (1) acute toxicity (2) organ toxicity (3) toxicological endpoints (4) toxicological pathways and (5) toxicity targets. The compounds exhibited slight activities for hepatotoxicity, carcinogenicity and mutagenicity while the compounds were inactive for immunotoxicity and cytotoxicity which needs to be experimentally verified through *in vivo* experiments. For Tox21-nuclear receptor signaling pathways, several parameters such as AhR, AR, AR-LBD, Aromatase, ER, ER-LBD, and PPAR-gamma were predicted for the designed compounds and for all the protein pathways the compounds have shown inactive probability. These results suggest that these compounds exhibit not only weak estrogenic, but also antiestrogenic, antiandrogenic, and anti-TH activities via different pathways. For Tox21-stress response pathways, parameters like nrf2/ARE, HSE, MMP, p53, and ATAD5 have been studied. All the compounds displayed inactive probability for all types of stress response pathways except Mitochondrial Membrane Potential (MMP) stress response pathway.

Molecular docking

Understanding how to predict interactions between proteins and small molecules is essential for identifying various biological processes, advancing drug development, and comprehending protein functions. A powerful approach for this purpose is protein-ligand blind docking, which identifies protein binding re-

gions, and foretelling a molecule's binding pose (32, 37-38). Alkaline phosphatase is an enzyme that is increased by a number of hepatobiliary disorders. Its increase is typically assumed to signify bile stasis. According to available reports, alkaline phosphatase is a significant prognostic factor for a number of malignancies, including colon, lung, and stomach cancer. Alkaline phosphatase increase is frequently interpreted as bile stasis brought on by liver metastases (39). To predict the best conformational position within the active region of target protein, all the designed azo coumarin derivatives (H-1 to H-5) were docked against alkaline phosphatase. The derivatives were docked into the active sites of human alkaline phosphatase (PDB ID: 1EW2). All the generated docked complexes were analyzed on the basis of minimum energy values expressed as binding energy (kcal/mol) and hydrogen/hydrophobic interactions. Docking results justified that all of designed compounds exhibited excellent binding affinities with the target protein. It was found that the molecules interact with different residues inside the active site of the alkaline phosphatase. The free binding energy for these derivatives was found to be in the range of -7.3 to -7.8 kcal/mol displaying good binding of these inhibitors inside the active site pocket of the protein. The 3D and 2D diagrams of interactions with the amino acid side chains of the target protein is shown in Figure 5 and Figure 6.

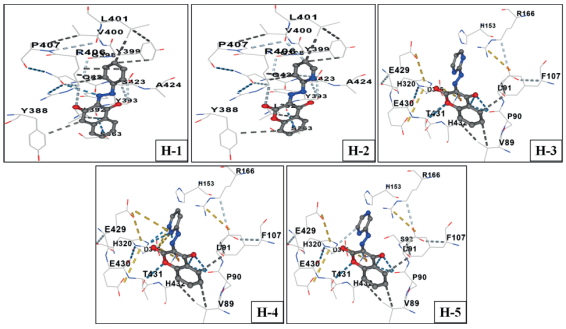

Figure 5. 3D-Binding modes of new azo coumarin derivatives (H-1 to H-5) in the active binding site of alkaline phosphatase

The basic chemical nuclei of all the designed compounds were the same and therefore most derivatives exhibited a good binding affinity with the target protein. The best docking score of -7.8 was shown by derivatives H-4 and H-5. However, other analogs showed a docking score of -7.3, -7.4 and -7.6 respectively. All the designed compounds showed well established H-bonding with different amino acid residues. The binding free energy and other details from docking studies are presented in Table 4.

The compounds H-4 and H-5 displayed three pi-cation interactions with ARG166, HIS432 and LYS87. The nitrogen of azo group, the lactone ring oxygen and the –OH on C-4 of coumarin moiety displayed hydrogen bond with THR431 and HIS432. Along with these, all molecules showed electrostatic and van der Waals interactions with other amino acid residues as shown in Figure 6. Such binding mode should have made these molecules well-fixed in the protein active site of the alkaline phosphatase.

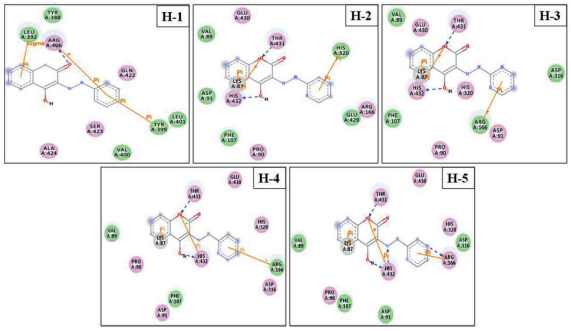

Figure 6. 2D-Interaction analysis of new azo coumarin derivatives (H-1 to H-5) in the active binding site of alkaline phosphatase

However, the other compounds also exhibited reasonably good interactions with the binding site amino acid residues and showed a good binding energy. The evaluated binding energy values reveal that all compounds fit favorably into the alkaline phosphatase active site displaying hydrogen bonding with different amino acid residues of the target protein. Our predicted results are in well agreement with the predicted in silico results. Therefore, these new

Table 4. Molecular docking results of the new azo coumarin derivatives

Sr. No.	Azo coumarin derivative	Binding Energy Kcal/Mol	Binding amino acid residues
1	H-1	-7.3	SER363, TYR388, LEU392, TYR393, GLY398, TYR399, VAL400, LEU40,1 ARG406, PRO407, GLN422, SER423, ALA424
2	H-2	-7.4	VAL89, PRO90, ASP91, SER92, PHE107, HIS153, ARG166, ASP316, HIS320, GLU429, GLU430, THR431, HIS432
3	H-3	-7.6	VAL89, PRO90, ASP91, PHE107, HIS153, ARG166, ASP316, HIS320, GLU429, GLU430, THR431, HIS432
4	H-4	-7.8	VAL89, PRO90, ASP91, PHE107, HIS153, ARG166, ASP316, HIS320, GLU429, GLU430, THR431, HIS432
5	H-5	-7.8	VAL89, PRO90, ASP91, SER92, PHE107, HIS153, ARG166, ASP316, HIS320, GLU429, GLU430, THR431, HIS432

derivatives containing a coumarin ring and heterocyclic amines joined through diazo group could be good scaffolds for designing new alkaline phosphatase inhibitors. These molecules also showed good ADMET, physicochemical properties and drug-likeness. These results collectively framed the way for the development of new azo coumarin derivatives as alkaline phosphates inhibitors.

Synthetic accessibility of the designed azo coumarin derivatives

The target compounds designed in this study can be synthesized according to Figure 7 for further examination. A cold solution of sodium nitrite (0.207 g, 3 mmol) was added dropwise into the solution of aromatic amines (3 mmol) dissolved in a mixture of conc. HCl and water (5 ml) in an ice bath. The temperature of the reaction was maintained below 5 °C. After the complete addition, the solution was kept for 15-30 min with occasional stirring to complete the diazotization. After completion of reaction as monitored by TLC, it was dropwise added into an ice-cold solution of 4-hydroxy coumarin (0.543 g, 3 mmol) in 10 ml of 2N NaOH. Then resultant mixtures were stirred at room temperature for 30 min to 1 hour. The colour products obtained were filtered and washed with water. Finally, the obtained products were dried and recrystallised by ethanol.

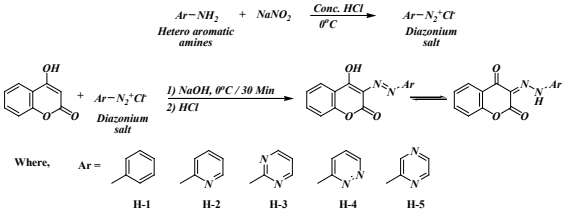

Figure 7. Possible synthetic scheme for new azo coumarin derivatives

Conclusion

In the present study, we designed the new azo coumarin derivatives by considering the advantages of important medicinal scaffold 4-hydroxycoumarin through molecular hybridization and computational methods. All the designed derivatives were virtually screened for their ADMET, physicochemical, drug-like ness and toxicity studies. All the compounds showed good pharmacodynamics, no violations in drug-likeness and devoid of any immunotoxicity and cytotoxicity. These compounds were further subjected for possible target prediction and the compounds were found to target enzymes. The predicted target was confirmed by molecular docking studies using alkaline phosphatase enzyme. All compounds exhibited reasonably good interactions with amino acid residues and showed a good binding energy. The evaluated binding energy values indicated that all com-

pounds fit favorably into the alkaline phosphatase active site displaying hydrogen bonding with different amino acid residues of the target protein. These results fit well with the predicted *in silico* results though these have to be experimentally verified. Therefore, these new derivatives containing a coumarin ring and heterocyclic amines joined through diazo group can become good drug candidate for designing new alkaline phosphatase inhibitors. These molecules also showed good ADMET, physicochemical properties and drug-likeness. These results collectively make the way for the development of new azo coumarin derivatives as possible alkaline phosphates inhibitors.

Acknowledgments

We are grateful to Dr. P. A. Inamdar, the President of MCE Society, Pune and the principal, Abeda Inamdar Senior college of Arts, Science and Commerce (autonomous), Pune for providing the lab facilities.

Conflict of interest: None.

Financial support

We are thankful to the Department of Science and Technology, Govt. of India for providing financial assistance under DST-FIST (0 Level) to Abeda Inamdar Senior College, Pune vide letter number SR/FST/COLLEGE-277/2018 dated 20th December 2018.

Ethics statement: None.

References:

1. Szumilak, M., Wiktorowska-Owczarek, A., & Stanczak, A. (2021). Hybrid Drugs-A Strategy for Overcoming Anticancer Drug Resistance. Molecules (Basel, Switzerland), 26(9), 2601. https://doi.org/10.3390/molecules26092601
2. Andricopulo, A. D., Salum, L. B., & Abraham, D. J. (2009). Structure-based drug design strategies in medicinal chemistry. Current topics in medicinal chemistry, 9(9), 771–790. https://doi.org/10.2174/156802609789207127
3. Bansal, Y., & Silakari, O. (2014). Multifunctional compounds: smart molecules for multifactorial diseases. European journal of medicinal chemistry, 76, 31–42. https://doi.org/10.1016/j.ejmech.2014.01.060
4. Geldenhuys, W. J., Youdim, M. B., Carroll, R. T., & Van der Schyf, C. J. (2011). The emergence of designed multiple ligands for neurodegenerative disorders. Progress in neurobiology, 94(4), 347–359. https://doi.org/10.1016/j.pneurobio.2011.04.010
5. Sultan, M. A., Galil, M. S. A., Al-Qubati, M., Omar, M. M., Barakat, A. (2020). Synthesis, molecular docking, druglikeness analysis, and ADMET prediction of the chlorinated ethanoanthracene derivatives as possible antidepressant agents. Appl. Sci. 10, 7727. https://doi.org/10.3390/app10217727
6. Singh, D. B., Gupta, M. K., Singh, D. V., Singh, S. K., & Misra, K. (2013). Docking and in silico ADMET studies of noraristeromycin, curcumin and its derivatives with Plasmodium falciparum SAH hydrolase: a molecular drug target against malaria. Interdisciplinary sciences, computational life sciences, 5(1), 1–12. https://doi.org/10.1007/s12539-013-0147-z
7. Isyaku, Y., Uzairu, A., & Uba, S. (2020). Computational studies of a series of 2-substituted phenyl-2-oxo-, 2-hydroxyl- and 2-acylloxyethylsulfonamides as potent anti-fungal agents. Heliyon, 6(4), e03724. https://doi.org/10.1016/j.heliyon.2020.e03724
8. Altaf, R., Nadeem, H., Iqbal, M. N., Ilyas, U., Ashraf, Z., Imran, M., & Muhammad, S. A. (2022). Synthesis, Biological Evaluation, 2D-QSAR, and Molecular Simulation Studies of Dihydropyrimidinone Derivatives

as Alkaline Phosphatase Inhibitors. ACS omega, 7(8), 7139–7154. https://doi.org/10.1021/acsomega.1c06833

9. Iqbal, Z., Iqbal, A., Ashraf, Z., Latif, M., Hassan, M., & Nadeem, H. (2019). Synthesis and docking studies of N-(5-(alkylthio)-1,3,4-oxadiazol-2-yl)methyl)benzamide analogues as potential alkaline phosphatase inhibitors. Drug development research, 80(5), 646–654. https://doi.org/10.1002/ddr.21542

10. Pangal, A., Shaikh, J. A., Khan, E. M. (2017). Current developments of C3-substituted coumarin hybrids as anti-cancer agents. Int. J. Pharm. Sci. Rev. Res. 42(1), 161-168.

11. Bubols, G. B., Vianna, D.daR., Medina-Remon, A., von Poser, G., Lamuela-Raventos, R. M., Eifler-Lima, V. L., & Garcia, S. C. (2013). The antioxidant activity of coumarins and flavonoids. Mini reviews in medicinal chemistry, 13(3), 318–334. https://doi.org/10.2174/138955713804999775

12. Pangal, A., & Ahmed, K. (2022). Synthesis and biological evaluation of coumarin-quinone hybrids as multifunctional bioactive agents. ADMET & DMPK, 11(1), 81–96. https://doi.org/10.5599/admet.1468

13. Pangal, A., Tambem, P., & Khursheed, A. (2023). Screening of 3-acetylcoumarin derivatives as multifunctional biological agents. Current Chemistry Letters, 12(2), 343-352. http://dx.doi.org/10.5267/j.ccl.2022.12.005

14. Hassan, M. Z., Osman, H., Ali, M. A., & Ahsan, M. J. (2016). Therapeutic potential of coumarins as antiviral agents. European journal of medicinal chemistry, 123, 236–255. https://doi.org/10.1016/j.ejmech.2016.07.056

15. Fylaktakidou, K. C., Hadjipavlou-Litina, D. J., Litinas, K. E., & Nicolaides, D. N. (2004). Natural and synthetic coumarin derivatives with anti-inflammatory/ antioxidant activities. Current pharmaceutical design, 10(30), 3813–3833. https://doi.org/10.2174/1381612043382710

16. Wang, X., Zhou, H., Wang, X., Lei, K., & Wang, S. (2021). Design, Synthesis, and In Vivo and In silico Evaluation of Coumarin Derivatives with Potential Antidepressant Effects. Molecules (Basel, Switzerland), 26(18), 5556. https://doi.org/10.3390/molecules26185556

17. Sánchez-Recillas, A., Navarrete-Vázquez, G., Hidalgo-Figueroa, S., Rios, M. Y., Ibarra-Barajas, M., & Estrada-Soto, S. (2014). Semisynthesis, ex vivo evaluation, and SAR studies of coumarin derivatives as potential antiasthmatic drugs. European journal of medicinal chemistry, 77, 400–408. https://doi.org/10.1016/j.ejmech.2014.03.029

18. Srivastav, V. K., Tiwari, M., Zhang, X., Yao, X-J. (2018). Synthesis and antiretroviral activity of 6-acetyl-coumarin derivatives against HIV-1 infection. Indian J Pharm Sci, 80(1), 108-117. http://doi.org/10.4172/pharmaceutical-sciences.1000335

19. Mali, H. M., Sabale, S. S., Degani, M. S., Borkute, R., Choudhari, A. S., Sarkar, D., Krishna, V. S., & Sriram, D. (2018). Rational design of coumarin derivatives as antituberculosis agents. Future medicinal chemistry, 10(20), 2431–2444. https://doi.org/10.4155/fmc-2018-0015

20. Pangal, A., Mujahidm, Y., Desai, B., Shaikh, J. A., Khursheed, A. (2022). Synthesis of 3-(2-(subsituted-(trifluoromethyl) phenylamino) acetyl)-2H-chromen-2-one derivatives as new anticancer agents. Current Chemistry Letters, 11(1), 105–112. http://dx.doi.org/10.5267/J.CCL.2021.8.004

21. Pangal, A., Shaikh, J. A., Mulani, M., & Khursheed, A. (2021). Synthesis, anticancer activities and in silico screening

of 3-acetylcoumarin hydrazone scaffolds. Journal of Advanced Scientific Research, 12(4-1), 225-233. https://doi.org/10.55218/JASR.s1202112425

22. Küpeli Akkol, E., Genç, Y., Karpuz, B., Sobarzo-Sánchez, E., & Capasso, R. (2020). Coumarins and Coumarin-Related Compounds in Pharmacotherapy of Cancer. Cancers, 12(7), 1959. https://doi.org/10.3390/cancers12071959

23. Irfan, A., Rubab, L., Rehman, M., Anjum, R., Ullah, S., Marjana, M., Qadeer, S. & Sana, S. (2020). Coumarin sulfonamide derivatives: An emerging class of therapeutic agents. Heterocyclic Communications, 26(1), 46-59. https://doi.org/10.1515/hc-2020-0008

24. Martins, P., Jesus, J., Santos, S., Raposo, L. R., Roma-Rodrigues, C., Baptista, P. V., & Fernandes, A. R. (2015). Heterocyclic Anticancer Compounds: Recent Advances and the Paradigm Shift towards the Use of Nanomedicine's Tool Box. Molecules (Basel, Switzerland), 20(9), 16852–16891. https://doi.org/10.3390/molecules200916852

25. Kerru, N., Gummidi, L., Maddila, S., Gangu, K. K., & Jonnalagadda, S. B. (2020). A Review on Recent Advances in Nitrogen-Containing Molecules and Their Biological Applications. Molecules (Basel, Switzerland), 25(8), 1909. https://doi.org/10.3390/molecules25081909

26. Arooj, M., Sakkiah, S., Kim, S., Arulalapperumal, V., & Lee, K. W. (2013). A combination of receptor-based pharmacophore modeling & QM techniques for identification of human chymase inhibitors. PloS one, 8(4), e63030. https://doi.org/10.1371/journal.pone.0063030

27. Alkhzem, A. H., Woodman, T. J., & Blagbrough, I. S. (2022). Design and synthesis of hybrid compounds as novel drugs and medicines. RSC Adv, 12(30), 19470-19484. https://doi.org/10.1039/D2RA03281C

28. Pawełczyk, A., Sowa-Kasprzak, K., Olender, D., & Zaprutko, L. (2018). Molecular Consortia-Various Structural and Synthetic Concepts for More Effective Therapeutics Synthesis. International journal of molecular sciences, 19(4), 1104. https://doi.org/10.3390/ijms19041104

29. Guan, L., Yang, H., Cai, Y., Sun, L., Di, P., Li, W., Liu, G., & Tang, Y. (2018). ADMET-score - a comprehensive scoring function for evaluation of chemical drug-likeness. MedChemComm, 10(1), 148–157. https://doi.org/10.1039/c8md00472b

30. Ibrar, A., Zaib, S., Jabeen, F., Iqbal, J., & Saeed, A. (2016). Unraveling the Alkaline Phosphatase Inhibition, Anticancer, and Antileishmanial Potential of Coumarin-Triazolothiadiazine Hybrids: Design, Synthesis, and Molecular Docking Analysis. Archiv der Pharmazie, 349(7), 553–565. https://doi.org/10.1002/ardp.201500392

31. Shaikh, J., Pangal, A., Tamboli, I., Pote, G., & Khursheed, A. (2022). Design and in silico evaluation of new azo barbituric acid analogs as possible anticancer agents. Hetercyclic letters, 2022; 12(4), 725-735. http://dx.doi.org/10.6084/m9.figshare.21647096

32. Mermer, A., Vakal, S. (2022). Pyrazine-chromene-3-carbohydrazide conjugates: Molecular docking and ADMET predictions on dual-acting compounds against SARS-CoV-2 Mpro and RdRp. J. Res. Pharm., 25(6), 953-966. http://dx.doi.org/10.29228/jrp.92

33. Isyaku, Y., Uzairu, A., & Uba, S. (2020). Computational studies of a series of 2-substituted phenyl-2-oxo-, 2-hydroxyl- and 2-acylloxyethylsulfonamides as potent anti-fungal agents. Heliyon, 6(4), e03724. https://doi.org/10.1016/j.heliyon.2020.e03724

34. Daina, A., & Zoete, V. (2016). A BOILED-Egg To Predict Gastrointestinal Absorption and Brain Penetration of Small Molecules. ChemMedChem, 11(11), 1117–1121. https://doi.org/10.1002/cmdc.201600182

35. Daina, A., Michielin, O., & Zoete, V. (2017). SwissADME: a free web tool to evaluate pharmacokinetics, drug-likeness and medicinal chemistry friendliness of small molecules. Scientific reports, 7, 42717. https://doi.org/10.1038/srep42717

36. Gfeller, D., Grosdidier, A., Wirth, M., Daina, A., Michielin, O., & Zoete, V. (2014). SwissTargetPrediction: a web server for target prediction of bioactive small molecules. Nucleic acids research, 42(Web Server issue), W32–W38. https://doi.org/10.1093/nar/gku293

37. Brackenridge, D. A., & McGuffin, L. J. (2021). Proteins and Their Interacting Partners: An Introduction to Protein-Ligand Binding Site Prediction Methods with a Focus on FunFOLD3. Methods in molecular biology (Clifton, N.J.), 2365, 43–58. https://doi.org/10.1007/978-1-0716-1665-9_3

38. Aqlan, F. M. S. (2021). Synthesis, ADMET and docking studies of novel pyrazoles incorporating coumarin moiety as tyrosine kinase (Src) inhibitors. Biointerface Research in Applied Chemistry, 11(5), 13706-13714. https://doi.org/10.33263/BRIAC115.1370613714

39. Annibali, O., Petrucci, M. T., Santini, D., Bongarzoni, V., Russano, M., Pisani, F., Venditti, O., Pantano, F., Rago, A., Siniscalchi, A., et. al. (2020). Alkaline phosphatase (alp) levels in multiple myeloma and solid cancers with bone lesions: Is there any difference? Journal of bone oncology, 26, 100338. https://doi.org/10.1016/j.jbo.2020.100338

40. Kim, S. H., Shin, K. H., Moon, S. H., Jang, J., Kim, H. S., Suh, J. S., & Yang, W. I. (2017). Reassessment of alkaline phosphatase as serum tumor marker with high specificity in osteosarcoma. Cancer medicine, 6(6), 1311–1322. https://doi.org/10.1002/cam4.1022

Current Trends in Biotechnology and Pharmacy
Vol. 18(3) 1935-1950, July 2024, ISSN 0973-8916 (Print), 2230-7303 (Online)
10.5530/ctbp.2024.3.39

“”Insilco Evaluation of *Psoralea corylifolia* for Novel Anti-Tubercular Compounds: Virtual Screening, Molecular Docking, and Dynamics Simulation Analysis”

Madhusudhanan J[1], Usharani S[2*]

[1]Department of Biotechnology, Anand Institute of Higher Technology, Kalasalingam Nagar IT Corridor, Chennai, Tamil Nadu 603 103, India;
[2]Department of Chemistry, S.I.V.E.T. College of Arts and Science, Velachery Main Road, Chennai, Tamil Nadu 600 073, India;
***Corresponding author:** usharani@sivet.in

Abstract

Mycobacterium tuberculosis, the causative agent of tuberculosis (TB), remains a significant global health concern, causing millions of infections and deaths each year. The emergence of drug-resistant strains of *M. tuberculosis* has further complicated the treatment of this infectious disease. Therefore, there is an urgent need to discover new and effective therapeutic strategies to combat TB. *P. corylifolia* was reported to possess antibacterial, anti-inflammatory, antifungal, antioxidant, estrogenic, antitumor, and immunomodulatory activities. The present study aimed to conduct an insilico evaluation of phytochemicals from the plant *Psorlea corylifolia* that are retrieved from databases and literature against potential targets of Mycobacterium tuberculosis. Around 69 compounds belonging to the plant was collected from previous literatures and they were subjected to SwissADME screening with various filters like Lipinski, Ghose, etc. Seven compounds have crossed these filters and ADMET prediction was done for these compounds using online tools like PreADME, ADMETlab2.0, etc. Additionally, molecular docking was performed for all seven compounds against three potential targets: 6B2Q, 6R9W, and 5W25 (protein structures related to Mycobacterium tuberculosis). Among the tested compounds, 2, 4-Di-tert-butylphenol exhibited interactions with all three targets, demonstrating favourable binding energy. The best docked complex was selected for a 100ns molecular dynamics simulation, which revealed stability between 70-90ns, indicating its potential interaction within a virtual biological environment. Further this compound requires *invitro* testing to know its ability to act as an anti-tuberculosis agent. These findings contribute to the identification of promising lead compounds for future drug discovery efforts against Mycobacterium tuberculosis.

Keywords: Insilico; *Mycobacterium tuberculosis; Psorlea corylifolia*, 2,4-Di-tert-butylphenol, Molecular Docking; Molecular Simulation; Anti-tubercular agent

Introduction

Mycobacterium tuberculosis, which causes tuberculosis (TB), continues to be one of the most prevalent causes of fatalities from a single infectious agent. Only three medications have been licensed and placed into the pharmaceutical market over the past 50 years, despite several attempts to find novel anti-TB treatments). Due to the rapid emergence of drug resistance and the lack of knowledge surrounding the cellular transition to dormancy that precedes it, many of the currently available anti-TB medications are ineffective. Additionally, nonrepli-

cating M. tuberculosis-fighting medications are currently scarce (1).

Psorlea corylifolia, a medicinal plant widely used in traditional medicine, has gained attention for its potential therapeutic properties. It contains a variety of bioactive compounds that have shown promising antimicrobial activities against several pathogens. In recent years, researchers have turned to *in silico* methods to explore the potential of Psorlea corylifolia and its bioactive compounds in combating *M. tuberculosis* (2).

In silico target validation is an essential step in drug discovery, enabling researchers to identify and validate potential protein targets that can be modulated by the bioactive compounds present in *Psorlea corylifolia.* By utilizing computational tools and databases, researchers can assess the drug-ability and functional significance of these targets, providing a foundation for subsequent analyses (3).

The crystal structure of the essential protein kinases A and B in Mycobacterium tuberculosis, represented by PDB ID 6B2Q (4), was chosen as one of the targets for the study. Targeting these protein kinases can potentially disrupt crucial cellular processes and inhibit the growth of MTB. Another target selected for investigation was the enoyl-ACP reductase, InhA, which is a validated drug target in MTB. InhA is involved in the synthesis of mycolic acids, essential components of the mycobacterial cell wall. The crystal structure of InhA in complex with the AP-124 inhibitor, represented by PDB ID 6R9W (5), was chosen to explore the binding interactions and potential inhibitory activity of *Psorlea corylifolia* against this target.

Additionally, the crystal structure of Aspartyl-t RNA synthetase (AspRS) from Mycobacterium tuberculosis, complexed with L-Aspartic Acid, represented by PDB ID 5W25, was selected as another target. AspRS plays a crucial role in protein synthesis by attaching aspartic acid to its cognate tRNA. Inhibition of AspRS can disrupt protein synthesis and potentially impair the survival of MTB (6). Through in silico target validation, molecular docking, and dynamics studies, we aim to investigate the binding affinity, potential inhibitory activity, and stability of *Psorlea corylifolia* compounds against the selected targets. These computational approaches will provide valuable insights into the interactions between *Psorlea corylifolia* and the target proteins, aiding in the identification of potential lead compounds for further experimental validation and development as novel anti-TB agents.

Materials and methods

Compound library preparation

The mass spectrometric data containing 69 compounds identified from the plant *Psorlea corylifolia* was retrieved from the literature (7,8). A compound library was prepared using these compounds along with canonical SMILES.

Physiochemical and ADME screening

The Canonical SMILES from the Library of Compounds were fed into the Swiss ADME prediction tool to obtain the physiochemical and ADME data. The screening was done using series of filters like Lipinski rule of 5, Ghose, Rotatable bonds, PAINS and Brenk (9).

Pharmacokinetics prediction

ADME prediction plays an important role in drug discovery and development as it helps assess the pharmacokinetic and pharmacodynamics properties of compounds. The ADME was predicted using the online tools Pre-ADME (10)and ADMETLAb2.0 (11). Pre ADME utilizes computational models and algorithms based on available databases and established methods to generate predictions for parameters like Lipophilicity, permeability, absorption, metabolism, etc., whereas ADMETLab2.0 gives all the ADME data along with clearance and half-life period of the compound.

Toxicity prediction

Toxicity prediction is an important step

in drug discovery and development to evaluate the potential adverse effects of chemical compounds on biological systems. Several online tools are available to assist in toxicity prediction, including Preadmet, Protox II, and GUSAR.

Acute rat toxicity model

The GUSAR (General Unrestricted Structure-Activity Relationships) computer program is designed to create models of quantitative correlations between an organic molecule's structure and other attributes. Quantitative Neighborhoods of Atoms (QNA) descriptors, Prediction of Activity Spectra for Substances (PASS), and Self-Consistent Regression predictions are used in the QSAR approach to model acute toxicity for rats. With four methods of pharmacological substance administration (oral, intraperitoneal, intravenous, and subcutaneous) for rats, QSAR models of relationships "structure - acute toxicity" were developed through the GUSAR software (12).

Ames test and carcinogenicity predictions

Protox II is an online tool designed specifically for predicting the potential toxicity of small organic molecules towards various toxicological endpoints. It utilizes a structure-activity relationship (SAR) approach and provides predictions for toxicity endpoints such as mutagenicity, carcinogenicity, hepatotoxicity, and developmental toxicity. Protox II combines chemical similarity searching and QSAR (Quantitative Structure-Activity Relationship) models to estimate toxicity risks based on the molecular structure of the compound (13).

Ligand and protein preparation

The Ligand preparation was done by retrieving the SDF format of the compounds from Pubchem. The Mol format was generated using Pymol and the energy minimization of the compound structure was achieved using the Avogadro tool. Similarly, based on the literature the target protein PDB file for Dual Inhibition of the Essential Protein Kinases A and B in Mycobacterium tuberculosis(6B2Q), Crystal structure of InhA in complex with AP-124 inhibitor (6R9W) and Crystal structure of Aspartyl-tRNA synthetase from Mycobacterium tuberculosis complexed with L-Aspartic Acid (5W25) was obtained from Protein Data bank (14). Polar hydrogens were added during preparation to avoid undesired interactions during docking, while water molecules and hetero atoms were removed from the protein crystal structure. Using Auto dock, Kollman and Gasteiger charges were added to the ligands and protein during preparation. Additionally, conversion of protein and ligand structures from the PDB format into the PDBQT (Protein Data Bank, Partial Charge (Q), & Atom Type (T)) formats was made with the help of Auto dock (15).

Protein structure validation

Protein structure model validation was done by using ERRAT ("https://servicesn.mbi.ucla.edu/ERRAT/), (16) Verify3D ("http://servicesn.mbi.ucla.edu/Verify3D/) and PROCHECK (17) ("https://www.ebi.ac.uk/thornton-srv/software/PROCHECK).

Molecular docking

Auto Dock Vina is a molecular docking tool used in computational drug discovery to predict how small molecules (ligands) bind to a target protein. Configuration files were created for both the proteins by setting suitable Cartesian coordinates to generate Grid box. The protein's X, Y, and Z attributes were noted after choosing a specific ligand posture from among those present in the protein crystal structure to determine the binding affinity (18). The protein molecules were kept rigid during the docking process. For ligand conformation searching, the Lamarckian Genetic Algorithm (LGA), which is a local search algorithm, was employed.

Molecular simulation

Molecular dynamics simulation was carried out using Desmond module via Maestro of Schrodinger suite 2020-3 in the Linux platform.

Molecular simulation was performed to study the stability of docked complex with the ligand for around 50ns. The molecular system was solvated with crystallographic water (TIP3P) molecules under cubic periodic boundary conditions for a 20 Å buffer region. The system was neutralized with 0.1 M of Na+ and Cl- ions (19).

Results and Discussion

Psorlea corylifolia- compound library screening

The Compounds were screened using the validated rules used as filters in many pharmaceutical companies, as follows Lipinski rule of 5, Ghose, Rotatable bonds, PAINS and Brenk. From 69 compounds about 7 were able to cross all the filters and they were depicted in the figure 1. These compounds were further considered for the study against the proteins involved in the cell wall biosynthesis of the targeted pathway. In a similar study, *Sravika et al., 2021* used these filters to estimate individual ADME parameters of the phytoconstituents from *Bauhinia acuminata* for screening of compounds (20)*conventional medicinal plants analysis have constantly increased multinationally because plants allow them to complement modern pharmacological approaches. As computer mechanics approach, i.e in silico screening and pharmacokinetic screening can augment active compounds among the candidates and indicate mechanism of action of medicinal plants. The plant is well known for its precautionary action in tuberculosis. It has been established to possess some pharmacological activities such as Cytotoxic [1] , antibacterial [2, 3] , anti-nociceptive [4] , thrombolytic activity [5] , antioxidant [6] , anthelmintic [7] , anti-diarrheal [8] , Hepatoprotective [9]. The present focus on the use of in silico ADME tool called Swiss ADME for pharmacological and pharmacognostic profiling of Bauhinia acuminata. The results of these studies can be further carried forward by researcher to investigate the in vitro and in vivo studies to reveal the pharmacological basis of traditional medicinal plants. Introduction The prehistoric people have great consciousness of the tradition of medicinal plants as herbal medicines. In the world, more than 80% of the living in minor developed countries reveal on customary medicine and humans are dependent on herbs for their basic requirements such as food stuffs, clothing, flavor, shelter, fragrance, and medicines (Divya and Mini, 2011 & Manoj Kumar Mishra, 2016, Gurib-Fakim, 2006 and Brijesh & Madhusudan, 2015*.

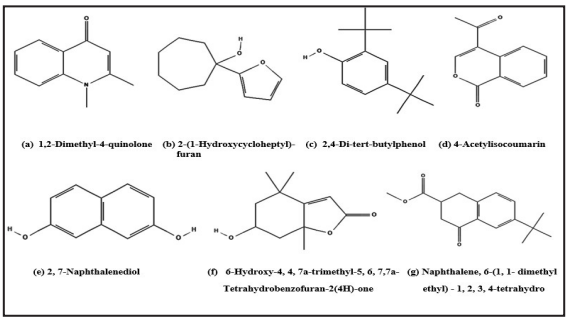

Figure 1: 2D structure of screened ligands

Physiochemical properties and drug likeness

The Physiochemical properties of the screened bioactive compounds were retrieved from swiss-ADME (Table 1). All the seven compounds were found to satisfy the Lipinski rule of five namely Molecular weight <500 g/mol, No of H-bond donors should be less than 5 and not more than 10 hydrogen bond acceptors (Table 2). The topological polar surface area was found to be less than 140 Å² describing the defined sum of polar atoms in the molecule. Moreover, the bioavailability scores of the compounds were computed based on their molecular weight, cLogP, number of hydrogen bond acceptors and hydrogen bond donor. In a previous Insilico validation study of 500 compounds focusing on different biological activity like antimicrobial, Antifungal, it was found that the predicted range of physiochemical properties exceeded the existing parameters even after applying all filters (21). The Log P (Octanol-Water partition coefficient) value remained within 5 indicating the water-soluble nature of compounds. According

to *Knoll et al., 2022* high lipophilicity indicates good permeation of compound through Mycobacterial cell wall (22). In the present study 2, 4-Di-tert-butylphenol exhibits moderate solubility with Log P value around 3.08 highlighting that it could penetrate through the cell wall of Mycobacterium and could exhibit potential activity at the target site.

Table 1: Physiochemical properties of predicted ligands

Ligands	Solubility and Lipophilicity							
	Molecular Formula	Molecular mass g/mol	No of H-bond acceptors	No of H-bond donors	Total polar surface Area Å²	Solubility (mg/mL)	Class	Log P
1,2-Dimethyl-4-quinolone	C11H11NO	173.21	1	0	22.00	2.83e-01	Soluble	2.07
2-(1-Hydroxycycloheptyl)-furan	C11H16O2	180.24	2	1	33.37	4.40e-01	Soluble	2.19
2,4-Di-tert-butylphenol	C14H22O	206.32	1	1	20.23	5.78e-03	Moderately soluble	3.08
2,7-Naphthalenediol	C10H8O2	160.17	2	2	40.46	3.61e-01	Soluble	1.31
4-Acetylisocoumarin	C11H8O3	188.18	3	0	47.28	9.55e-01	Soluble	1.75
6-Hydroxy-4,4,7a-trimethyl-5,6,7,7a-tetrahydrobenzofuran-2(4H)-one	C11H16O3	196.24	3	1	46.53	4.04e+00	Very soluble	1.88
Naphthalene, 6-(1,1-dimethyl ethyl)-1,2,3,4-tetrahydro	C16H20O3	260.33	3	0	43.37	8.12e-02	Soluble	2.88

Table 2: Drug likeness

Ligands	Lipinski rule of 5	Ghose	Bioavailability score
1,2-Dimethyl-4-quinolone	Yes; 0 violation	Yes ; No violation	0.55
2-(1-Hydroxycycloheptyl)-furan	Yes; 0 violation	Yes ; No violation	0.55
2,4-Di-tert-butylphenol	Yes; 0 violation	Yes ; No violation	0.55
2,7-Naphthalenediol	Yes; 0 violation	Yes ; No violation	0.55
4-Acetylisocoumarin	Yes; 0 violation	Yes ; No violation	0.55
6-Hydroxy-4,4,7a-trimethyl-5,6,7,7a-tetrahydrobenzofuran-2(4H)-one	Yes; 0 violation	Yes ; No violation	0.55
Naphthalene, 6-(1,1- dimethyl ethyl)- 1,2,3,4-tetrahydro	Yes; 0 violation	Yes ; No violation	0.55

ADMET prediction

The gastrointestinal absorption (GIA) of the identified compounds was evaluated using PreADME and the results are presented in Table 3A. 2, 7-Naphthalenediol was estimated to have low GIA, while 2, 4-Di-tert-butylphenol and 1, 2-Dimethyl-4-quinolone was predicted to have high potential to be absorbed in the gastrointestinal tract. High GIA is considered an advantage during oral administration. Thus, both 2, 4-Di-tert-butylphenol and 1, 2-Dimethyl-4-quinolone has good probability of being absorbed in the intestinal cells and exerts

its biological activity. The Caco2 permeability study can aid in the selection of appropriate excipients to enhance the absorption of poorly permeable compounds. Values predicted using PreADME suggest that the Caco2 permeability of the compounds are within the moderate range. The skin permeation (LogKp) suggests that 2,4-Di-tert-butylphenol compound possess the less negative value of – 3.87 cm/s indicating its good skin permeability whereas 6-Hydroxy-4,4,7a-trimethyl-5,6,7,7a-tetrahydrobenzofuran-2(4H)-one was predicted to contain moderate to high negative value of -6.79 cm/s depicting relatively low skin permeability. P-gp inhibitors are molecules that may block P-gp from excreting pharmaceuticals into cells, boosting the intracellular concentration and bioavailability of co-administered medications. In the current study it was found that compounds 1,2-Dimethyl-4-quinolone, 2,4-Di-tert-butylphenol and Naphthalene, 6-(1,1- dimethyl ethyl)- 1,2,3,4-tetrahydro are inhibitors of P-Glycoprotein indicating that these substances can overcome drug resistance and improve the therapeutic efficacy of drug by suppressing P-gp. Similarly, all the 7 compounds were found to be BBB permeable. The % plasma binding protein was found to be 100 for 2-(1-Hydroxycycloheptyl)-furan and 2, 4-Di-tert-butylphenol and least % of 23.88 for 6-Hydroxy-4, 4, 7a-trimethyl-5, 6, 7, 7a-tetrahydrobenzofuran-2(4H)-one once again highlighting that 2, 4-Di-tert-butylphenol has better systemic circulation. In an insilico study performed by *Khamouli et al., 2019* overall ADME predictions of amino-pyrimidine derivatives showed GIA of 90.926%, Caco2 around 15-18% and skin permeability -2.704 to -3. 721 cm/s respectively. Similarly, the plasma binding protein was found to be around 87% with moderate BBB penetration and some compounds are P-glycoprotein inhibitors (23). These predictions reveals that the GIA, Plasma binding protein, Caco2 permeability and BBB were found to be comparatively similar or more in the current study highlighting better Absorption and distribution property of the compound.

Table 3A: ADME Prediction of Screened compounds

COMPOUND NAME	ABSORPTION			DISTRIBUTION		
	Human intestinal Absorption	Caco-2 permeability	Log Kp (skin permeation) (cm/s)	P-glycoprotein inhibitor	BBB penetration	Plasma Protein Binding
1,2-Dimethyl-4-quinolone	100.000000	54.5989	-5.89	Yes	Yes	58.502030
2-(1-Hydroxycycloheptyl)-furan	95.451419	43.0929	-5.78	No	Yes	100.000000
2,4-Di-tert-butylphenol	100.000000	44.8684	-3.87	Yes	Yes	100.000000
2,7-Naphthalenediol	91.618383	20.3624	-5.93	No	Yes	95.587064
4-Acetylisocoumarin	98.036259	21.3184	-6.52	No	Yes	49.326538
6-Hydroxy-4,4,7a-trimethyl-5,6,7,7a-tetrahydrobenzofuran-2(4H)-one	93.378046	21.5562	-6.79	No	Yes	23.881949
Naphthalene, 6-(1,1-dimethyl ethyl)-1,2,3,4-tetrahydro	98.213233	22.3895	-5.62	Yes	Yes	92.984636

Compound metabolism impacts a substance's distribution, excretion, and absorption. A class of enzymes known as cytochrome P450 (CYP) monooxygenases affects how drugs are metabolized and eliminated from the body. The predicted metabolism of the identified compounds against six isomers of CYP is displayed in the table 3B. ADME prediction study done by *Aguinaldo et al., 2022,* revealed that caffeic acid extracted from *Cocos nucifera* caffeic acid was non-inhibitor of CYP1A2, CYP2C19, CYP2C9, CYP2D6, and CYP3A4. Results also demonstrate that caffeic acid is a non-substrate of CYP1A2, CYP2C19, CYP2D6, and CYP3A4 (24) whereas in the present study, it was found that except 1, 2-Dimethyl-4-quinolone all other compounds are inhibitors of CYP2C9 and CYP3A4. Also, other than compounds 1, 2-Dimethyl-4-quinolone, 2, 4-Di-tert-butylphenol and 6-Hydroxy-4, 4, 7a-trimethyl-5, 6, 7, 7a-tetrahydrobenzofuran-2(4H)-one remaining were found to be the inhibitors of CYP2C19. On the other hand, none of the compounds showed inhibition against CYP2D6. While focussing on CYP substrates, 2, 4-Di-tert-butylphenol and Naphthalene, 6-(1, 1- dimethyl ethyl) - 1, 2, 3, 4-tetrahydro were found act as CYP3A4 substrates whereas no compound acts as a CYP2D6 substrates. From these data it has been predicted that among seven compounds most of them were found to be inhibitors of CYP2C19, CYP2C9 and CYP3A4 highlighting the metabolism of the compounds studied.

Table 3B: ADME Prediction of Screened compounds

COMPOUND NAME	METABOLISM						EXCRETION	
	CYP3A4 substrate	CYP3A4 inhibition	CYP2C19 inhibition	CYP2D6 substrate	CYP2D6 inhibition	CYP2C9 inhibition	$T_{1/2}$ (half-life period)	Clearance rate (ml/min/kg)
1,2-Dimethyl-4-quinolone	Weakly	No	No	No	No	No	0.345	5.226
2-(1-Hydroxycycloheptyl)-furan	No	Yes	Yes	No	No	Yes	0.255	8.533
2,4-Di-tert-butylphenol	Yes	Yes	No	No	No	Yes	0.324	6.300
2,7-Naphthalenediol	No	Yes	Yes	No	No	Yes	0.866	16.596
4-Acetylisocoumarin	No	Yes	Yes	No	No	Yes	0.618	3.049
6-Hydroxy-4,4,7a-trimethyl-5,6,7,7a-tetrahydrobenzofuran-2(4H)-one	Weakly	Yes	No	No	No	Yes	0.720	8.814
Naphthalene, 6-(1,1-dimethyl ethyl)-1,2,3,4-tetrahydro	Yes	Yes	Yes	No	No	Yes	0.193	7.212

A key pharmacokinetic factor that is related to drug bioavailability is drug clearance (CL). It is also a crucial factor in determining how frequently to administer drugs to reach steady-state concentrations. Suthar et al explains the half Life ($T_{1/2}$) of the compound explains the Volume of distribution and clearance of Drug. It falls under two category $T_{1/2}$> 3 (Category 0-

$T_{1/2}$ -) and $T_{1/2}$ ≤3 (Category 1- $T_{1/2}$+) The Output value is the probability of being $T_{1/2}$+ within the range 0 to 1. The values between 0-0.3 remarks excellent half-life of the compound whereas 0.3-0.7 gives us moderate half-life (25). In the present study, the compound Naphthalene,6-(1, 1- dimethyl ethyl) - 1, 2, 3, 4-tetrahydro had good half-life value of 0.193 whereas 2, 7-Naphthalenediol had poor half-life of 0.866. Also, the clearance rate was found to be relatively low for 4-Acetylisocoumarin with 3.049 ml/min/kg whereas 2, 7-Naphthalenediol exhibited higher clearance rate indicating that it can be rapidly excreted from the circulation. This implies that the compounds exhibited comparatively moderate half-life and clearance rate.

Toxicity panel

Rat toxicity model

The Acute toxicity prediction in Rat model was done using GUSAR Online and the results are tabulated Table 4. GUSAR gave predictions on rat model with Different routes of administration like Intraperitoneal, Intravenous, Oral and Subcutaneous whose LD50 are expressed in mg/kg. The globally standardized system of Classification and Labelling of Chemicals (GHS) defines the following hazardous classes as mentioned in (26): Class 1: if ingested, fatal (LD_{50} 5≤ mg/kg); Class 2 substances are deadly if consumed (5<LD_{50}≤50 mg/kg), hazardous if ingested (50<LD_{50}≤ 300 mg/kg), toxic if ingested (300<LD_{50}≤ 2000 mg/kg), potentially harmful if ingested (2000<LD50≤5000 mg/kg), and non-toxic (LD_{50}>5000 mg) substances. Previous research conducted by *Halder et al., 2019* confirms that *Psoralea corylifolia* was found to contain Neobavaisoflavone, a phytochemical which is predicted to possess an LD50 of 2500 mg/kg, and hence better than Dapsone, which is chemically produced (27). In contrast to the previous study, where the LD50 ranged between 2000 and 5000, the current investigation revealed that the LD 50 values of substances in all drug delivery routes, including IP, IV, SC, and oral, were expected to be larger than 5000mg/kg and thus found to be harmless. From these predictions, it was clear that the current study contains compounds with LD50 values that fall within the range indicating that they are non-toxic.

Table 4: Results of LD 50 value of the compound estimated with rat toxicity model

Ligands	Rat IP LD50 (mg/kg)	Rat IV LD50 (mg/kg)	Rat Oral LD50 (mg/kg)	Rat SC LD50 (mg/kg)
1,2-Dimethyl-4-quinolone	471,000	59,100	1327,000	732,200
2-(1-Hydroxycycloheptyl)-furan	326,700	37,890	858,600	486,800
2,4-Di-tert-butylphenol	797,100	72,050	1743,000	492,900
2,7-Naphthalenediol	483,900	98,270	1011,000	642,100
4-Acetylisocoumarin	380,600	39,010	2676,000	1275,000
6-Hydroxy-4,4,7a-trimethyl-5,6,7,7a-tetrahydrobenzofuran-2(4H)-one	479,300	20,150	3038,000	215,300
Naphthalene, 6-(1,1- dimethyl ethyl)-1,2,3,4-tetrahydro	612,100	36,540	1418,000	423,700

IP - Intraperitoneal route of administration Oral - Oral route of administration

IV - Intravenous route of administration SC - Subcutaneous route of administration

Ames test and carcinogenicity

AMES toxicity which is the test for mutagenicity. To prevent the creation of hazardous mutagenic and potentially carcinogenic medications, it is necessary to estimate the AMES toxicity since mutagenicity is a key end point of toxicity and has a strong connection to carcinogenicity. Except 2, 4-Di-tert-butylphenol rest of the compounds are reported to be mutagen. Other toxicity predictions like Hepatotoxicity, Carcinogenicity, Immunotoxicity, mutagenicity and Cytotoxicity has been done using protox2 which revealed that the compounds 2,4-Di-tert-butylphenol, 2,7-Naphthalenediol and Naphthalene, 6-(1,1- dimethyl ethyl)- 1,2,3,4-tetrahydro exhibited inactive remarks in all the above-mentioned toxicity parameters including Carcinogenicity Mouse and Rat model (Table 5). *Castro et al., 2021* conducted an evaluation of toxicity for compounds Isoeleutherin and Eleutherin isolated from a herb where insilico predictions revealed that both the compounds are positive towards rat carcinogenicity model and negative in mouse carcinogenicity model with medium risk in cytotoxicity (28). Whereas in the present study the compound 2,4-Di-tert-butylphenol was found to be a non-mutagen and negative or inactive in terms of all toxicity studies highlighting that this compound can be considered for further study.

Table 5: Toxicity panel

Ligand	Ames test	Carcinogenicity Mouse model	Carcinogenicity Rat model	Hepatotoxicity	Carcinogenicity	Immunotoxicity	Mutagenicity	Cytotoxicity
1,2-Dimethyl-4-quinolone	mutagen	Negative	Positive	Inactive	Inactive	Inactive	Active	Inactive
2-(1-Hydroxycycloheptyl)-furan	mutagen	Positive	Negative	Inactive	Inactive	Inactive	Inactive	Inactive
2,4-Di-tert-butylphenol	non-mutagen	Negative	Negative	Inactive	Inactive	Inactive	Inactive	Inactive
2,7-Naphthalenediol	mutagen	Negative	Negative	Inactive	Inactive	Inactive	Active	Inactive
4-Acetylisocoumarin	mutagen	Negative	Positive	Inactive	Active	Inactive	Inactive	Inactive
6-Hydroxy-4,4,7a-trimethyl-5,6,7,7a-tetrahydrobenzofuran-2(4H)-one	mutagen	Negative	Negative	Inactive	Active	Inactive	Inactive	Inactive
Naphthalene, 6-(1,1-dimethyl ethyl)-1,2,3,4-tetrahydro	mutagen	negative	negative	Inactive	Inactive	Inactive	Inactive	Inactive

Protein model validation

PROCHECK analysis and Ramachandran plot validation for the target proteins has been done following (29) protocol and has been illustrated in Figure 2, 3 and 4. In Target protein 6B2Q with more than 90.2% of the residues were found to be in favoured and altogether 9.6 % residues were found in additional and generously allowed regions, which validate the quality of homology models. Similarly, other proteins namely 6R9W and 5W25 shows around 91.6 and 88.2% of the residues in favoured region indicating better quality of protein model. The overall G-factor for 6B2Q, 6R9W and 5W25 were 0.12, 0.10 and 0.15. The modelled structures were also validated by other structure verification servers such as Verify 3D and Errat. Verify 3D assigned a 3D-1D score of >=0.1 for all the modelled proteins.

Table 6: Evaluation of Protein Model Quality

Protein Name	ERRAT Quality Score	Procheck	Verify 3D
6B2Q	92.7007	Out of 8 evaluations, Errors: 3 Warning: 3 Pass: 2	86.95 % of the residues have average 3D-1D score of >= 0.1
6R9W	96.1792	Out of 8 evaluations, Errors: 4 Warning: 2 Pass: 2	68.49 % of the residues have average 3D-1D score of >= 0.1
5W25	88.2459	Of 9 evaluations, Errors: 2 Warning: 3 Pass: 4	84.05% of the residues have averaged 3D-1D score >= 0.1

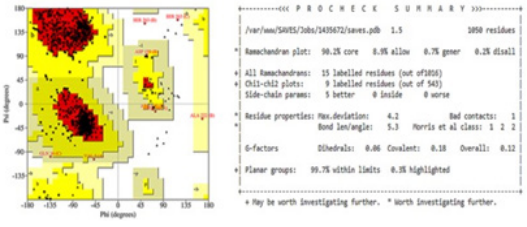

Figure 2: Ramachandran plot of protein 6B2Q obtained from procheck analysis

This implies that the models are compatible with their sequence. ERRAT showed overall quality factor 92.7007, 96.1792 and 88.2459 for 6B2Q, 6R9W and 5W25 respectively (Table 6). *Hamid et al., 2021* performed computational analysis of 3D structure of two catalytic proteins MOCS1A and MOCS1B where procheck analysis have been done and The Ramachandran plot statistics for model proteins MOCS1A and MOCS 1B revealed that for MOCS1A about 80% residues are in the allowed region and 3.6% residues (only 12 residues) are in disallowed region. For MOCS1B, more than 90% residues are in the allowed region and 1.8% residues (only 10 residues) are in disallowed region (30). Contrasting the current and previous study it can be inferred from Ramachandran plots that most data appear in the favoured region suggesting that the modelled structure is acceptable.

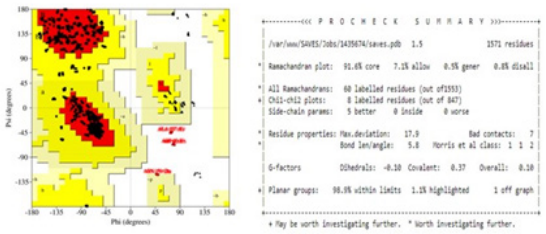

Figure 3: Ramachandran plot of protein 6R9W obtained from procheck analysis

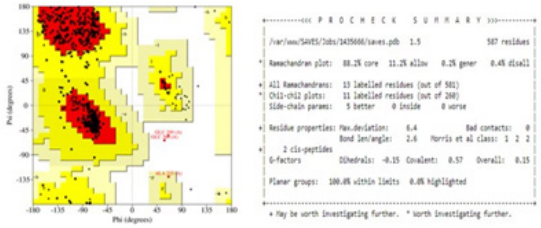

Figure 4: Ramachandran plot of protein 5W25 obtained from procheck analysis

Molecular docking

Molecular docking was done using Auto dock vina and their interactions are visualized using UCSF Chimera tool as per (31)many methods of molecular modeling have been em-

ployed to study complex biological and chemical systems. Experimental strategies are integrated with computational approaches for the identification, characterization, and development of novel drugs and compounds. In modern drug designing, molecular docking is an approach that explores the confirmation of a ligand within the binding site of a macromolecule. To date, many software and tools for docking have been employed. AutoDock Vina (in UCSF [University of California, San Francisco] Chimera. Docking was carried out with the seven screened compounds against the targets 6B2Q, 6R9W and 5W25. Among the docked compounds 2, 4-Di-tert-butylphenol exhibited strong binding energy of -8.8, -10.0 and -7.1 kcal/mol against all the three targets 6B2Q, 6R9W and 5W25 respectively (Table 7). They formed H-bonds with the amino acid residues Val98 A, Gly 96 A and Gly 563 A of the aforementioned corresponding targets (Refer Figure 5, 6 and 7). Similarly in terms of interactions, 2, 7-Naphthalenediol showed four H-bond interactions against 5W25 with the binding energy of -5.8 kcal/mol. Furthermore, 2-(1-Hydroxycycloheptyl)-furan and 4-Acetylisocoumarin displayed moderate binding energies of -5.6 and -5.5 kcal/mol against 6B2Q and 5W25. In a docking study conducted by *Wlodarchak et al., 2108* against 6B2Q, best binding affinity was found to be -8.87 kcal/mol for imidazopyridine aminofurazans (32) In another study nearly 25 bioactive pyrimidine derivatives have been docked against 6R9W where one of the derivatives showed better score of -11.59kcal/mol indicating its best interaction against the target (33). According to these two pioneering findings, the binding energy for 2, 4-Di-tert-butylphenol in the current research was discovered to be very similar with binding energy ranging between -8.8 and -10.0 kcal/mol.

Table 7: Docking scores of 6B2Q, 6R9W and 5W25 with the Compounds along with Bond Length

S.NO	Ligands	6B2Q				6R9W				5W25			
		Binding energy (Kcal/mol)	H-donor	H-acceptor	Bond length(Å)	Binding energy (Kcal/mol)	H-donor	H-acceptor	Bond length(Å)	Binding energy (Kcal/mol)	H-donor	H-acceptor	Bond length(Å)
1	1,2-Dimethyl-4-quinolone	-6.3	Asp 159 C	Ligand	5.558	-7.5	Gly 96A	Ligand	5.563	-5.6	Glu 230 A	Ligand	4.793
2	2-(1-Hydroxycycloheptyl)-furan	-5.6	Ligand	Gly 145 A	4.746	-6.5	Ligand	Ser 152 D	4.063	-5.8	Ligand	Arg 132 A	3.131
							Ligand	Ser 166 C	5.418				
3	2,4-Di-tert-butylphenol	-8.8	Ligand	Val 98 A	2.355	-10.0	Ligand	Gly 96 A	4.387	-7.1	Ligand	Gly 563 A	4.510
			Val 98 A	Ligand	2.823								
4	2,7-Naphthalenediol	-6.8	Val 98 A	Ligand	2.840	-7.9	Ligand	Gly 96 D	3.674	-5.8	Ligand	Ala 535 A	3.148
							Val 65 D	Ligand	2.361		Ligand	Gly 488 A	2.699
											Ligand	Asp 701 A	2.702
							Ligand	Leu 63 D	2.347		Ligand	Glu 485 A	2.942
5	4-Acetylisocoumarin	-6.8	Val 98 A	Ligand	3.755	-7.9	Gly 96 D	Ligand	3.405	-5.5	Gly 563 A	Ligand	5.064

6	6-Hydroxy-4,4,7a-trimethyl-5,6,7,7a-tetrahydrobenzofuran-2(4H)-one	-6.0	Leu 97 A	Ligand	2.912	-8.0	Ligand	Ser 166 D	3.324	-5.9	Ligand	Arg 492 A	3.250
7	Naphthalene, 6-(1,1-dimethyl ethyl)-1,2,3,4-tetrahydro	-7.6	Thr 21 D	Ligand	4.831	-7.6	Met 155B	Ligand	2.861	-5.8	Val 564 A	Ligand	4.292

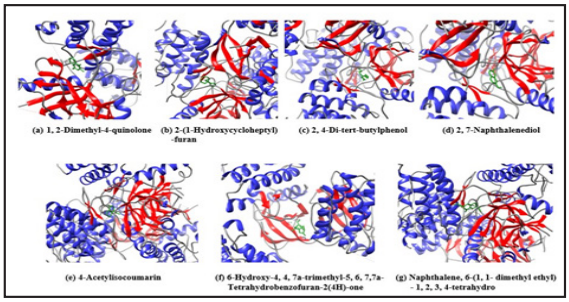

Figure 5: Visualization of interaction of Ligands with the target protein 6B2Q

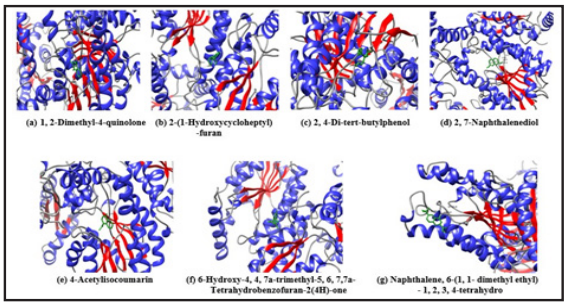

Figure 6: Visualization of interaction of Ligands with the target protein 6R9W

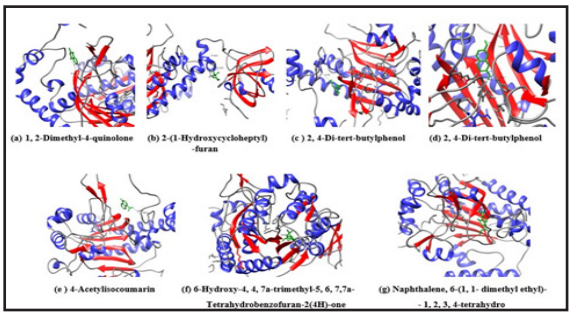

Figure 7: Visualization of interaction of Ligands with the target protein 5W25

Overall, the results indicate that the tested ligands have the potential to interact with the target proteins of Mycobacterium tuberculosis, suggesting their possible therapeutic relevance. The observed binding energies and hydrogen bonding interactions provide insights into the strength and specificity of ligand-protein interactions (1). Also, the current docking study highlights that compound 2, 4-Di-tert-butylphenol shows promising binding affinity against all the targets and hence the docked complex with better binding efficiency namely 6R9W_2, 4-Di-tert-butylphenol was further considered for Molecular dynamic simulation.

Molecular simulation

Numerous dynamical, structural, and energetic details about the simulated system are revealed by MD simulations. For the purpose of running the simulations, the top-ranked docked pose 6R9W_2, 4-Di-tert-butylphenol based on free binding energy scores was selected as the structural model. The built trajectories of all the simulated systems were analysed in terms of its RMSD and Protein ligand Histogram. Complex stability was checked by analysis of the interaction map and the RMSD (root mean square deviation) plot of the ligand and protein. RMSD of the protein gives insights to the structural conformation throughout the simulation.The changes of the order of 1-3 Å is acceptable for small molecules.Here it was found to be around 2.4-3.3 Å with slight fluctuations from the beginning and it attained equilibration between 70- 90 ns (Figure 8). *Alzain et al., 2023* conducted an insil-

ico multitarget approach where 18 cytosporone E analogues were screened against 6R9W by docking and simulation using desmond schrodinger exhibited RMSD value below 3Å which reflected the stability of the compounds with few fluctuations (34). On comparing the present and previous study the RMSD and the stability was found to be more or less similar displaying that the compound, 2, 4-Di-tert-butylphenol can be considered as a potential anti-tubercular agent which requires further *invitro* evaluations to be marketed as drug molecule.

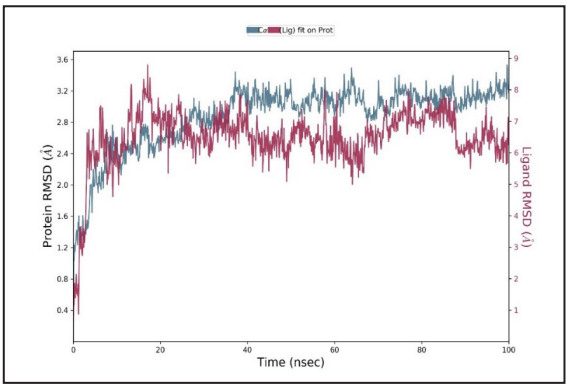

Figure 8: RMSD plot for the simulated 6R9W_2, 4-Di-tert-butylphenol complex

The protein Ligand contacts histogram depicts different types of interactions namely H-bond, Hydrophobic , Ionic and Water bridges. The stacked bar charts are normalized over the course of trajectory. In the Figure 9, H-bond interaction was seen with the aminoacid residues Met 98, Gly 96, ser 94, Arg 43 and Lys 165 indicating that there was a specific interaction maintained for about 30-50% of the simulation time of 100ns. Other than H-bond interactions, few hydrophobic contacts was observed at residue Met98, Ile 16, Phe41, Met 161, Ala 164 and Met 199 displaying the interaction of aromatic or aliphatic group on the ligand (Figure 9). According to *Alzain et al., 2023* water bridges are commonly found in the histogram since it mediates the hydrogen-bonded protein-ligand interactions. In their study, the average Hydrogen and hydrophobic bonds formed between the derivatives and the target was 5 that comprises of aminoacid residues like Phe149, Tyr 158, Trp222, Thr196 and Glu219 (34). This indicates that the current study had better H-bond interactions throughout the simulation time equally to that of the prior study.

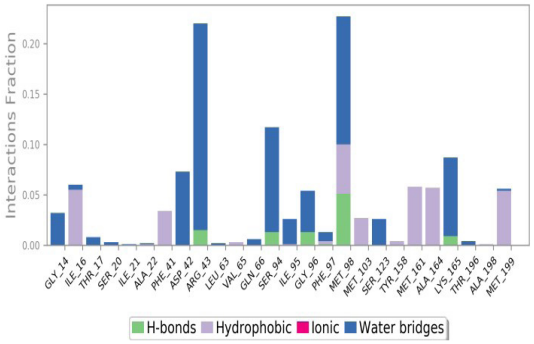

Figure 9: Protein Ligand Contacts Histogram

Conclusion

Overall, the study focused on in-silico evaluation of phytochemicals from *Psorlea corylifolia* against potential targets of Mycobacterium tuberculosis. Sixty-nine compounds from the plant were screened using SwissADME with various filters, resulting in the identification of seven compounds that passed these filters. ADME prediction using tools like PreADME and ADMETlab2.0 provided insights into the pharmacokinetic properties of these compounds. Furthermore, molecular docking against three potential targets related to Mycobacterium tuberculosis revealed better interaction between the compound 2, 4-Di-tert-butylphenol and the targets. Molecular dynamics simulation of the best docked complex demonstrated stability within a virtual biological environment. These findings highlight the potential of 2, 4-Di-tert-butylphenol as a lead compound for further investigation as an anti-tuberculosis agent. However, in vitro testing is necessary to validate its efficacy and determine its ability to act against Mycobacterium tuberculosis. The identified lead compound from this study contribute to ongoing drug discovery efforts against Tuberculosis.

References

1. Hanwarinroj C, Phusi N, Kamsri B, Kamsri P, Punkvang A, Ketrat S, et al. Discovery of novel and potent InhA inhibitors by an in silico screening and pharmacokinetic prediction. Future Med Chem. 2022;14(10):717–29.
2. Newton SM, Lau C, Gurcha SS, Besra GS, Wright CW. The evaluation of forty-three plant species for in vitro antimycobacterial activities; isolation of active constituents from Psoralea corylifolia and Sanguinaria canadensis. J Ethnopharmacol. 2002;79(1):57–67.
3. Liao J, Wang Q, Wu F, Huang Z. In silico methods for identification of potential active sites of therapeutic targets. Molecules. 2022;27(20):7103.
4. Sukumar S, Krishnan A, Khan MKA. Protein kinases as antituberculosis targets: the case of thymidylate kinases. Front Biosci. 2020;25(9):1636–54.
5. Prasad MS, Bhole RP, Khedekar PB, Chikhale R V. Mycobacterium enoyl acyl carrier protein reductase (InhA): A key target for antitubercular drug discovery. Bioorg Chem. 2021;115:105242.
6. Ho QTV. Bringing mycobacterial secretion inhibitors to maturation. 2023;
7. Kumar A, AlGhamdi KM, Khan AA, Ahamad R, Ghadeer A, Bari A. Psoralea corylifolia (babchi) seeds enhance proliferation of normal human cultured melanocytes: GC--MS profiling and biological investigation. Open Chem. 2023;21(1):20220292.
8. Kumar SR, Chozhan K, Murugesh KA, Rajeswari R, Kumaran K. Gas chromatography-Mass spectrometry analysis of bioactive compounds in chloroform extract of Psoralea corylifolia L. J Appl Nat Sci. 2021;13(4):1225–30.
9. Daina A, Michielin O, Zoete V. SwissADME: a free web tool to evaluate pharmacokinetics, drug-likeness and medicinal chemistry friendliness of small molecules. Sci Rep. 2017;7(1):42717.
10. Angamuthu P, Sharon A, Arunkumar R, HARISHA B, Arvind T, Alluru M, et al. SCREENING OF NOVEL AMINOPYRIMIDINE DERIVATIVES AGAINST HUMAN CDK-8 ENZYME: AN INSILICO APPROACH. Int J Res Pharm Chem Anal. 2023;2(1).
11. Xiong G, Wu Z, Yi J, Fu L, Yang Z, Hsieh C, et al. ADMETlab 2.0: an integrated online platform for accurate and comprehensive predictions of ADMET properties. Nucleic Acids Res. 2021;49(W1):W5--W14.
12. Askerova UF. PREDICTION OF ACUTE TOXICITY FOR (Z)-3-(2-PHENYLHYDRAZINYLIDENE) BENZOFURAN-2 (3H)-ONE AND ITS DERIVATIVES FOR RATS USING GUSAR PROGRAM.
13. Ramireddy VSR, Kurakula R, Chellam PV, James A, van Hullebusch ED. Systematic computational toxicity analysis of the ozonolytic degraded compounds of azo dyes: Quantitative structure-activity relationship (QSAR) and adverse outcome pathway (AOP) based approach. Environ Res. 2023;231:116142.
14. Baskaran KP, Arumugam A, Kandasamy R, Alagarsamy S. In silico method for prediction of maximum binding affinity and ligand-protein interaction studies on Alzheimer's disease. Int J Res Granthaalayah. 2020;8:362–70.
15. Dhorajiwala TM, Halder ST, Samant L. Comparative in silico molecular docking analysis of l-threonine-3-dehydrogenase, a protein target against African trypanosomiasis using selected phytochemicals. J Appl Biotechnol Reports. 2019;6(3):101–8.
16. Saman S, Chen C-C, Malak N, Khan A, Nasreen N, Khan A, et al. Ethanolic Ex-

tracts of Datura innoxia Have Promising Acaricidal Activity against Rhipicephalus microplus as It Blocks the Glutathione S-Transferase Activity of the Target Tick. Genes (Basel). 2022;14(1):118.

17. Ghosh M, Akhter N, Zobayer N. An in silico based approach towards the characterization with feature identification and analogy modeling of human osteoclast protein. Int J Pept Res Ther. 2021;27(3):2111–24.

18. Che X, Liu Q, Zhang L. An accurate and universal protein-small molecule batch docking solution using Autodock Vina. Results Eng. 2023;19:101335.

19. Das SK, Mahanta S, Tanti B, Tag H, Hui PK. Identification of phytocompounds from Houttuynia cordata Thunb. as potential inhibitors for SARS-CoV-2 replication proteins through GC--MS/LC--MS characterization, molecular docking and molecular dynamics simulation. Mol Divers. 2022;26(1):365–88.

20. Sravika N, Priya S, Divya N, Jyotsna PMS, Anusha P, Kudumula N, et al. Swiss ADME properties screening of the phytochemical compounds present in Bauhinia acuminata. J Pharmacogn Phytochem. 2021;10(4):411–9.

21. Pinlac RKL, Comia LET, Epino GNT, Fernandez RM, Madrid HS, Salvacion ASR, et al. Benchmarking the physicochemical properties of 500 compounds for absorption, distribution, metabolic, excretion, and toxicity (ADMET) property prediction in Caenorhabditis elegans. Anim Biol Anim Husb. 2021;13(2).

22. Knoll KE, van der Walt MM, Loots DT. In silico drug discovery strategies identified ADMET properties of decoquinate RMB041 and its potential drug targets against Mycobacterium tuberculosis. Microbiol Spectr. 2022;10(2):e02315--21.

23. Khamouli S, Belaidi S, Lanez T. Molecular doking and ADMET studies of amino-pyrimidine derivaties as mycobacterium tuberculosis Ser/Thr protein kinases B inhibitors. J Fundam Appl Sci. 2019;11(2):914–39.

24. Aguinaldo RMG, Castillo SMJ, Emlan JK, Gomez ACG, Crisostomo ABC, de Grano RVR. In silico evaluation of caffeic acid from coconut (Cocos nucifera L.) husks as a potential inhibitor of the human factor Xa. J Pharmacogn Phytochem. 2022;11(3):1–6.

25. SUTHAR S, PAL D, NASKAR A, LANJHIYANA SK, JAIN SK. DESIGN OF ETHANOLIC BIOISOSTERES OF MIGLITOL AS NOVEL ALPHA-GLUCOSIDASE ENZYME INHIBITOR FOR DIABETES MELLITUS.

26. Vawhal PK, Jadhav SB, Kaushik S, Panigrahi KC, Nayak C, Urmee H, et al. Coumarin-Based Sulfonamide Derivatives as Potential DPP-IV Inhibitors: Pre-ADME Analysis, Toxicity Profile, Computational Analysis, and In Vitro Enzyme Assay. Molecules. 2023;28(3):1004.

27. Halder ST, Dhorajiwala TM, Samant LR. Multiple docking analysis and In silico absorption, distribution, metabolism, excretion, and toxicity screening of anti-leprosy phytochemicals and dapsone against dihydropteroate synthase of Mycobacterium leprae. Int J Mycobacteriology. 2019;8(3):229–36.

28. Castro ALG, Cruz JN, Sodré DF, Correa-Barbosa J, Azonsivo R, de Oliveira MS, et al. Evaluation of the genotoxicity and mutagenicity of isoeleutherin and eleutherin isolated from Eleutherine plicata herb. using bioassays and in silico approaches. Arab J Chem. 2021;14(4):103084.

29. Roy S, Maheshwari N, Chauhan R, Sen NK, Sharma A. Structure prediction and functional characterization of secondary metabolite proteins of Ocimum. Bioinformation. 2011;6(8):315.

30. Hamid M, Batool J, Qaisar A, Paracha RZ, others. Identification and Computational Analysis of 3D-Structure Of MOCS1. 2021;

31. Butt SS, Badshah Y, Shabbir M, Rafiq M. Molecular Docking Using Chimera and Autodock Vina Software for Nonbioinformaticians. JMIR Bioinforma Biotechnol. 2020;1(1):e14232.

32. Wlodarchak N, Teachout N, Beczkiewicz J, Procknow R, Schaenzer AJ, Satyshur K, et al. In silico screen and structural analysis identifies bacterial kinase inhibitors which act with $β$-lactams to inhibit mycobacterial growth. Mol Pharm. 2018;15(11):5410–26.

33. Magar VK, Sonawane L, Patwekar S. Molecular Docking Study Of Few Novels Pyrimidine Derivatives On Validated Target Enoyl Acyl Coa Reductase. Lat Am J Pharm. 2023;42(3):777–91.

34. Alzain AA, Makki AA, Ibraheem W. Insights into the Inhibition of Mycolic Acid Synthesis by Cytosporone E Derivatives for Tuberculosis Treatment Via an In Silico Multi-Target Approach. Chem Africa. 2023;1–21.

Current Trends in Biotechnology and Pharmacy
Vol. 18(3) 1951-1961, July 2024, ISSN 0973-8916 (Print), 2230-7303 (Online)
10.5530/ctbp.2024.3.40

The Role of trnH-pbsA Spacer Gene in *Eucalyptus* Species Identification and its Importance in Phylogenetics

G. Jayaraj

Centre For Research and Dept. of Botany and Biotechnology,
Andhra Loyola College (Autonomous), Vijayawada 520 008, Andhra Pradesh.
*Corresponding author: jgorantla3@gmail.com

Abstract

Our present study is made to use **t**he trnH-psbA spacer gene data to resolve some phylogenetic relationships among the *Eucalyptu*s speices. The species included are *E. moorei, E.affn. moorei, E. dives, E. mitchelliana, E. pauciflora* and E. *stellulata.* There were successful amplifications of DNA for the seven *Eucalyptus* species using gene trnH-psbA. The trnH-psbA spacer is the short with 476 bps. It is to be complimented with rbcL, MatK and trnH-psbA gene study. The trnH-psbA spacer is showing 21 SNPs out of 476 bps segment. The mean length is 733 bps long. Amplification success rate is almost 100%. For each species there are multiple good quality sequences available for the sequence alignment. The trnH-psbA spacer has discriminated 5 species clearly from the rest and the other 3 species are also separated from each other though the distance between them is not significantly noticeable.

Key words: trnH-psbA spacer, SNPs, variable gene, phylogenetics, complementary

Introduction

In the past few decades, the Genomic research has undergone tremendous changes. There have been several newer technical advances created to help the structural and functional aspects of genes, chromosomes and sometimes the entire genome. e.g. the sequencing of the entire Human genome, of *Arabidopsis, Rice, o*r *Popular* genomes. There are several other researches are taking place recently. It includes the *Eucalyptus* that has the sequencing of the entire genome. It has a wider application. Genetic information can help us with a good resolution of species boundaries. This will eventually may give insights into the patterns and rates of evolutionary diversification among species.

In DNA Barcoding we use a short selection DNA (portion of a gene) in order to identify a species. This is called DNA barcoding. The DNA barcoding is a newer system created to provide accurate and automatable species identifications by using short and variable standardized gene regions as species tags or species identity. This has initiated a new method/ technique and eventually led to the formation of Consortium for the Barcode of Life (5). Our objective of this project is to obtain DNA barcodes from all species of *Eucalyptus* for all over the world, from different geographical and climatic regions. Our challenge is also to find out a very suitable region which shows enough variation within it to discriminate among species yet conserved enough to be present.

A critique of barcoding

The advocates of DNA barcoding say that this technology would revitalize biological collections and speed up species identification and inventories. There are only 1.7 million specimens that have been identified by taxonomists

and about 10-20 million more which have not been named or explained.

The opponents of barcoding argue that this technology would destroy the traditional systematics and turn it into a service industry (6). These fears are allayed and in all cases DNA barcoding are applied only in conjunction with classical approach where species are simply unknown or no attempts have been made to delimit them. Therefore, barcoding as originally intended would be limited in its applicability. The DNA barcoding address by matching DNA sequences to 'known' species. As in the words of CBOL "barcoding is neither a substitution for alpha taxonomy nor about interfering phylogenies (20). Apart from being a diagnostic tool, barcode sequences per se and their ever-increasing taxonomic coverage could become an unprecedented resource for taxonomy and systematic studies. In future in plants multiple markers is likely to be a necessity and it is already being explored (5). It is possible some taxa can be established from the sequence variation alone and re-identified unequivocally while awaiting morphological analysis and formal description, i.e. the 'reverse taxonomy'. Using DNA barcoding the present research is carried out in order to find out the phylogenetic relationship of 6 closely related and 2 distantly related eucalypts.

It has been reported that the Chloroplasts are maternally inherited in most Angiosperms and for the eucalypts too this has been demonstrated by Byrne et al., (1993) (1). in *E. nitens* of eastern Australia. Schael et al., (1999) (19). showed a uniparental inheritance of the chloroplast genome and lack of recombination. The variations in the chloroplast genome are ordered accordingly. Since the Chloroplast genome is non- recombining, asexually inherited and evolves slowly, these characters are useful for the estimation of the extension of gene flow between species. Many studies in recent years have been focused on the chloroplast DNA variations in eucalypts because of their economic and ecological significance apart from other important genomic studies. Eucalypts have dominated different land scape of Australia over the thousands of centuries.

***trnH-PsbA* gene and barcoding:**

Kress et al., (2005) (5). Shaw et al., (2005) (20). and other researchers showed that trnH-psbA region is one of the most valuable non-coding regions of plastid genome. It has been shown that this region with highest variable sites makes it a good candidate for the species discrimination. However, there are problems to align the sequences because of high rates of insertions/deletions. Kress et al., (2006) (12). found that *trnH-psbA* spacer is very short (less than 300 bp). The alignment of *trnH-psbA* spacer across bigger families of angiosperms remains highly ambiguous. There exists also great length deference. In contrast with the indels problem for phylogenetic construction, Kress et al., (2005) (5), think that indels would ultimately enhance the information needed for species identification. The highest divergence is provided by trnH-psbA spacer from the studies.

Materials and Methods

Finding the suitable regions of the genome

In the present study we are taking into consideration multi locus region *trnH-psbA* of the genome for the barcoding of *8 Eucalypt* species. The psbA-trnH intergenic spacer is one of the most variable non-coding regions of the plastid genome in Angiosperms. It has highest percentage of variable sites (20). In some group of plants, it is relatively short, having less than 300 bps (12). The The chloroplast gene rbcL encodes the large subunit of ribulose bisphosphate carboxylase in plants.

The taxa selection for barcoding

The taxa selected for the study includes *E. moorei, E.affn. moorei, E. dives, E. mitchelliana, E. pauciflora* and E. *stellulata* . These are considered to be a highly evolved group in eucalypts. Their mallee form is said to be of recent origin on the evolutionary scale of eucalypts and it is an adaptation to the poor soil and dry

climatic conditions (Ian Brooker personal communication). The other two species (in the present study) included as a close out- group are *E. globulus* and *E. nitens* and they evolved much before the mallee forms. Of the seven species in this study, *E. moorei*, *E. affn. moorei*, *E. dives*, and *E. pauciflora* came from one population each of Nerega region of New South Wales. The *E. mitchelliana* specimens were collected from one plantation of South Australia. *E. stellulata* collections came from one population of Black Mountain of Canberra, ACT. The *E. globulus* and *E. nitens* collections came from Central Victoria- one population each respectively. There were 30 specimens collected for each of the eight species for DNA barcoding from each population. After extracting the DNA from each specimen, the DNA is pooled for a each one.

DNA extraction

About 5-7g of leaves were cut, avoiding the thicker part of the midrib and petiole and any large dead regions. They were immersed in liquid nitrogen. Immediately after liquid N2 evaporates, grind 30-40 seconds in coffee grinder. The powder was resuspended in 40 ml of extraction buffer (recipe below) in small plastic beaker. Polytron (homogenize) for 20-30 seconds at 3/4 speed. This procedure is followed using a standard protocol.

Preparation of eucalypt extraction buffer

For 1 L buffer preparation 100 mM Tris, 100 mM Tris 12.1 g, 25 mM EDTA 50 ml, 0.35 M Sorbitol 64 g, 100 mM Boric acid 6.2 g 1 M

Preparation of eucalypt extraction buffer

For 1 L buffer preparation 100 mM Tris, 100 mM Tris 12.1 g, 25 mM EDTA 50 ml, 0.35 M Sorbitol 64 g, 100 mM Boric acid 6.2 g 1 M NaCl. 58.4 g were weighed and taken in a 2 L beaker. The pH to 8.0 was added before 2% PVP 40,000 20 g was added. Then the following chemicals 10% PEG 8000 100 g, 0.5% BSA 5 g, 0.1 % spermine 1 g, 0.1% spermidine 1 g were added. We prepared the wash buffer with the following chemicals for 1 L. 50 mM Tris50 ml (of 1M, pH8.0), 25 mM EDTA 50 ml (of 0.5 M EDTA, pH 8.0), 0.35 M Sorbitol 64 g. Sodium metabisulphite was added to extraction buffers and wash buffer to 10 mM just prior to use (about 0.2 g per 100 ml – or 10ml per liter of a 1M soln, = 95g/L). PVP 40,000 20 g was added. Then the following chemicals 10% PEG 8000 100 g, 0.5% BSA 5 g, 0.1 % spermine 1 g, 0.1% spermidine 1 g were added.

Primers The universal primers are selected for the genes matK, rbcL, and intergeneric spacers- ITS and trnH-psbA (11). After extracting the DNA individually from all the specimens of each species, the DNA for 30 specimens is pooled together for each is species. The DNA quality is checked using standard protocol before the PCR amplifications are done.

Table 1. Primer sequences used in this study (listed 5'- to -3' end)

psbA- trnH	GTTATGCATGAACGTAATGCTC (1) CGCGCATGGTGGATTCACAATCC (2)

PCR amplification

The non-coding as well as coding regions of matK*, trnH-psbA, ITS and rbcL were* amplified and sequenced by following the protocol usnign the universal. primer pairs (Table 3.1) with TaqF2 (Fisher Biotech, Australia) polymerase.

All PCR amplifications were performed in 20 µl reaction with specific primers annealing temperature. The PCR reactions were consisted of 2 µl of 10xbuffer, 1 µl of 10mM dNTP, 1.6 µl of 25 mM $MgCl_2$, 0.5 µl of each primer (20µM), 1µl pooled genomic DNA (~45ng/µl), 12.9 µl distilled water and 0.5 µl Taq F2 DNA polymerase (5 units/µl; Fisher Biotech, Australia). The amplifications were performed on an ABI thermal cycler (GeneAmp^R PCR System 2700) with initial denaturing at 94°C for 1 min, 35 cycles of 94°C 30 s, primers specific annealing temperature for 30 s and 2-3 min at 72°C followed by a 10 min extension at 72°C.

EgrNAM1 genomic sequences were amplified from randomly selected sixteen trees and both parents DNA using PfuTurbo DNA polymerase (Strata gene, USA). The 100 µl PCR reactions were performed in 10 µl of 10xPCR buffer, 1 µl of 25mM each dNTPs, 2.5 µl of 20 µM each primer mix, 2 µl of 100 ng/µl DNA template, 2 µl of 2.5 U/µl PfuTurbo DNA polymerase (Strata gene, USA) and 80 µl of distilled water. DNA was amplified using the same thermal cycler following same amplification program as used in above mentioned genes with initial denaturing at 95˚C instead of 94˚C. All PCR products were confirmed by gel electrophoresis using a 1% agarose gel and purified by QIAGEN gel extraction kit (Hilden, Germany). Purified PCR product was then quantified by gel electrophoresis comparing with a 100bp gene ladder (Fermentas, Australia).

Cloning of PCR products

All purified DNA amplicons were ligated into the pGEM-T Easy vector using the pGEM-T Easy vector kits (Promega, USA). Ten microliters ligation mixtures contained 5 µl of 2xRapid Ligation Buffer, 1µl of pGEM-Teasy vector (50ng), 3 µl PCR products (25-30ng/µl), 1µl of T4 DNA Ligase (3U/µl) and 1 µl distilled water. A positive control was included for checking transformation and ligation efficiency, and used control insert DNA instead of PCR product as template. A no template negative control was also included. Two microliters of each ligation reaction were transformed into bacterial cells (JM109 and DH5α) by heat-shocking for 50 second at 42˚C water bath, and plated out in LB/ampicillin/IPTG/X-Gal medium, and then incubated at 37˚C for overnight. Twenty-four white colonies were picked and cultured in 5 ml LB/ampicillin medium for overnight at 37˚C and plasmid DNA isolated using the QIAprep Spin Miniprep kit (Hilden, Germany). In the case of *EgrNAM1*, DNA from 18 trees were ligated, transformed and plated out separately following the procedure described above. A single positive colony was picked from each individual and cultured for plasmid DNA preparation. The sizes of all inserts were verified by digestion with *Not*I followed by gel electrophoresis. Each 10 µl digestion reaction was consisted of 1 µl of buffer D, 0.1 µl of BSA, 1 µl of plasmid DNA, 0.20 µl of *Not*I (Invitrogen, USA) and 7.70 µl of distilled water and was incubated at 37˚C in a water bath for 2-3 hours.

Sequencing

Twenty-four different amplicons of each fragment of *EgrHB1*and EgrPAAPA*,* and 18 amplicons of each fragment of *EgrNAM1* were sequenced in both directions using pGEM-Teasy vector Forward (5’ GTAAAACGACGGCCAGT 3’) and Reverse (5’ CAGGAAACAGCTATGAC 3’) primers. Further sequences of large gene fragments were obtained using internal primers. Sequencing was carried out using Big Dye Terminator version 3.1 reagents and an ABI PRISM sequence analyzer using 1/8 reaction volume. Plasmid DNA (0.8 µl) was added to 14.2 µl of distilled water, 1µl of Big Dye version 3.1 mix, 3.5 µl of 5x sequencing buffer and 0.5 µl of each primer (10µM). Cycle sequencing used an initial step at 94˚C for 5 min, then 30 cycles of denaturation at 96˚C for 10 s, annealing at 50˚C for 5 s, and extension at 60˚C for 4 min. The products were precipitated using ethanol, dried down under vacuum and sent to the John Curtin School of Medical Research (JCMSR) for gel separation.

Sequences analysis

Sequences were verified manually and contigs were assembled using the computer software program MEGA version 3.1 (Kumar et al., 2004). Multiple sequence alignments were made using the same program and adjusted manually. All chromatograms and SNPs were visually checked using Sequencer 4.6 (Gene Codes, Corporation, Ann Arbor. Michigan, USA) to exclude any sequencing errors. Philip analysis is done using the Philip version. Reference.

Results and Discussion

There were successful amplifications of DNA for the eight eucalypt species using 4 DNA barcode, trnH-psbA.. The trnH-psbA spacer is the short with 476 bps. The mean length is 733 bps long. Amplification success rate is almost 100%. For each species in each gene there are multiple good quality sequences available for the sequence alignment. They varied 4- 10 good quality sequences for each species in each gene. Looking at the Single Nucleotide Polymorphic (SNPs) sites, the trnH-psbA spacer showing 21 SNPs out of 476 bps segment. The trnH-psbA spacer has 4.41% variability and the rbcL showing only 1.57% variability.

gor1700505glo		A	A	C	C	G	T	T	
'gor170_0515mit'		T	A	G	T	G	C	T	
'gor170_0526nit'		A	A	C	T	A	T	T	
'gor170_0534ste'		A	A	G	T	G	C	T	
'gor170_0695Amo'		A	A	G	T	G	C	T	
'gor170_0706moo'		A	A	G	T	G	C	T	
'gor170_0719pau'		A	A	G	T	G	C	C	
'gor170_0731div'		A	C	G	T	G	C	T	

Figure 2: Variable sites

trnH-psbA spacer shows higher divergence (up to 0.29) The intraspecific divergence values are found to be very negligible (up to 0.008). In the present the study two of the trnH-psbA is able to meet the barcode criteria well by showing greater interspecific variability.

Discussion

Until now there are a few successful findings to give us most suitable DNA barcodes for land plants. These studies helped to focus on the generic level discrimination using barcodes or above this level. One of the prime objectives of this investigation was to compare the cpDNA region of *E. moorei* complex (*E. moorei* and *E. affn. moorei*). The study also included very closely related taxa such as *E. dives, E. stellulata, E. pauciflora* and *E. mitchelliana*. There is a question of the true (disputed) identity of *E. affn. moorei* coming from a disjunct population with diagnostically different morphological features from that of *E. moorei*. The following genes have provided very useful information for the phylogenetic study of eight taxa of eucalypts.

trnH-psbA

It is relatively shorter and the average length is 476 bp. It is the second most variable segment in the present study. The amplification and sequencing are easily done. There are alignment problems because of large number of indels. For example, E. *globulus* sequences contain 28 indels in the short fragment length of 476.

Table 2: Barcode genes' sequence analysis and SNPs comparisons

Gene	No. Bases	No. SNPs	No. of Taxa useful SNPs	% SNPs
trnH-psbA	476	21	7	4.41

gor1700505glo	A	A	C	C	G	T	T	-	-	A	A	A	C	C	G	G	T	T	T	T	T
'gor170_0505glo'	A	A	C	C	G	T	T	-	-	A	A	A	C	C	G	G	T	T	T	T	T
'gor170_0507glo'	A	A	C	C	G	T	T	-	-	A	A	A	A	T	G	G	T	T	T	T	T
'gor170_0509glo'	A	A	C	C	G	T	T	-	-	A	A	A	A	T	G	G	T	T	T	T	T
'gor170_0515mit'	T	A	G	T	G	C	T	T	A	A	A	A	A	T	A	A	T	T	T	T	A
'gor170_0517mit'	T	A	G	T	G	C	T	T	A	A	A	A	A	T	G	G	T	T	T	T	G
'gor170_0518mit'	T	A	G	T	G	C	T	T	A	A	A	A	A	T	G	G	T	T	T	T	G
'gor170_0521mit'	T	A	G	T	G	C	T	T	A	A	A	A	A	T	G	G	T	T	T	T	G
'gor170_0526nit'	A	A	C	T	A	T	T	T	A	A	A	A	A	T	A	G	C	T	T	T	T
'gor170_0528nit'	A	A	C	T	A	T	T	T	A	G	A	A	A	T	G	G	T	T	T	T	T
'gor170_0529nit'	A	A	C	T	A	T	T	T	A	A	A	A	A	T	A	G	T	T	T	T	T

‘gor170_0530nit’	A	A	C	T	A	T	T	T	A	A	A	A	A	T	G	G	T	T	T	T	T
‘gor170_0532nit’	A	A	C	T	A	T	T	T	A	A	A	A	A	T	A	G	T	T	T	A	T
‘gor170_0534ste’	A	A	G	T	G	C	T	T	A	A	A	A	A	T	G	G	T	T	T	T	G
‘gor170_0535ste’	A	A	G	T	G	C	T	T	A	A	A	A	A	T	A	G	T	T	T	T	A
‘gor170_0536ste’	A	A	G	T	G	C	T	T	A	A	A	A	A	T	G	G	T	T	T	T	G
‘gor170_0538ste’	A	A	G	T	G	C	T	T	A	A	A	A	A	T	G	G	T	T	T	T	G
‘gor170_0541ste’	A	A	G	T	G	C	T	T	A	A	A	A	A	T	A	G	T	T	T	T	A
‘gor170_0542ste’	A	A	G	T	G	C	T	T	A	A	A	A	A	T	A	G	T	T	T	T	G
‘gor170_0695Amo’	A	A	G	T	G	C	T	T	A	A	A	A	A	T	G	G	T	T	T	T	G
‘gor170_0696Amo’	A	A	G	T	G	C	T	T	A	A	A	A	A	T	G	G	T	T	T	T	G
‘gor170_0698Amo’	A	A	G	T	G	C	T	T	A	A	A	A	A	T	G	G	T	C	T	T	G
‘gor170_0700Amo’	A	A	G	T	G	C	T	T	A	A	A	A	A	T	G	G	T	T	T	T	G
‘gor170_0702Amo’	A	A	G	T	G	C	T	T	A	A	A	A	A	T	G	G	T	T	T	T	G
‘gor170_0703Amo’	A	A	G	T	G	C	T	T	A	A	A	A	A	T	G	G	T	T	T	T	G
‘gor170_0706moo’	A	A	G	T	G	C	T	T	A	A	A	A	A	T	G	G	T	T	T	T	G
‘gor170_0708moo’	A	A	G	T	G	C	T	T	A	A	A	A	A	T	G	G	T	T	T	T	G
‘gor170_0710moo’	A	A	G	T	G	C	T	T	A	A	G	A	A	T	G	G	T	T	T	T	G
‘gor170_0712moo’	A	A	G	T	G	C	T	T	A	A	A	A	A	T	G	G	T	T	T	T	G
‘gor170_0714moo’	A	A	G	T	G	C	T	T	G	A	A	A	A	T	G	G	T	T	T	T	G
‘gor170_0716moo’	A	A	G	T	G	C	T	T	A	A	G	A	A	T	G	G	T	T	T	T	G
‘gor170_0719pau’	A	A	G	T	G	C	C	G	A	A	A	A	A	T	G	G	T	T	T	T	G
‘gor170_0720pau’	A	A	G	T	G	C	C	G	A	A	A	A	A	T	A	G	T	T	T	T	A
‘gor170_0722pau’	A	A	G	T	G	C	C	G	A	A	A	A	A	T	A	G	T	T	T	T	A
‘gor170_0724pau’	A	A	G	T	G	C	C	G	A	A	A	A	A	T	G	G	T	T	G	T	G
‘gor170_0725pau’	A	A	G	T	G	C	C	G	A	A	A	A	A	T	G	G	T	T	T	T	G
‘gor170_0727pau’	A	A	G	T	G	C	C	G	A	A	A	A	A	T	G	G	T	T	T	T	G
‘gor170_0731div’	A	C	G	T	G	C	T	T	A	A	A	C	A	T	G	G	T	T	T	T	G
‘gor170_0732div’	A	C	G	T	G	C	T	T	A	A	A	C	A	T	G	G	T	T	T	T	G
‘gor170_0733div’	A	C	G	T	G	C	T	T	A	A	A	C	A	T	G	G	T	T	T	T	G
‘gor170_0734div’	A	C	G	T	G	C	T	T	A	A	A	C	A	T	G	G	T	T	T	T	G
‘gor170_0737div’	A	C	G	T	G	C	T	G	A	A	A	A	A	T	G	G	T	T	T	T	G
‘gor170_0739div’	A	C	G	T	G	C	T	T	A	A	A	C	A	T	G	G	T	T	T	T	G

Figure 1: trnH-PsbA spacer sequences

The others have 7-9 indels. The taxonomically useful SNPs have clearly discriminated 5 species, namely, *E. dives, E. globulus, E. mitchelliana, E. nitens* and *E. pauciflora.* The *E. stellulata* has shown 5 single nucleotide substitutions and indicating that 50% chances of recognizing a separate species based on the molecular data. There are also 3 single nucleotide substitutions in the case of *E. moorei* that are different from the *E. affn. moorei*. The 62.5% success rate of interspecific variations using this barcode makes it a good candidate as ear-

lier reported (11) that can be recommended as one of the most useful non-coding regions for cp DNA barcode studies.

Table. 4 Sequence length and percent intra-specific sequence divergence for four plastid regions of 8 eucalypts

Species	Gene
	trnH-psbA length(bp) %divergence
E. affin. *moorei*	447/1 0.002
E. moorei	447/2 0.004
E. dives	447/2 0.004
E. globulus	447/2 0.004
E. mitchelliana	447/0 0.000
E. nitens	447/2 0.004
E. pauciflora	447//0 0.000
E. stellulata	447/2 0.004

We can explain the lack of clear discrimination between *E. moorei and E. affn. moorei* and *E. stellulata* because of strong chloroplast sharing among the closely related eucalypts. As it is reported earlier that hybridization or introgressions are very common among the species of the same subgenus in eucalypts which come from the same geographical regions.

Implications of the present study and future prospects

The present research findings highlight the importance of matK (coding region) and trnH-psbA to a great. Two of them are better suited for low-level taxonomic investigations than other coding and non-coding barcodes so far reported. The matK which has been recommended as an important barcoding gene recently (15). Kress, 2007 (13) proved again its great resolving power at interspecific discrimination. The trnH-psbA is also found to be easily amplifiable with the universal primers and has shown good number of variable sites in the sequence analysis. In spite of large number of indels, this gene has yielded relatively significant PIC values. The trnH-psbA spacers discriminated 5 species clearly from the rest and the other 3 species are also separated from each other though the distance between them is not significantly noticeable.

This present work has focused on a small group consisting of five blue ashes, one Peppermint and two symohyomyrts (eight closely related) Eucalyptus taxa. These are said to be one of the most rapidly evolving group of individuals in the genus *Eucalyptus.*

There are many reports of interspecific hybridizations and introgressions. It is not always easy to distinguish the hybrids because the hybrids share the maternal plastid DNA. Therefore, the choice of this study actually enters into a problem-group area in a sense this might be a good start with a problem group and apply the DNA barcodes for the 8 closely related taxa is challenging. Sometimes we also know the fact that discrimination of some taxa might be lost with greater taxonomic and geographic sampling. This gives us a grasp of things on a minor scale before launching a large-scale study.

Conclusion

In the Phylip tree construction based on Nucleic Acid sequence Maximum likelihood method has given us comparative confidence limits of interspecific divergence of eight closely related Eucalyptus species. Among the eight taxa, there are five species with significant confidence levels. They are as following. *E. dives*

Figure 3: trnH-PsbA - Phylogenetic tree (UPGMA)

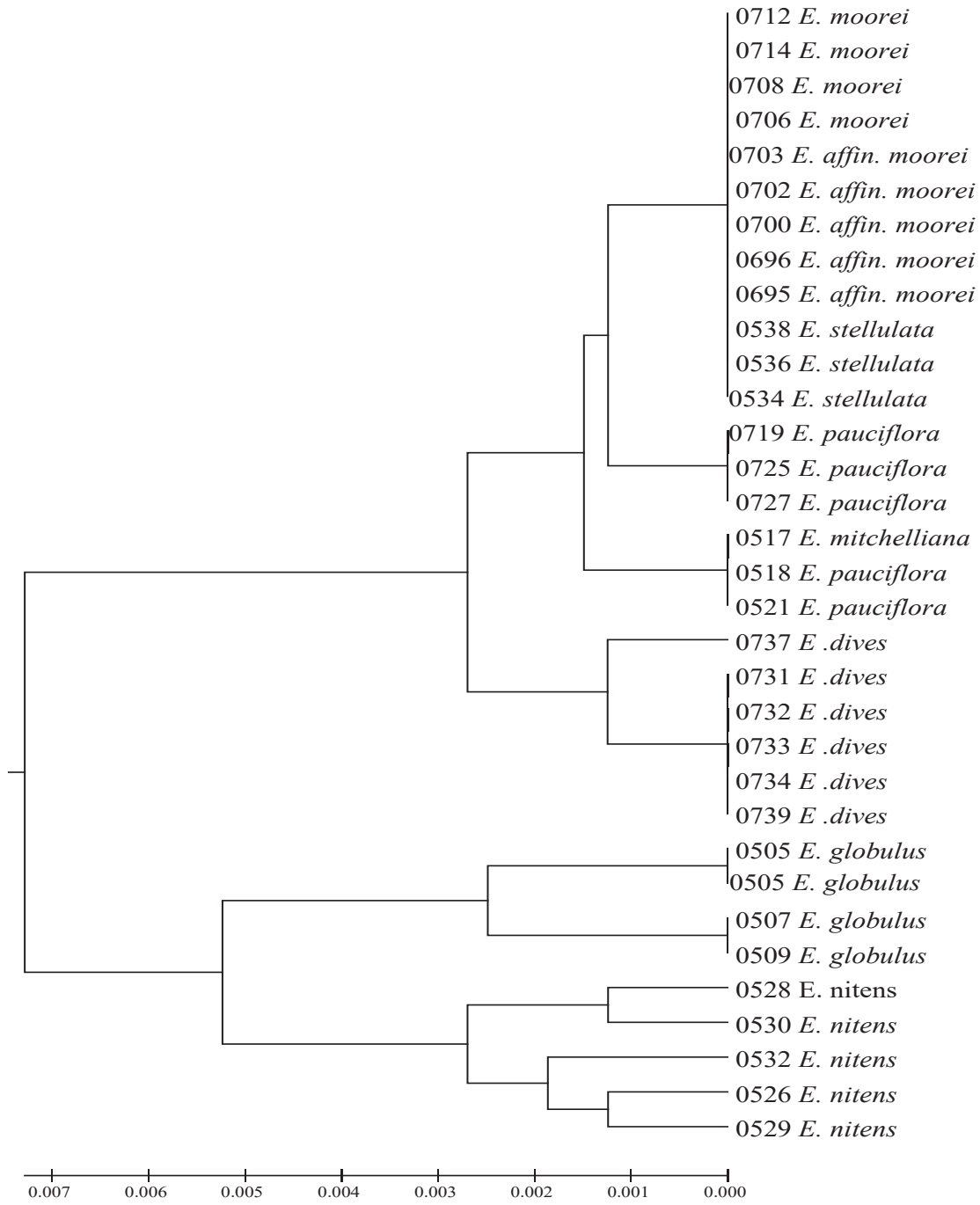

Figure 3: trnH-PsbA - Phylogenetic tree (UPGMA)

0.17 confidence, *E. pauciflora* 0.18 confidence, *E. mitchelliana* 0.37 confidence, *E. globulus* 010 confidence, and *E. nitens* 0.24 confidence. These levels of confidence are positively significant. In other three cases of *E. stellulata*, *E. moorei* and *E. affn. moorei* the confidence limits are insignificant.

Table 4: DNA sequence homology of trnH-PsbA gene (%)

Gene	Species	*E.dives*	*E.globulus*	*E.mitchelliana*	*E.Affin.moorei*	*E.moorei*	*E.nitens*	*E.pauciflora*	*E.stellulata*
	E. dives	**1**							
	E. globulus	**0.99**	**1**						
	E. mitchelliana	**0.99**	**0.98**	**1**					
trnH-psbA	***E. affin. moorei***	**0.99**	**0.98**	**0.99**	**1**				
	E. moorei	**0.99**	**0.98**	**0.99**	**0.99**	**1**			
	E. nitens	**0.98**	**0.98**	**0.98**	**0.98**	**0.98**	**1**		
	E. pauciflora	**0.98**	**0.99**	**0.98**	**0.99**	**0.99**	**0.97**	**1**	
	E. stellulata	**0.99**	**0.99**	**0.99**	**0.99**	**0.98**	**0.98**		**1**

These form a one taxonomic complex. We can also call this an aggregated species based on molecular data. But the taxonomic identity of *E. steullulata* is well defined based on morphological characters. There is an ambiguity about the identity of the disputed E. *aft. moorei*. Our present study using 4 different cp DNA and nrDNA-ITS barcodes have not resolved the issue fully although it has indicated us some haplotypes of *E. moorei*/ *E. affn*. *moorei*. It is recommended (Ian Brooker personal communication, 2008) to make a collection from a population of Blackheath, New South Wales, for this species complex in order to do a comparative study based on morphological characters as well as molecular data. This might either clarify or brings out useful information for identifying *E. affn. moorei* as a different species or consider it still part *E. moorei* species complex. We can also use some low-copy nuclear genes to resolve the identity and position of *E. affn . moorei*.

There are many success stories so far reported using either a single cp DNA barcode or in combination two or three in different individual groups of land plants. But there is no consensus as yet if an individual or a multilogues barcodes that would work very well in plants belonging to different families coming from various geographical locations of the planet. Some taxonomist's view (Chase et al 2003) (9). that DNA barcodes based on uniparentally inherited markers can never reflect the complexity that exists in nature.

There are ambiguities created as far as species limits are concerned by barcodes in some cases. Therefore, some taxonomists have a suspicion or skepticism of barcodes. They are critical of this work. For most taxonomists it is important to have a reasonable barcode based on multiple low copy nuclear DNA loci, a multi-locus barcode system (MBC). This would mean look-

ing for identification of conserved flanking regions containing variable sites. These sites may be introns of appropriate size. These conserved sites would serve as universal PCR priming locations. The reasons for MBC are because of detection of hybridization/ introgression cannot be reliably done by examining a single cp DNA region.

The starting presupposition was to identify all the 8 species of this group using 4 cp DNA barcodes coding and non-coding and expected them to be taxonomically discriminated based on molecular data. The findings are not far from the objectives. Though there is no 100% perfection of the results, these have clarified and illumined the understanding that matK gene and trnH-psbA spacer are better suited for low-level molecular phylogenetic studies in eucalypts. Therefore, it is not a question of mathematical precision of usefulness of data but the value and the significance of the information it has provided us in order to enhance the ongoing search for the most suited barcode regions for plant identification in a wider concern for recording and preserving the biodiversity on our planet .The regions included for this kind of study are trnH-psbA spacer, there are many other non-coding regions of cpDNA investigated but they are not recorded or not explored yet. Because of these reasons we have little information about relative rate of evolution among different non-coding regions. Each research group designed its own experiments to test different barcodes on different group of plants. Some of the works are on a large scale. However, there is no consensus as yet. Apart from various recommendations, some of the latest such as Lahaye et al (2007) (15). which correctly classified 90% of the species by using matK and trnH-psbA (either alone or in combination)? The final agreements seem to be in the direction of using multiple regions than one. The latest CBOL' conference in Taipei proposal is for using matK, trnH-psbA and atpF-H. The present findings are in the direction of above research work.

References

1. Byrne, M., G. F. Moran, et al. (1993). "Restriction map and maternal inheritance of chloroplast DNA in *Eucalyptus nitens*." Journal of Heredity 84(3): 218-220.

2. Byrne, M. and B. Hines (2004). "Phylogeographical analysis of cpDNA variation in *Eucalyptus loxophleba* (*Myrtaceae*)." Australian Journal of Botany 52(4): 459-470.

3. Byrne, M., B. MacDonald, et al. (2002). "Phylogeographical patterns in chloroplast DNA variation within the *Acacia acuminata* (*Leguminosae : Mimosoideae*) complex in Western Australia." Journal of Evolutionary Biology 15(4): 576-587.

4. Chase, M. W., S. Knapp, et al. (2003). "Molecular systematics, GISH and the origin of hybrid taxa in Nicotiana (Solanaceae)." Annals of Botany 92(1): 107-127.

5. Chase, M. W., N. Salamin, et al. (2005). "Land plants and DNA barcodes: short-term and long-term goals." Philosophical Transactions of the Royal Society B-Biological Sciences 360(1462): 1889-1895.

6. Ebach, M. C. and C. Holdrege (2005). "More Taxonomy, Not DNA Barcoding." BioScience 55(10): 823-824.

7. Freeman, J. S., H. D. Jackson, et al. (2001). "Chloroplast DNA phylogeography of Eucalyptus globulus." Australian Journal of Botany 49(5): 585-596.

8. Freeman, J. S., H. D. Jackson, et al. (2001). "Chloroplast DNA phylogeography of Eucalyptus globulus." Australian Journal of Botany 49(5): 585-596.

9. Kress, W. J. and T. Htun (2003). "A second species of Smithatris (*Zingiberaceae*) from Myanmar." Novon 13(1): 68-71.

10. Kress, W. J., V. A. Funk, et al. (2005). "Mapping biological diversity." Plant Conservation: A Natural History Approach: 209-235.

11. Kress, W. J., A. Z. Liu, et al. (2005). "The molecular phylogeny of Alpinia (*Zingiberaceae*): A complex and polyphyletic genus of gingers." American Journal of Botany 92(1): 167-178.

12. Kress, W. J. and G. A. Krupnick (2006). "The future of Floras: new frameworks, new technologies, new uses." Taxon 55(3): 579-580.

13. Kress, W. J., M. F. Newman, et al. (2007). "An analysis of generic circumscriptions in tribe Alpinieae (*Alpiniodeae : Zingiberaceae*)." Gardens' Bulletin (Singapore) 59(Part 1-2): 113-127.

14. Kumar, S., K. Tamura, et al. (2004). "MEGA3: Integrated software for molecular evolutionary genetics analysis and sequence alignment." Briefings in Bioinformatics 5: 150-163.

15. Jackson, H. D., D. A. Steane, et al. (1999). "Chloroplast DNA evidence for reticulate evolution in Eucalyptus (Myrtaceae)." Molecular Ecology 8(5): 739-751.

16. Lahaye, R., J. Klackenberg, et al. (2007). "Phylogenetic relationships between derived Apocynaceae s.l. and within Secamonoideae based on chloroplast sequences." Annals of the Missouri Botanical Garden 94(2): 376-391.

17. McKinnon, G. E., D. A. Steane, et al. (1999). "Incongruence between chloroplast and species phylogenies in Eucalyptus subgenus Monocalyptus (Myrtaceae)." American Journal of Botany 86(7): 1038-1046.

18. McKinnon, G. E., D. A. Steane, et al. (1999). "Incongruence between chloroplast and species phylogenies in Eucalyptus subgenus Monocalyptus (Myrtaceae)." American Journal of Botany 86(7): 1038-1046.

19. Newmaster SG, F. A., Ragupathy S (2006). "DNA barcoding in land plants: evaluation of rbcL in a multigene tiered approach." Canadian Journal of Botany-Revue Canadienne De Botanique 84: 335-341

20. Schaal, B. A., D. A. Hayworth, et al. (1998). "Phylogeographic studies in plants: problems and prospects." Molecular Ecology 7(4): 465-474.

21. Shaw, J., E. B. Lickey, et al. (2005). "The tortoise and the hare II: relative utility of 21 noncoding chloroplast DNA sequences for phylogenetic analysis." Am. J. Bot. 92(1): 142-166.

22. Schindel, D. E. and S. E. Miller (2005). "DNA barcoding a useful tool for taxonomists." Nature 435(7038): 17-17.

23. Steane, D. A. and D. J. Mabberley (1998). "Rotheca (Lamiaceae) revived." Novon 8(2): 204-206.

24. Taberlet, P., E. Coissac, et al. (2007). "Power and limitations of the chloroplast trnL (UAA) intron for plant DNA barcoding." Nucleic Acids Research 35(3).

25. Tautz, M. M. a. D. (2005). "Reverse taxonomy: an approach towards determining the diversity of meiobenthic organisms based on ribosomal RNA signature sequences." Philos Trans R Soc Lond B Biol Sc 360: 1462.

Current Trends in Biotechnology and Pharmacy
Vol. 18(3) 1962-1967, July 2024, ISSN 0973-8916 (Print), 2230-7303 (Online)
10.5530/ctbp.2024.3.41

Trends in the Indian Patent Scenario: A Meta-Analysis

Sumana Ande[1*], Rama Rao Nadendla[2]

[1]Department of Regulatory Affairs, Chalapathi Institute of Pharmaceutical Sciences, Guntur, Andhra Pradesh.
[2]Professor and Principal, Chalapathi Institute of Pharmaceutical Sciences, Guntur, Andhra Pradesh.
*Corresponding author: sumana.ande@gmail.com

Abstract

This trend analysis delves into the landscape of Indian patents from 2012 to 2022, aiming to identify and evaluate significant trends and changes in innovation. The primary objectives of this research include discerning patenting patterns, exploring innovative domains, assessing the impacts of legislative modifications, and projecting future developments. Through a comprehensive analysis of patent data, it seeks to ascertain prevalent technological domains, key influencing factors, and India's competitive standing within the global innovation landscape. The report underscores sector-specific patenting trends, placing emphasis on the emergence of new industries such as artificial intelligence, renewable energy, pharmaceuticals, and telecommunications. It illuminates India's evolving research and development objectives by scrutinizing patent filing rates, trends in technical collaborations, and the country's participation in the global arena. Additionally, it considers how changes in policy frameworks and regulations may influence patent activities. Our findings reveal a substantial increase in patent applications across various industries, with notable surges observed in technology, pharmaceuticals, and renewable energy sectors. Notably, this analysis underscores the necessity for continual policy support and increased investments in research and development to harness the full potential of Indian innovation. This comprehensive analysis provides strategic insights into future innovation trajectories, contributing to a nuanced understanding of India's patent landscape over the past decade.

Key words: Indian patents, innovation trends, patenting patterns

Introduction

In the context of the modern interconnected global economy, the importance of intellectual property rights is paramount. A key objective outlined by the Indian government for sustainable development is the promotion of innovation. The National Intellectual Property Rights (IPR) Policy aspires to create an environment where intellectual property drives creativity and innovation for the collective benefit of society. Various government initiatives such as Make in India, Start-up India, Digital India, and Skill India have effectively demonstrated their capability to foster innovation. The Atal Innovation Mission plays a pivotal role in nurturing innovation within educational institutions across the nation. Aligned with the IPR policy, the Office of the Controller General of Patents, Designs, and Trademarks has entrusted CIPAM, the cell for IPR Promotion and Management, with the responsibility of facilitating the establishment and commercialization of intellectual property assets. Notably, there has been a significant rise in the number of filings for intellectual property rights, prompting a capacity-building transformation within the Intellectual

Property Offices. This transformation includes an increased number of Examiners who have received specialized training in patents. Since October 2013, the Patent Office has functioned as an international searching and examining authority, and the growing preference of more applicants choosing the IPO for global search is a positive indication (1). The provision of Expedited Examination as a service for applicants registered as start-ups and choosing the Indian Patent Office for their international application is a commendable development. Moreover, the establishment of a specialized Quality Assurance Division within the Patent Office ensures quality in all operational aspects. Patents serve as a significant source of original and pioneering technical knowledge. The volume of patents originating from a country is a reliable indicator of its technological prowess and competitiveness. Analyzing patent trends aids in forecasting technology trajectories and shaping policy decisions effectively (2).

The primary aim here is to conduct in-depth research into the current patenting landscape in India, specifically through an examination of Indian patent trends spanning from 2012 to 2022. This comprehensive trend analysis method identifies and evaluates patenting patterns, unveiling crucial elements, predominant technological domains, and India's competitive position within the global innovation industry. This analysis not only aids in devising innovative approaches to obtain patents but also helps in understanding the reasons behind patent refusals.Top of Form

Materials and Methods

The study's methodological framework aimed to scrutinize trends and patterns in patent applications spanning diverse invention categories from 2012 to 2022, along with identifying the contributing factors to patent rejections. The information used for this study was sourced from the official Intellectual Property website of India. The comprehensive analysis involved an examination of the total count of patent applications filed, examined, granted, and those either disposed of or denied, which were sourced from the annual reports published by the Intellectual Property Office (IPO). These reports can be accessed at https://ipindia.gov.in/annual-reports-ipo.htm(3). All patents issued by the IPO during the years 2012 to 2022 conformed to the established inclusion criteria (3). A record sheet was meticulously structured to compile and organize the primary data obtained. The record sheet was created using Microsoft Office Word 2022, and subsequently, the data were imported into Microsoft Office Excel 2022 for comprehensive analysis and further processing. The compiled record sheet provides a comprehensive overview of patent filing and examination trends in various fields of invention from 2012 to 2022, including the total number of patents filed, examined, disposed of or granted, and granted across different fields. The collected data were methodically organized, entered into the Microsoft Office Excel 2022 program, and underwent a rigorous statistical analysis to draw conclusive insights.

Results and Discussion

This study reviewed, examined, and resolved all Indian patent applications filed from 2012 to 2022. The results are presented in Table 1 and Graph 1. Tables 2 and 3 provide a detailed breakdown of the data, offering insights into the evolving landscape of patent acquisition in India. These tables are valuable resources for researchers, policymakers, and industry stakeholders.

Table 1: Scenario of Indian patents from 2012-2022

Year	2012-13	2013-14	2014-15	2015-16	2016-17	2017-18	2018-19	2019-20	2020-21	2021-22
Filed	43,674	42,951	42,763	46,904	45,444	47,854	50,659	56,267	58,503	66,440
Examined	12,268	18,615	22,631	16,851	28,967	60,330	85,426	80,080	73,165	66,571
Granted	4,126	4,227	5,978	6,326	9,847	13,045	15,283	24,936	28,385	30,073
Disposal	9,027	11,411	14,316	21,987	30,271	47,695	50,884	55,945	52,755	35,990

Table 2: Number of patent applications filed from 2012-2022 under major fields of invention (14)(15).

YEAR	CHEMICAL	PS	PS&T	CS&E	COMMUNICATION	ELECTRICAL	PHYSICS	BIO-MEDICAL	ME	OTHERS	TOTAL
2012-2013	6812	2954	1425	4424	4163	3568	2593	1053	10198	6484	43674
2013-2014	6769	2507	1050	4410	4039	4371	2230	612	11318	5645	42951
2014-2015	6454	2640	1059	4285	4380	4031	2529	1669	10031	5685	42763
2015-2016	6463	2966	1230	5988	5770	4102	2852	1579	10164	5790	46904
2016-2017	5911	2122	1158	6443	5315	4141	2693	1048	10715	5898	45444
2017-2018	6343	2741	1116	6089	5486	4278	2996	1095	11573	6137	47854
2018-2019	6560	2683	1100	5540	6308	4703	3659	812	12414	6880	50659
2019-2020	5198	5622	1309	11126	6862	4587	2646	3508	10359	5050	56267
2020-2021	8809	80	1508	11930	6660	3743	2842	4911	10540	7480	58503
2021-2022	5173	5179	858	15575	7314	4286	3007	5288	11969	7791	66440

Table 3: Number of patent applications granted from 2012-2022 under major fields of invention (16)(17).

YEAR	CHEMICAL	PS	PS&T	CS&E	COMMUNICATION	ELECTRICAL	PHYSICS	BIO-MEDICAL	ME	OTHERS	TOTAL
2012-2013	1289	344	169	510	273	188	65	0	749	539	4126
2013-2014	1111	256	165	690	375	237	109	0	645	638	4226
2014-2015	1533	389	295	835	538	376	142	0	1047	823	5978
2015-2016	1683	370	279	810	414	362	175	0	1414	819	6326
2016-2017	2673	551	562	1049	805	579	260	0	1939	1429	9847
2017-2018	3376	733	747	1028	1031	818	568	150	2514	2080	13045
2018-2019	4242	761	701	1074	1414	1253	703	290	2857	1988	15283
2019-2020	4848	1930	923	2141	2692	2451	1349	565	5301	2736	24936
2020-2021	6074	1264	1745	2049	2857	2637	1396	703	6348	3312	28385
2021-2022	4279	3317	893	2459	3238	3084	1609	982	6832	3380	30073

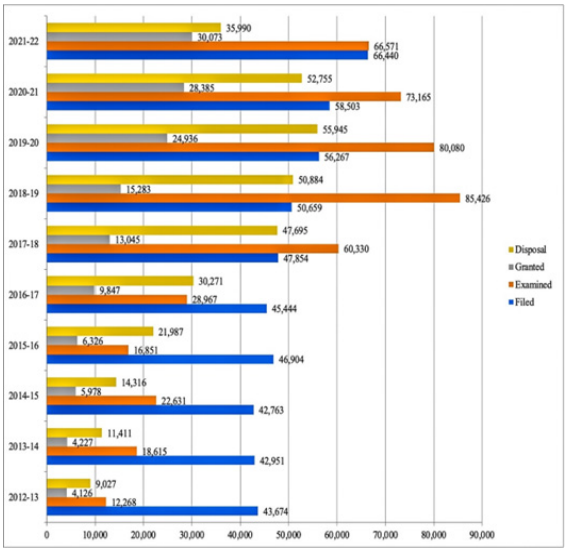

Graph 1: Patent trends in India during 2012-2022

Graphs 2 and 3 provide a comprehensive overview of the patenting landscape in India over the last decade, shedding light on distinctive trends in patent filings and grants across various fields of invention (Graph 2 and Graph 3). The total number of patents filed and granted under 2012-2022 are represented as pie charts with the percentages (Fig 1 and Fig 2).

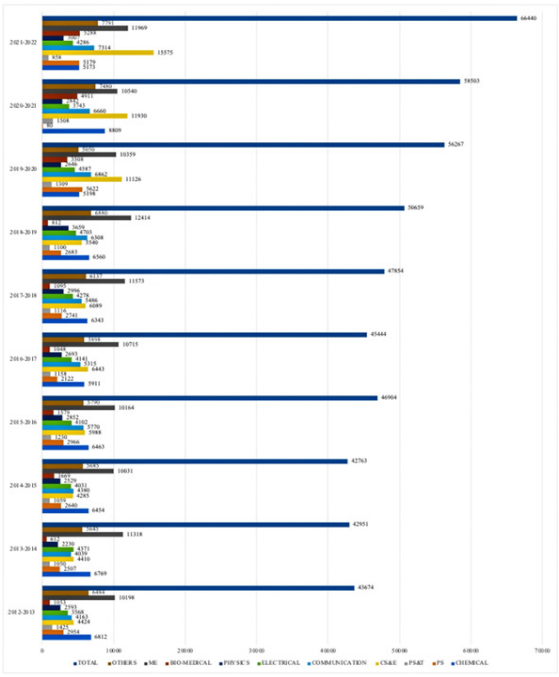

Graph 2: Patent applications filed under major fields of invention from 2012-2022

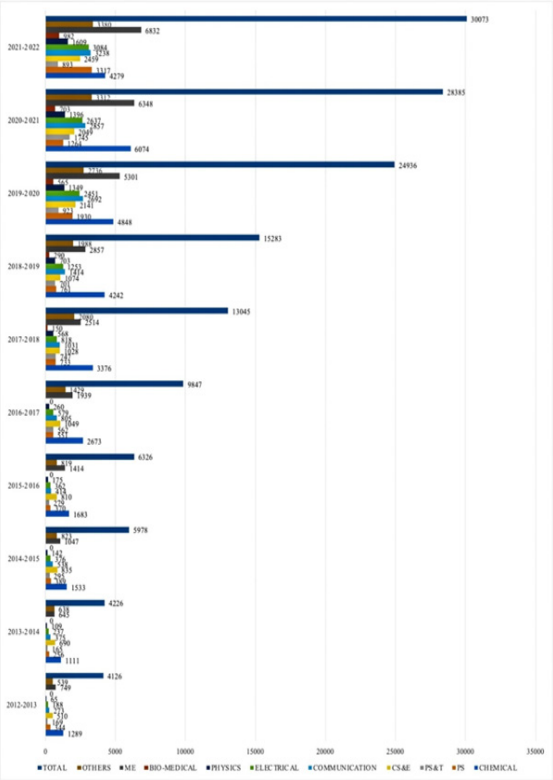

Graph 3: Patent applications granted under major fields of invention from 2012-2022

Throughout the analysed period, mechanical engineering consistently emerged as the frontrunner in terms of the number of patents filed. Concurrently, the field of chemicals secured the highest count of patents granted (4-13). This established a clear dichotomy in the dynamics of patent acquisition, with mechanical engineering dominating in filings and the chemical domain excelling in actual grants. A notable inflection point surfaced in the Fiscal year 2019-20. Despite mechanical engineering maintaining its stronghold on the highest number of patents granted, the landscape of filings underwent a remarkable shift. The forefront transitioned to the dynamic realms of computer science and electronics, signifying a significant pivot in innovation trends (11).

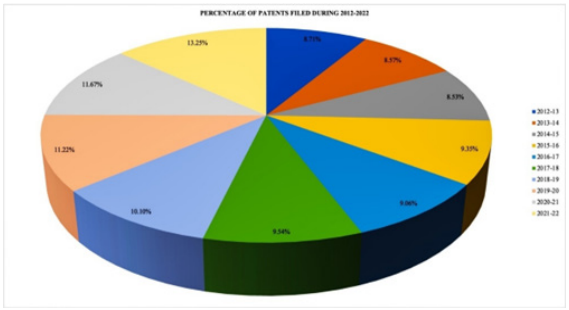

Figure 1: Percentage of patents filed from 2012-2022

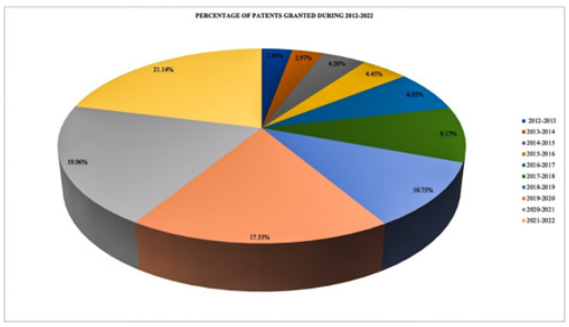

Figure 2: Percentage of patents granted from 2012-2022

The percentage growth of patent filings from 2012 to 2022 revealed a fluctuating yet overall ascending trend in submissions: 43,674 patent applications in 2012–2013 showcased a marginal 1.1% increase from the prior year (4), while 42,951 applications in 2013–14 saw a slight 1.65% decrease (5). Subsequent years witnessed varied patterns: 42,763 filings in 2014–15 with a modest decline (6), a surge to 46,904 applications in 2015–2016, marking an increase of nearly 10% from the previous year (7). The two-year period from 2016 to 2017 experienced a minor decrease to 45,444 patent applications, demonstrating a 3.2% decline. Notably, the domestic filing percentage saw a rise to 29.2% in 2016–17, indicating a 1.2% increase (8). The following years displayed a positive trajectory with increasing submissions: 47,854 in 2017–18 (a 5.3% increase) (9), 50,659 in 2018–2019 (a 5.9% rise) (10), 56,279 in 2019–2020 (an 11.1% increase) (11), 58,503 in 2020–2021

(a 3.97% rise) (12), and 66,440 in 2021–2022, marking a substantial increase of 13.57% from the preceding year (13). Moreover, there were notable elevations in the percentage of domestically filed patent applications, indicating an increasing trend over the years.

This trend analysis not only provides insights into the current patenting landscape in India but also serves as a valuable tool for understanding the diverse areas of dominance in patent acquisition across different fields of invention. For instance, the surge in computer science and electronics filings could guide strategic considerations for those seeking patents in cutting-edge technologies.

The analysis encompassed an extensive evaluation of Indian patents from 2012 to 2022, revealing significant trends and variations in the patenting landscape. The study involved an examination of patent applications, grant rates, and their distribution across multiple fields of invention.

Across the ten-year period, the observed percentage growth of patents filed depicted varying trends. Notably, the number of patent applications exhibited fluctuations year-on-year, with occasional rises and declines in the filing rates. These statistics highlight the changing dynamics of innovation and patent submissions within India.

The trend analysis underscored the evolving patenting patterns, shedding light on the prevailing dominance in specific fields of invention. This insight is crucial in understanding the sectors garnering the most patent activity and serves as a strategic guide for emerging areas that require focus for increased patent acquisition. This comprehensive study not only delineates the prevailing patent trends but also presents a roadmap for identifying fields with significant potential for enhanced patent acquisition.

Conclusion

The comprehensive analysis of patent trends offers valuable insights into the landscape of patent application filings, innovation trajectories, and the diverse patenting endeavour's across multiple inventive sectors in India. This study indicates a noticeable upsurge in patent activity over the years, signifying a growing interest in patenting activities across various fields. The fluctuating trends in patenting activity underscore the dynamic nature of innovation in different invention categories, culminating in the issuance of patents. It's apparent that while there is a notable number of patent applications, only a fraction of these are successfully granted, while the remainder face rejection for various reasons. Reasons for patent rejections encompass aspects such as lack of innovation, issues related to inventive steps, failure to disclose biological material sources, and inadequacies in providing a detailed innovation description. Additionally, the consideration of prior community experiences, whether local or indigenous, plays a significant role in the patent rejection process.

References

1. Indian patent office, vision and mission, https://ipindia.gov.in/vision-patent.htm
2. Sanjay V. Jadhav, Kailas R. Jagdeo. (2020). Recent Patenting Trends in India-A Critical Study. International Journal of Creative Research Thoughts; 8(4):469-75.
3. IPR Annual Reports, https://ipindia.gov.in/annual-reports-ipo.htm
4. Office of the Controller General of Patents, Designs & Trade Marks. Annual report (2012-2013), pp.5
5. Office of the Controller General of Patents, Designs & Trade Marks. Annual report (2013-2014), pp.5
6. Office of the Controller General of Patents, Designs & Trade Marks. Annual report (2014-2015), pp.6

7. Office of the Controller General of Patents, Designs & Trade Marks. Annual report (2015-2016), pp.5
8. Office of the Controller General of Patents, Designs & Trade Marks. Annual report (2016-2017), pp.10
9. Office of the Controller General of Patents, Designs & Trade Marks. Annual report (2017-2018), pp.7
10. Office of the Controller General of Patents, Designs & Trade Marks. Annual report (2018-2019), pp.7
11. Office of the Controller General of Patents, Designs & Trade Marks. Annual report (2019-2020), pp.6
12. Office of the Controller General of Patents, Designs & Trade Marks. Annual report (2020-2021), pp.6
13. Office of the Controller General of Patents, Designs & Trade Marks. Annual report (2021-2022), pp.6
14. Office of the Controller General of Patents, Designs & Trade Marks. Annual report (2016-2017), pp.46
15. Office of the Controller General of Patents, Designs & Trade Marks. Annual report (2021-2022), pp.37
16. Office of the Controller General of Patents, Designs & Trade Marks. Annual report (2016-2017), pp.47
17. Office of the Controller General of Patents, Designs & Trade Marks. Annual report (2021-2022), pp.38